

Thermophoresis of electrolyte solutions and protein-ligand systems

Inaugural-Dissertation

zur

Erlangung des Doktorgrades

der Mathematisch-Naturwissenschaftlichen Fakultät

der Universität zu Köln

vorgelegt von

Shilpa Mohanakumar

aus Kerala, India

Köln, 2023

Berichterstatte: Prof. Dr. Simone Wiegand
(Gutachter) Prof. Dr. Annette Schmidt
Prof. Dr. Uwe Ruschewitz

Tag der mündlichen Prüfung: 28.04.2023

Abstract

Thermophoresis or thermodiffusion is the mass transport driven by a temperature gradient. This thesis focuses on the thermophoretic motion of ionic compounds in a biological context and is motivated by a practical application, in which thermodiffusion is used to monitor protein-ligand reactions. Proteins are complex molecules containing non-ionic and ionic groups. While recent studies of non-ionic compounds found a strong correlation between thermodiffusion and hydration, it is unclear how this correlation changes when molecules are charged. To separate ionic from non-ionic contributions, it is reasonable to look first into the thermophoretic motion of simple salts without large organic side groups and to study in the next step complex protein-ligand systems, which typically contain hydrophobic and hydrophilic groups. The systematic studies of aqueous solutions of simple salts should reveal differences between ionic and non-ionic systems and should give further information about ion and ion specific effects. Due to the high complexity of protein-ligand systems, complementary methods should be used to gain a better understanding of the interactions between different components that are present in the system. This will help to understand how the thermophoretic behavior of the free protein differs from that of the protein-ligand complex formed.

Study of the thermophoretic behavior of ionic systems indicates that several correlations, which were found for aqueous solutions of non-ionic solutes are no longer valid for ionic solutes. For non-ionic solutes hydrogen bonds primarily influence the thermophoretic behavior. In case of ionic solutes, although both electrostatic interactions and hydrogen bonds are present, it is found that thermophoretic behavior is influenced by electrostatic interactions. Focusing on the specific ion effects for ionic systems in the context of the Hofmeister series, a change of the anion is found to influence the thermophoretic behavior more than a change of the cation. Further, a correlation between thermophoretic behavior and hydrophilicity of the ionic solutes is found, which underlines the sensitivity of thermodiffusion to changes in hydration. Based on this sensitivity, a preliminary model is developed for describing the non-monotonous variation of Soret coefficient S_T with concentration for aqueous solutions of alkali iodide salts. To study the thermodiffusion of binding reactions, we also use complementary methods such as Isothermal Titration Calorimetry (ITC) and a thermophoretic microfluidic cell. As systems, we have chosen EDTA-CaCl₂ and protein-ligand systems (binding of Bovine Carbonic Anhydrase I (BCA I) with two aryl sulfonamide lig-

ands). To gain deeper insight into the complex formation reactions thermophoretic data (non-equilibrium process) are compared with thermodynamic data (equilibrium process) to establish a mathematical relation between S_T and Gibb's free energy ΔG . For EDTA-CaCl₂ and protein-ligand systems, the derived relation holds valid, which enables calculation of ΔG at a particular temperature from S_T .

Kurzzusammenfassung

Thermophorese oder Thermodiffusion ist der durch ein Temperaturgefälle hervorgerufene Massentransport. Diese Arbeit befasst sich mit dem thermophoretischen Bewegung biologischer oder biokompatibler ionischer Verbindungen und ist durch eine praktische Anwendung motiviert, bei der die Thermodiffusion zur Charakterisierung von Protein-Ligand-Reaktionen eingesetzt wird. Proteine sind komplexe Moleküle, die nicht-ionische und ionische Gruppen enthalten. Während neuere Studien bei nicht-ionischen Verbindungen eine starke Korrelation zwischen Thermodiffusion und Hydratation finden, ist unklar, wie sich diese Korrelation ändert, wenn die Moleküle geladen sind. Um die ionischen von den nicht-ionischen Beiträgen zu trennen, ist es sinnvoll, zunächst die thermophoretische Bewegung von einfachen Salzen ohne große organische Seitengruppen zu untersuchen und im nächsten Schritt komplexe Protein-Ligand-Systeme zu analysieren, die typischerweise hydrophobe und hydrophile Gruppen enthalten. Die systematischen Untersuchungen von wässrigen Lösungen einfacher Salze sollen Unterschiede zwischen ionischen und nicht-ionischen Systemen aufzeigen und weitere Informationen über ionische und ionenspezifische Effekte liefern. Aufgrund der hohen Komplexität von Protein-Ligand-Systemen sollten komplementäre Methoden eingesetzt werden, um ein besseres Verständnis der Wechselwirkungen zu gewinnen. Dies wird helfen zu verstehen, wie sich das thermophoretische Verhalten des freien Proteins von dem des gebildeten Protein-Liganden-Komplexes unterscheidet.

Die Untersuchung des thermophoretischen Verhaltens ionischer Systeme zeigt, dass mehrere Korrelationen, die für wässrige Lösungen nicht-ionischer Stoffe gefunden wurden, für ionische Stoffe nicht mehr gültig sind. Bei nicht-ionischen Stoffen beeinflussen vor allem Wasserstoffbrückenbindungen das thermophoretische Verhalten. Bei ionischen gelösten Stoffen sind sowohl elektrostatische Wechselwirkungen als auch Wasserstoffbrückenbindungen vorhanden, und es zeigt sich, dass das thermophoretische Verhalten auch durch die elektrostatischen Wechselwirkungen beeinflusst wird. Betrachtet man die spezifischen Ioneneffekte für ionische Systeme im Rahmen der Hofmeister-Reihe, so stellt man fest, dass eine Änderung des Anions das thermophoretische Verhalten stärker prägt als eine Änderung des Kations. Darüber hinaus finden wir eine Korrelation zwischen dem thermophoretischen Verhalten und der Hydrophilie des ionischen gelösten Stoffes, was die Sensitivität der Thermodiffusion gegenüber Änderungen der Hydratation unterstreicht. Auf der Grundlage dieser Empfindlichkeit wird ein vorläufiges Modell zur Beschreibung der nicht-monotonen Variation des

Soret-Koeffizienten S_T mit der Konzentration für wässrige Lösungen von Alkali-Iodid-Salzen entwickelt. Um die Thermodiffusion von Bindungsreaktionen zu untersuchen, verwenden wir auch komplementäre Methoden wie die Isothermale Titrationskalorimetrie (ITC) und eine thermophoretische Mikrofluidikzelle. Als Systeme haben wir EDTA-CaCl₂ und Protein-Liganden-Systeme gewählt (Bindung von Rinder-Kohlensäureanhydrase I (BCA I) mit zwei Arylsulfonamid-Liganden). Um einen tieferen Einblick in die Komplexbildungsreaktionen zu erhalten, werden thermophoretische Daten (Nicht-Gleichgewichtsprozess) mit thermodynamischen Daten (Gleichgewichtsprozess) verglichen, um eine mathematische Beziehung zwischen S_T und der freien Gibb-Energie ΔG herzustellen. Für EDTA-CaCl₂ und Protein-Ligand-Systeme gilt die abgeleitete Beziehung, die die Berechnung von ΔG bei einer bestimmten Temperatur aus S_T ermöglicht.

Contents

1	Introduction	1
1.1	Introduction to thermodiffusion	1
1.2	Applications of thermophoresis	2
1.2.1	MicroScale Thermphoresis (MST)	2
1.3	Theoretical descriptions and simulations of thermodiffusion in different systems	4
1.3.1	Aqueous systems	4
1.3.2	Colloidal systems	4
1.3.3	Simulations	6
1.4	Experimental studies of thermodiffusion in different systems	8
1.4.1	Low molecular aqueous systems	8
1.4.2	Colloidal systems	10
1.4.3	Protein-ligand systems	11
1.5	Experimental methods and materials	12
1.5.1	Description of IR-TDFRS setup used	12
1.5.2	Measurement of refractive index contract factors	14
1.5.3	Isothermal Titration Calorimetry	14
1.5.4	Sample preparation	16
1.6	Outline of the thesis	17
2	Thermodiffusion of Aqueous Solutions of Various Potassium Salts	21
3	Towards Understanding Specific Ion Effects in Aqueous Media using Thermodiffusion	33

4	Overlapping hydration shells in salt solutions causing non-monotonic Soret coefficients with varying concentration	43
5	Thermophoretic Microfluidic Cells for Evaluating Soret Coefficient of Colloidal Particles	53
6	Complementary Experimental Methods to Obtain Thermodynamic Parameters of Protein Ligand Systems	63
7	Discussion and Conclusion	79
7.1	Discussion	79
7.1.1	Correlation with hydrophilicity	80
7.1.2	Effect of cluster formation	82
7.1.3	Changes in the hydration shell	84
7.1.4	Thermodiffusion of complexes	86
7.1.4.1	IR-TDFRS measurements	87
7.1.4.2	Measurements using a thermophoretic microfluidic cell	89
7.1.4.3	Factors affecting thermodiffusion of complexes	89
7.1.5	Connecting parameters of equilibrium (ITC) and non-equilibrium (IR-TDFRS) experimental techniques	90
7.2	Conclusion	92
7.2.1	Thermodiffusion of aqueous salt solutions	92
7.2.2	Development of a thermophoretic microfluidic cell	94
7.2.3	Thermodiffusion of binding reactions	94
7.3	Outlook	96
	Acknowledgement	99
	Bibliography	101

Appendix	113
Supporting Information	113
Declaration of Individual Contribution	190
Erklärung zur Dissertation	193
Lebenslauf	193

1 Introduction

1.1 Introduction to thermodiffusion

Mass transport that is driven by a temperature gradient is known as thermodiffusion, also termed thermophoresis or Ludwig-Soret effect. Thermophoresis in liquid mixtures was first reported by Carl Ludwig in 1856 and later systematically investigated by Soret [1]. In a multi-component mixture along a temperature gradient ∇T , the mass flux \vec{j} is given by

$$\vec{j} = -\rho D \nabla c - \rho c(1-c) D_T \nabla T, \quad (1.1)$$

where D_T is the thermal diffusion coefficient, ρ is the mass density and c is the concentration given as mass fraction [2]. Along with the thermodiffusion, there is also Fickian diffusion which is characterized by the diffusion coefficient D . At steady state, the ratio of concentration gradient that is generated upon the induction of temperature gradient is equal to the Soret coefficient S_T given by

$$S_T \equiv \frac{D_T}{D} = -\frac{1}{c(1-c)} \frac{\Delta c}{\Delta T}. \quad (1.2)$$

S_T , which has a unit of K^{-1} , can have a positive or negative value. The thermophobic component of the mixture, which enriches on the cold side, has a positive Soret coefficient, while the thermophilic one enriches on the warm side and has a negative S_T .

Thermophoresis combined with other effects like convection can be used as an effective tool for partial separation of components in a mixture. Different applications of thermophoresis depict that the process strongly depends on a variety of molecular properties such as molar

mass, size, charge, hydration shell, etc. [3]. Although this is an extensively studied field, there is still a limited microscopic understanding of the effect in fluid mixtures.

1.2 Applications of thermophoresis

The earliest application of thermophoresis was in 1939 for the isotope separation of chlorine gas in a thermogravitational column [4]. Later in 1944, it was used for the uranium isotope separation in the Manhattan project [5]. But it has to be noted that, on an application level thermogravitational columns have been replaced by other instruments for isotope separation due to its high energy costs and technical difficulties in maintaining. It has also been reported that thermodiffusion influences the distribution of different crude oil components in hydrocarbon reservoirs [6]. Around the twentieth century, another important application of the thermophoretic effect was developed, which is Thermal Field-Flow Fractionation (Th-FFF). This was primarily used to characterize and fractionate polymers like polystyrene [7, 8]. Although Th-FFF has been applied to many different synthetic polymers and colloids [9, 10], there have been certain limitations of this technique with respect to low molar mass polymers. For low molecular mass systems, due to small S_T , a high temperature gradient of the order of 10^6 K/m is required [11]. Further, an application of thermophoresis which is most relevant in biological systems is discussed in detail in the forthcoming section.

1.2.1 MicroScale Thermphoresis (MST)

An extensive study of biomolecular interactions is fundamental nowadays to provide a good understanding of the biological processes that happen in living systems. It turned out that the thermophoretic behavior of a free protein differs from that of the protein-ligand complex which led to the development of a commercial instrument, MicroScale Thermophoresis (MST). MST monitors the movement of inherently fluorescent molecules or fluorescently labeled molecules in a temperature gradient at different ligand concentrations [12–14]. Thermophoresis depends on a variety of molecular properties. For biological reactions, a change in hydration is expected to change thermophoretic motion. During a MST experiment, a temperature gradient is induced by an infrared laser in a solution with fluorescently labeled

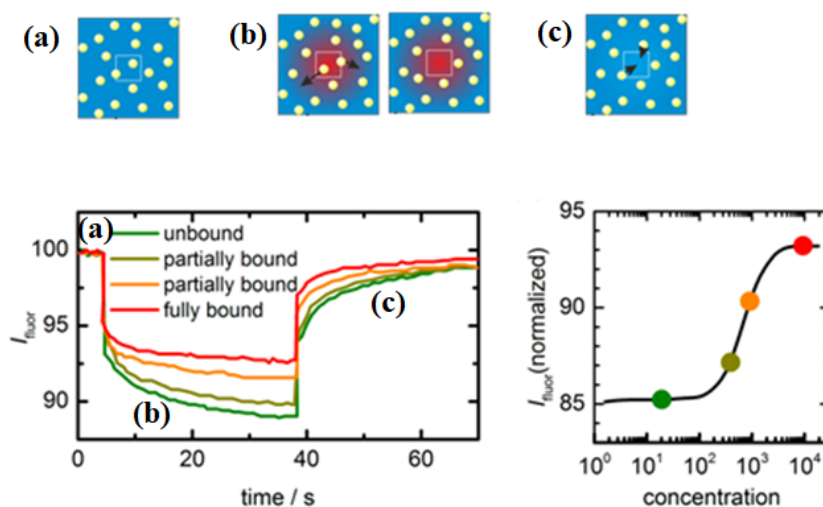


Figure 1.1: Thermophoresis signal obtained from a typical MST experiment

biomolecules or inherently fluorescent biomolecules. Once a temperature gradient occurs, thermodiffusion sets in, and the corresponding fluorescence intensity is detected which is proportional to the S_T of the studied biomolecule. When the ligand is titrated to the solution, binding between the ligand and biomolecule occurs which is accompanied by changes in the hydration layer of the biomolecule. This, in turn, changes the thermodiffusive behavior and is reflected as a change in the fluorescence intensity. A typical signal obtained from an MST experiment and a schematic representation of the process is shown in Fig. 1.1. Change in fluorescence intensity is reported as a titration curve and is utilized to extract information about the equilibrium constant of the binding reaction. MST has proven to be a very efficient technique to extract information about the changes that happen in the hydration layer.

MST has several advantages over other techniques such as simplicity, low sample volume, etc. [12]. Since the technique uses fluorescent detection, a fluorescent label is attached or the inherent fluorescence of a molecule is used if available. One of the important drawbacks of the technique lies in this fluorescent labeling as it might influence the binding of the ligand. Although MST uses thermophoresis, it doesn't give access to Soret and thermal diffusion coefficients.

1.3 Theroretical descriptions and simulations of thermodiffusion in different systems

1.3.1 Aqueous systems

Thermodiffusion of non-polar and polar aqueous mixtures shows prominent differences owing to the latter's ability to form hydrogen bonds. This can often be seen in the temperature dependence of S_T . For several aqueous systems, a change in the sign of S_T is observed with temperature [15,16]. In general, aqueous solutions exhibit a typical temperature dependence where the solute shows a lower S_T value at low temperatures and gradually increases with temperature. The following empirical equation has been proposed by Iacopini and Piazza [17] to characterize the temperature dependence behavior of aqueous solutions.

$$S_T(T) = S_T^\infty \left[1 - \exp\left(\frac{T^* - T}{T_0}\right) \right], \quad (1.3)$$

where S_T^∞ , T^* and T_0 are empirical parameters that refer to the Soret coefficient at infinite temperature, the temperature at which sign change of S_T occurs and a parameter to describe the curvature respectively. Sign change in S_T has been explained using a concept of free energy minimization [18]. At lower temperatures, where the enthalpy contribution dominates, the system has a largely undisturbed hydrogen bond network of water which minimizes the free energy. This moves the solute towards the warm side. With increasing temperature, entropy dominates and the high translational and orientational entropy of water leads to an enrichment on the warm side [18].

1.3.2 Colloidal systems

The study of thermodiffusion in colloidal particles was initiated by Ruckenstein in 1981 [19], where a connection between the thermophoresis of solid colloidal particles and the Marangoni effect is made. Theoretical concepts of thermodiffusion in colloids consider two contributions;

1.3 Theoretical descriptions and simulations of thermodiffusion in different systems 5

the first one being the specific interaction between the surface group of colloidal particles with the solvent molecules and the second contribution due to the interaction between the colloid particles. A study by Dhont [20] for uncharged colloids expressed collective and thermal diffusion coefficient in terms of the osmotic pressure. Later, the thermal diffusion coefficient of interacting colloidal spheres is derived in terms of the inter colloidal pair-interaction potential and hydrodynamic interaction functions [21]. This study is based on the Smoluchowski equation which is then generalized to a temperature gradient.

For charged colloids at very dilute concentrations, inter colloidal interactions can be neglected. In such highly diluted solutions, dispersion interaction between colloidal particles and the solvent and the formation of a double layer dominates the physical properties of colloids. S_T at high dilutions is termed as single-particle Soret coefficient. Different theoretical approaches have been developed for the derivation of single particle S_T of charged colloids. A model for single spherical ionic ferrocolloids in terms of a spherical potential has been derived by Morozov [22]. Later an expression for S_T of colloidal particles was proposed by Bringuier and Bordon [23] in terms of the total internal energy of the particle, based on Brownian motion. In the theory by Dhont, S_T is derived by considering the electrostatic energy that is necessary to build up the double layer [24]. In this study, an expression for the contribution of an electrical double layer to the single-particle thermal diffusion coefficient is derived in terms of the surface charge density of the colloidal sphere, the electrostatic screening length, and its core radius, to within the Debye-Hückel approximation [24, 25]. The theory proposed by Würger *et al.* starts from a Navier-Stokes equation and considers the additional forces that arise once a temperature gradient is applied [26]. Braun calculated the Soret coefficient for a charged colloid from the analogy of the colloid's surface and its double layer with an electric capacitor [27]. Both the above mentioned theories are limited to thin double layers and lead to the same expression of single particle Soret coefficient.

Electric double layer has often been reported to have an effect on the thermodiffusion of colloid systems [25, 28]. Theoretical approaches which look into the effect of double layer formation can be classified into two groups. Within the first group, temperature induced deformations in the electric double layer are neglected [24, 26, 27, 29]. The second approach considers the resulting flow within the double layer once the temperature gradient is applied [30]. Along with this, the interaction of the colloid with the surrounding solvent

occurs and this force leads to a solvent flow around the colloid [30,31]. Thus, the total thermophoretic force acting will have a contribution from the aforementioned force and the friction force resulting from the solvent flow.

All the above mentioned concepts were originally developed for spherical colloids but were later extended to nonspherical colloids as well [32]. The theory which existed for thermal diffusion of charged spheres is extended to long and thin charged rods. This leads to an expression for S_T in terms of the Debye length, the rod-core dimensions, and the surface charge density. The theory developed here predicts that the thermal diffusion coefficient of a rod like colloid is equal to that of a spherical bead with a diameter of dimension same as that of the rod-core, and with the same surface charge density, multiplied by the number of beads [32]. This is found to be accurate for arbitrary Debye lengths, including very thin double layers.

1.3.3 Simulations

A challenging part of studying thermophoresis is the involvement of different parameters as discussed before, which are interconnected and in reality, sometimes cannot be altered without changing another. This makes it difficult to separate the contributions experimentally. Here is where the importance of simulations, especially molecular dynamics (MD) simulation comes into the picture. Simulations have the main advantage of changing parameters independently. Along with this, simulations also help to get a closer insight microscopically which will in turn provide information about changes in molecular interactions. Of MD simulations, there are equilibrium and non-equilibrium molecular dynamics (EMD and NEMD, respectively), of which NEMD simulations are mainly used for studying thermophoretic behavior of different systems. [33,34].

There have been several systems where the thermodiffusive properties have been computed by simulations. In the case of benzene/cyclohexane [35] simulation study reported behavior similar to what has been observed experimentally. Big particle systems like polymer solutions [36] and colloidal systems have also been studied with simulations [37,38]. NEMD simulations of three heptane isomers in benzene show the same trend as experimental data

1.3 Theoretical descriptions and simulations of thermodiffusion in different systems 7

where S_T increases with the increasing degree of branching of heptane. For *n*-heptane, simulated S_T at all mole fractions have a value 40% lower than experimental S_T [39]. Whereas, simulated and experimental S_T values in binary mixtures of spherical molecules in carbon tetrachloride agreement agreed within 10-20% [40].

Thermophoretic properties of several polar non-ionic mixtures have also been studied with the help of simulations. For the ethanol/water system a sign change in S_T with the composition of ethanol which experimentally [41], was also reported with MD simulations [42]. Simulation data obtained in this study were in good agreement with experimental data that have been obtained with three different methods [41–43]. Also, a sign change in S_T of acetone/water and dimethylsulfoxide(DMSO)/water mixtures, with varying water content was predicted by simulations [44]. Later this was confirmed experimentally for both systems with a reasonable agreement between the experimental and simulation data [45], except for the equimolar mixture of acetone/water. For urea/water, thermal diffusion measurements showed a change in the temperature dependence of S_T with concentration; where at low concentrations there was a positive slope ($S_T/\partial T > 0$) and at high concentrations, a negative slope ($S_T/\partial T < 0$) [46]. S_T obtained from NEMD simulations also predicted the sign change in the slope as observed in experiments. With the help of simulations, it was concluded that the transition concentration at which the change from positive slope to negative slope occurs is determined by the solute-solvent interactions, mainly influenced by the hydrogen bonds. Simulations also predict that this phenomenon is primarily enthalpic in its origin. Thus, simulations further provided evidence for the fact that thermophoresis is sensitive to the nature of solute-solvent interactions. Artola *et al.* used EMD simulation to predict the concentration dependence of S_T for ethanol/water system, using two different models [47]. Concentration at which a sign change in S_T is observed from simulations coincides with experimental results [48]. However, simulations underestimate the magnitude of S_T except at sign changing concentration [47].

The Soret coefficient of an aqueous solution of LiCl has been studied as a function of temperature and concentration using simulations [49]. This study predicts a minimum in S_T with concentration at low temperatures which disappears with increasing temperature. From simulations, minimum is observed around 2.5 mol/kg at 240 K. Experimental study of an aqueous solution of LiCl also predicts a minimum in S_T with concentration, but at a lower

concentration of around 0.5 mol/kg at 273 K [50]. This simulation study also predicted that the diameter of an anion has a significant impact on the concentration at which minimum is observed [49].

1.4 Experimental studies of thermodiffusion in different systems

1.4.1 Low molecular aqueous systems

There have been several studies that report the thermodiffusive behavior of aqueous low molecular weight systems [15, 46, 51] and polymer solutions [41]. Although Eq. 1.3 which describes temperature dependence of S_T holds for several biological systems [3, 52], it has failed to describe the temperature dependence of S_T for several systems like ethanol in water, ethylene glycol oligomers in water, etc. [53]. For certain solutes like formamide, the validity of the equation depends on the concentration as well [54]. At dilute concentrations of formamide solution, temperature dependence can be described using Eq. 1.3, but fails at higher concentrations. Temperature dependence of S_T for aqueous solutions of monovalent organic salts, tetramethylammonium and tetrabutylammonium hydroxides (TMAOHF and TBAOH respectively) shows contrasting behaviors. While S_T of TMAOH increases with temperature, that of TBAOH decreases with temperature [55]. The thermodiffusion behavior of aqueous non-ionic systems is mainly dominated by the hydrogen bond network that is present. Maeda *et al.* found that the difference in the number of hydrogen bond donor and acceptor sites on ethylene glycols and crown ethers is linearly correlated to the temperature dependence of their Soret coefficients [53]. For low molecular ionic systems, S_T generally shows an increase with temperature, which is successfully described using Eq. 1.3 [56]. This increase is steep at low temperatures and flattens out at high temperatures.

For many aqueous solutions, it is found that the sign of S_T changes with temperature [51, 52, 56–58]. Often a sign change in S_T with temperature depends on concentration and has been observed experimentally for various systems [15, 41, 51]. For example, in ethanol/water system [41], ethanol tends to accumulate on the colder side at low concentra-

tions of ethanol. With an increase in the concentration of ethanol, there is a sign change in S_T and tends to accumulate on the warmer side.

Thermophoretic behavior of non-ionic systems (small amide molecules) in water has been systematically studied [54]. To describe the temperature and concentration dependence of amides in water an empirical equation can be used which has been originally developed for non-polar mixtures by Wittko and Köhler [59]

$$S_T(m, T) = \alpha(m)\beta(T) + S_T^i, \quad (1.4)$$

with polynomial serial expansions for $\alpha(m)$ and $\beta(T)$

$$\begin{aligned} \alpha(m) &= a_0 + a_1m + a_2m^2 + a_3m^3 + \dots, \\ \beta(T) &= 1 + b_1(T - T_0) + b_2(T - T_0)^2 + \dots \end{aligned} \quad (1.5)$$

T_0 is an arbitrary reference temperature, set to $T_0 = 25^\circ\text{C}$ and S_T^i is a temperature and concentration independent constant. Although, S_T^i of non-polar mixtures can be related to their differences in mass and moment of inertia this is not possible for aqueous non-polar systems [3, 57]. It has to be noted here that a_0 and S_T^i are no independent parameters.

Concentration dependence of thermodiffusion behavior of various salt systems has been studied by Tanner [60, 61]. Later Snowdon and Turner calculated the heat of transfer of these salts from the measured S_T [62, 63]. They found out that the additivity of the ionic contributions holds for the heat of transfer of univalent salts, but not for the multivalent ones. Concentration dependence of salt systems like NaCl and KCl has also been studied very extensively [15]. Aqueous solutions of both these salts show a sign change in S_T with concentration [15]. Another interesting behavior of these salt solutions is a minimum in S_T with concentration. There exists no theoretical explanation for the occurrence of this minimum yet. Chanu [64] and later Gaeta [15] have connected this minimum to the perturbation of water structure once ions are introduced into the system. Additional structural changes are observed with an increase in salt concentration. Several studies indicate that thermodiffusion for aqueous ionic systems is also influenced by the charges present in addition to the extensive hydrogen bond network [3].

1.4.2 Colloidal systems

Colloidal systems have been used as model systems to test derived theoretical approaches [24,25,32,65]. Several experimental studies indicate that the thermodiffusive behavior of colloids is influenced by size, charge, interfacial tension, Brownian motion, and hydrodynamic interaction. Size dependence of S_T for hard and soft colloids has been studied by several groups [66–71]. A study of a non-ionic microemulsion (surfactant AOT/isooctane/water) showed a linear dependence of S_T on with radius of the particle. Linear dependence of S_T on size dependence has also been confirmed for several other non-ionic microemulsions. Naumann *et al.* observed this dependence for water/n-decane/pentaethylene glycol mono dodecyl ether which is also a non-ionic microemulsion [66,68]. These studies indicate that D_T is independent of the size of the particle which is in agreement with the molar mass dependence of D_T of polymers with high molar masses [72]. Size dependence of thermodiffusive behavior has also been studied for charged colloids. Duhr and Braun found out that for carboxyl-modified polystyrene beads, S_T varies linearly with the square of the radius and D_T varies linearly with the radius [73]. Braibanti *et al.* repeated the measurement for the same particle in a mixture of H_2O+D_2O (1:1) and found a linear radial dependence of S_T in contrast to what has been observed by Duhr and Braun [70]. Unfortunately, thermophoretic data of different colloids with different radii which have been synthesized by different methods cannot be compared since thermophoretic properties very much depend upon grafting, surface charge densities, etc. [71,74].

Charge effects in colloidal systems have also been studied by experiments. A systematic study of thermal diffusion of dilute solution of Ludox silica particles has been carried out by Ning *et al.* [25]. S_T of Ludox silica particles is measured as a function of Debye length and surface charge density of colloids. At high salt concentration (lower Debye length) S_T of Ludox particle measured is lower than that at low salt concentration (higher Debye length). A reasonable agreement with the experimental data and theoretical prediction were found in this study [25]. S_T of polystyrene (PS) particles also showed an increase with Debye length [27]. Eslahian *et al.* studied PS particles in the presence of different salts as a function of concentration [75,76]. They compared the thermophoretic behavior of colloidal particles in presence of different ions as they are ordered in Hofmeister series. S_T of PS particles show an increase with anions going from kosmotropic to chaotropic. Besides, changing anion is found to have a stronger effect on thermophoretic behavior than changing cation [76].

Experiments also focused on studying thermophoretic properties of non-spherical colloidal particles. Thermodiffusion behavior of a dilute solution of colloidal rod (bare fd-virus) has been studied by Wang *et al.* [32]. S_T of fd-viruses show an increase with Debye length and weak dependence on rod-concentration when the ionic strength is kept constant. Theory that existed for the thermal diffusion of charged spheres were extended to describe the thermal diffusion of long and thin charged rods [32]. Later, thermodiffusive behavior of fd-virus grafted with a polymer (polyethylene glycol) has been investigated [77]. Debye length dependence of grafted fd-virus was also described with an expression derived for charged rods. D_T of bare virus strongly increases with Debye length whereas that of grafted virus shows only very weak increase [77]. Thermodiffusive behavior of a mutant of fd-virus showed a sign change with salt concentration [78]. At low salt concentration, system depicted a thermophobic behavior and changes to thermophilic behavior with increasing salt concentration. This study also indicate that structural changes of the surrounding water majorly influence the thermodiffusive behavior [78].

1.4.3 Protein-ligand systems

In recent years, thermophoresis has emerged as a promising tool to monitor biomolecular interactions. As mentioned before, thermophoresis is very sensitive to changes in the hydration layer. Most of the biomolecular interactions, such as protein-ligand binding are accompanied by a change in the hydration layer of the biomolecule once the ligand binds to it. A schematic representation of this change is shown in Fig. 1.2. How those hydration layer changes influence the thermophoretic behavior is not understood on a microscopic physical level. Binding reactions are quite complex and are strongly influenced by a variety of factors including temperature, concentration, pH, ionic strength, etc. Several studies report that these factors as well affect the thermophoretic behavior [3,29,79].By combining thermophoresis with other existing experimental methods, the binding mechanism can be unveiled to a vaster extent [80].

One of the protein-ligand systems, which has been extensively studied using thermodiffusion is the binding of protein streptavidin with ligand biotin [80,81]. These studies show that the temperature sensitivity of S_T is less for the complex compared to free protein. This is an indication that the complex is more hydrophilic than the free protein. This is because several hydrogen bond sites are deep in the pocket and are longer accessible once biotin is bound

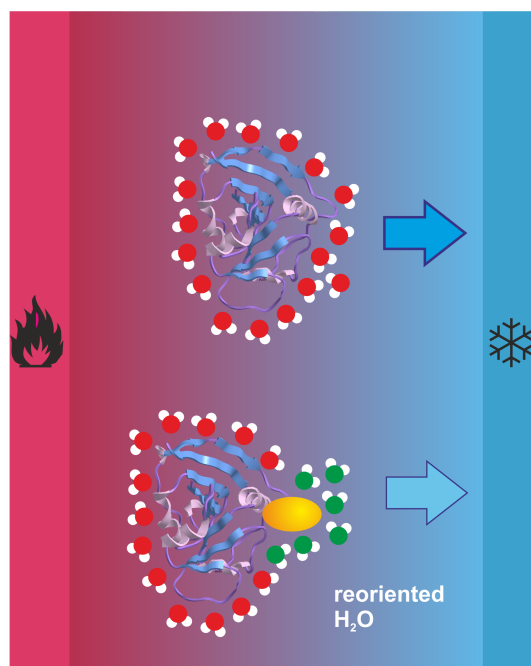


Figure 1.2: Schematic representation of how the hydration layer around the protein changes once the ligand binds and the influence of this change on thermophoresis

to protein [82, 83]. Precise answers about the origin and exact mechanism of the changes that happen in thermodiffusion with complex formation can only be attained through the investigation of several other systems.

1.5 Experimental methods and materials

1.5.1 Description of IR-TDFRS setup used

We use Infra-red Thermal Diffusion Forced Rayleigh Scattering (IR-TDFRS) for the measurement of thermodiffusive properties. This technique has been used to measure the thermophoretic properties of various binary solutions, microemulsions, polymer and protein solutions [3, 51, 58, 77, 81, 84, 85]. A temperature grating is created inside the sample by the interference of two laser beams. A schematic illustration of how this is achieved is shown in Fig. 1.3. An IR-laser beam ($\lambda=980$ nm) is used which is split into two parts and crossed at a small angle inside the sample. Interference of these laser beams leads to a periodic inten-

sity grating inside the sample. Since water has an absorption around this wavelength [86], a periodic temperature grating is generated around 100 μs after the laser is switched on. Thermodiffusive movement of the solutes leads to a concentration grating in addition to this temperature grating. Both these concentration and temperature differences result in a refractive index contrast of the solution. A read out laser beam ($\lambda=633\text{ nm}$) is used to measure the heterodyne intensity of the refracted beam against time. Measured intensity is fitted using the following equation [87]

$$\xi_{het}(t) = 1 - \exp\left(-\frac{t}{\tau_{th}}\right) - \frac{A}{\tau - \tau_{th}} \left\{ \tau \left[1 - \exp\left(-\frac{t}{\tau}\right) \right] - \tau_{th} \left[1 - \exp\left(-\frac{t}{\tau_{th}}\right) \right] \right\}, \quad (1.6)$$

where $\tau_{th} = 1/(q^2 D_{th})$ and $\tau = 1/(q^2 D)$ are the heat and mass diffusion times respectively, with the thermal diffusion coefficient D_{th} , the mass diffusion coefficient D , and the grating vector q . As can be seen in Eq. 1.6, measured heterodyne intensity is proportional to the refractive index contrast factors. Soret coefficient, S_T is then calculated from the amplitude of the concentration signal A with the following equation

$$S_T = \frac{A}{c(1-c)} \frac{(\partial n/\partial T)_{p,c}}{(\partial n/\partial c)_{p,T}}, \quad (1.7)$$

with the refractive index contrast factors $(\partial n/\partial T)_{p,c}$ and $(\partial n/\partial c)_{p,T}$ being measured independently. As can be seen in Fig. 1.3, there is a writing and read out laser beam. A pockels cell is used to achieve a phase shift in grating by 180° . To measure the grating vector and monitor the excitation function, a small fraction of the writing beam is reflected into a CCD camera and an avalanche diode respectively, before passing through the sample. The refracted readout laser beam is passed through an IR filter and the intensity is detected by another avalanche diode.

The sample cell is kept inside a cell holder which is thermostated by an external thermostat that can be controlled using the measurement software. Inside the cell holder, the temperature is measured using a PT 100 temperature sensor. Before filling solutions into an optical quartz sample cell (Hellma) with an optical path length of 0.2 mm, they were filtered through a 0.2 μm filter (Whatman Anotop 10).

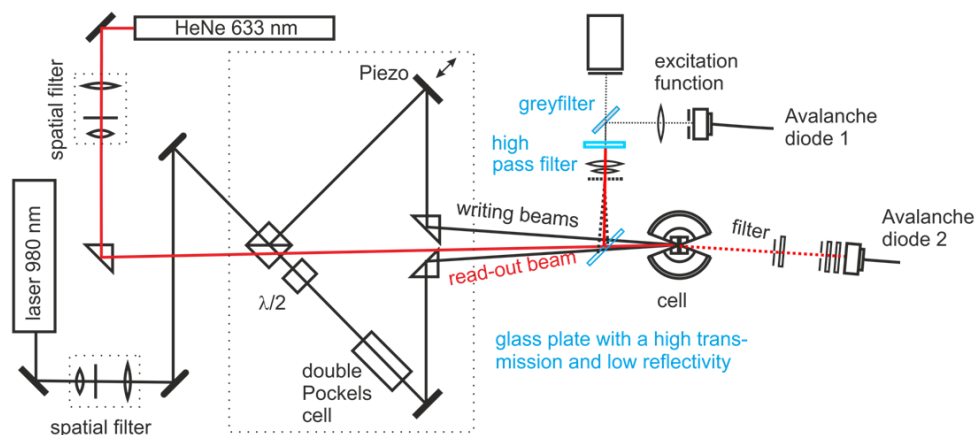


Figure 1.3: Schematic illustration of Infra-red Thermal Diffusion Forced Rayleigh Scattering (IR-TDFRS) used to measure thermodiffusion properties in this work.

1.5.2 Measurement of refractive index contract factors

Auxiliary parameters, $(\partial n/\partial T)_{p,c}$ and $(\partial n/\partial c)_{p,T}$, are required to be measured independently for each sample to quantify the concentration signal measured. The refractive index increments with temperature at constant pressure and concentration, $(\partial n/\partial T)_{p,c}$ is measured interferometrically [88], in a range of 5K around the temperature of interest with a heating rate of 1.6 mK/s. This always includes the highest and lowest temperature measured with IR-TDFRS. The refractive index change with concentration at constant pressure and temperature, $(\partial n/\partial c)_{p,T}$ is measured with an Abbe refractometer (Anton Paar Abbemat MW) at a wavelength of 632.8 nm. Refractive indices at five concentrations around the desired contraction are measured. The slope of the linear interpolation of the refractive index as a function of concentration gives $(\partial n/\partial c)_{p,T}$.

1.5.3 Isothermal Titration Calorimetry

To measure the thermodynamic parameters associated with a binding reaction, we used Isothermal Titration Calorimetry (ITC) which is a standard method [89]. This technique directly measures the change in heat associated with a binding reaction and has been extensively used to study the thermodynamics of protein-ligand binding [90]. It has also been widely used in the field of drug discovery to measure thermodynamic parameters of molecular interactions including target protein interactions with ligands [91], protein-DNA

interactions [92, 93], lipid-DNA interactions, lipid-lipid interactions, etc. A highly sensitive calorimetric technique like ITC can be used to measure the change in Gibb's free energy ΔG , enthalpy ΔH , and entropy ΔS once the ligand binds to the protein. In addition to this, binding affinity K_d and stoichiometry m of binding is also measured.

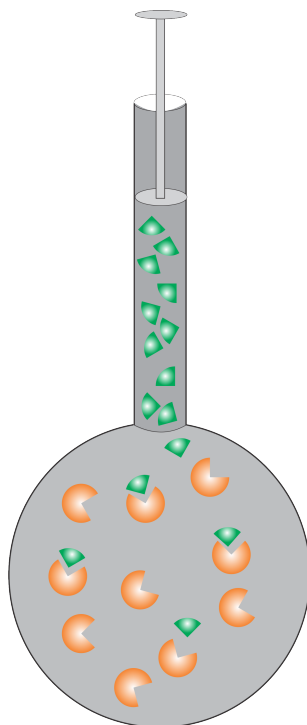


Figure 1.4: Schematic representation of the sample cell of Isothermal Titration Calorimetry (ITC) on which the measurement for this work has been done. The green minor sector indicate the ligand/molecule being injected and orange major sector indicate the macromolecule

An illustration of the sample cell of the ITC instrument in which the measurement takes place is shown in Fig. 1.4. Two identical cells, one sample cell, and one reference cell are placed in an adiabatic jacket, which is usually maintained at a temperature below the measurement temperature. [94]. The reference cell usually contains buffer or a solution that has a similar heat capacity as the interacting components in the sample cell. Initially, both the cells are heated to the measurement temperature. At thermal equilibrium, the power required to maintain both the cells at a constant temperature gives the baseline [94]. As can be seen in Fig. 1.4 sample cell has an opening into which a syringe is placed. Injection of the ligand into the cell will lead to a heat change due to the reaction taking place. The temperature of both cells is monitored by a thermocouple device. If the reaction is exothermic, the sample cell requires less power to maintain thermal equilibrium with the

reference cell. Change in this power requirement for each injection over a given time is measured. The data measured is presented as a plot of power against time. A series of injections will gradually saturate binding sites available on the protein. Once this happens, the heat that is measured corresponds to the heat that is released when the ligand is being dissolved in the solution of the cell. This heat which is referred to as heat of dilution is not related to the binding event and hence needs to be subtracted from the binding isotherm.

1.5.4 Sample preparation

Aqueous salt systems: We studied the thermodiffusive behavior of 11 different aqueous sodium and potassium salt solutions. Potassium salts that have been chosen are; Potassium chloride (KCl), potassium bromide (KBr), potassium iodide (KI), potassium acetate (CH_3COOK), potassium thiocyanate (KSCN), and potassium carbonate (K_2CO_3). Sodium salt systems are as follows; sodium iodide (NaI), sodium acetate (CH_3COONa), sodium thiocyanate (NaSCN), and sodium carbonate (Na_2CO_3). Additionally, the thermodiffusive behavior of lithium iodide (LiI) is also studied. All the salt systems are purchased from Sigma Aldrich (purity $\geq 99\%$) and used without further purification. A stock solution of higher concentration is prepared and the required concentrations were made up from this stock solution. Stock is made by weighing the required amount of salt and adding deionized water from a Millipore filter unit ($0.22 \mu\text{M}$)

EDTA- CaCl_2 system:

For TDFRS measurements, higher concentrations are required due to the poor signal to noise ratio. Hence EDTA (1 mM) and CaCl_2 (10 mM) were used by weighing and dissolving in MES buffer. EDTA (Sigma Aldrich, purity $\geq 99\%$) and CaCl_2 (Merck, purity $\geq 99.5\%$) solutions are prepared in 2-(N-morpholino)ethanesulfonic acid (MES) buffer of 10 mM, pH 5.8. For ITC measurements, a calibration kit (Malvern Panalytical) is used as received as it required lower concentrations. EDTA ($100 \mu\text{M}$) and CaCl_2 (1 mM) were used for ITC measurements. Solutions were used as received from Malvern Panalytical without further purification.

Bovine Carbonic Anhydrase I (BCA I)- ligand system: Sodium phosphate buffer (20 mM, pH 7.4) is used for the preparation of solutions of protein and ligand. Buffer solution was prepared by dissolving the desired amount of Sodium Phosphate Dibasic Heptahydrate and Sodium Phosphate Monobasic Monohydrate in Millipore water.

The final pH of the solution is adjusted to 7.4 by adding NaOH. Bovine Carbonic Anhydrase I (BCA I) is the target protein that is used in this study with a molecular weight of 29 kDa. Amino acid sequence of this protein is given by MASPDWGYDGENGPEHWGKLYPIANGNNQSPIDIKTSETKRDPSTLKLPLSVSYNPATAKEI VNVGHSFHVNFEDSDNRSVLKGGPLSESYRLRQFHFHWGITDDCGSEHLVDGAKFSAELH LVHWN-SAKYPSFADAASQADGLALIGVLVKVGQANPNLQKVLDAKAVKNKNKKAPFTNFDPSVLLPPSLDYWAYSGLTHPPLHESVTWIIFKETISVSSEQLAQFRSLLANAEGDREV HIKQNNRPPQPLNGRTVKASF. Two ligands belonging to the group of aryl sulfonamides are used to monitor the interaction with protein; 4-fluorobenzenesulfonamide (4FBS) (Sigma Aldrich, purity $\geq 98\%$) and pentafluorobenzenesulfonamide (PFBS) (Sigma Aldrich, purity $\geq 98\%$).

The concentration of BCA I and ligand solutions was determined using UV-Vis absorption spectroscopy. Calibration curves (absorbance vs concentration) for BCA I, PFBS, and 4FBS were prepared starting from the stock solution of 1 mg/mL and measuring the absorbance maxima at 280, 268, and 257 nm, respectively. For BCA I, the concentration of the solution was reconfirmed using the molar extinction coefficient of BCA I ($51.0 \times 10^3 \text{ M}^{-1} \text{ cm}^{-1}$) and absorbance measured at 280 nm [95]. For ITC experiments, of BCA I–PFBS system protein and ligand concentrations of 10 μM and 110 μM were used respectively, while for BCA I–4FBS we had to increase protein and ligand concentrations to 20 μM and 300 μM , respectively. For IR-TDFRS experiments, BCA I and ligand concentrations of 10 μM and 110 μM were used. Prepared solutions were filtered through a 0.2 μm filter (Whatman Anotop 10) and filled into a quartz cell (Hellma) with an optical path length of 0.2 mm.

1.6 Outline of the thesis

The main motivation of the thesis is to investigate the thermophoretic behavior of ionic compounds in a biological context, primarily to study protein-ligand reactions. Since protein-ligand systems are complex due to the different ionic and non-ionic groups present, it is appropriate to look into the individual thermophoretic contributions of these groups. Hence, the work mainly consists of two parts as discussed below.

The first three chapters focus on the thermodiffusive behavior of aqueous solutions of

simple salts, which act as buffer systems (chapters 2-4). These chapters compare the thermophoretic behavior of simple ionic systems to that of non-ionic systems, which have been studied before [57]. Systematic studies of the thermodiffusive behavior of simple salts (concentration and temperature dependence) have been carried out to investigate whether a correlation between thermodiffusion and hydration holds as in the case of non-ionic systems. Temperature dependence of S_T for ionic solutes follow the typical behavior of hydrophilic non-ionic solutes. Chapter 2 reports thermodiffusive behavior of various potassium salts with the anions ranging from hydrophilic "carbonate" to hydrophobic "thiocyanate" covering the whole of the Hofmeister series. It is found that the thermophoretic behavior of ionic systems is also influenced by electrostatic interactions that are present in addition to the hydrogen bonds. Besides, changing the anion is found to influence thermodiffusive and diffusive behaviors. To further explore the effect of ion specificity on thermodiffusion, cation of the salt systems are changed, which is discussed in chapter 3. Exchanging the cation is found to have a stronger influence on the diffusive behavior than on the thermodiffusive behavior. Based on the thermophoretic results, a strong correlation between S_T^i (which is a temperature and concentration independent constant) and $\log P$ (hydrophilicity of the solute) is observed. This result further supported the sensitivity of thermodiffusion to the changes in hydration. Above mentioned observation is further used to explain the non-monotonous variation of S_T with concentration, which has been observed for aqueous solution of alkali iodide salts. A preliminary model is developed to explain the behavior of S_T with concentration in chapter 4. Although results based on this model successfully predict a minimum in S_T with concentration as observed in experiments, a deviation from experimental values is observed at higher concentrations.

In the second part of the thesis, we continue with colloidal particles, protein and protein-ligand complexes. As the solutes are larger, more complex, and often dissolved in a buffer solution we develop a thermophoretic microfluidic cell, which can be operated under a confocal microscope (chapter 5). This cell can be used for the quantification of S_T of systems, which are inherently fluorescent or fluorescently labeled. In chapter 5, the developed cell is validated by measuring S_T of fluorescently labeled polystyrene particles and comparing it with IR-TDFRS measurements. With the help of this developed microfluidic cell, the first step to studying the protein-ligand system is to look into the difference in the thermophoretic behavior of free protein and compare it with that of the protein-ligand complex formed.

In chapter 6 we investigate binding reactions by TDFRS, the new developed microfluidic cell, and Isothermal Titration Calorimetry (ITC). We study the complex formation of EDTA-CaCl₂ and binding of protein BCA I with two ligands; 4FBS and PFBS. To gain deeper insight into the complex formation, thermophoretic data (non-equilibrium process) is compared with thermodynamic data (equilibrium process). A mathematical correlation is found between the parameters S_T and Gibb's free energy of binding ΔG . This correlation is first validated for the simple binding reaction of EDTA with CaCl₂ and is later extended and tested for both the protein-ligand systems. Thermophoretic measurements combined with ITC measurements give more information about the binding processes. S_T of free protein is also measured with the developed microfluidic cell, by fluorescently labeling the protein with dye ATTO 532. With the help of ITC, it is found that fluorescent labeling significantly alters the binding process, probably blocking the binding site of the ligand by the dye.

This is followed by a discussion that highlights the results obtained including the effect of ion specificity, charge, hydrophilicity, and hydration on thermophoresis. This section also includes a discussion on the changes in thermophoresis once the complex formation occurs. In the last section of the conclusion and outlook, further experiments and simulations that need to be conducted to gain more insights into the above-mentioned research problems are discussed.

2 Thermodiffusion of Aqueous Solutions of Various Potassium Salts

Thermodiffusion of aqueous solutions of various potassium salts

Cite as: J. Chem. Phys. 154, 084506 (2021); doi: 10.1063/5.0038039

Submitted: 18 November 2020 • Accepted: 4 February 2021 •

Published Online: 26 February 2021



View Online



Export Citation



CrossMark

Shilpa Mohanakumar,¹  Jutta Luettmmer-Strathmann,^{2,a)}  and Simone Wiegand^{1,b)} 

AFFILIATIONS

¹IBI-4: Biomacromolecular Systems and Processes, Forschungszentrum Jülich GmbH, D-52428 Jülich, Germany

²Department of Physics and Department of Chemistry, The University of Akron, Akron, Ohio 44325-4001, USA

Note: This paper is part of the JCP Special Collection in Honor of Women in Chemical Physics and Physical Chemistry.

a) Electronic mail: jutta@uakron.edu

b) Also at: Chemistry Department – Physical Chemistry, University Cologne, D-50939 Cologne, Germany.

Author to whom correspondence should be addressed: s.wiegand@fz-juelich.de

ABSTRACT

Thermophoresis or thermodiffusion has become an important tool to monitor protein–ligand binding as it is very sensitive to the nature of solute–water interactions. However, the microscopic mechanisms underlying thermodiffusion in protein systems are poorly understood at this time. One reason is the difficulty to separate the effects of the protein system of interest from the effects of buffers that are added to stabilize the proteins. Due to the buffers, typical protein solutions form multicomponent mixtures with several kinds of salt. To achieve a more fundamental understanding of thermodiffusion of proteins, it is therefore necessary to investigate solutions of buffer salts. For this work, the thermodiffusion of aqueous potassium salt solutions has been studied systematically. We use thermal diffusion forced Rayleigh scattering experiments in a temperature range from 15 °C to 45 °C to investigate the thermodiffusive properties of aqueous solutions of five potassium salts: potassium chloride, potassium bromide, potassium thiocyanate, potassium acetate, and potassium carbonate in a molality range between 1 mol/kg and 5 mol/kg. We compare the thermophoretic results with those obtained for non-ionic solutes and discuss the thermophoresis of the salts in the context of ion-specific solvation according to the Hofmeister series.

© 2021 Author(s). All article content, except where otherwise noted, is licensed under a Creative Commons Attribution (CC BY) license (<http://creativecommons.org/licenses/by/4.0/>). <https://doi.org/10.1063/5.0038039>

I. INTRODUCTION

Thermophoresis, also known as thermodiffusion or the Ludwig–Soret effect, is sensitive to the nature of solute–solvent interactions.^{1,2} Nowadays, there are two major applications of this effect in aqueous solutions of biological and biocompatible compounds. The first is the accumulation of molecules in thermophoretic traps by a combination of thermodiffusion and convection.^{3,4} The second application is based on the change in the thermophoretic response of a protein when a ligand binds.^{5,6} This is the operating principle of MicroScale Thermophoresis (MST) that allows the determination of binding constants.⁵ The origin for the change in the thermophoretic behavior of the molecules upon binding is not understood on a microscopic level. Recent studies suggest that changes in the hydration layer of the protein upon

ligand binding and electrostatic effects influence the thermophoretic response.^{2,6,7}

In a macroscopic description, the diffusion flux \vec{j} in a binary fluid of mass density ρ not only originates from a concentration but also from a temperature gradient,

$$\vec{j} = -\rho D \nabla w - \rho w(1-w) D_T \nabla T, \quad (1)$$

where w is the mass fraction of the solute, and D and D_T are mass and thermal diffusion coefficients, respectively. In the steady state with $\vec{j} = 0$, the Soret coefficient $S_T = D_T/D$ is proportional to the established concentration difference divided by the applied temperature difference. S_T can be positive indicating that the solute accumulates

in the colder region (thermophobic response) or negative indicating that the solute moves toward the warmer region (thermophilic response).^{2,8}

Thermophoresis of protein–ligand systems relevant to biomedical applications is complicated as those systems are stabilized in buffer solutions containing a variety of salts. This makes protein solutions examples of multi-component mixtures, a class of systems known to have complex thermodiffusive properties.⁹ In addition, salt concentrations in protein solutions are typically low to moderate (physiological concentration is 150 mM) and beyond the Debye–Hückel and Poisson–Boltzmann approximations. To gain a better understanding of the thermophoretic response of protein–ligand systems, it is therefore essential to separate the effects of the protein system of interest from the effects of the buffer. As a first step, we investigate thermal diffusion in aqueous salt solutions in this work.

For salts in protein solutions, it is well known that not just the charges but the types of the ions affect protein solubility, stability, and function. Ion specific effects are also important in aqueous salt solutions and may be described by the Hofmeister series,^{10,11} which ranks ions according to their degree of hydration.¹¹ In general, ion specific effects are larger for anions than for cations. Since hydration/solvation dominates the thermodiffusive behavior of non-ionic solutes in water, we expect differences in ion-specific hydration to lead to differences in thermophoretic behavior. Furthermore, salts are known to modify the dynamics and thermodynamics of aqueous solutions,¹² which will certainly have an impact on the heat transfer thus influencing thermodiffusion. To explore these effects, we focus in this work on salts with a common cation and a series of anions. In the following, we briefly summarize what is known about the thermophoresis of ionic and non-ionic water soluble solutes.

Ionic water soluble solutes: The majority of the recent thermophoretic studies of charged systems concentrate on large solutes such as (bio)macromolecules and colloids.^{13–24} So far, there are no recent systematic temperature and concentration dependent studies of aqueous salt solutions. Almost a century ago, Tanner reported positive Soret coefficients for more than 20 different salts as a function of concentration at a fixed temperature around 35 °C.²⁵ In his studies, S_T of half of the investigated salts increased with increasing salt concentration, while S_T of the other salts showed a decrease. An unusual concentration dependence of S_T has been reported by Gaeta *et al.*²⁶ for sodium and potassium chloride. They found two sign inversions and a minimum of S_T in a very low concentration range of the order 10^{-1} mol/L. A more recent study²⁷ could not reproduce this observation because it was not possible to get reliable data below 0.5 mol/L. Another indication for a minimum of S_T as a function of concentration was observed experimentally²⁸ and by computer simulations¹ for lithium chloride.

Non-ionic water soluble solutes: Hydrogen-bond contributions to the Soret effect have been systematically investigated in recent years.² As illustrated in Fig. 1, a weakening of hydrogen bonds between the solute molecules and water leads to an increase in S_T and a decrease in $\Delta S_T(\Delta T) = S_T(T + \Delta T) - S_T(T)$, the change of S_T in a certain temperature range ΔT . It turns out that $\Delta S_T(\Delta T)$ for many systems shows a clear correlation with the logarithm of a partition coefficient P , which is a measure for the hydrophilicity of the solute.² Most commonly P describes the

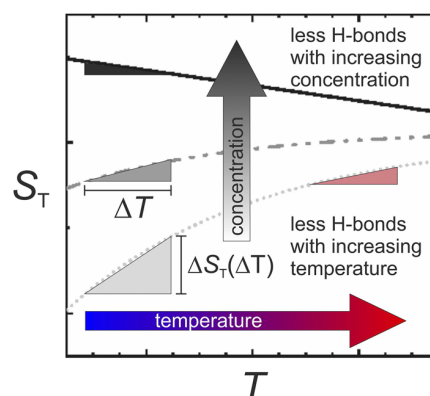


FIG. 1. Illustration of the temperature dependence of the Soret coefficient S_T for diluted and concentrated non-ionic solutes. The lines represent Soret coefficients for high (solid), intermediate (dashed-dotted), and low (dotted) concentrations. The colored triangles illustrate $\Delta S_T(\Delta T) = S_T(T + \Delta T) - S_T(T)$, the change of S_T in a certain temperature range ΔT . By increasing the solute concentration or the temperature, the number of hydrogen bonds between the solute and water is reduced. This leads to an increase in S_T and a decrease in $\Delta S_T(\Delta T)$.

concentration ratio in the two phases 1-octanol and water ($c_{\text{octanol}}/c_{\text{water}}$). The influence of temperature on S_T can be described by an equation proposed by Iacopini and Piazza,¹⁵

$$S_T^{\text{hyd}} = S_T^{\infty} \left[1 - \exp\left(\frac{T^* - T}{\tilde{T}}\right) \right], \quad (2)$$

where S_T^{∞} , T^* , and \tilde{T} are empirical parameters that refer to the Soret coefficient at infinite temperature, the temperature at which a sign change of S_T^{hyd} occurs, and a parameter to describe the curvature, respectively. The superscript hyd indicates that S_T is mainly determined by hydration effects. This equation holds for numerous biological systems^{2,29} but fails to describe the temperature dependence of certain substances such as ethanol³⁰ or ethylene glycol oligomers in water.³¹ For solutes such as formamide, Eq. (2) holds at dilute concentrations and deviates at higher concentrations.⁴ Note that a sign change of S_T with increasing temperature and concentration may occur if the solute shows thermophilic behavior at low concentrations and temperatures. The sign change with temperature was explained qualitatively using a concept of free energy minimization.³²

Reichl *et al.*²¹ expanded Eq. (2) by adding an electric double layer contribution (S_T^{DL}), a contribution from the Seebeck effect (S_T^{SE}), and an ideal gas term ($1/T$) to describe the Soret coefficient of DNA strands of different lengths in aqueous solutions of various salts as a function of temperature as follows:

$$S_T = S_T^{\text{DL}} + S_T^{\text{SE}} + S_T^{\text{hyd}} + 1/T. \quad (3)$$

While there are explicit expressions for S_T^{DL} and S_T^{SE} , there is no theory for hydration effects. Reichl *et al.*²¹ accounted for those effects

by applying Eq. (2) with adjustable parameters. In accordance with the Hofmeister series,¹⁰ we expect that the hydration layer will depend on the chemical nature of the salt. Therefore, the hypothesis of the additivity of the various contributions to the Soret coefficient underlying Eq. (3) has to be carefully examined for different salts.

Wittko and Köhler³³ proposed another empirical ansatz to describe the temperature and concentration dependence of the Soret coefficient $S_T(m, T)$,

$$S_T(m, T) = \alpha(m)\beta(T) + S_T^i, \quad (4)$$

with polynomial serial expansions for $\alpha(m)$ and $\beta(T)$,

$$\begin{aligned} \alpha(m) &= a_0 + a_1m + a_2m^2 + a_3m^3 + \dots, \\ \beta(T) &= 1 + b_1(T - T_0) + b_2(T - T_0)^2 + \dots \end{aligned} \quad (5)$$

While Wittko and Köhler used the molar fraction as the concentration variable, we employ the molality m of the solution. The parameter T_0 is an arbitrary reference temperature, set to $T_0 = 25^\circ\text{C}$, and S_T^i is a temperature and concentration independent constant. For non-polar systems, S_T^i can be expressed as

$$S_T^i = a_M\delta M + b_I\delta I, \quad (6)$$

where δM and δI are the mass and moment of inertia difference (between the solute and solvent), respectively, and a_M and b_I are adjustable parameters. Recent work shows that Eqs. (4)–(6) may be used to describe the Soret coefficients of amides in water. However, the relation between S_T^i and the mass and moment of inertia differences expressed in Eq. (6) fails in general for polar solutes.³⁴

Some insight into microscopic processes underlying thermophoresis can be gained by discussing diffusion in the absence of temperature gradients. Due to ion pairing and complex formation, the diffusing entities in electrolyte solutions are changing with increasing concentration, which also implies that different entities respond to an applied temperature gradient. For example, in LiCl aqueous solutions, single ions diffuse at very low concentrations ($c < 0.1$ mol/L), ion pairs at intermediate concentrations (0.1 mol/L $< c < 1$ mol/L), and ions with clouds of counter ions at high concentrations ($c > 1$ mol/L).¹ In experiments on aqueous KSCN solutions, Bian *et al.*³⁵ observed cluster formation, with clusters containing multiple anions and the cluster size increasing with concentration. In the case of organic salts, hydrogen bonding may also play an important role so that water molecules might be pulled with the moving entities thereby slowing down the diffusion. The theoretical description of diffusion in electrolyte solutions dates back to Nernst³⁶ and Onsager and Fuoss.³⁷ The latter employed the Debye–Hückel ion-atmosphere model to derive an expression for the diffusion coefficient that includes electrophoretic effects. This approach has been extended and improved over the years.^{37–45} Most theoretical approaches predict that the diffusion coefficients of simple salts show a minimum at low concentrations (0.1 mol/L $< c^* < 1$ mol/L) and a monotonous increase at higher

concentrations. Theories based on the mean-spherical approximation are limited to concentrations less than about 2 mol/L because they assume that the solvent may be described as a dielectric continuum.⁴² For the best description of experimental data, the hydration layer of the cations has to be taken into account, which is accomplished by assigning effective diameters to the cations.^{42–44} For example, Gao *et al.*⁴⁵ described the cationic diameter as $\sigma^+ = \sigma_0^+ + \lambda_{\text{hyd}}(m)$, where σ_0^+ is the Pauling diameter and the parameter λ_{hyd} , being twice the thickness of the hydration layer, is assumed to depend on the salt concentration. They were able to reproduce the minimum in the mutual diffusion coefficient observed for many solutions of simple salts as well as the monotonous decay of the diffusion coefficient with concentration observed in aqueous ammonium nitrate solutions.⁴⁶ For this last system, the infinite dilution value λ_0 of λ_{hyd} was roughly a factor five larger than σ_0^+ . Gao *et al.* assumed that the diffusion slows down due to the formation of ion pairs. However, as the obtained hydration layer thickness $\lambda_{\text{hyd}}^0/2$ at infinite dilution corresponds to a large number of water layers around the ion, other explanations might be considered.

To achieve a more fundamental understanding of thermomodification of aqueous salt solutions, we investigated the five potassium salts displayed in Fig. 2 together with their probable position according to the Hofmeister series.^{10,11} For potassium chloride (KCl), potassium bromide (KBr), and potassium thiocyanate (KSCN), we expect that the thermophoretic behavior is predominantly determined by ionic effects, while for potassium acetate (CH₃COOK) and potassium carbonate (K₂CO₃), contributions due to hydrogen bonds should become more important. There are two reasons for including the divalent salt K₂CO₃: first, we can investigate how much its behavior deviates or follows the general trend of monovalent salts, and second, carbonate is very hydrophilic and allows us to cover a wide hydrophilicity range of anions. To investigate whether ionic and non-ionic contributions to the Soret coefficient can be separated, we performed systematic measurements in a temperature range from 15 °C to 45 °C and a concentration range of 1 mol/kg–5 mol/kg.

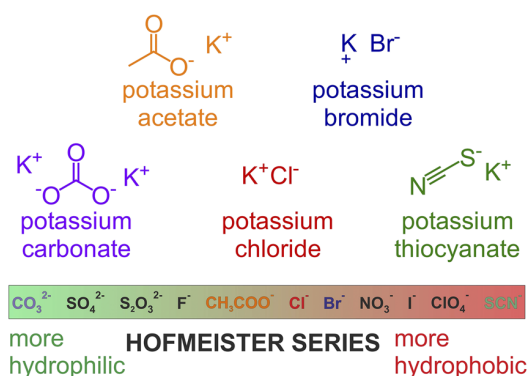


FIG. 2. Sketch of the investigated potassium salts and their probable position according to the Hofmeister series.^{10,11} From left to right in the series, the salts generally become more hydrophobic.

II. METHODS AND MATERIAL

A. Sample preparation and properties

The investigated substances, potassium chloride, potassium bromide, potassium acetate, potassium carbonate, and potassium thiocyanate, were purchased from Sigma Aldrich and were used without further purification. The salts used were of purity $\geq 99\%$. The solutions were prepared with distilled and deionized water. Before filling solutions into an optical quartz cell (Hellma) with an optical path length of 0.2 mm, they were filtered through a 0.2 μm filter (Whatman Anotop 10). A stock solution of the highest concentration was prepared, and the required concentrations were made up from this stock solution. The stock solution was made by weighing the required amount of salt and adding water into it. We filled at least two cells and measured each cell at least two times at the same temperature.

A crucial point in the interpretation of S_T is the number of ionic species present in the solution. Since CH_3COOK and K_2CO_3 are salts of weak acids, the pH value and with it the valency of the anion are expected to depend on the salt concentration. We performed pH-measurements, calculated microspecies distributions, and found that, in the concentration range investigated in this work, only the anions CH_3COO^- and CO_3^{2-} exist in the solution (cf. Sec. VI and Fig. 23 of the [supplementary material](#)). Thus, a distribution of anions with different valencies was ruled out.

The auxiliary parameters, concentration and temperature dependence of the refractive index, were measured independently. The refractive index as a function of concentration was measured with an Abbe refractometer (Anton Paar Abbemat MW) at a wavelength of 632.8 nm. We measured the refractive index for seven concentrations to determine $(\partial n/\partial c)_{p,T}$. The refractive index change on temperature, $(\partial n/\partial T)_{p,c}$, was measured interferometrically.⁴⁷ All data are shown in the [supplementary material](#).

B. Thermal diffusion forced Rayleigh scattering

Infrared-Thermal diffusion forced Rayleigh scattering (IR-TDFRS), a transient grating technique, is employed to measure the thermodiffusion.^{8,18} Two infrared laser beams are used to create a holographic grating inside the sample, which in turn creates a temperature grating due to the inherent absorption of water in that wavelength range. This leads to the migration of particles in the temperature gradient resulting in a concentration grating. Both temperature and concentration gradients give rise to changes in the refractive index of the sample. The heterodyne scattering intensity $\zeta_{\text{het}}(t)$ of the readout beam is measured and fitted with

$$\zeta_{\text{het}}(t) = 1 - \exp\left(-\frac{t}{\tau_{\text{th}}}\right) - A(\tau - \tau_{\text{th}})^{-1} \times \left\{ \tau \left[1 - \exp\left(-\frac{t}{\tau}\right) \right] - \tau_{\text{th}} \left[1 - \exp\left(-\frac{t}{\tau_{\text{th}}}\right) \right] \right\}. \quad (7)$$

With the lifetimes $\tau_{\text{th}} = (D_{\text{th}}q^2)^{-1}$ and $\tau = (Dq^2)^{-1}$ of the temperature and concentration grating, respectively, where q , D_{th} , and D denote the grating wave vector, the thermal diffusivity, and the mutual diffusion coefficient, respectively. When the so-called contrast factors, the change of refractive index with temperature

and concentration, $(\partial n/\partial T)_{c,p}$ and $(\partial n/\partial c)_{T,p}$, are known, the Soret coefficient can be calculated from the amplitude A as follows:

$$A = \left(\frac{\partial n}{\partial w} \right)_{p,T} \left(\frac{\partial n}{\partial T} \right)_{p,w}^{-1} S_T w(1-w). \quad (8)$$

Low concentrations and small S_T values will result in a small amplitude of A , which makes the analysis difficult.

III. RESULTS

A. Concentration dependence

The concentration dependence of the Soret coefficient S_T for all considered aqueous salt solutions is shown in Fig. 3. The lines in Fig. 3 are fits to Eq. (4), which gives a satisfactory description of all studied systems. In all cases, third order and second order polynomials have been used to describe the concentration and temperature dependence of S_T , respectively. The simplest salts investigated in this study are potassium chloride (KCl) and potassium bromide (KBr). The concentration dependence of S_T of KCl solutions was studied

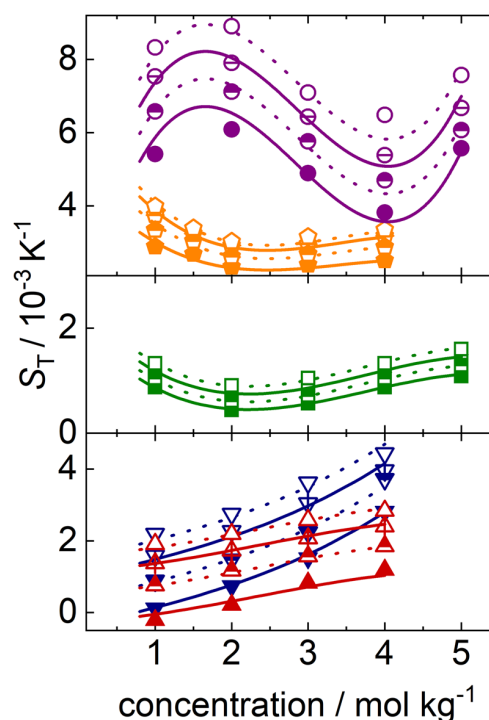


FIG. 3. Soret coefficients of all investigated systems as a function of concentration for temperatures between 15 °C and 45 °C. The markers indicate the temperature, filled symbols (15 °C), half filled symbols (25 °C), half crossed symbols (35 °C), and open symbols (45 °C), and the salts, KCl (red up-pointing triangles), KBr (blue down-pointing triangles), KSCN (green squares), CH_3COOK (orange pentagons), and K_2CO_3 (violet circles). The lines are fits to Eq. (4).

before by Gaeta *et al.*²⁶ at 30 °C and by Tanner²⁵ at 36.4 °C. Deviations between our experimental measurements at 30 °C and the reported values lie around 4%–51% with the highest difference observed for a molality of 4 mol/kg (Fig. 1 of the [supplementary material](#)). The study by Gaeta *et al.*²⁶ reported a minimum of S_T at 0.4 mol/L. Due to experimental constraints, we were not able to measure at concentrations below 1 mol/kg. Our S_T values show a monotonous increase with concentration for these two systems, and there is no indication for a minimum at low concentrations.

We also studied aqueous solutions of potassium thiocyanate (KSCN), potassium acetate (CH_3COOK), and potassium carbonate (K_2CO_3). In the case of KSCN, S_T initially shows a decrease with concentration up to 2 mol/kg and then increases again at higher concentrations. Such a minimum has been previously reported for some salts systems such as KCl, NaCl, and LiCl.^{26,28} The range over which S_T varies with concentration for KSCN is smaller compared to that of KCl and KBr. In the forthcoming parts, we will refer to the concentration at which the minimum of S_T is observed as m^* . The other investigated salts, CH_3COOK , a monovalent salt, and K_2CO_3 , a divalent salt, exhibit a more complex behavior of S_T . Both salts show a minimum in S_T with concentration as observed for KSCN. For CH_3COOK , S_T decays with concentration until m^* and saturates at higher concentrations. S_T of K_2CO_3 , on the other hand, shows a weak increase between 1 mol/kg and 2 mol/kg, then it drops until a minimum is reached at $m^* \approx 4$ mol/kg, and then S_T increases once

more at higher concentrations. The increase in S_T at high concentrations is a general observation, which holds for all investigated salt systems.

The diffusion coefficient D and its concentration dependence differ between the systems. On the basis of the obtained results, salts can be classified into two groups. KCl, KBr, and CH_3COOK belong to the first group, where D increases with concentration. The diffusion coefficient of the divalent salt K_2CO_3 has a slight decrease with concentration, which is more pronounced at higher temperatures. For KSCN, there is a clear decay in the magnitude of D with concentration at all temperatures. [Figure 4](#) shows the diffusion coefficients of KCl and KSCN as two representatives of the two classes at 25 °C in comparison with literature results.^{48–50} The measured diffusion coefficients for all potassium salts and temperatures are shown in the [supplementary material](#).

The concentration dependence of the thermodiffusion coefficient D_T is similar to that of S_T . In the case of KSCN, K_2CO_3 , and CH_3COOK , D_T shows a minimum, as was also observed for S_T . For CH_3COOK and K_2CO_3 , the spread of D_T observed at the highest temperature of 45 °C is a factor two to three larger compared to that at 15 °C. All results for D_T are included in the [supplementary material](#).

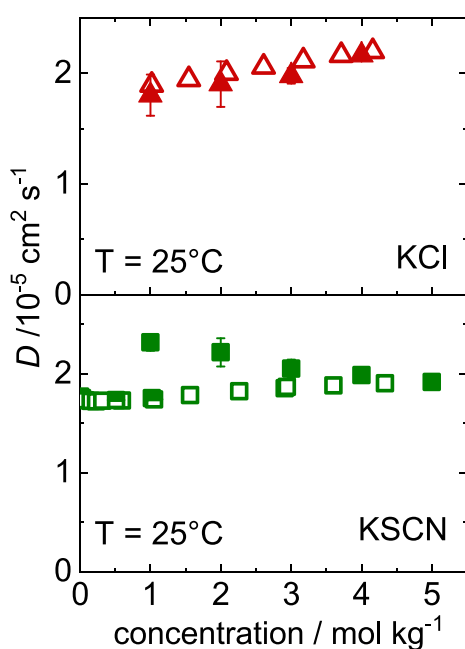


FIG. 4. Diffusion coefficients of KCl (red triangles) and KSCN (green squares) compared with literature values. Filled symbols correspond to our results, and open and half filled symbols correspond to literature results for KSCN by Mitchell *et al.*⁴⁸ (open squares) and Ribeiro *et al.*⁴⁹ (half filled squares) and for KCl by Gosting (open triangles).⁵⁰

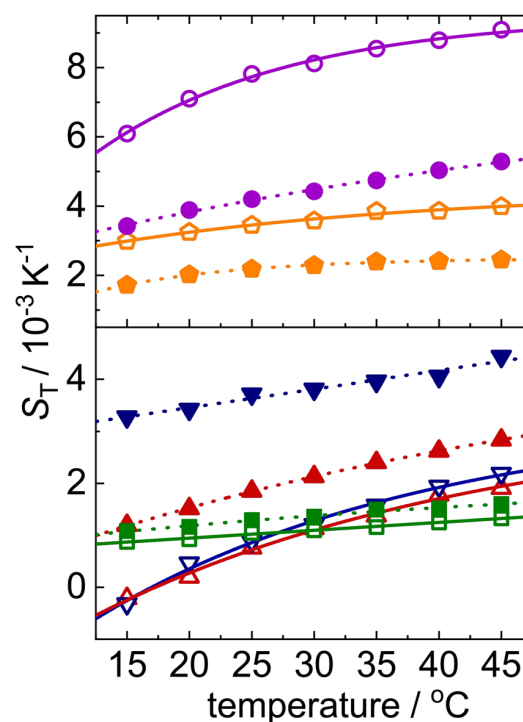


FIG. 5. Soret coefficients as a function of temperature for all investigated aqueous solutions of potassium salts at 4 mol/kg (solid symbols) and 1 mol/kg (open symbols): KCl (red up-pointing triangles), KBr (blue down-pointing triangles), KSCN (green squares), CH_3COOK (orange pentagons), and K_2CO_3 (violet circles). The lines are fits to Eq. (2).

B. Temperature dependence

The Soret coefficient against temperature for the lowest and highest concentration of 1 mol/kg (open symbols) and 4 mol/kg (solid symbols) of the studied potassium salts in water is shown in Fig. 5. Curves are fitted according to Eq. (2). For all studied systems, S_T shows an increase with temperature indicating a more thermophobic behavior with increasing temperature. A more detailed look into the temperature dependence of S_T and its change from low to high concentrations suggest that the investigated systems can be divided into two groups. For salts such as KCl, KBr, and KSCN, the magnitude of S_T increases with concentration, while the temperature dependence of S_T , characterized by $\Delta S_T(\Delta T)$ (cf. Sec. I), shows a decrease with increasing concentration. Note that $\Delta S_T(\Delta T)$ of KSCN is almost concentration independent, and its temperature dependence is weak. The scenario is different for K_2CO_3 and CH_3COOK . For these salts, the magnitude of S_T decreases with increasing concentration. While the temperature dependence of S_T is weak for CH_3COOK at both concentrations, for K_2CO_3 , $\Delta S_T(\Delta T)$ decreases with concentration. The thermal diffusion coefficient D_T behaves similar to S_T and shows a monotonous increase with temperature. The temperature dependence of the diffusion coefficient D is dominated by the decrease in viscosity with increasing temperature leading to a monotonous increase of D with temperature for all systems (see the [supplementary material](#) for more details).

IV. DISCUSSION

A. Concentration dependence

1. Soret coefficient: Empirical fitting

As mentioned in Sec. I, the Soret coefficient of nonpolar systems can be described successfully with Eq. (4), and the temperature and concentration independent parameter S_T^i can be expressed as a function of differences of mass and moment of inertia of the solute and solvent [see Eq. (6)]. We applied Eq. (4) to describe the temperature and concentration dependence of the investigated aqueous potassium salt solutions and determined S_T^i from fits to our experimental data. Additionally, we have included previously investigated aqueous solutions of amides.³⁴ To compare with Eq. (6), we calculated absolute mass and moment of inertia differences as described in the [supplementary material](#). The fitting of S_T^i to Eq. (6) yields $a_M = (-1.2 \pm 0.1) \text{ K}^{-1} \text{ g mol}^{-1}$ and $b_I = (-2.1 \pm 0.4) \text{ K}^{-1} \text{ g mol}^{-1} \text{ \AA}^2$. Rutherford⁵¹ and Debuschewitz and Köhler⁵² analyzed S_T^i for benzene systems. Converted to absolute mass and moment of inertia differences (see the [supplementary material](#)), Rutherford's values for substituted benzene systems are $a_M = (-1.0 \pm 0.1) \text{ K}^{-1} \text{ g mol}^{-1}$ and $b_I = (-1.5 \pm 0.4) \text{ K}^{-1} \text{ g mol}^{-1} \text{ \AA}^2$ and those by Debuschewitz and Köhler for benzene-cyclohexane mixtures are $a_M = (-1.1 \pm 0.1) \text{ K}^{-1} \text{ g mol}^{-1}$ and $b_I = (-3.5 \pm 0.4) \text{ K}^{-1} \text{ g mol}^{-1} \text{ \AA}^2$. Our values are close to the literature values.

Figure 6 shows the correlation between the calculated $S_T^i(\text{calc})$ using a_M and b_I with Eq. (6) and S_T^i obtained from the fit of the experimental data according to Eq. (4). The linear regression of $S_T^i(\text{calc})$ vs S_T^i results in a regression coefficient of $R = 0.7$. The amide solutes have comparatively a low mass difference and do not vary much among themselves in terms of S_T^i . The masses of the potassium salts cover a larger range: KCl shows the highest negative

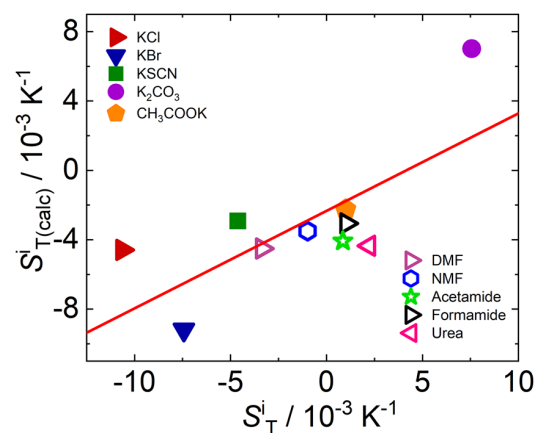


FIG. 6. Comparison of the constant contribution to the Soret coefficient, S_T^i , determined from fits of experimental data to Eq. (4) with values calculated from the correlation $S_T^i(\text{calc}) = a_M \delta M + b_I \delta I$ with $a_M = -1.2 \text{ K}^{-1} \text{ g mol}^{-1}$ and $b_I = -2.1 \text{ K}^{-1} \text{ g mol}^{-1} \text{ \AA}^2$ for all systems investigated in this work and for aqueous solutions of amides.³⁴ The solid line represents a linear regression as discussed in the text.

value, whereas K_2CO_3 (divalent salt) has the highest positive value of S_T^i .

In a recent study of aqueous solutions of amides,³⁴ it was found that S_T^i decays linearly with $\log P$, where $\log P$ is a parameter describing the hydrophilicity of the solute molecule, determining the interactions with water. Notice that the hydrophilicity scale defined by $\log P$ is not completely identical to Hofmeister's order. In particular, the SCN^- anion is not the least hydrophilic anion but slightly more hydrophilic than Cl^- and Br^- according to the $\log P$ -scale. To study whether a similar dependence holds for potassium salts, we present in Fig. 7 S_T^i values as a function of $\log P$ for all investigated salts. For

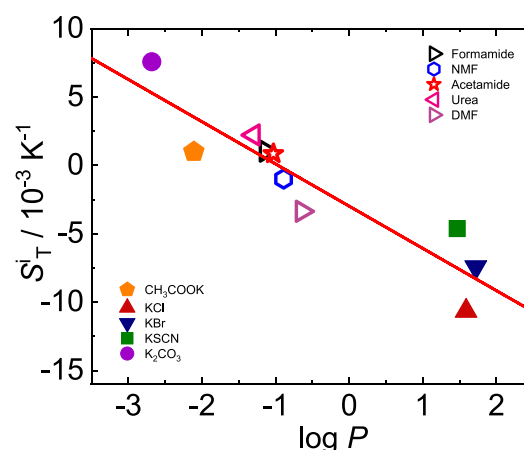


FIG. 7. S_T^i values for all investigated systems as a function of $\log P$ containing ionic and non-ionic contributions.

comparison, we include also previously investigated amide systems. Note that, for salts, $\log P$ has contributions from ionic and nonionic species. S_T^i shows a decrease with $\log P$, and the linear correlation leads to a slightly better regression coefficient of $R = 0.9$ compared to the fit using a_M and b_I [cf. Fig. (6)]. This confirms that, in the case of polar substances, the thermophoretic behavior is more influenced by specific interactions than by physical parameters such as mass and moment of inertia. Due to the strong correlation between S_T^i and $\log P$ for ionic and non-ionic water soluble solutes, we suggest expressing S_T^i by

$$S_T^i = \gamma_P \log P + \sigma_{\text{intercept}}, \quad (9)$$

where the parameter γ_P represents the slope obtained in a fit of the data to a straight line and $\sigma_{\text{intercept}}$ is the intercept. We find $\gamma_P = (-3.1 \pm 0.5) \times 10^{-3} \text{ K}^{-1}$ and $\sigma_{\text{intercept}} = (-3.0 \pm 0.7) \times 10^{-3} \text{ K}^{-1}$. The correlation between $\log P$ and S_T^i may be related to the solute's ability to form hydrogen bonds. Consequently, this relation is probably limited to molecules, which are small enough not to coil or fold, so that the entire surface of the molecules is accessible by the solvent. Although there is certainly also a correlation between S_T^i and δM and δI , it is not possible to separate this contribution from the influence of the solute–water interactions described by $\log P$.

Another relevant parameter obtained from a fit to Eq. (4) is b_1 describing the temperature dependence in first order. For amide systems, it was observed that b_1 increases non-linearly with $\log P$ and the b_1 -values spread over a three-times larger range compared to non-polar systems.³⁴ If we include the b_1 -values of potassium salts, we can no longer identify a correlation between b_1 and $\log P$ (cf. Fig. 24 of the supplementary material). While in the case of the amide systems the solute molecule with the most negative $\log P$ -value shows also the most negative b_1 -value, we find for CH_3COOK with $\log P = -2.1$ a positive b_1 . Therefore, the correlation between b_1 and the capacity of the solute to form hydrogen bonds are altered by charge effects.

2. Diffusion coefficient

Since the amplitude of the concentration signal [cf. Eq. (8)] becomes very small below 0.5 mol/kg, we could not obtain reliable values for the diffusion coefficient in the concentration range where typically a minimum can be observed. The minimum of D with concentration is often related to ion-pair formation, which reduces the movement of the ions.⁴⁸ Apart from ion pairing, solvent–solute association can also contribute to the behavior of D . When solute–solvent interactions are more favored, the probability of ions being surrounded by solvent molecules increases leading to a larger size and reduced diffusion coefficient of the entity.^{48,53}

In the intermediate to high concentration range investigated in this work, the diffusion coefficients of aqueous solutions of KCl and KBr show a monotonous increase with concentration for all temperatures. Except for the lowest temperature, the same holds true for the diffusion coefficient of CH_3COOK in water (cf. Fig. 14 of the supplementary material). This observed trend follows the theoretically predicted behavior for simple aqueous electrolyte solutions.^{37,40,43} While for KCl and KBr the concentration dependent slope is almost the same for all temperatures, the slope decreases for CH_3COOK with decreasing temperature. At the lowest investigated

temperature of $T = 15^\circ\text{C}$, the diffusion coefficient of CH_3COOK is almost temperature independent. This slightly different behavior might be related to the capability to form hydrogen bonds between the two oxygens of the acetate group of CH_3COO^- and water. With increasing temperature, the influence due to the hydrogen bonds diminishes so that at higher temperatures the diffusion is dominated by the charge of the salt. This idea is supported by the observation that the measured diffusion coefficients of non-ionic amides in water also show a decrease with increasing concentration (cf. Fig. 8). For most of the investigated amides, the derivative of the diffusion coefficient with concentration decreases slightly with lowering the temperature (cf. Fig. 27 of the supplementary material).

The measured diffusion coefficients of aqueous K_2CO_3 and KSCN solutions decrease with concentration (cf. Figs. 4 and 18 of the supplementary material). In the case of KSCN, the derivative of the diffusion coefficient with concentration is temperature independent within the error bars. For the divalent salt K_2CO_3 , the negative slope becomes more pronounced with increasing temperature. The decreasing diffusion coefficient of KSCN with concentration can be explained by cluster formation, which was reported by Bian *et al.*³⁵ In the investigated concentration regime between 1 mol/kg and 5 mol/kg, the percentage of ion clusters increases approximately from 30% to 70%, whereas also the number of anions in the cluster doubles from 3 to 6. Both effects will lead to a decrease in the mutual diffusion coefficient. The thermal diffusion and the Soret coefficient of KSCN show a minimum around 2 mol/kg. On the one hand, it is known that D_T is very sensitive to the solute–solvent interface. On the other hand, it is not expected that the water interfaces of the formed clusters change with concentration. This suggests that the minimum might be a concentration effect. While at low concentrations interactions between water and salt clusters dominate, at higher concentrations interactions between the clusters become more important. With K_2CO_3 , we have a divalent

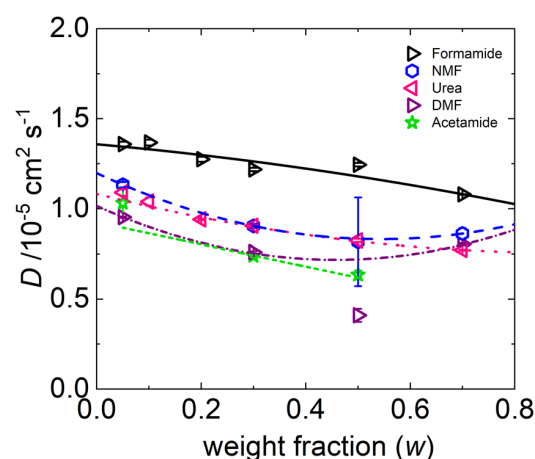


FIG. 8. Diffusion coefficients of various aqueous solutions of amides at $T = 20^\circ\text{C}$. The unpublished diffusion coefficients have been determined in the thermophoretic study by Niether *et al.*³⁴ The lines are a guide to the eye.

salt, which can also form hydrogen bonds. At this time, we can only conclude that this particular divalent salt does not follow the same trend as the monovalent salts and that more experiments are required.

B. Temperature dependence

As shown in Fig. 5, the temperature dependence of S_T of all salts, even those with a positive $\log P$, can be described by Eq. (2) at low and high concentrations. This is in contrast to the aqueous solutions of amides. Only S_T of the two most hydrophilic amides, urea and formamide, exhibited the typical temperature dependence at low concentrations in water, while S_T of the other amides shows a decrease with temperature.³⁴ Furthermore, for many non-ionic water soluble solutes, the change of the Soret coefficient with temperature $\Delta S_T(\Delta T)$ decays linearly with $\log P$ (cf. Fig. 7 of Ref. 34). The underlying physical reason for this correlation is the solutes' ability to form hydrogen bonds. In the case of the salts investigated here, the correlation between $\Delta S_T(\Delta T)$ and $\log P$ observed for non-ionic solutes cannot be confirmed (cf. Fig. 26 of the [supplementary material](#)). Note that only for two of the salts investigated here, potassium acetate and potassium carbonate, both being able to form hydrogen bonds and both being very hydrophilic, $\Delta S_T(\Delta T)$ shows a similar trend in respect of $\log P$ as the non-ionic amides (cf. Fig. 26 of the [supplementary material](#)).

The aqueous solutions of amides, which cannot be described by Eq. (2), tend to form micro-heterogeneities.^{54–57} The physical reason is probably connected to their more hydrophobic nature leading to the formation of clusters instead of the formation of hydrogen bonds with water. Experiments and simulations on aqueous salt solutions^{35,58–60} reveal the formation of ion clusters at concentrations above about 1 mol/kg.^{58–60} However, for potassium salts, we do not observe a decay of the Soret coefficient with temperature as in the case of the non-ionic solutes. Ren *et al.*⁶⁰ simulated highly concentrated (16.7M) aqueous KSCN solutions over a wide range of temperatures (300 K–800 K) at constant density and investigated the cluster size distributions. They find shifts to larger clusters for the anions and to smaller clusters for the cations as the temperature increases. They also examine cluster size distributions as a function of concentration for a temperature of 300 K and find smaller clusters at lower concentrations. If the temperature trends persist at lower concentrations and for a system at constant pressure, one would expect a very small change in cluster size distribution over the temperature range investigated in this work. This suggests that the observed changes in the diffusion and Soret coefficients are due to thermodynamics and changes in the interactions at the interface between salt clusters and water.

One striking difference between non-ionic and ionic solutes is in the effect of concentration on the temperature dependence of the Soret coefficient, as illustrated in Fig. 9. For a typical non-ionic solute, the behavior of S_T changes from increasing with temperature to decreasing with temperature as the concentration increases. This is correlated with the solvation of the solutes, which decreases as the concentration increases. Only very hydrophilic non-ionic solutes have S_T values that increase with temperature for all concentrations. In contrast, the Soret coefficients of ionic solutes show the typical temperature dependence of very hydrophilic solutes over the entire concentration range. This can be explained by cluster formation and

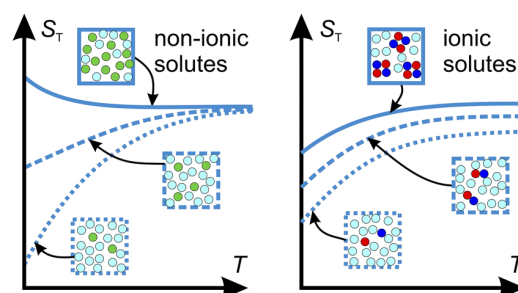


FIG. 9. Schematic comparison of the temperature dependence of S_T for non-ionic and ionic solutes at different concentrations: low (dotted line), intermediate (dashed line), and high (solid line).

growth of the salts with increasing concentrations. Even at high salt concentrations, the clusters are hydrated by water since the fraction of ions in the interfaces decreases when more ions are part of larger clusters.

V. CONCLUSION

Thermophoresis is an excellent tool to monitor protein–ligand binding as it is very sensitive to the nature of solute–solvent interactions. The process involves hydrophobic, hydrophilic, and ionic entities as chemical (side) groups of the proteins and ligands and as buffer components. In this work, we studied systematically a set of potassium salts to gain a better understanding of thermodiffusion in electrolyte solutions. We initiated the study of aqueous salt solutions to reduce the complexity compared to protein–ligand systems. However, due to the presence of charges and the complex nature of water, even aqueous salt solutions are complex systems. This study shows how sensitive the Soret effect is to the ion species.

For all salts studied in this work, it is possible to describe the temperature and concentration dependence of S_T with Eq. (4), an ansatz originally developed for non-polar binary mixtures. While for non-polar compounds, the temperature and concentration independent parameter S_T^I correlates well with mass and moment of inertia differences, for the salts, S_T^I is more closely correlated with $\log P$. The previously investigated amides also follow this relation, which suggests that solute–water interactions dominate mass and size effects for charged and polar systems. Other correlations³⁴ found for aqueous solutions of non-ionic solutes are no longer valid for salt solutions. In particular, the correlations between $\Delta S_T(\Delta T)$ and $\log P$ as well as $\Delta S_T(\Delta c)$ and $\log P$ fail in the case of salts (cf. Figs. 25 and 26 of the [supplementary material](#)).

Previous studies²¹ express the Soret coefficient as a sum [cf. Eq. (3)] including two ionic contributions, one due to the electric double layer and another due to the Seebeck effect. The latter leads to an ion-specific offset, and the double layer contribution is constant for thin double layers (in the sub-nanometer range) expected at high salt concentrations. It is also assumed that the hydration contribution in Eq. (3) can be described by the empirical approach of Iacopini *et al.*¹⁵ and is the same for all ions. For the high salt concentrations studied here, this assumption is not correct since we find

an ion-specific effect on S_T that correlates with both the Hofmeister series and $\log P$. This shows that, at higher salt concentrations, salt-specific properties become more important than the non-specific ionic contributions due to the double layer and the Seebeck effect.

To study the influence of the double layer thickness, very low salt concentrations between 2 mM and 20 mM would have to be investigated. To our best knowledge, there are no existing methods that work for small molecules in the millimolar range. Due to insufficient optical contrast, optical techniques such as beam deflection, thermal lens, and digital interferometry have similar problems to measure small molecules at low concentrations as the TDFRS method employed here. MicroScale thermophoresis (MST) requires fluorescent labeling, which would lead to inaccurate results for small molecules. Thermogravimetric columns could be used to measure at concentrations up to one order of magnitude below our range, however, this is still too concentrated and requires measurement times several 100 times longer.

Another important question to address is what is diffusing. With increasing concentration, the diffusing entities change from single ions over ion pairs to ion clusters. The salt solutions investigated here are in the concentration range of ion clusters. For KSCN, it has been observed that the number and size of clusters increases with concentration.³⁵ This explains the decrease in the diffusion coefficient with increasing concentration, while the observed minima in D_T and S_T are more difficult to understand. A possible explanation could be that at higher concentrations, interactions between clusters become more important than cluster–water interactions, which dominate at lower concentrations. In addition, the interface between diffusing entity and solvent may change with concentration, which can have a pronounced effect on the thermophoretic properties. To achieve a deeper understanding of thermodiffusion in aqueous salt solutions, more systematic experiments need to be carried out, accompanied by computer simulations.

SUPPLEMENTARY MATERIAL

The [supplementary material](#) shows the diffusion and thermal diffusion coefficients and Soret for potassium bromide (KBr), potassium chloride (KCl), potassium carbonate (K_2CO_3), potassium acetate (CH_3COOK), and potassium thiocyanate (KCNS) in water at various temperatures, the refractive index contrast factors as a function of temperature, and the refractive index values as a function of temperature and concentration. pH dependence on concentration of CH_3COOK and K_2CO_3 is also shown. Fitting parameters of the investigated systems to Eqs. (4) and (5), dependence of b_1 on $\log P$ (ionic + non-ionic), dependence of $\Delta S_T(c)$ and $\Delta S_T(T)$ on $\log P$ (ionic + non-ionic), and selected diffusion coefficients of aqueous amide solutions from previous studies that have been used here for comparison have also been included.

DEDICATION

This paper honors Johanna (Anneke) Maria Henrica Levelt Sengers, who performed groundbreaking work on critical phenomena. Anneke has mentored and inspired many students, including one of the authors, to pursue careers in physical chemistry/chemical

physics, during her career at NIST. She has received many awards such as the 2003 Women in Science Award and was elected to the National Academy of Sciences (NAS).

ACKNOWLEDGMENTS

We thank Fernando Bresme, Wim Briels, Sandra Greer, Doreen Niether, and Annette Schmidt for fruitful discussions. We are grateful to Jan Dhont for inspiring ideas and his generous support of our work. S.M. acknowledges support from the International Helmholtz Research School of Biophysics and Soft Matter (BioSoft). Calculator Plugins were used for calculation (of $\log P$ and pKa values), Marvin 16.5.2.0, 2016, ChemAxon (<http://www.chemaxon.com>).

DATA AVAILABILITY

The data that support the findings of this study are available within the article and its [supplementary material](#) and from the corresponding author upon reasonable request.

REFERENCES

- 1 S. Di Lecce, T. Albrecht, and F. Bresme, "The role of ion-water interactions in determining the Soret coefficient of LiCl aqueous solutions," *Phys. Chem. Chem. Phys.* **19**, 9575–9583 (2017).
- 2 D. Niether and S. Wiegand, "Thermophoresis of biological and biocompatible compounds in aqueous solution," *J. Phys.: Condens. Matter* **31**, 503003 (2019).
- 3 P. Baaske, F. M. Weinert, S. Duhr, K. H. Lemke, M. J. Russell, and D. Braun, "Extreme accumulation of nucleotides in simulated hydrothermal pore systems," *Proc. Natl. Acad. Sci. U. S. A.* **104**, 9346–9351 (2007).
- 4 D. Niether, D. Afanasenkau, J. K. G. Dhont, and S. Wiegand, "Accumulation of formamide in hydrothermal pores to form prebiotic nucleobases," *Proc. Natl. Acad. Sci. U. S. A.* **113**, 4272–4277 (2016).
- 5 M. Jerabek-Willemsen, T. André, R. Wanner, H. M. Roth, S. Duhr, P. Baaske, and D. Breitsprecher, "Microscale thermophoresis: Interaction analysis and beyond," *J. Mol. Struct.* **1077**, 101–113 (2014).
- 6 D. Niether, M. Sarter, B. W. Koenig, J. Fitter, A. M. Stadler, and S. Wiegand, "Thermophoresis: The case of streptavidin and biotin," *Polymers* **12**, 376 (2020).
- 7 M. Sarter, D. Niether, B. W. Koenig, W. Lohstroh, M. Zamponi, N. H. Jalarvo, S. Wiegand, J. Fitter, and A. M. Stadler, "Strong adverse contribution of conformational dynamics to Streptavidin–Biotin binding," *J. Phys. Chem. B* **124**, 324–335 (2020).
- 8 *Thermal Nonequilibrium Phenomena in Fluid Mixtures*, Lecture Note in Physics, edited by W. Köhler and S. Wiegand (Springer, Berlin, 1 edition, 2002), Vol. LNP584.
- 9 W. Köhler and K. I. Morozov, "The Soret effect in liquid mixtures—A review," *J. Non-Equilib. Thermodyn.* **41**, 151–197 (2016).
- 10 Y. Zhang and P. S. Cremer, "Interactions between macromolecules and ions: The Hofmeister series," *Curr. Opin. Chem. Biol.* **10**, 658–663 (2006).
- 11 A. Salis and B. W. Ninham, "Models and mechanisms of Hofmeister effects in electrolyte solutions, and colloid and protein systems revisited," *Chem. Soc. Rev.* **43**, 7358–7377 (2014).
- 12 M. Andreev, A. Chremos, J. de Pablo, and J. F. Douglas, "Coarse-grained model of the dynamics of electrolyte solutions," *J. Phys. Chem. B* **121**, 8195–8202 (2017).
- 13 E. Bringuier and A. Bourdon, "Colloid transport in nonuniform temperature," *Phys. Rev. E* **67**, 011404 (2003).
- 14 S. Duhr and D. Braun, "Why molecules move along a temperature gradient," *Proc. Natl. Acad. Sci. U. S. A.* **103**, 19678–19682 (2006).

- ¹⁵S. Iacopini, R. Rusconi, and R. Piazza, "The 'macromolecular tourist': Universal temperature dependence of thermal diffusion in aqueous colloidal suspensions," *Eur. Phys. J. E* **19**, 59–67 (2006).
- ¹⁶J. K. G. Dhont, S. Wiegand, S. Dühr, and D. Braun, "Thermodiffusion of charged colloids: Single-particle diffusion," *Langmuir* **23**, 1674–1683 (2007).
- ¹⁷J. K. G. Dhont and W. J. Briels, "Single-particle thermal diffusion of charged colloids: Double-layer theory in a temperature gradient," *Eur. Phys. J. E* **25**, 61–76 (2008).
- ¹⁸P. Blanco, H. Kriegs, M. P. Lettinga, P. Holmqvist, and S. Wiegand, "Thermal diffusion of a stiff rod-like mutant Y21M fd-virus," *Biomacromolecules* **12**, 1602–1609 (2011).
- ¹⁹A. Majee and A. Würger, "Collective thermoelectrophoresis of charged colloids," *Phys. Rev. E* **83**, 061403 (2011).
- ²⁰K. A. Eslahian, A. Majee, M. Maskos, and A. Würger, "Specific salt effects on thermophoresis of charged colloids," *Soft Matter* **10**, 1931–1936 (2014).
- ²¹M. Reichl, M. Herzog, A. Götz, and D. Braun, "Why charged molecules move across a temperature gradient: The role of electric fields," *Phys. Rev. Lett.* **112**, 198101 (2014).
- ²²B. T. Huang, M. Roger, M. Bonetti, T. J. Salez, C. Wiertel-Gasquet, E. Dubois, R. Cabreira Gomes, G. Demouchy, G. Mériquet, V. Peyre, M. Kouyaté, C. L. Filomeno, J. Depeyrot, F. A. Tourinho, R. Perzynski, and S. Nakamae, "Thermoelectricity and thermodiffusion in charged colloids," *J. Chem. Phys.* **143**, 054902 (2015).
- ²³J. Burelbach, D. Frenkel, I. Pagonabarraga, and E. Eiser, "A unified description of colloidal thermophoresis," *Eur. Phys. J. E* **41**, 7 (2018).
- ²⁴Z. Wang, D. Niether, J. Buitenhuis, Y. Liu, P. R. Lang, J. K. G. Dhont, and S. Wiegand, "Thermophoresis of a colloidal rod: Contributions of charge and grafted polymers," *Langmuir* **35**, 1000–1007 (2019).
- ²⁵C. C. Tanner, "The Soret effect. Part 1," *Trans. Faraday Soc.* **23**, 75–95 (1927).
- ²⁶F. S. Gaeta, G. Perna, G. Scala, and F. Bellucci, "Non-isothermal matter transport in sodium-chloride and potassium chloride aqueous solutions. 1. Homogeneous system (thermal-diffusion)," *J. Phys. Chem.* **86**, 2967–2974 (1982).
- ²⁷F. Römer, Z. Wang, S. Wiegand, and F. Bresme, "Alkali halide solutions under thermal gradients: Soret coefficients and heat transfer mechanisms," *J. Phys. Chem. B* **117**, 8209–8222 (2013).
- ²⁸J. Colombani, J. Bert, and J. Dupuy-Philon, "Thermal diffusion in (LiCl, RH₂O)," *J. Chem. Phys.* **110**, 8622–8627 (1999).
- ²⁹Y. Kishikawa, S. Wiegand, and R. Kita, "Temperature dependence of Soret coefficient in aqueous and nonaqueous solutions of pullulan," *Biomacromolecules* **11**, 740–747 (2010).
- ³⁰A. Königer, B. Meier, and W. Köhler, "Measurement of the Soret, diffusion, and thermal diffusion coefficients of three binary organic benchmark mixtures and of ethanol–water mixtures using a beam deflection technique," *Philos. Mag.* **89**, 907–923 (2009).
- ³¹K. Maeda, N. Shinyashiki, S. Yagihara, S. Wiegand, and R. Kita, "Ludwig-Soret effect of aqueous solutions of ethylene glycol oligomers, crown ethers, and glycerol: Temperature, molecular weight, and hydrogen bond effect," *J. Chem. Phys.* **143**, 124504 (2015).
- ³²Z. Wang, H. Kriegs, and S. Wiegand, "Thermal diffusion of nucleotides," *J. Phys. Chem. B* **116**, 7463–7469 (2012).
- ³³G. Wittko and W. Köhler, "On the temperature dependence of thermal diffusion of liquid mixtures," *Europhys. Lett.* **78**, 46007 (2007).
- ³⁴D. Niether, H. Kriegs, J. K. G. Dhont, and S. Wiegand, "Peptide model systems: Correlation between thermophilicity and hydrophilicity," *J. Chem. Phys.* **149**, 044506 (2018).
- ³⁵H. Bian, X. Wen, J. Li, H. Chen, S. Han, X. Sun, J. Song, W. Zhuang, and J. Zheng, "Ion clustering in aqueous solutions probed with vibrational energy transfer," *Proc. Natl. Acad. Sci. U. S. A.* **108**, 4737–4742 (2011).
- ³⁶W. Nernst, "Zur Kinetik der in Lösung befindlichen Körper," *Z. Phys. Chem.* **2**, 613 (1888).
- ³⁷L. Onsager and R. M. Fuoss, "Irreversible processes in electrolytes diffusion, conductance, and viscous flow in arbitrary mixtures of strong electrolytes," *J. Phys. Chem.* **36**, 2689–2778 (1932).
- ³⁸H. J. V. Tyrrell and K. R. Harris, *Diffusion in Liquids* (Butterworths, London, 1984).
- ³⁹M. J. Pikal, "Ion-pair formation and the theory of mutual diffusion in a binary electrolyte," *J. Phys. Chem.* **75**, 663–675 (1971).
- ⁴⁰O. Bernard, T. Cartailleur, P. Turq, and L. Blum, "Mutual diffusion coefficients in electrolyte solutions," *J. Mol. Liq.* **73-74**, 403–411 (1997).
- ⁴¹J. F. Dufrêche, O. Bernard, and P. Turq, "Mutual diffusion coefficients in concentrated electrolyte solutions," *J. Mol. Liq.* **96-97**, 123–133 (2002).
- ⁴²S. Van Damme, J.-F. Dufrêche, and J. Deconinck, "Influence of ion properties on the equilibrium and transport properties of electrolyte solutions," *J. Phys. Chem. B* **110**, 1015–1019 (2006).
- ⁴³G.-H. Gao, H.-B. Shi, and Y.-X. Yu, "Mutual diffusion coefficients of concentrated 1:1 electrolyte from the modified mean spherical approximation," *Fluid Phase Equilib.* **256**, 105–111 (2007).
- ⁴⁴S. Van Damme and J. Deconinck, "Relaxation effect on Onsager coefficients of mixed strong electrolytes in the mean spherical approximation," *J. Phys. Chem. B* **111**, 5308–5315 (2007).
- ⁴⁵A. C. F. Ribeiro, J. J. S. Natividade, A. J. M. Valente, and V. M. M. Lobo, "Diffusion of electrolytes and non-electrolytes in aqueous solutions: A useful strategy for structural interpretation of chemical systems," in *Advances in Kinetics and Mechanism of Chemical Reactions*, edited by G. E. Zaikov, A. J. M. Valente and L. L. Iordanskiĭ (Apple Academic Press, Oakville, Ont., Point Pleasant, N.J., 2013), pp. 21–33.
- ⁴⁶G. J. Janz, G. R. Lakshminarayanan, M. P. Klotzkin, and G. E. Mayer, "Diffusion of silver nitrate in concentrated aqueous solutions," *J. Phys. Chem.* **70**, 536–539 (1966).
- ⁴⁷A. Becker, W. Köhler, and B. Müller, "A scanning Michelson interferometer for the measurement of the concentration and temperature derivative of the refractive index of liquids," *Ber. Bunsen-Ges. Phys. Chem.* **99**, 600–608 (1995).
- ⁴⁸J. P. Mitchell, J. B. Butler, and J. G. Albright, "Measurement of mutual diffusion coefficients, densities, viscosities, and osmotic coefficients for the system KSCN-H₂O at 25 °C," *J. Solution Chem.* **21**, 1115 (1992).
- ⁴⁹A. C. F. Ribeiro, V. M. M. Lobo, and J. J. S. Natividade, "Diffusion coefficients in aqueous solutions of potassium sulfocyanate at 298.15 K," *J. Mol. Liq.* **94**, 61–66 (2001).
- ⁵⁰L. J. Gosting, "A study of the diffusion of potassium chloride in water at 25° with the Gouy interference method," *J. Am. Chem. Soc.* **72**, 4418–4422 (1950).
- ⁵¹W. M. Rutherford, "Effect of mass distribution on the isotopic thermal diffusion of substituted benzenes," *J. Chem. Phys.* **81**, 6136–6139 (1984).
- ⁵²C. Debuschewitz and W. Köhler, "Molecular origin of thermal diffusion in benzene plus cyclohexane mixtures," *Phys. Rev. Lett.* **87**, 055901 (2001).
- ⁵³A. Katz and S. Ben-Yaakov, "Diffusion of seawater ions. Part II. The role of activity coefficients and ion pairing," *Mar. Chem.* **8**, 263–280 (1980).
- ⁵⁴Y. Lei, H. Li, H. Pan, and S. Han, "Structures and hydrogen bonding analysis of *N,N*-dimethylformamide and *N,N*-dimethylformamide–water mixtures by molecular dynamics simulations," *J. Phys. Chem. A* **107**, 1574–1583 (2003).
- ⁵⁵A. K. H. Weiss, T. S. Hofer, B. R. Randolf, A. Bhattacharjee, and B. M. Rode, "Hydrogen bond formation of formamide and *N*-methylformamide in aqueous solution studied by quantum mechanical charge field-molecular dynamics (QMCD-MD)," *Phys. Chem. Chem. Phys.* **13**, 12173–12185 (2011).
- ⁵⁶V. Vasudevan and S. H. Mushrif, "Force field parameters for *N,N*-dimethylformamide (DMF) revisited: Improved prediction of bulk properties and complete miscibility in water," *J. Mol. Liq.* **206**, 338–342 (2015).
- ⁵⁷J. A. Aguilar-Pineda, G. A. Méndez-Maldonado, E. Núñez-Rojas, and J. Alejandro, "Parametrisation of a force field of acetamide for simulations of the liquid phase," *Mol. Phys.* **113**, 2716–2724 (2015).
- ⁵⁸S. A. Hassan, "Computer simulation of ion cluster speciation in concentrated aqueous solutions at ambient conditions," *J. Phys. Chem. B* **112**, 10573–10584 (2008).
- ⁵⁹J.-H. Choi and M. Cho, "Ion aggregation in high salt solutions. II. Spectral graph analysis of water hydrogen-bonding network and ion aggregate structures," *J. Chem. Phys.* **141**, 154502 (2014).
- ⁶⁰G. Ren, L. Chen, and Y. Wang, "Dynamic heterogeneity in aqueous ionic solutions," *Phys. Chem. Chem. Phys.* **20**, 21313–21324 (2018).

3 Towards Understanding Specific Ion Effects in Aqueous Media using Thermodiffusion



Towards understanding specific ion effects in aqueous media using thermodiffusion

Shilpa Mohanakumar¹ and Simone Wiegand^{1,2,a}

¹ IBI-4: Biomacromolecular Systems and Processes, Forschungszentrum Jülich GmbH, D-52428 Jülich, Germany

² Chemistry Department–Physical Chemistry, University Cologne, D-50939 Cologne, Germany

Received 28 October 2021 / Accepted 10 January 2022 / Published online: 01 February 2022

© The Author(s) 2022

Abstract Specific ion effects play an important role in scientific and technological processes. According to Hofmeister, the influence on the hydrogen bond network depends on the ion and leads to a specific order of the ions. Also thermodiffusion the mass transport caused by a temperature gradient is very sensitive to changes of the hydrogen bond network leading to a ranking according to hydrophilicity of the salt. Hence, we investigate various salt solutions in order to compare with the Hofmeister concept. We have studied three different sodium salts in water as a function of temperature (25–45°C) and concentration (0.5–5 mol kg⁻¹) using Thermal Diffusion Forced Rayleigh Scattering (TDFRS). The three anions studied, carbonate, acetate and thiocyanate, span the entire range of the Hofmeister series from hydrophilic to hydrophobic. We compare the results with the recent measurements of the corresponding potassium salts to see to what extent the cation changes the thermodiffusion of the salt.

1 Introduction

In recent years, thermodiffusion or thermophoresis, which is the mass transport caused by a temperature gradient has gained a lot of interest [1–3]. In the steady state, the Soret coefficient $S_T = D_T/D$ is defined as the ratio of the thermal diffusion D_T and the diffusion coefficient D . A positive and negative S_T corresponds to accumulation of the solute molecules in the cold and the warm region, respectively. The established concentration difference $\Delta c = -c(1-c)S_T\Delta T$ depends also on the applied temperature difference ΔT and the mass fraction c . The research boost in biophysics and bio medicine in recent years can mainly be attributed to the detection of binding reactions via the change in thermophoresis [1, 4]. MicroScale Thermophoresis (MST) gives access to the dissociation constant K_d and molar ratio n , but the physical origin for the change in the thermophoretic behavior upon binding is so far microscopically not understood. It is known that during the binding with the ligand structural modifications of the protein occur and additionally the interfacial waters and the hydrogen bond network play an important role [5]. From previous thermophoretic studies of non-ionic compounds it has been revealed that thermodiffusion is strongly correlated with the hydrophilicity of the solute molecules [6].

Specific ion effects are important in numerous fields of science and technology [7, 8]. Since the pioneering work of Hofmeister, it is known that most aqueous physicochemical processes not only depend on ion concen-

tration and valency, but also on the ion type [9–11]. For instance, cells use the ionic selectivity of ion channels to process information through the organism [12]. Different simulation models [13, 14] show a hypothetical variation in temperature at the level of the ion channels, due to the flow of the ions from the inside to the outside, during the genesis of the action potential. Such a non-uniform temperature gradient could then lead to a concentration gradient due to thermodiffusion and influence the signaling. Systematic studies of aqueous potassium salt solutions show that thermodiffusion is also sensitive to the specific ions [15]. This study has illustrated that the thermophoretic behavior of the anion correlates with its position in the Hofmeister series [10, 16]. Ion specific effects influence also the stability, solubility, reactivity and function of bio-molecules [17, 18]. It is argued that the water molecules in the hydration layer of the protein and the dynamics of hydrogen bond networks are influenced by the salts effecting the proteins, but the mechanism is not understood on a microscopic level [19]. Hofmeister [9, 20, 21] developed an empirical concept that ranks both cations and anions based on salt-specific effects, especially their ability to salt out proteins [10, 16, 22]. Fig. 1 shows the Hofmeister series for cations and anions as we know it today. Ions at the left end of the series are well hydrated (*hydrophilic*) and are called “*cosmotropic*” (water structure maker). Ions at the right end of the series are poorly hydrated (*hydrophobic*) and are also referred to as “*chaotropes*” (water structure breaker) [23]. These ion-specific effects are greater for anions than for cations. Since ions are known to change

^a e-mail: s.wiegand@fz-juelich.de (corresponding author)

the structure and dynamics of water, this also affects the heat of transfer and thus thermal diffusion [24].

For aqueous solutions the *temperature* dependence of S_T can often be described using an empirical equation proposed by Iacopini and Piazza [25],

$$S_T(T) = S_T^\infty \left[1 - \exp\left(\frac{T^* - T}{T_0}\right) \right]. \quad (1)$$

where S_T^∞ , T^* and T_0 are adjustable parameters that refer to the S_T at infinite temperature, the temperature at which a sign change of S_T occurs, and a parameter to describe the curvature, respectively. The temperature dependence of S_T flattens with increasing temperature indicating that fewer hydrogen bonds can break. Eq. 1 describes the temperature dependence of many diluted non-ionic solutes in water [3, 26], but fails for others like ethanol in water [27]. However, while S_T of ionic solutes can be described for all concentrations by Eq. 1 this is not the case for salts with larger organic side groups at low and for non-ionic solutes at higher concentrations [6, 15, 28, 29].

To describe the *temperature* and *concentration* dependence the following empirical Ansatz suggested by Witko and Köhler [30] can be used,

$$S_T(m, T) = \alpha(m)\beta(T) + S_T^i \quad (2)$$

with polynomial serial expansions for $\alpha(m)$ and $\beta(T)$

$$\begin{aligned} \alpha(m) &= a_0 + a_1m + a_2m^2 + a_3m^3 + \dots, \\ \beta(T) &= 1 + b_1(T - T_0) + b_2(T - T_0)^2 + \dots \end{aligned} \quad (3)$$

m is the molality, T_0 is an arbitrary reference temperature, set to $T_0 = 25^\circ\text{C}$ and S_T^i is a temperature and concentration independent constant. Although the approach was originally developed for non-polar systems it can also be used to describe the temperature and concentration dependence of polar aqueous solutions [6, 15]. In our recent study of polar systems we observed a correlation between S_T^i and $\log P$ [15]. The partition coefficient P is a measure for the relative difference of solubility for a solute in two different solvents. Most commonly used is the octanol/water partition coefficient, because it is used for modeling physiological and environmental transport processes and an important parameter for drug compounds [31, 32]. In a system where a solute can diffuse freely between two phases, P is the ratio of its equilibrium concentration in octanol over that in water, so a negative $\log P$ signifies stronger hydrophilicity. Further $\log P$ of a given solute molecule is proportional to its activity coefficient in water $\log \gamma_{water}$ and is used as a measure of solute-solvent interactions in aqueous solutions [33].

In order to get a physical picture of the thermodiffusion of salt solutions, we also need to identify the diffusing entity. With increasing concentration, ion pairs and larger clusters can form in solution. This implies different entities respond to the applied temperature

gradient and the solutions might be inhomogenous containing different entities [15, 29, 34, 35]. There are several theoretical models to describe the concentration dependence of the experimentally determined diffusion coefficient D in electrolyte solutions [36–38]. The theories which provide an accurate fit to the experimental data are generally valid only at dilute concentrations since they are based on Debye-Hückel ion atmosphere model that includes electrophoretic effects [39–41]. Ions are in general moving under the influence of two forces:

1. a gradient of the chemical potential, which is the main contribution to the movement of ions
2. an electric field produced by the motion of oppositely charged ions

Based on the early work by Nernst [36] and later by Onsager and Fuoss [37] D can be described as follows:

$$D = (D_0 + \Delta_n) \left(1 + c \left(\frac{d \ln \gamma_{\pm}}{dc} \right) \right) \quad (4)$$

where D_0 is the Nernst limiting value of the diffusion coefficient, c is the concentration of solute in moles per volume and γ_{\pm} is the mean molar activity coefficient of the salt. Δ_n is the contribution from the electrophoretic term which was introduced by Onsager and Fuoss [37] into the Nernst-Hartley equation [36]. This theoretical approach predicts a minimum in D at low concentrations and then a constant increase at high concentrations. To achieve a good description of the experimental data an effective cationic diameter is used to account for the hydration layer [42]. The theoretical approach fails to describe a drop of the diffusion coefficient due to aggregation as observed for example for potassium thiocyanate (KSCN) [15, 19, 35, 43].

The change of the diffusing entity with concentration has also been observed in computer simulations of aqueous solution of LiCl [34]. They find single ion diffusion at low concentrations $c < 0.1$ mol/l, ion pairs at intermediate concentrations between 0.1 and 1 mol/L and ion clouds with counter ions at high concentrations $c > 1$ mol/L. Simulations carried out in aqueous solutions of potassium and sodium salts depicted two scenarios of cluster formation [19, 44–46]. In some salt solutions closely packed ion clusters are formed with increasing concentration, while others build spatially extended ion networks similar to the water network exhibiting an exceptionally high solubility limit in liquid water. For many salts the ion structures do not change, when the cation is exchanged, but for some systems a change from ion cluster formation to network-like structures is observed. Another molecular dynamic study investigated the cation influence by comparing potassium and sodium acetate in aqueous solution [47]. Their study revealed that the association constant to form ion pairs is higher in case of the cation Na^+ compared K^+ . In general it is expected that hydration of simple anions are quite different, both structurally and dynamically,

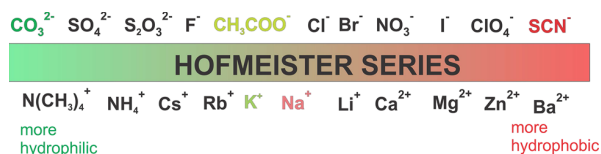


Fig. 1 Sketch of the cations and anions of the investigated salts with their probable position according to the Hofmeister series [22,49]. From left to right, the ions in general becomes more hydrophobic

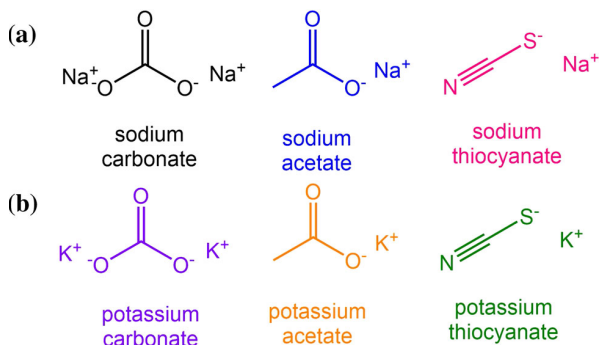


Fig. 2 **a** Chemical structure of the investigated sodium salts and **b** the structure of the investigated corresponding potassium salts [15]. The color of the chemical structures corresponds to that of the symbols in the figures

from hydration of cations, so that a single concept of water structure will not suffice to characterize it [48].

In the previous study the anions of the salts studied covered the entire range of the Hofmeister series, while the cation potassium was always the same [15]. In this work we want to explore the specific effects of cations and have studied corresponding sodium and potassium salts with carbonate (CO_3^{2-}), acetate (CH_3COO^-), thiocyanate (SCN^-) as anions. The probable positions of the chosen ions in the Hofmeister series are displayed in Fig. 1 [22,49]. The left end of the series corresponds to the more “hydrophilic” ions while at the right end the “hydrophobic” ions are located.

The chemical structures of the investigated salt are shown in Fig. 2. For carbonate and acetate salts studied, we expect the thermodiffusive behavior to be dominated by hydrogen bonds as both the cations and anions are hydrophilic. For thiocyanate salts, the thermophoretic behavior will have contributions from ionic as well as hydrogen bonding effects. To investigate whether these hypotheses is in line with the results and how it depends on the cation, we systematically investigate these salts in a temperature range of 15 to 45°C with concentration being varied from 0.5 to 5 mol kg⁻¹.

2 Experimental section

2.1 Sample preparation

Deionized water from a Millipore filter unit (0.22 μm) was used to prepare all aqueous solutions. Potas-

sium carbonate (K_2CO_3), sodium carbonate (Na_2CO_3), potassium acetate (CH_3COOK), sodium acetate (CH_3COONa), potassium thiocyanate (KSCN) and sodium thiocyanate (NaSCN) were purchased from Sigma-Aldrich and used without further purification. The salts were of purity $\geq 99\%$. Solutions ranging from concentration 0.5–5 mol kg⁻¹ were prepared using a stock solution at a high concentration.

An optical quartz cell (Hellma) with an optical path length of 0.2 mm were used for measurement of the thermophoretic properties using infrared thermal diffusion forced Rayleigh scattering (IR-TDFRS). Prepared solutions were filtered through a 0.2 μm filter (Whatman Anotop 10) and filled into this quartz cell. All measurements are performed in the temperature range between 15 and 45°C. Measurements were performed at least two times in different cells with freshly prepared samples. The experimental methods which are used to measure thermodiffusion are explained in detail in Supporting Information.

3 Results

3.1 Concentration dependence of S_T and D_T

The concentration dependence of S_T for all studied salt solutions is shown in Fig. 3. The lines in Fig. 3 correspond to the fit corresponding to Eq. (2). An example of the raw IR-TDFRS signal for NaSCN at $T = 25^\circ\text{C}$ is shown in the Supporting Information (Fig. S5). Except for Na_2CO_3 , third order and second order polynomials have been used to describe the concentration and temperature dependence of S_T , respectively. For Na_2CO_3 for which measurements were not possible above 2 mol kg⁻¹ due to its solubility limit, first order polynomials of concentration and temperature have been used to describe the data.

The overview Fig. 3 shows that as the hydrophilicity of the anion decreases, the magnitude of the Soret coefficient also decreases. The values for the two cations are very similar. It has been noted that at low concentrations (≤ 2 mol kg⁻¹), all sodium salts have a stronger tendency to accumulate on the cold side. All sodium salts have lower solubility than the corresponding potassium salts, with the difference being most pronounced for the two carbonate salts. S_T of the divalent salt K_2CO_3 oscillates, while S_T of the corresponding sodium salt decays monotonously with concentration in the accessible range. A previously reported $S_T = 8.21 \times 10^{-3} \text{ K}^{-1}$ value of Na_2CO_3 at 0.5 [50] agrees well with our S_T -value of $8.19 \times 10^{-3} \text{ K}^{-1}$. CH_3COOK shows a shallow minimum in S_T , while CH_3COONa decreases monotonously with concentration. Both thiocyanate salts show a minimum in S_T with concentration at 2 mol kg⁻¹. This minimum in S_T shown by KSCN , NaSCN and CH_3COOK has been previously reported for certain other salts like KCl , NaCl and LiCl [51,52]. Although, several salts exhibit this behavior, the physical reason for this minimum is not yet clear [15].

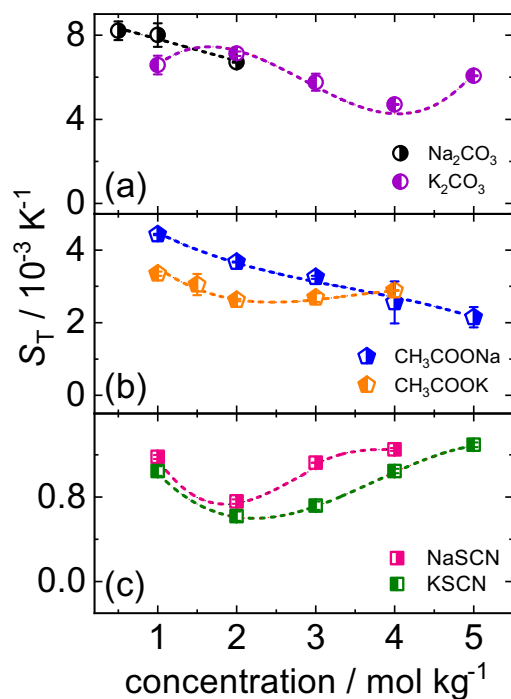


Fig. 3 Soret coefficient of **a** K_2CO_3 (violet circles), Na_2CO_3 (black circles), **b** CH_3COOK (orange pentagons), CH_3COONa (blue pentagons), **c** KSCN (green squares) and NaSCN (pink squares) in water as a function of concentration at $T = 25^\circ\text{C}$. The lines are fits according to Eq. 2. Further information is given in the text

The concentration dependence of D_T has a similar behavior to that of S_T for all systems studied. This is shown in the Supporting Information (Fig. S6).

3.2 Temperature dependence S_T and D_T

In the following we will discuss the temperature dependence of S_T , which is for diluted solutes related to their hydrophilicity. Figure 4 shows the temperature dependence of S_T of four salts (Na_2CO_3 , K_2CO_3 , NaSCN and KSCN) at two concentrations (1 and 4 mol kg^{-1}). The line is a fit according to Eq. (1). In general, S_T shows an increase with temperature indicating system get more thermophobic with increasing temperature. For carbonates (K_2CO_3 and Na_2CO_3), S_T decreases with increasing concentration, while for thiocyanate salts (KSCN and NaSCN), magnitude of S_T increases with concentration. Acetate salts (CH_3COOK and CH_3COONa), exhibits behavior similar to carbonate salts which is shown in Supporting Information (cf. Fig. S1).

Although, for non-ionic solute molecules and many bio molecules the temperature sensitivity, $\Delta S_T(\Delta T) = S_T(T + \Delta T) - S_T(T)$ decreases with increasing temperature, while $\Delta S_T(\Delta T)$ barely changes for salts. The temperature dependence of S_T of ionic solutes is different from the behavior of non-ionic solutes which has been studied before [6]. For non-ionic solutes only the

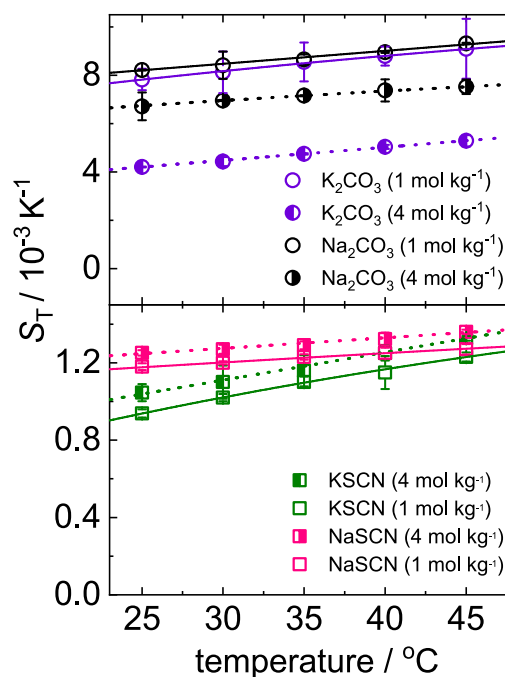


Fig. 4 Soret coefficient of Na_2CO_3 , K_2CO_3 , NaSCN and KSCN as a function of temperature. Open and half-filled symbols correspond to concentrations 1 and 4 mol kg^{-1} respectively. The half-filled symbols correspond to the symbols used in Fig. 3. The lines correspond to a fit according to Eq. 1

most hydrophilic solutes exhibited at very low concentrations a temperature dependence of S_T described by Eq. 1 [6], whereas S_T of all investigated salts can be described for all concentrations by Eq. 1. This difference in behavior could be an effect of cluster formation at higher concentrations [19]. Those formed clusters are well hydrated thus behaving like diluted solutions of clusters. Additionally, the temperature sensitivity, $\Delta S_T(\Delta T) = S_T(T + \Delta T) - S_T(T)$ decreases for non-ionic solutes with increasing temperature, while this slope barely changes for the salts, which might be related to the fact that ionic interactions show a weaker temperature dependence than hydrogen bonds.

Due to decrease of the viscosity with increasing temperature, we expect that the diffusion coefficient D increases with temperature. This is observed for all the studied salts. As in the case of concentration dependence, D_T shows a similar trend as S_T . For further information, see Supporting Information (cf. Fig. S7).

3.3 Concentration dependence of D

The dependence of the diffusion coefficient D on concentration at 25°C is shown in Fig. 5. The studied salts can be classified in three groups. The first group (cf. Fig. 5a) shows a slight increase of D , in the second group (cf. Fig. 5b) D is independent of concentration and the third group (cf. Fig. 5c) shows a decrease of D

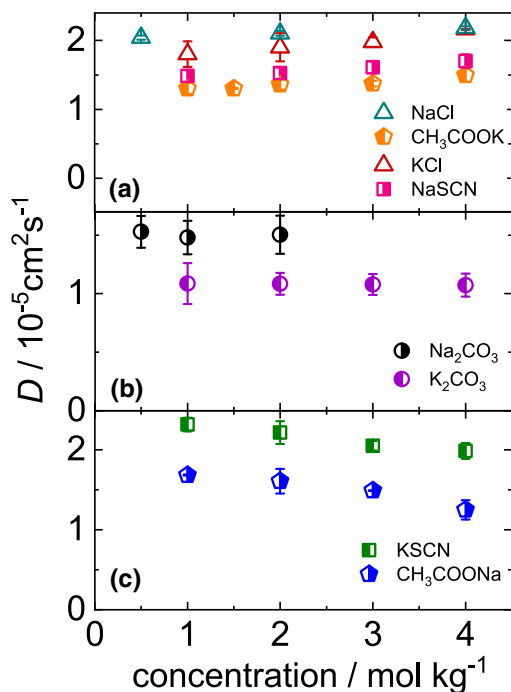


Fig. 5 **a** Diffusion coefficient of **a** CH_3COOK (orange left-half-filled pentagons), NaSCN (pink right-half-filled squares) and Na_2CO_3 (black right-half-filled circles) as function of concentration at $T = 25^\circ\text{C}$. For comparison we show also the literature values of sodium chloride (NaCl) (green open triangle down) [53] and potassium chloride (KCl) (red open triangle up) [15]. **b** Diffusion coefficient of aqueous Na_2CO_3 (black right-half-filled circles) and K_2CO_3 (violet left-half-filled circles) solutions as function of concentration at $T = 25^\circ\text{C}$. **c** Diffusion coefficient of KSCN (green left-half-filled squares) and CH_3COONa (blue right-half-filled pentagons) as function of concentration at $T = 25^\circ\text{C}$. Symbols correspond to the symbol used for S_T of the same salt in Fig. 3

with concentration. In the investigated concentration regime none of the salts shows a clear minimum as predicted by theories [42]. The diffusion coefficient of the third group with KSCN and CH_3COONa decays with concentration. From molecular dynamic simulations it is known that both salts form network structures, which are interlinked with the water network slowing down the diffusion at higher concentrations [19, 46].

4 Discussion

4.1 Concentration and temperature dependence of S_T

For comparison of the concentration dependence of S_T for the various salt systems we introduce $\Delta S_T(\Delta c)$ as $\Delta S_T(\Delta c) = S_T(2 \text{ mol kg}^{-1}) - S_T(1 \text{ mol kg}^{-1})$. The concentration dependence of the salt systems studied

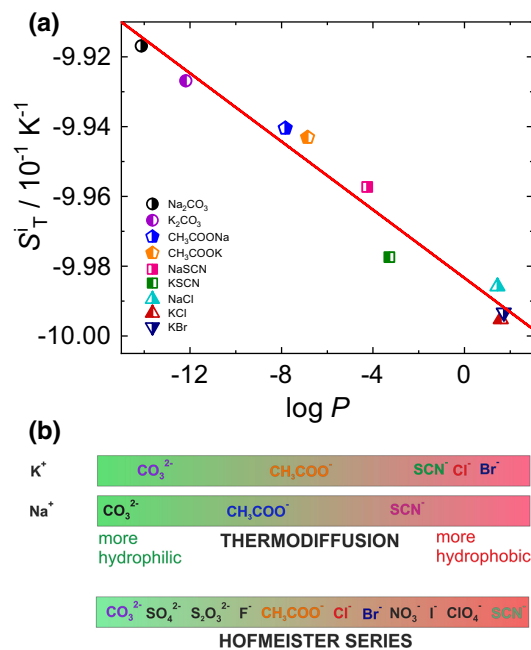


Fig. 6 **a** S_T^i values of all studied systems plotted as function of $\log P$. Note, that $\log P$ is the sum of an ionic and non-ionic contribution. The S_T^i values of KCl and KBr have been previously reported [15]. S_T^i of NaCl was obtained by fitting the S_T values reported by Wang *et al.* [53]. First order polynomials of concentration and temperature have been used to fit the data using Eq. 2 for NaCl . **b** Sequence of the anions based on S_T^i for the two investigated cations in comparison with the Hofmeister series

indicates that, with the exception of CH_3COONa , all salts show an increase in thermophobicity at higher concentrations. For CH_3COONa , the thermophobicity decreases monotonously with increasing concentration. A decay of the Soret coefficient with increasing concentration ($\Delta S_T(\Delta c) < 0$) has also been observed for ethanol [27, 54], for acetamide and *N*-methyl-formamide in water [6]. In all systems, $\Delta S_T(\Delta T)$ increases as a function of concentration, resulting in a temperature-independent intersection point ($\Delta S_T(\Delta T) = 0$), if we plot S_T versus concentration.

Except for K_2CO_3 and NaSCN , $\Delta S_T(\Delta c)$ is nearly independent of temperature (see also supporting information Figs. S2, S3 and S4). For K_2CO_3 , $\Delta S_T(\Delta c)$ shows a weak increase with temperature, while for KSCN it shows a decrease with temperature. The physical origin of this behavior is not yet clear. While the change in the concentration dependence of S_T for different temperatures of non-ionic solutes can be related to the fact that the thermophobic behavior of these systems is determined exclusively by hydrogen bonds, which show a strong temperature dependence, the electrostatic interactions are less temperature dependent.

We used Eq. 2 to describe the concentration and temperature dependence of S_T and determined the parameter S_T^i for all salt systems studied. We set $a_0 = 0$ as

it is strongly coupled to S_T^i . Note, that the observed correlation between S_T^i and $\log P$ remains, when a_0 is fixed. Figure 6 shows that S_T^i depends linearly on $\log P$. The most hydrophilic salt, Na_2CO_3 has the highest S_T^i -value and KBr, the most hydrophobic salt has the lowest S_T^i . Both investigated cations potassium and sodium follow the same overall trend and show no systematic deviations. Note, that S_T^i of non-polar systems is correlated with the difference in mass and moment of inertia of the two compounds [2]. The correlation between S_T^i and $\log P$ holds apparently for ionic as well as for non-ionic water soluble solutes and is most probably related to ability of molecules to form hydrogen bonds, but so far there is no microscopic theory [15]. It should also be noted that the correlation is likely to be limited to molecules small enough that they do not coil or fold, so that the entire surface of the molecule is accessible to the solvent.

As already discussed in Sect. 1, Hofmeister series arranges ions on the basis of their decreasing hydrophilicity [23]. $\log P$ is the parameter that defines the hydrophilicity of a solute molecule. A negative value of $\log P$ indicates that the molecule has a higher affinity towards aqueous phase (hydrophilic in nature). On the other hand, a positive value denotes a higher concentration in the organic phase (hydrophobic in nature) [55, 56]. Based on the $\log P$ -dependence of S_T^i we can define a new hydrophobic-hydrophilic scale for the anions displayed in Fig. 6b. The anions CO_3^{2-} , CH_3COO^- and SCN^- have independent of the cation the same order as in the Hofmeister Series, while Cl^- and Br^- are more hydrophobic than SCN^- according to their thermodynamic behavior. Note that, corresponding to the $\log P$ -scale Na^+ is slightly more hydrophilic than K^+ , which is reversed in the Hofmeister series. This difference is not completely understood, but might be related to the fact that Hofmeister ranks individual ions and not complete salts.

For non-ionic systems it is known that changes of the Soret coefficient $\Delta S_T(\Delta T)$ and $\Delta S_T(\Delta c)$ in a certain temperature ΔT and concentration Δc interval correlate with $\log P$. For the investigated salts we define $\Delta S_T(\Delta T) = S_T(50^\circ\text{C}) - S_T(20^\circ\text{C})$ at 1 mol kg^{-1} and $\Delta S_T(\Delta c)$ as mentioned before in Sect. 4.1 at $T = 25^\circ\text{C}$. Figure 7 displays $\Delta S_T(\Delta T)$ and $\Delta S_T(\Delta c)$ as function of $\log P$. For comparison we show also the results for the previously investigated non-ionic systems [6]. The solid and dotted lines are linear fits for ionic and non-ionic systems, respectively. Note, that for non-ionic solutes $\Delta S_T(\Delta T) = S_T(50^\circ\text{C}) - S_T(20^\circ\text{C})$ at 5wt% and $\Delta S_T(\Delta c) = S_T(50\text{wt}\%) - S_T(5\text{wt}\%)$ at $T = 10^\circ\text{C}$. Neither $\Delta S_T(\Delta T)$ nor $\Delta S_T(\Delta c)$ shows a pronounced $\log P$ -dependence as observed for the non-ionic solutes. Thus, $\Delta S_T(\Delta T)$ and $\Delta S_T(\Delta c)$ of the salts are nearly independent of the hydrophilicity of the salt, in clear contrast to non-ionic solutes, which are very sensitive to a change in $\log P$. Hydrophilic, non-ionic solutes form more hydrogen bonds with water, the number of which decreases when the temperature or concentration is increased. This then also leads to a strong

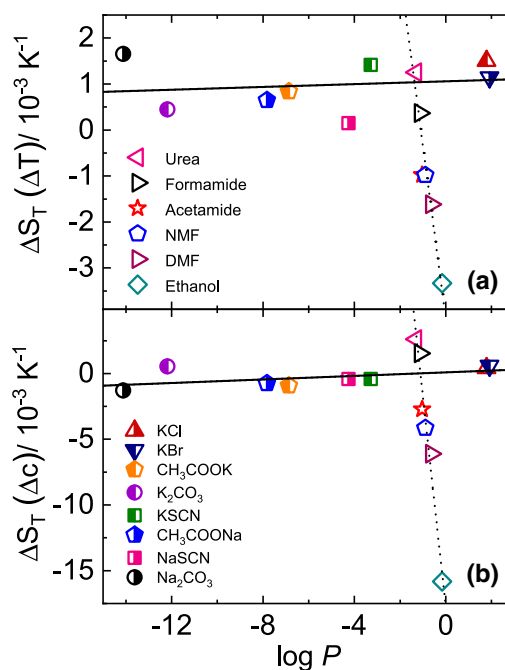


Fig. 7 **a** Change of $\Delta S_T(\Delta T)$ and **b** change of $\Delta S_T(\Delta c)$ as function of $\log P$ for the investigated salt systems in comparison with some previously studied non-ionic systems [6]. The solid and dotted lines are linear fits for ionic and non-ionic systems, respectively. Further information is given in the text

decrease of $\Delta S_T(\Delta T)$ and $\Delta S_T(\Delta c)$ with increasing $\log P$. For ionic solutes $\Delta S_T(\Delta T)$ and $\Delta S_T(\Delta c)$ are more or less independent of $\log P$. Therefore, we assume that the thermophoretic behavior ionic solutes at the first order are determined by electrostatic interactions, which are independent of the hydrophilicity. Further studies are required to investigate whether the thermophoretic behavior shows some correlation with $\log P$ at much lower concentrations or for salts with larger organic side groups.

4.2 Concentration dependence of D

The measurement of the diffusion coefficient gives information about the entities and their interactions diffusing in the temperature gradient (cf. Sect. 3). Figure 8 clearly demonstrates that changing the cation can have a noticeable effect on the diffusion coefficient of salts. It shows that the diffusion coefficient of sodium thiocyanate in water at 25°C increases with concentration, while that of the corresponding potassium salts decreases. Differences are also observed for aqueous solutions of the acetate-anions, but in this case the diffusion coefficient of the sodium salt in water decreases, while the corresponding potassium salt shows a slight increase with concentration (cf. Fig. 5a and c). The decrease of the diffusion coefficient might be related to the stronger association of Na^+ compared to K^+ in the

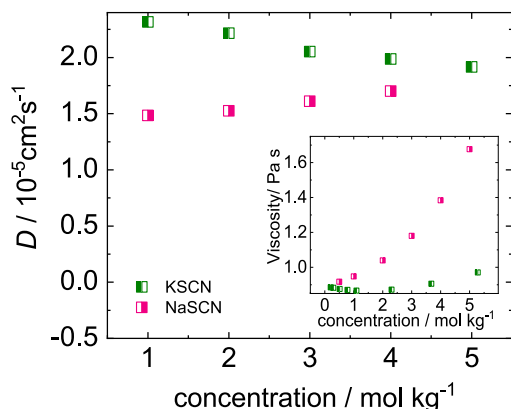


Fig. 8 Change of diffusion coefficient D and viscosity of thiocyanate salts studied with concentration at a temperature of 25°C

presence of the acetate anion [47]. For aqueous KSCN solutions the formation of network structures [19, 46] as well as the formation of clusters have been reported [35]. For both scenarios a decrease of the diffusion coefficient with increasing concentration is expected.

The measured diffusion coefficient depends inversely on the viscosity of the solutions. In the inset of Fig. 8 literature values of the viscosity of both thiocyanate salts are displayed [57]. It is obvious that the change of the cation has also a prominent effect on the viscosity. Considering the viscosity we would expect that the diffusion of NaSCN should show a more pronounced decrease with increasing concentration compared to KSCN. This is obviously not the case, therefore we looked also into the differences in the chemical potential of the two salt solutions. According to Eq. 4 the diffusion coefficient depends on the mean activity coefficient. Comparing the term $1 + c(d \ln \gamma_{\pm} / dc)$ for NaSCN and KSCN solutions, we find that the increase of the term for NaSCN is four times larger than for KSCN (cf. Supporting Information Sect. S7). This might be the reason that we observe a weak increase of D for NaSCN with concentration although a recent work predicts for both salts cluster formation with increasing concentration [35]. Note, that the clustering for NaSCN is less pronounced, as the percentage of clustered ions at 4 mol/kg is 60% and 67% for NaSCN and KSCN, respectively. Therefore, the cluster formation dominates the diffusion only for KSCN.

5 Conclusion

We have investigated the thermophoretic properties of various aqueous sodium salt solutions as function of temperature and concentration and compared the results with those measured for the corresponding potassium salts to explore the influence of the cation exchange.

It turned out that the temperature and concentration dependence of the Soret coefficient is only marginally influenced by the exchange of the cation (cf. Figs. 3 and 4). The shape of the curves is similar although not identical. The diffusion coefficient D is influenced by the exchange of the cation. While D of CH_3COOK and NaSCN in water shows a weak increase with concentration the corresponding salts CH_3COONa and KSCN show a decay (cf. Fig. 5a and c). For both divalent salts we observe no dependence on the concentration. Therefore, we can only conclude that the exchange of cation can influence the behavior, but so far we were not able to identify a trend. And the influence is especially visible in the diffusion, but not so much in the thermophoretic behavior.

As already observed for the studied potassium salts the temperature dependence of the Soret coefficient can be described for all concentration with Eq. 1. While for non-ionic systems the $\Delta S_T(\Delta T)$ changes with concentration, the ionic systems show only a shift of S_T . This is also the reason that in contrast to the non-ionic systems $\Delta S_T(\Delta c)$ and $\Delta S_T(\Delta T)$ are almost independent of $\log P$, while for non-ionic systems a strong dependence is found (cf. Fig. 7).

Further we were able to describe the temperature and concentration dependence of S_T using Eq. 2 and observed that the parameter S_T^i shows a linear correlation with $\log P$. The here investigated anions have the same sequence as in the Hofmeister series. Deviations are found for Cl^- and Br^- . The sequence of the two investigated cations Na^+ and K^+ is reversed. But as the cations lie very close together within the Hofmeister Series, more experiments need to be performed covering the entire range.

Our studies, thus explore the effect of both cations and anions on the thermophoretic properties of salt systems, which play a crucial role in science and technology [8, 11, 14]. In this study we have chosen rather simple experimental conditions by looking into aqueous salt solutions. In order to learn more about the role of the thermodiffusion of ions and the coupling of thermal and electric fields it would also be desirable to perform studies in biological cells or thermoelectric devices. This is still a big challenge for future studies.

Supplementary information The online version contains supplementary material available at <https://doi.org/10.1140/epje/s10189-022-00164-8>.

Acknowledgements We thank Fernando Bresme, Wim Briels, Nils Hansen, Namkyu Lee, Jutta Luettmmer-Strathmann, Daniel Markthaler, Doreen Niether, Annette Schmidt and Nils Zimmermann for fruitful discussions. We are grateful to Jan Dhont for inspiring ideas and his generous support of our work. SM acknowledges support from the International Helmholtz Research School of Biophysics and Soft Matter(BioSoft). We used Marvin 16.5.2.0, 2016, ChemAxon with the calculator plugin to calculate $\log P$. Further information can be found at <http://www.chemaxon.com>.

Funding Information Open Access funding enabled and organized by Projekt DEAL.

Author contribution statement

SM and SW conceived and planned the experiments. SM carried out the experiments and analyzed the data. SM and SW contributed to the interpretation of the results. SM took the lead in writing the manuscript. Both authors provided critical feedback and helped shape the research, analysis and manuscript.

Open Access This article is licensed under a Creative Commons Attribution 4.0 International License, which permits use, sharing, adaptation, distribution and reproduction in any medium or format, as long as you give appropriate credit to the original author(s) and the source, provide a link to the Creative Commons licence, and indicate if changes were made. The images or other third party material in this article are included in the article's Creative Commons licence, unless indicated otherwise in a credit line to the material. If material is not included in the article's Creative Commons licence and your intended use is not permitted by statutory regulation or exceeds the permitted use, you will need to obtain permission directly from the copyright holder. To view a copy of this licence, visit <http://creativecommons.org/licenses/by/4.0/>.

References

1. M. Jerabek-Willemsen, T. Andre, R. Wanner, H.M. Roth, S. Duhr, P. Baaske, D. Breitsprecher, Microscale thermophoresis: interaction analysis and beyond. *J. Mol. Struct.* **1077**, 101–113 (2014)
2. W. Köhler, K.I. Morozov, The soret effect in liquid mixtures - a review. *J. Non-Equil. Thermodyn.* **41**, 151–197 (2016)
3. D. Niether, S. Wiegand, Thermophoresis of biological and biocompatible compounds in aqueous solution. *J. Phys. Condens. Matter* **31**, 503003 (2019)
4. M. Asmari, R. Ratih, H.A. Alhazmi, S. El Deeb, Thermophoresis for characterizing biomolecular interaction. *Methods* **146**, 107–119 (2018)
5. P. Mehrabi, E.C. Schulz, R. Dsouza, H.M. Müller-Werkmeister, F. Tellkamp, R.J.D. Miller, E.F. Pai, Time-resolved crystallography reveals allosteric communication aligned with molecular breathing. *Science* **365**, 1167–1170 (2019)
6. D. Niether, H. Kriegs, J.K.G. Dhont, S. Wiegand, Peptide model systems: correlation between thermophilicity and hydrophilicity. *J. Chem. Phys.* **149**, 044506 (2018)
7. W. Kunz, J. Henle, B.W. Ninham, 'zur lehre von der wirkung der salze' (about the science of the effect of salts): Franz hofmeister's historical papers. *Curr. Opin. Colloid Interface Sci* **9**, 19–37 (2004)
8. J. Miikka, J.A. Manzanares, K. Kontturi, Thermal potential of ion-exchange membranes and its application to thermoelectric power generation. *J. Membr. Sci* **499**, 234–244 (2016)
9. F. Hofmeister, Zur Lehre von der Wirkung der Salze. *Archiv f. Experiment. Pathol. u. Pharmakol.* **24**, 247–260 (1888)
10. Yanjie Zhang, Paul S. Cremer, Interactions between macromolecules and ions: the hofmeister series. *Curr. Opin. Struct. Biol.* **10**, 658–663 (2006)
11. Werner Kunz, *Specific ion effects* (World Scientific, Singapore and Hackensack NJ, 2010)
12. R. Sacco, P. Airoldi, A.G. Mauri, J.W. Jerome, Three-dimensional simulation of biological ion channels under mechanical, thermal and fluid forces. *Appl. Math. Model.* **43**, 221–251 (2017)
13. D.P. Chen, R.S. Eisenberg, J.W. Jerome, C.W. Shu, Hydrodynamic model of temperature change in open ionic channels. *Biophys. J.* **69**, 2304–2322 (1995)
14. A. El Hady, B.B. Machta, Mechanical surface waves accompany action potential propagation. *Nat. Commun.* (2015)
15. S. Mohanakumar, J. Luettmmer-Strathmann, S. Wiegand, Thermomodification of aqueous solutions of various potassium salts. *J. Chem. Phys.* **154**, 084506 (2021)
16. A. Salis, B.W. Ninham, Models and mechanisms of hofmeister effects in electrolyte solutions, and colloid and protein systems revisited. *Chem. Soc. Rev.* **43**, 7358–7377 (2014)
17. P.L. Nostro, B.W. Ninham, S. Milani, A.L. Nostro, G. Pesavento, P. Baglioni, Hofmeister effects in supramolecular and biological systems. *Biophys. Chem.* **124**, 208–213 (2006)
18. H. Zhao, Protein stabilization and enzyme activation in ionic liquids: specific ion effects. *J. Chem. Technol. Biot.* **91**, 25–50 (2016)
19. J.H. Choi, H.R. Choi, J. Jeon, M. Cho, Ion aggregation in high salt solutions. vii. the effect of cations on the structures of ion aggregates and water hydrogen-bonding network. *J. Chem. Phys.* **147**, 154107 (2017)
20. F. Hofmeister, Zur Lehre von der Wirkung der Salze. *Archiv f. Experiment. Pathol. u. Pharmakol.* **25**, 1–30 (1888)
21. F. Hofmeister, Zur Lehre von der Wirkung der Salze. *Archiv f. Experiment. Pathol. u. Pharmakol.* **28**, 210–238 (1891)
22. H.I. Okur, J. Hladílková, K.B. Rembert, Y. Cho, J. Heyda, J. Dzubiella, P.S. Cremer, P. Jungwirth, Beyond the hofmeister series: ion-specific effects on proteins and their biological functions. *J. Phys. Chem. B* **121**, 1997–2014 (2017)
23. B. Kang, H. Tang, Z. Zhao, S. Song, Hofmeister series: insights of ion specificity from amphiphilic assembly and interface property. *ACS Omega* **5**, 6229–6239 (2020)
24. M. Andreev, A. Chremos, J. de Pablo, J.F. Douglas, Coarse-grained model of the dynamics of electrolyte solutions. *J. Phys. Chem. B* **121**, 8195–8202 (2017)
25. S. Iacopini, R. Rusconi, R. Piazza, The macromolecular tourist: universal temperature dependence of thermal diffusion in aqueous colloidal suspensions. *Eur. Phys. J. E* **19**, 59–67 (2006)
26. Y. Kishikawa, S. Wiegand, R. Kita, Temperature dependence of soret coefficient in aqueous and nonaqueous solutions of pullulan. *Biomacromolecules* **11**, 740–747 (2010)
27. A. Königer, B. Meier, W. Köhler, Measurement of the soret, diffusion, and thermal diffusion coefficients

- of three binary organic benchmark mixtures and of ethanol-water mixtures using a beam deflection technique. *Philos. Mag.* **89**, 907–923 (2009)
28. D. Niether, D. Afanasenkau, J.K.G. Dhont, S. Wiegand, Accumulation of formamide in hydrothermal pores to form prebiotic nucleobases. *Proc. Natl. Acad. Sci USA* **113**, 4272–4277 (2016)
 29. A.L. Sehnem, D. Niether, S. Wiegand, A.M.F. Neto, Thermodiffusion of monovalent organic salts in water. *J. Phys. Chem. B* **122**, 4093–4100 (2018)
 30. G. Wittko, W. Köhler, On the temperature dependence of thermal diffusion of liquid mixtures. *Europhys. Lett.* **78**, 46007 (2007)
 31. C.A. Lipinski, F. Lombardo, B.W. Dominy, P.J. Feeney, Experimental and computational approaches to estimate solubility and permeability in drug discovery and development settings. *Adv. Drug. Deliver. Rev.* **46**, 3–26 (2001)
 32. C.A. Lipinski, F. Lombardo, B.W. Dominy, P.J. Feeney, Experimental and computational approaches to estimate solubility and permeability in drug discovery and development settings. *Adv. Drug Deliv. Rev.* **64**, 4–17 (2012)
 33. U. Avico, E.C. Signoretti, P. Zuccaro, Activity-coefficients and partition-coefficients as parameters for the evaluation of biological-activity - a linear relationship between log-gamma and log-p. *Farmaco-Edizione Scientifica* **35**, 590–595 (1980)
 34. S. Di Lecce, T. Albrecht, F. Bresme, The role of ion-water interactions in determining the soret coefficient of licl aqueous solutions. *Phys. Chem. Chem. Phys.* **19**, 9575–9583 (2017)
 35. H. Bian, X. Wen, J. Li, H. Chen, S. Han, X. Sun, J. Song, W. Zhuang, J. Zheng, Ion clustering in aqueous solutions probed with vibrational energy transfer. *P. Natl. Acad. Sci.* **108**, 4737–4742 (2011)
 36. W. Nernst, Zur kinetik der in lösung befindlichen körper. *Z. Phys. Chem.* **2U**, 613–637 (1888)
 37. L. Onsager, R.M. Fuoss, Irreversible processes in electrolytes diffusion, conductance, and viscous flow in arbitrary mixtures of strong electrolytes. *J. Phys. Chem. US* **36**, 2689–2778 (1932)
 38. A.C.F. Ribeiro, J.J.S. Natividade, A.J.M. Valente, V.M.M. Lobo, Diffusion of electrolytes and non-electrolytes in aqueous solutions: a useful strategy for structural interpretation of chemical systems. *Adv. Kinet. Mech. Chem. React.*, 21–33, (2013)
 39. A. Anderko, P. Wang, M. Rafal, Electrolyte solutions: from thermodynamic and transport property models to the simulation of industrial processes. *Fluid. Phase. Equilib.* **194**, 123–142 (2002)
 40. W.R. Fawcett, A.C. Tikanen, Role of solvent permittivity in estimation of electrolyte activity coefficients on the basis of the mean spherical approximation. *J. Phys. Chem.* **100**, 4251–4255 (1996)
 41. P. Debye, E. Hückel, Zur theorie der elektrolyte. i. gefrierpunktserniedrigung und verwandte erscheinungen. *Phys. Z.*, 24(185):305, (1923)
 42. G.H. Gao, H.B. Shi, Y.X. Yu, Mutual diffusion coefficients of concentrated 1:1 electrolyte from the modified mean spherical approximation. *Fluid. Phase. Equilib.* **256**, 105–111 (2007)
 43. S. Kim, H. Kim, J.H. Choi, M. Cho, Ion aggregation in high salt solutions: ion network versus ion cluster. *J. Chem. Phys.* **141**, 124510 (2014)
 44. S.A. Hassan, Computer simulation of ion cluster speciation in concentrated aqueous solutions at ambient conditions. *J. Phys. Chem. B* **112**, 10573–10584 (2008)
 45. A.A. Chen, R.V. Pappu, Quantitative characterization of ion pairing and cluster formation in strong 1:1 electrolytes. *J. Phys. Chem. B* **111**, 6469–6478 (2007)
 46. J. H. Choi, M. Cho, Ion aggregation in high salt solutions. ii. spectral graph analysis of water hydrogen-bonding network and ion aggregate structures. *J Chem Phys*, 141:154502, (2014)
 47. H.V.R. Annapureddy, L.X. Dang, Molecular mechanism of specific ion interactions between alkali cations and acetate anion in aqueous solution: a molecular dynamics study. *J. Phys. Chem. B* **116**, 7492–7498 (2012)
 48. S. Nihonyanagi, S. Yamaguchi, T. Tahara, Counterion effect on interfacial water at charged interfaces and its relevance to the hofmeister series. *J. Am. Chem. Soc.* **136**, 6155–6158 (2014)
 49. M. Virginia, S.J.C. Vincent, What is the fundamental ion-specific series for anions and cations? ion specificity in standard partial molar volumes of electrolytes and electrostriction in water and non-aqueous solvents. *Chem. Sci.* **8**, 7052–7065 (2017)
 50. H. Lü, D.G. Leaist, Thermal diffusion with hydrolysis in aqueous solutions of sodium carbonate. *Can. J. Chem.* **69**, 1584–1588 (1991)
 51. F. S. Gaeta, G. Perna, G. Scala, F. Bellucci, Non-isothermal matter transport in sodium-chloride and potassium chloride aqueous solutions . 1. homogeneous system (thermal-diffusion). *J. Phys. Chem.-US*, 86:2967–2974, (1982)
 52. J. Colombani, J. Bert, J. Dupuy-Philon, Thermal diffusion in (licl, rh₂o). *J. Chem. Phys.* **110**, 8622–8627 (1999)
 53. F. Römer, Z. Wang, S. Wiegand, F. Bresme, Alkali halide solutions under thermal gradients: soret coefficients and heat transfer mechanisms. *J. Phys. Chem. B* **117**, 8209–8222 (2013)
 54. P. Kolodner, H. Williams, C. Moe, Optical measurement of the soret coefficient of ethanol/water solutions. *J. Chem. Phys.* **88**, 6512–6524 (1988)
 55. A. Leo, C. Hansch, D. Elkins, Partition coefficients and their uses. *Chem. Rev.* **71**, 525–616 (1971)
 56. H. Cumming, C. Rücker, Octanol-water partition coefficient measurement by a simple 1h nmr method. *ACS Omega* **2**, 6244–6249 (2017)
 57. G.J. Janz, B.G. Oliver, G.R. Lakshminarayanan, G.E. Mayer, Electrical conductance, diffusion, viscosity, and density of sodium nitrate, sodium perchlorate, and sodium thiocyanate in concentrated aqueous solutions. *J. Phys. Chem.* **74**, 1285–1289 (1970)

4 Overlapping hydration shells in salt solutions causing non-monotonic Soret coefficients with varying concentration



Cite this: *Phys. Chem. Chem. Phys.*,
2022, 24, 27380

Overlapping hydration shells in salt solutions causing non-monotonic Soret coefficients with varying concentration†

Shilpa Mohanakumar,^a Hartmut Kriegs,^a W. J. Briels^{ab} and Simone Wiegand^{*,ac}

We investigate the thermodiffusive properties of aqueous solutions of sodium iodide, potassium iodide and lithium iodide, using thermal diffusion forced Rayleigh scattering in a concentration range of 0.5–4 mol kg⁻¹ of solvent, large enough to deal with associated salts, and a temperature range of 15 to 45 °C. All systems exhibit non-monotonic variations of the Soret coefficient S_T with concentration, with a minimum at one mol kg⁻¹ of solvent in all three cases. We take this as an indication that the relevant length and energy scales are very similar in all cases. On this basis we develop an intuitive picture in which the relevant objects are the fully hydrated salt molecules, including all water molecules that behave differently from bulk water. Preliminary, somewhat sketchy calculations indicate that indeed Soret coefficients begin to rise beyond concentrations where the fully hydrated particles are randomly close packed. Indications are given as to why the model will fail at large concentrations.

Received 2nd September 2022,
Accepted 28th October 2022

DOI: 10.1039/d2cp04089a

rsc.li/pccp

1 Introduction

Thermophoresis, also called thermodiffusion or Ludwig–Soret effect, describes mass transport in temperature gradients and is one of the interesting unsolved puzzles in physical chemistry. Nowadays the most prominent application of this effect is in the determination of binding constants in protein–ligand reactions,^{1,2} but the effect also plays an important role in, for example, the conversion of waste heat into electricity by means of thermogalvanic cells.^{3–5} In both cases a deeper understanding of thermodiffusion of ions in aqueous solutions is desirable. Since the pioneering work of Hofmeister, it is known that many physicochemical processes in aqueous salt solutions do not only depend on ion concentrations and valencies, but also on the ion type.^{6–8} We therefore present experimental results of thermodiffusion in a range of concentrations and temperatures of solutions of three different salts with equal valencies but of different ion type, *in casu* lithium, sodium and potassium iodide.

In principle, in systems like ours there are four mass fluxes, *i.e.* those of the two types of ions, the one of the intact, non-dissociated salt molecules, and that of the solvent. Because of macroscopic electro-neutrality the two ionic fluxes must be equal. If we further assume that the dissociation equilibrium does not change with the very small temperature changes, the flux of the intact salt molecules must be equal to that of the individual ions. At the end we are left with only two independent mass fluxes, that of the solvent and that of the solute as a whole. From a phenomenological point of view we are therefore left with binary systems. From a microscopic point of view, the measured transport coefficients are combinations of those of the individual components.

In a binary fluid mixture exposed to a temperature gradient a stationary non-equilibrium state sets in, where the ordinary diffusive mass flux of the solute, proportional to the diffusion coefficient D , balances a thermophoretic mass flux of the solute, proportional to the thermal diffusion D_T . The Soret coefficient S_T defined as the ratio D_T/D describes the value of the concentration gradient that develops as a result of the applied temperature gradient. It can be positive, indicating that the solute accumulates in the cold region, or negative, in case the solute moves towards the warm region.^{9,10} Especially in aqueous systems, variations of concentration or temperature may lead to sign changes and non-monotonous variations of S_T . While early studies of more than 20 different salts in water indicated monotonous behavior of the Soret coefficient with concentration,¹¹ later works reported a minimum of S_T for

^a IBI-4: Biomacromolecular Systems and Processes, Forschungszentrum Jülich GmbH, D-52428 Jülich, Germany. E-mail: s.wiegand@fz-juelich.de

^b University of Twente, Computational Chemical Physics, Postbus 217, 7500 AE Enschede, The Netherlands. E-mail: w.j.briels@utwente.nl

^c Chemistry Department – Physical Chemistry, University Cologne, D-50939 Cologne, Germany

† Electronic supplementary information (ESI) available. See DOI: <https://doi.org/10.1039/d2cp04089a>



aqueous solutions of various salts.^{12–14} A recent indication for a minimum of S_T with concentration was observed experimentally¹⁵ and by computer simulations¹⁶ for lithium chloride at very low temperatures. The simulations showed that the minimum disappeared with increasing temperature, and especially that artificially decreasing the size of the anion increased the depth of the minimum. Until now, all these phenomena are basically not understood on a microscopic level.^{10,17–19}

According to Onsager's irreversible thermodynamics^{20–22} the Soret coefficient S_T of a binary mixture may be written as

$$S_T = \frac{Q^*}{RT^2} \left(1 + \frac{\partial \ln \gamma_{\pm}}{\partial \ln c} \right)^{-1}, \quad (1)$$

where γ_{\pm} is the activity coefficient of the salt and c the mass fraction of salt. Moreover, Q^* is an unknown quantity, containing both thermodynamic and kinetic contribution, and which is called the heat of transfer. Several expressions for Q^* have been suggested in the literature, some including kinetic contributions,²³ others ignoring them altogether.^{17,24–26} The simplest of these models is the one of Prigogine,¹⁷ who relates sign changes with concentration to a stronger cross interaction compared to the like-like interactions. This energetic concept works fine for many aqueous mixtures with ethanol,²⁷ saccharides,²⁸ methylformamides²⁹ and anionic surfactant sodiumdodecyl sulfate micelles in the presence of NaOH.³⁰ It also rationalizes the sign of the Soret coefficient in aqueous salt solutions at very low concentrations, *i.e.* below the dissociation limit.^{14,15} In general, reasonable agreement may be found for non-polar mixtures, but all models fail for polar mixtures.²⁵ We have applied eqn (1), using the model of Kempers with thermodynamic data from several ref. 31–33 but have not been able to represent our results with any accuracy.

Variations of the Soret coefficient S_T with temperature often follow an empirical equation proposed by Iacopini and Piazza³⁴

$$S_T(T) = S_T^{\infty} \left[1 - \exp\left(\frac{T^* - T}{T_0}\right) \right] \quad (2)$$

with obvious interpretations of the various adjustable parameters. In particular T^* is the temperature where the Soret coefficient changes sign, possibly outside the range of experimental data. Eqn (2) in particular does a good job with diluted aqueous solutions.^{10,34,35} As we will see below, also S_T of halides follows this equation for all concentrations. This is not the case, however, for larger organic salts at low, and for non-ionic solutes at higher concentrations.^{29,36–38}

Several computer simulation studies of thermodiffusion have appeared in the literature, some of which have been cited above, but none of these addresses salt solutions over a range of temperatures and concentrations. We will therefore not review these studies here in any detail. However, because we will refer to them on several occasions below, we do briefly discuss the results of thermophoretic simulations of binary Lennard-Jones mixtures by Artola and Rousseau.³⁹ All particles in their simulations were of equal mass and equal size. Simulations were performed over the full range of mole-fractions and a

range of temperatures. Moreover they studied several different systems by varying like-like (ϵ_{AA} , ϵ_{BB}) and cross-interactions (ϵ_{AB}). Clearly, with Lennard-Jones energies $\epsilon_{AA} = \epsilon_{BB}$, and ϵ_{AB} such that component A goes to cold at small mole-fractions x_A , component B must go to cold at small mole-fractions x_B , *i.e.* at large mole-fractions x_A ; as a consequence component A will go to hot at large mole-fractions x_A . The Soret coefficient of component A must therefore obey $S_T(x_A) = -S_T(1 - x_A)$, and change sign at $x_A = x_B = \frac{1}{2}$. From the simulations it follows that in all cases the Soret coefficient changes linearly with mole-fraction, and indeed obeys the rule just mentioned. Moreover, it was found that changing k_{AB} in $\epsilon_{AB} = k_{AB} \sqrt{\epsilon_{AA}\epsilon_{BB}}$ changes the slope of this line, while varying the ratio $\psi = \epsilon_{BB}/\epsilon_{AA}$ induces a vertical (or horizontal if you prefer) shift of the line. Before ending this paragraph on computer simulations we mention one more study on Lennard-Jones mixtures by Bresme *et al.*,⁴⁰ where the authors perform in depth calculations of all properties of their mixtures relevant for testing several theories proposed to describe Soret coefficients so far. Their calculations are restricted however to one particular set of Lennard-Jones parameters, and therefore cannot be used for our purposes (see below).

Even when no theoretical explanation for the occurrence of a minimum in the Soret coefficient with variations of concentration is available, some hypotheses/speculations concerning the origin of the phenomenon may be found in the literature. Chanu,¹³ and later Gaeta *et al.*¹⁴ pointed at the perturbation of local order of water in the neighborhood of the ions and its dependence on salt concentration as a possible starting point for an understanding of the non-monotonous dependence of Soret. This picture of perturbed water goes back to Frank and Wen.⁴¹ Evidently, in dense solutions, solvent molecules must organize their structure in order to accommodate to the presence of the solutes. Indeed, strong variations of water densities around NaI, among other salts, have been confirmed in a paper by simulations and neutron diffraction experiments^{42–46} and around CO₂ by Mitev *et al.*⁴⁷ A closer look at the structure in the latter case reveals that water molecules very close to the solute are strongly bound to that solute, either by expressing their negative oxygen atom to the slightly positive carbon atom on CO₂, or by embracing the slightly negative oxygen atom on CO₂ with their hydrogen atoms. Similar structures may be assumed to occur around dissolved salt molecules. Beyond this first shell of water molecules, a second shell of decreasingly perturbed water molecules is needed to gradually adjust to bulk water. As a result, the CO₂ molecule plus perturbed water is roughly a sphere with a radius of about 6–7 Å.⁴⁷

In this paper we will adopt a similar picture for salt solutions. For simplicity we assume that the measured effective transport coefficients may be attributed to non-dissociated salt molecules. Further discussion of this assumption will be given in Section 3.1. We define three types of particles, the bare salt molecule consisting of a cation paired with an iodide ion, the hydrated salt molecule (HSP) consisting of a bare salt molecule



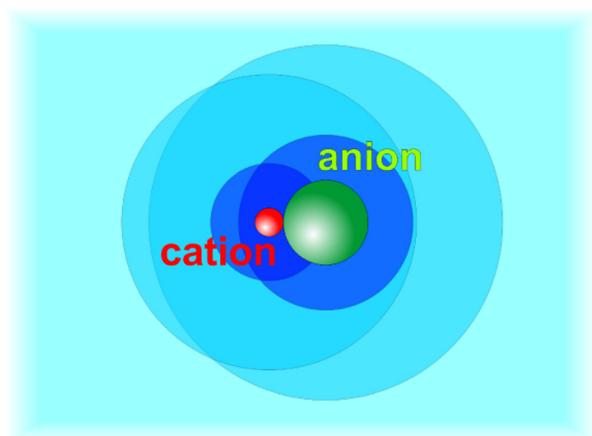


Fig. 1 Model of a hydrated salt molecule with a first shell of tightly bound water molecules (dark blue) and a second shell of perturbed water (light blue). For simplicity the molecule including the two hydration shells will be assumed spherical.

plus a first layer of Z strongly bound solvent molecules, and the fully hydrated salt molecule (FHP) consisting of the hydrated salt molecule plus the shell of perturbed water molecules. A caricaturist picture of these definitions is shown in Fig. 1. We expect that the Soret coefficient will change monotonously with concentration up to random close packing of the FHPs, beyond which the behavior will change. Random close packing occurs at a volume fraction of $\phi = 0.64$,⁴⁸ which with a radius of 6–7 Å corresponds to a molality of about 1.0 mole of salt per kilogram of water. This indeed turns out to roughly coincide with the minimum of Soret in all systems that we studied. We will use this observation as the starting point of our analysis of the thermophoresis of salt solutions with molalities on the order of one mole kg^{-1} of water.

2 Results

2.1 Concentration dependence

We used Infrared Thermal Diffusion Forced Rayleigh Scattering (IR-TDFRS) to investigate the thermophoretic behavior quantitatively. A schematic diagram of the setup is discussed in ESI† (Section S1) By way of example, we present in Fig. 2 the diffusion coefficient D , the thermal diffusion coefficient D_T , and the Soret coefficient S_T of NaI at four different temperatures as function of concentration. The solid lines are guides to the eye. As a measure of concentration we use molality m , *i.e.* the number of moles of salt per kilogram of water. At all temperatures D_T shows a minimum around a molality of 1 mol kg^{-1} , which survives in S_T , only slightly smoothed by increasing D . In all cases the diffusion coefficient D increases monotonously with concentrations, with the increase at higher concentrations being less than that at lower concentrations, due to an increase of viscosity with increasing salt concentration.⁴⁹ At the lowest measured temperature S_T and D_T change sign twice with concentration. Around $m = 1$ mol kg^{-1} NaI is

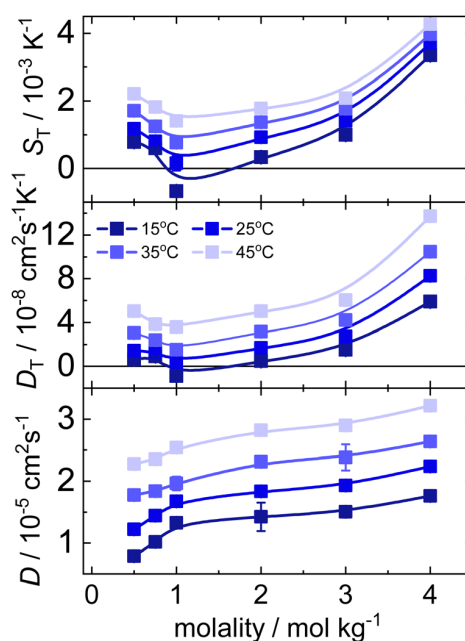


Fig. 2 Concentration dependence of Soret coefficient S_T , thermodiffusion coefficient D_T and diffusion coefficient D of NaI at four different temperatures as indicated in the inset. The lines are guides to the eye.

thermophilic (goes to hot), while at lower and higher concentrations it reveals thermophobic behavior (goes to cold). Potassium and lithium iodide behave similarly, but none of them shows a double sign change (*cf.* Fig. S4 and S5, ESI†).

Fig. 3 displays the concentration dependence of S_T values at 25 °C of the three iodide salts that have been studied. The lines are guide to the eye. All S_T of the investigated systems show a minimum with concentration, around 1 mol kg^{-1} , as has been observed for several other electrolytes.^{13–15,38} The concentration at which the minimum is observed varies only marginally for different salt systems. The steepest decay at low concentrations is found for LiI, which is the most hydrophilic of the investigated systems.

2.2 Temperature dependence

Fig. 4 shows the measured S_T as function of temperature at a molality of 1 and 4 mol kg^{-1} . The curves have been fitted using eqn (2). The Soret coefficient shows an increase with increasing temperature for all salt systems investigated, which is typical for aqueous solutions at low concentrations. At 1 mol kg^{-1} S_T of KI and NaI show a sign change with temperature (*cf.* Fig. 4a), while LiI, as expected from the previous literature, shows thermophilic behavior at all concentrations.⁵⁰ Additionally, S_T of LiI remains almost constant with increasing concentration, while the thermophobicity of the other salts increases with concentration.

In a previous investigation where S_T of a number of electrolytes had been studied at 0.01 mol kg^{-1} of water, Snowden and Turner⁵¹ found at 25.3 °C the largest negative value of S_T for LiI, $-1.44 \times 10^{-3} \text{ K}^{-1}$. Also, in our study LiI exhibits large negative



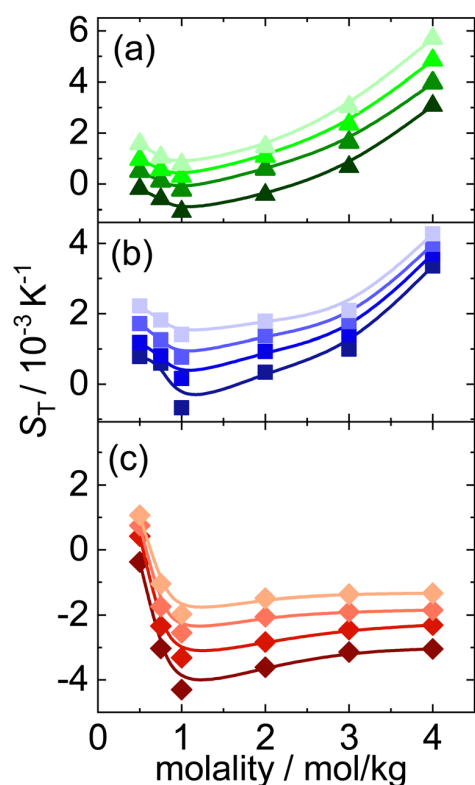


Fig. 3 Concentration dependence of Soret coefficient S_T of KI (upper panel), NaI (middle panel) and LiI (lower panel) at all measured temperatures. In each panel temperatures are 15, 25, 35 and 45 °C in that order, with the lowest temperature corresponding to the darkest set of symbols. Lines are guides to the eye.

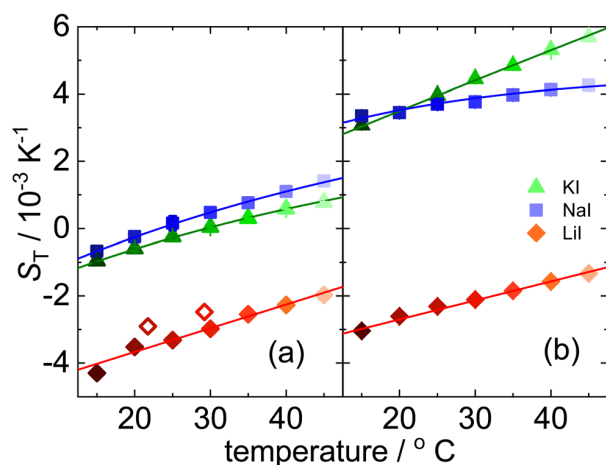


Fig. 4 Temperature dependence of Soret coefficient S_T of KI, NaI and LiI at molalities of 1 (left panel) and 4 (right panel) mol kg^{-1} respectively. The open symbols mark data points by Caldwell.⁵⁰ Darkest symbol corresponds to the lowest temperature of 15 °C with gradually fading to lighter symbols towards higher temperatures.

S_T values in comparison to KI and NaI (*cf.* Fig. 4). In a previous study of LiI Caldwell *et al.*⁵⁰ reported a S_T value of

$-2.69 \times 10^{-3} \text{ K}^{-1}$, while we found an 11% lower value of $-3.01 \times 10^{-3} \text{ K}^{-1}$ under the same conditions.

Fig. S6, S7 and S8 in the ESI,[†] display the temperature dependence of D_T and D . Both D_T and D show an increase with temperature. The increase in D is associated with the decrease in viscosity with temperature.

3 Discussion

3.1 Concentration dependence

In this section we infer from the characteristics of the data presented above a coarse grain picture that, in our view, contains the relevant elements to model the physics of our systems. In the second part we present results from some quick, but rather incomplete calculations on the basis of this model.

3.1.1 Rationalizing the results. Two things immediately stand out in all plots of Soret coefficients in Fig. 3. First, the data at low concentrations roughly depend linearly on concentration, with the slope being pretty constant for all systems and all temperatures. Second, the concentration where the minimum occurs varies only marginally among the different salts. The first observation agrees with the findings of Artola and Rousseau discussed in Section 1, while the second is consistent with the assumption that, at least at low concentrations, all salt molecules behave like equally big spherical particles.

It is known that in all cases that we consider about 80% of the salt molecules are dissociated into independent ions, while only 20% of them exist as non-dissociated, intact salt molecules.^{52–54} We notice, however, that also among the dissociated ions the cation–anion pair correlation functions have very strong first peaks, mainly as a result of the strong Coulomb interactions. In agreement with the second of the above findings we therefore assume that on average we may treat the salt molecules as single particles, sometimes consisting of strongly bound ion pairs, sometimes consisting of more loosely bound ion pairs, and sometimes even as single anions. A particle like this is called a bare salt molecule from now on. The properties attributed to such a bare salt molecule must be considered to be effective properties, very much as discussed in Section 1. Clearly, the model that we describe below will become less applicable with increasing cation sizes. If needed, a more realistic, but also more complicated model may be devised along similar lines. Referring to Fig. 1, we recall the definition of hydrated salt molecule (HSP), consisting of a bare salt molecule plus the first layer of strongly attached water molecules, and the fully hydrated salt molecule (FHP), consisting of an HSP plus the layer of perturbed water molecules. The radius of such an FHP will be denoted R_{HS} . We obtain an estimate of this radius by assuming that the FHPs are randomly close packed when the molality is equal to m_{min} . The volume fraction of FHPs ϕ is given as

$$\phi = \frac{N_s V_{\text{HS}}}{V} = N_{\text{AV}} \frac{\rho m}{m_0 M_w + m M_s} V_{\text{HS}} = N_{\text{AV}} \mathcal{M} V_{\text{HS}}, \quad (3)$$

where m is the molality of the solution, m_0 is the molality of water, *i.e.* the number of water molecules in one kilogram of water, M_s and M_w are the molar masses of salt and water respectively, and \mathcal{M}



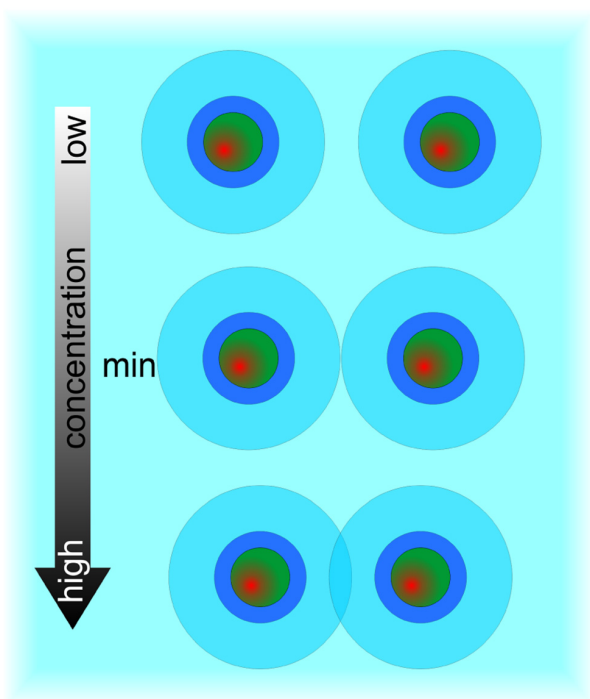


Fig. 5 Hydrated salt molecules overlapping with increasing concentration. The green–red sphere represents the bare salt molecule, after adding the blue shell of strongly attached water molecules we get the salt particle (HSP), while after adding next the outer light blue shell of perturbed water we arrive at the hydrated salt molecule, called FHP. At concentrations above m_{\min} the outer shells overlap as shown in the bottom row.

is called the molarity, the number of moles of salt per liter of solution. V_{HS} is the volume of one FHP, *i.e.* one hydrated salt molecule or anion, N_s is the number of salt molecules in volume V , and ρ is the density of the solution. With $m_{\min} = 1.0 \text{ mol kg}^{-1}$ for all systems and a random close packed volume fraction $\phi_{\text{rcp}} = 0.64$, we obtain $R_{\text{HS}} = 6.3 \text{ \AA}$; this is a very reasonable value according to Mitev *et al.*⁴⁷

On increasing the concentration beyond m_{\min} , the outer hydration shells of the salt molecules begin to overlap, as shown in Fig. 5. This gives rise to a type of depletion interaction between the salt molecules, which we will now explain. First we notice that concentrations are never large enough for the tightly bound water molecules, constituting the first solvation layer, of two different salt molecules or anions to touch. Therefore we take HSPs as the coarse grain particles in our model. Similarly we define coarse water particles to consist of several water molecules. The energy of a salt solution is then written as

$$E = \sum_{i=1}^{N_s-1} \sum_{j=i+1}^{N_s} \phi_{\text{ss}}^0(r_{ij}) + \sum_{i=1}^{N_w-1} \sum_{j=i+1}^{N_w} \phi_{\text{ww}}(r_{ij}) + \sum_{i=1}^{N_s} \sum_{j=1}^{N_w} \phi_{\text{sw}}(r_{ij}) + E^{\text{self}}. \quad (4)$$

Here ϕ_{ss}^0 denotes the interaction potential between two coarse salt particles, *i.e.* two HSPs at a distance r_{ij} , ϕ_{ww} that between

two coarse water particles and ϕ_{sw} that between an HSP and a coarse water particle. E^{self} is an additional self energy depending on the configuration of all HSPs collectively, which is the key quantity in our model.

When one molecule of salt is dissolved in water, the change of energy has two contributions, one negative contribution when the first layer of water molecules is bound to the salt, and one positive contribution that takes into account the perturbation of the outer hydration shell. The total increase of energy will be negative. At low concentrations, when the FHPs do not overlap, a total energy E^0 proportional to the number of salt particles will be released. When two FHPs do overlap, the energies gained by attaching the strongly bound water shells to each of the bare salt molecules, *i.e.* by creating the HSPs, are the same as for two non-overlapping FHPs, but the energy paid to create the outer shells of the FHPs is diminished by a positive amount, proportional to the overlap of the two outer shells. This holds for any pair of overlapping hydration shells. The self energy therefore reads

$$E^{\text{self}} = E^0 - \sum_{i < j}^{N_s} \kappa \frac{1}{4} H_{ij}^2 (3 - H_{ij}) \quad H_{ij} \geq 0 \quad (r_{ij} \leq 2R_{\text{HS}}) \\ = 0 \quad H_{ij} \leq 0 \quad (r_{ij} \geq 2R_{\text{HS}}) \quad (5a,b)$$

where $H_{ij} = 1 - r_{ij}/2R_{\text{HS}}$ is half the thickness of the overlap, divided by R_{HS} , and κ is a positive constant with the dimensions of energy. With this we get for the total energy of the solution

$$E = \sum_{i=1}^{N_s-1} \sum_{j=i+1}^{N_s} \phi_{\text{ss}}^{\text{total}}(r_{ij}) + \sum_{i=1}^{N_w-1} \sum_{j=i+1}^{N_w} \phi_{\text{ww}}(r_{ij}) + \sum_{i=1}^{N_s} \sum_{j=1}^{N_w} \phi_{\text{sw}}(r_{ij}), \quad (6a)$$

$$\phi_{\text{ss}}^{\text{total}}(r_{ij}) = \phi_{\text{ss}}^0(r_{ij}) - \kappa \frac{1}{4} H_{ij}^2 (3 - H_{ij}) = : \phi_{\text{ss}}^0(r_{ij}) + \phi_{\text{ss}}^{\text{overlap}}(r_{ij}) \quad (6b)$$

where we have omitted the unimportant constant E^0 . Evidently, with increasing concentrations the assumed pairwise-additivity of the correction to the self-energy becomes inaccurate.

On the energy scales that we are interested in, coarse salt particles may be considered to be impenetrable particles interacting through dipole–dipole interactions, so ϕ_{ss}^0 may well be approximated by a Lennard-Jones potential. Given the dimensions as shown in Fig. 1 the radius of a coarse salt particle is about one half of R_{HS} , so the salt–salt Lennard-Jones potential has a σ of about R_{HS} , and therefore a range of about $2\sigma = 2R_{\text{HS}}$, which is equal to that of the overlap potential $\phi_{\text{ss}}^{\text{overlap}}$. For computational purposes it is often most convenient to have water particles of about the same size as that of the salt particle. Clearly for coarse water–water and salt–water interactions somewhat more soft potentials seem to be preferable, although Lennard-Jones potentials have been used for this purpose as well. For a review see Hadley and McCabe.⁵⁵ This concludes the description of our coarse grain picture of salt solutions at low concentrations.



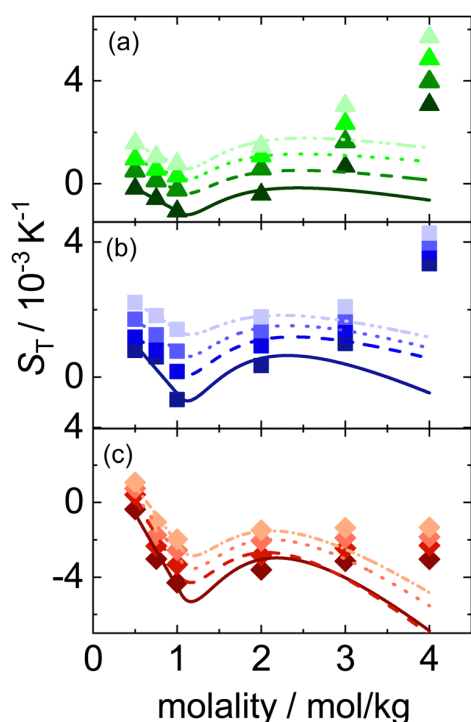


Fig. 6 Concentration dependence of Soret coefficient S_T of KI (upper panel), NaI (middle panel) and LiI (lower panel) at four different temperatures. In each panel temperatures are 15, 25, 35 and 45 °C in that order, with the lowest temperature corresponding to the darkest set of symbols. Lines correspond to fits that have been obtained with our model (for details see Section 3.1).

3.1.2 Estimated predictions. In order to test the validity of this model one has to perform simulations or try to extract information otherwise. Here we will present the results of some rather sketchy calculations on the basis of the results published by Artola and Rousseau for Lennard-Jones mixtures. To this end we assume Lennard-Jones potentials for coarse water–water and salt–water interactions and map the total coarse salt–salt potential $\phi_{ss}^{\text{total}}(r_{ij}) = \phi_{ss}^0(r_{ij}) + \phi_{ss}^{\text{overlap}}(r_{ij})$ on some effective Lennard-Jones potential ϕ_{ss}^{eff} . With these we next make use of the reported data in the paper of Artola and Rousseau. Details of the calculations are presented in the Appendix to this paper. Evidently, mapping the sum of $\phi_{ss}^0(r_{ij})$ and $\phi_{ss}^{\text{overlap}}(r_{ij})$, with rather different distance dependencies, to an effective Lennard-Jones potential, must be approximate. We assume, however, that for concentrations not too far above m_{min} the approximation works acceptably. The results obtained with this method must be considered as a proof of principle. The final verdict has to be given by means of a simulation study. Until then, the model remains somewhat speculative, although intuitively appealing.

The results of our calculations are shown as the lines in Fig. 6. It is clearly seen that the predicted Soret coefficients increase as soon as the outer hydration shells of the big spheres begin to overlap. At larger concentrations, however, they decay again while experimental data continue to increase. Apart from

the numerical inadequacies already mentioned, also the model itself will become inadequate at the larger concentrations. First, the pairwise additive corrections to the self energies will become inappropriate, and next, at even higher concentrations, one can imagine that it is profitable to form clusters of salt particles and expel the water molecules from these altogether to minimize the energy stored in the perturbed hydration shells. Both effects will lower the average salt–salt interactions faster than is done within the present model, and will drive salt to the cold.

3.2 Temperature dependence

As can be seen in Fig. 4 S_T of all investigated systems shows an increase in thermophobicity with temperature and can be successfully described by eqn (2) for all concentrations studied. The same behavior has been recently observed for other simple salts without large organic groups,^{38,56} which is in contrast to the temperature dependence of S_T observed for larger organic salts^{37,57} and non-ionic solutes in water.²⁹ For a typical non-ionic solute, the behavior of S_T changes from increasing with temperature to decreasing with temperature as the concentration increases. It is assumed that this is correlated with the hydration of the solutes, which decreases as the concentration increases. In contrast, the Soret coefficients of simple ionic solutes show the typical temperature dependence described by eqn (2) over the entire concentration range. This might be explained by cluster formation and growth of the salts with increasing concentrations. At high salt concentrations, these clusters are hydrated by water as the fraction of ions in the interfaces decreases when more ions are part of larger clusters. This results in diluted solutions of clusters, which still exhibit the typical temperature dependence of diluted aqueous solutions.

4 Conclusion

We have studied the thermophoretic properties of three iodide salt solutions over a range of temperatures and concentrations. For all three salts, LiI, NaI and KI, the variation of the Soret coefficient with concentration exhibits a minimum for all four temperatures that we investigated. On the basis of various theoretical expressions combined with the best thermodynamic enthalpies and activity coefficients available, we were not able to describe this minimum. On the contrary, in most cases we predicted a maximum in Soret coefficient with concentration.

All experimental data share the same characteristics. First, Soret coefficients at low concentrations decay linearly with concentration, and second, in all cases a minimum occurs at one and the same concentration of one mole of salt per kilogram of solvent. From this we infer that the relevant objects in all systems are to a large extent equally big and behave like ideally dissolved particles at low concentrations. From the concentration where the minimum occurs we obtain an estimate for the size of these objects, which coincides with that of a salt molecule including the full hydration shell of strongly



attached and perturbed water molecules. Beyond the concentration where the Soret coefficient is minimal, the hydrated objects begin to overlap which leads to stronger interactions between salt molecules, much like depletion interactions do in colloid-polymer solutions. Preliminary, somewhat sketchy calculations indicate that indeed the Soret coefficient increases when concentrations increase beyond one mole of salt per kilogram of water. The model only holds at concentrations not very much larger than close packing of the big hydrated objects. At even larger concentrations the pair wise approximation on which the model is built may not be accurate enough. Moreover at large concentrations it may be energetically profitable for the system to expel the water between the salt molecules and form salt clusters.

Conflicts of interest

There are no conflicts to declare.

Appendix

In this appendix we describe how we map our model on the binary Lennard-Jones model of Artola and Rousseau in order to be able to make use of their numerical data on S_T for these systems. We summarize the data of these authors as

$$S_T(x) = -\frac{1}{140}[k-1][x-x_0], \quad (7a)$$

$$x_0 = 0.635\frac{1}{\psi} - 0.142, \quad (7b)$$

where x is the mole fraction of A-particles and k and ψ are set parameters. Their relation to the Lennard-Jones potential parameters is according to $\varepsilon_{AB} = k\sqrt{\varepsilon_{AA}\varepsilon_{BB}}$ and $\psi = \varepsilon_{BB}/\varepsilon_{AA}$. The values of x_0 are obtained from the simulations and have been fitted by us as in eqn (7b).

As noticed in the main text, the radius of the bare salt molecule plus the attached water layer is about half the radius of the fully hydrated salt molecule. Moreover, our concentrations will never be large enough that the attached water layers become perturbed as well. Given these two facts, we consider one salt molecule together with Z attached water molecules to be one LJ_s particle of diameter σ equal to R_{HS} . A LJ_w particle then consists of $Z + \alpha$ water molecules, such that it has the same diameter and preferably the same mass as the salt particles. With this we calculate the Lennard-Jones mole-fractions for salt according to

$$x = \frac{N_s}{N_s + \frac{N_w - ZN_s}{Z + \alpha}} = (Z + \alpha)\frac{m}{m_0 + \alpha m}. \quad (8)$$

Since there is no definite way to decide about the size of a particle of $Z + \alpha$ water molecules we settle for $\alpha = 1$. All Lennard-Jones potentials have the same value for σ , which plays no further role in what follows.

We now must decide about the values of k and ψ . These are determined by the three epsilon values $\varepsilon_{AA} = \varepsilon_{ss}^{\text{eff}}$, $\varepsilon_{BB} = \varepsilon_{ww}$ and $\varepsilon_{AB} = \varepsilon_{sw}$, of which ε_{ww} and ε_{sw} remain constant throughout this appendix. Moreover only values of $\varepsilon_{ss}^{\text{eff}}/\varepsilon_{ww}$ are needed explicitly. First, we determine $\varepsilon_{ss}^0/\varepsilon_{ww} = 1/\psi^0$ by putting the overlap potential to zero for molalities less than m_{min} . By fitting the experimental data in this range with eqn (7) we get k^0 and ψ^0 for the zeroth order potentials. For molalities larger than m_{min} we assume that the total salt-salt potential, $\phi_{ss}^{\text{total}}(r_{ij})$ may be approximated by the effective Lennard-Jones potential

$$\phi_{ss}^{\text{eff}}(r_{ij}) = \phi_{ss}^0(r_{ij}) + \frac{\tilde{\phi}_{ss}^{\text{overlap}}(r^{\text{NN}})}{\phi_{ss}^0(r^{\text{NN}})}\phi_{ss}^0(r_{ij}), \quad (9)$$

where r^{NN} is the average nearest neighbor distance between salt molecules. This gives rise to an effective ε^{eff} given as

$$\varepsilon_{ss}^{\text{eff}} = \varepsilon_{ss}^0 + \kappa \frac{\tilde{\phi}_{ss}^{\text{overlap}}(r^{\text{NN}})}{\phi_{ss}^0(r^{\text{NN}})}, \quad (10)$$

where the tildes indicate that factors bearing the dimensions of energy have been taken out, *i.e.* $\tilde{\phi}_{ss}^0 = \phi_{ss}^0/\varepsilon^0 = \phi^{\text{LJ}}/\varepsilon$, *etc.* Since both the numerator and the denominator in the last term are negative, the effective epsilon is larger than the pure epsilon, so binding becomes stronger. In order to complete the calculation of k and ψ as function of concentration we must relate r^{NN} to the concentration. To this end we approximate

$$r^{\text{NN}}(\mathcal{M}) = 1 + \left(\frac{\mathcal{M}_{\text{min}}}{\mathcal{M}}\right)^{1/3}. \quad (11)$$

For $\mathcal{M} = \mathcal{M}_{\text{min}}$ we get $r^{\text{NN}} = 2$, and for very large concentrations $r^{\text{NN}} = 1$.

We now have available all information to calculate k and ψ as functions of concentration:

$$\frac{1}{\psi(\mathcal{M})} = \frac{1}{\psi^0} + A \frac{\tilde{\phi}_{ss}^{\text{overlap}}(r^{\text{NN}}(\mathcal{M}))}{\phi_{ss}^0(r^{\text{NN}}(\mathcal{M}))}, \quad (12a)$$

$$k(\mathcal{M}) = k^0 \sqrt{\psi(\mathcal{M})/\psi^0}, \quad (12b)$$

where $A = \kappa/\varepsilon_{ww}$ is an adjustable parameter. Putting these values into eqn (7) we calculate S_T for any concentration.

Acknowledgements

We thank Fernando Bresme, Julia Burkhardt, Niels Hansen, Jutta Luettmer-Strathmann, Daniel Markthaler, Gunwoo Park, Annette Schmidt and Nils Zimmermann for fruitful and helpful discussions. We are grateful to Jan Dhont and Peter Lang for inspiring ideas and his generous support of our work. SM acknowledges the support of the International Helmholtz Research School of Biophysics and Soft Matter (BioSoft).

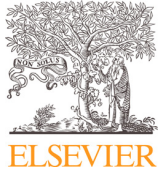


References

- 1 M. Jerabek-Willemsen, T. Andre, R. Wanner, H. M. Roth, S. Duhr, P. Baaske and D. Breitsprecher, *J. Mol. Struct.*, 2014, **1077**, 101–113.
- 2 D. Niether, M. Sarter, B. W. Koenig, J. Fitter, A. M. Stadler and S. Wiegand, *Polymers*, 2020, **12**, 376.
- 3 B. T. Huang, M. Roger, M. Bonetti, T. J. Salez, C. Wiertel-Gasquet, E. Dubois, R. Cabreira Gomes, G. Demouchy, G. Mériguet, V. Peyre, M. Kouyaté, C. L. Filomeno, J. Depeyrot, F. A. Tourinho, R. Perzynski and S. Nakamae, *J. Chem. Phys.*, 2015, **143**, 054902.
- 4 M. Jokinen, J. A. Manzanares, K. Kontturi and L. Murtoimäki, *J. Membr. Sci.*, 2016, **499**, 234–244.
- 5 N. Jaziri, A. Boughamoura, J. Mueller, B. Mezghani, F. Tounsi and M. Ismail, *Energy Rep.*, 2020, **6**, 264–287.
- 6 F. Hofmeister, *Arch. Exp. Pathol. Pharmacol.*, 1888, **24**, 247–260.
- 7 Y. Zhang and P. S. Cremer, *Curr. Opin. Chem. Biol.*, 2006, **10**, 658–663.
- 8 W. Kunz, *Specific ion effects*, World Scientific, Singapore and Hackensack NJ, 2010.
- 9 *Thermal nonequilibrium phenomena in fluid mixtures*, ed. W. Köhler and S. Wiegand, Springer, Berlin, 1st edn, 2002, vol. LNP584.
- 10 D. Niether and S. Wiegand, *J. Phys.: Condens. Matter*, 2019, **31**, 503003.
- 11 C. C. Tanner, *Trans. Faraday Soc.*, 1927, **23**, 75–95.
- 12 J. Chanu, *J. Chim. Phys. Phys.-Chim. Biol.*, 1958, **55**, 743–753.
- 13 J. Chanu, in *Advances in Chemical Physics*, ed. I. Prigogine, John Wiley & Sons, Inc, Hoboken, NJ, USA, 1967, pp. 349–367.
- 14 F. S. Gaeta, G. Perna, G. Scala and F. Bellucci, *J. Phys. Chem.*, 1982, **86**, 2967–2974.
- 15 J. Colombani, J. Bert and J. Dupuy-Philon, *J. Chem. Phys.*, 1999, **110**, 8622–8627.
- 16 S. Di Lecce, T. Albrecht and F. Bresme, *Phys. Chem. Chem. Phys.*, 2017, **19**, 9575–9583.
- 17 I. Prigogine, L. Debrouckere and R. Amand, *Physica*, 1950, **16**, 851–860.
- 18 P. Polyakov and S. Wiegand, *J. Chem. Phys.*, 2008, **128**, 034505.
- 19 Z. Wang, H. Kriegs and S. Wiegand, *J. Phys. Chem. B*, 2012, **116**, 7463–7469.
- 20 S. R. de Groot, *Thermodynamics of irreversible processes*, North Holland, Amsterdam, 1966.
- 21 R. Haase, *Thermodynamik der Irreversiblen Prozesse*, Steinkopff, Heidelberg, 1963, vol. 8.
- 22 S. Kjelstrup, D. Bedeaux, E. Johannessen and J. Gross, *Nonequilibrium thermodynamics for engineers*, World Scientific, Hackensack, NJ, 2nd edn, 2017.
- 23 K. Shukla and A. Firoozabadi, *Ind. Eng. Chem. Res.*, 1998, **37**, 3331–3342.
- 24 L. J. T. M. Kempers, *J. Chem. Phys.*, 2001, **115**, 6330–6341.
- 25 M. G. Gonzalez-Bagnoli, A. A. Shapiro and E. H. Stenby, *Philos. Mag.*, 2003, **83**, 2171–2183.
- 26 M. Hartung and W. Köhler, *Eur. Phys. J. E: Soft Matter Biol. Phys.*, 2009, **29**, 117–121.
- 27 A. Königer, B. Meier and W. Köhler, *Philos. Mag.*, 2009, **89**, 907–923.
- 28 P. Blanco, H. Kriegs, B. Arlt and S. Wiegand, *J. Phys. Chem. B*, 2010, **114**, 10740–10747.
- 29 D. Niether, H. Kriegs, J. K. G. Dhont and S. Wiegand, *J. Chem. Phys.*, 2018, **149**, 044506.
- 30 D. Vigolo, S. Buzzaccaro and R. Piazza, *Langmuir*, 2010, **26**, 7792–7801.
- 31 D. Lide, T. J. Bruno and J. R. Rumble, *CRC handbook of chemistry and physics: A ready-reference book of chemical and physical data*, 100th edn, 2019.
- 32 R. Heyrovská, *Chem. Phys. Lett.*, 1989, **163**, 207–211.
- 33 J. A. Myers, S. I. Sandler and R. H. Wood, *Ind. Eng. Chem. Res.*, 2002, **41**, 3282–3297.
- 34 S. Iacopini, R. Rusconi and R. Piazza, *Eur. Phys. J. E: Soft Matter Biol. Phys.*, 2006, **19**, 59–67.
- 35 Y. Kishikawa, S. Wiegand and R. Kita, *Biomacromolecules*, 2010, **11**, 740–747.
- 36 D. Niether, D. Afanasenkau, J. K. G. Dhont and S. Wiegand, *Proc. Natl. Acad. Sci. U. S. A.*, 2016, **113**, 4272–4277.
- 37 A. L. Sehnem, D. Niether, S. Wiegand and A. M. F. Neto, *J. Phys. Chem. B*, 2018, **122**, 4093–4100.
- 38 S. Mohanakumar, J. Luettmer-Strathmann and S. Wiegand, *J. Chem. Phys.*, 2021, **154**, 084506.
- 39 P. A. Artola and B. Rousseau, *Phys. Rev. Lett.*, 2007, **98**, 125901.
- 40 O. R. Gittus and F. Bresme, On the microscopic origin of Soret coefficient minima in liquid mixtures, <https://arxiv.org/pdf/2207.12864>.
- 41 H. S. Frank and W.-Y. Wen, *Discuss. Faraday Soc.*, 1957, **24**, 133.
- 42 M. Carrillo-Tripp, H. Saint-Martin and I. Ortega-Blake, *J. Chem. Phys.*, 2003, **118**, 7062–7073.
- 43 A. K. Soper and K. Weckström, *Biophys. Chem.*, 2006, **124**, 180–191.
- 44 R. Mancinelli, A. Botti, F. Bruni, M. A. Ricci and A. K. Soper, *J. Phys. Chem. B*, 2007, **111**, 13570–13577.
- 45 J. Gujt, M. Bešter-Rogač and B. Hribar-Lee, *J. Mol. Liq.*, 2014, **190**, 34–41.
- 46 P. Gallo, D. Corradini and M. Rovere, *J. Mol. Liq.*, 2014, **189**, 52–56.
- 47 K. Hermansson, P. D. Mitev and W. J. Briels, *J. Phys. Chem. B*, 2021, **125**, 13886–13895.
- 48 G. D. Scott and D. M. Kilgour, *J. Phys. D: Appl. Phys.*, 1969, **2**, 863–866.
- 49 D. E. Goldsack and R. Franchetto, *Can. J. Chem.*, 1977, **55**, 1062–1072.
- 50 D. R. Caldwell, *J. Phys. Chem.*, 1975, **79**, 1882–1884.
- 51 P. N. Snowdon and J. C. R. Turner, *Trans. Faraday Soc.*, 1960, **56**, 1409–1418.
- 52 R. Heyrovská, *Croat. Chem. Acta*, 1997, **70**, 39–54.
- 53 I. S. Joung and T. E. Cheatham, *J. Phys. Chem. B*, 2009, **113**, 13279–13290.
- 54 A. K. Borkowski, Z. A. Piskulich and W. H. Thompson, *J. Phys. Chem. B*, 2021, **125**, 350–359.
- 55 K. R. Hadley and C. McCabe, *Mol. Simul.*, 2012, **38**, 671–681.
- 56 S. Mohanakumar and S. Wiegand, *Eur. Phys. J. E: Soft Matter Biol. Phys.*, 2022, **45**, 10.
- 57 A. L. Sehnem, A. M. F. Neto, R. Aquino, A. F. C. Campos, F. A. Tourinho and J. Depeyrot, *Phys. Rev. E: Stat., Nonlinear, Soft Matter Phys.*, 2015, **92**, 042311.



5 Thermophoretic Microfluidic Cells for Evaluating Soret Coefficient of Colloidal Particles



Contents lists available at ScienceDirect

International Journal of Heat and Mass Transfer

journal homepage: www.elsevier.com/locate/hmt

Thermophoretic microfluidic cells for evaluating Soret coefficient of colloidal particles

Namkyu Lee^a, Shilpa Mohanakumar^a, Simone Wiegand^{a,b}^a IBI-4, Forschungszentrum Jülich, 52428, Germany^b Universität zu Köln, 50939, Germany

ARTICLE INFO

Article history:

Received 24 February 2022

Revised 13 April 2022

Accepted 5 May 2022

Keywords:

Thermophoresis

Microfluidics

Temperature gradient

Soret coefficient

Colloidal particles

ABSTRACT

Thermodiffusion or thermophoresis gained much interest in bio, chemical, and energy engineering. Although there are several methods to measure thermophoresis, they consume large sample volumes, are limited to binary mixtures, and give only indirect access to the applied temperature profile. Herein, we propose a thermophoretic microfluidic cell for quantitative measurements of the Soret coefficient of colloids. The actual microscale measuring channel lies between cooling and heating channels to achieve a one-dimensional temperature gradient. Fluorescence lifetime imaging microscopy with Rhodamine B is utilized to measure the spatial temperature profile in the channel. The fluorescence intensity of fluorescently labeled polystyrene particles with a diameter of 25 nm is used to monitor the concentration profile. The observed temperature and concentration profiles are one-dimensional, as gradients in the longitudinal and height directions can be neglected. In the investigated temperature range, the averaged difference between the measured Soret coefficients with the cell and determined with the Thermal Diffusion Forced Rayleigh Scattering set-up is less than 8%.

© 2022 Elsevier Ltd. All rights reserved.

1. Introduction

Thermodiffusion or thermophoresis is a process which occurs in non-isothermal systems, when a temperature gradient drives not only a heat flux, but also a mass flux [1]. This coupling of heat and mass fluxes leads to a concentration profile and plays a role in natural and technical transport processes with temperature gradients, e.g. petrology (rock formation), petroleum reservoirs and as separation techniques [2]. Also, as it is one of the few known mechanisms which allows the accumulation of substance against diffusion it is discussed in the context of the origin-of-life question [3,4]. In the recent years, it has turned out that the thermophoretic response of proteins and protein-ligand complexes can be used to characterize the binding affinity between ligand and protein utilizing the so-called microscale thermophoresis device (MST) [5–7]. Furthermore, the effect also needs to be considered in the development of liquid thermoelectric cells used to convert waste heat into electricity [8–10]. In those cells, charged colloidal particles are added to increase the energy conversion efficiency. To improve our still poor understanding of physicochemical effect and to develop improved theoretical concepts of thermophoresis in those multi-component systems, quantitative measurements are desirable [11].

Thermophoresis is the particle movement driven by a temperature gradient [6], which is expressed by the flux equation [12]

$$\vec{j} = -\rho D \nabla c - \rho c(1-c) D_T \nabla T \quad (1)$$

with the net mass flux j , the particle density ρ , the diffusion coefficient D , the mass fraction c of the solute, the thermal diffusion coefficient D_T and the temperature T . In the steady state ($\vec{j} = 0$), the Soret coefficient, S_T , is defined as $S_T \equiv D_T/D$. The Soret coefficient S_T is a measure for the resulting concentration difference Δc , if a certain temperature difference ΔT is applied. Despite many theoretical approaches and simulations [2,13–16], there is so far no microscopic theory which predicts S_T quantitatively. While mass, shape and moment of inertia are important for thermodiffusive properties of non-polar substances, the thermodiffusion of polar and especially aqueous solutions is governed by the hydrophilicity of the solute molecules, pH and ionic strength [6].

There are several experimental methods to measure the Soret coefficient quantitatively, such as thermal lens (TL) [17,18], Thermal Diffusion Forced Rayleigh Scattering (TDFRS) [19,20], beam deflection [21–23] and thermogravitational columns (TCs) [24]. Except for TCs, all other methods use optical detection and depend on the optical refractive index contrast due to temperature and concentration changes. Therefore, they are limited to binary or specific ternary systems unless two wavelengths are implemented us-

E-mail addresses: n.lee@fz-juelich.de (N. Lee), s.wiegand@fz-juelich.de (S. Wiegand).

ing the dispersion to analyze ternary systems [25]. For the multi-component mixtures, TC, which uses the interaction of free convection and thermodiffusive flow, is a good choice [24,26] as samples are drawn from the column and analyzed according to their composition. However, TCs consume sample volumes in the order of 30 mL [24], which are not affordable for biological samples only available in small amounts of a few micro liter.

To overcome limitations of conventional measurement methods, advanced microfluidic devices have been suggested [27–30]. In general, microfluidic devices consume small sample volumes ($\sim \mu\text{L}$) and provide short equilibrium times so that they are suitable for biological samples. An instrument utilizing the thermophoretic effect is MST [28] which has been widely used for investigating diseases such as influenza [31], corona [32] and Alzheimer [33]. While the strengths of MST are a low detection limit (~ 1 pM) and a fast response time to measure the protein-ligand binding constant, it gives only qualitative values for the Soret coefficient. Researchers have also used microfluidic channels to quantify the Soret coefficient [27,29,30]. The main difficulty of microfluidic cells is the reliable determination of the temperature and concentration profile. Some experiments measure the temperature outside the actual measuring channel and assume a one-dimensional temperature profile propagating into the measuring channel [27,30]. Otherwise, the temperature dependence of the fluorescence intensity in the measuring channel is used [29,34]. Both methods are prone to errors, since it can easily be affected by changes in external condition such as the surrounding temperature for the first method or by photobleaching of the dye or reflections in the latter method [35].

In order to obtain reliable thermophoretic results, several points need to be considered. As S_T is proportional to $\Delta c/\Delta T$, a large temperature gradient causes a larger and easier to measure concentration difference. On the other hand, larger gradients can induce free convection, which mixes the solution and decreases the concentration differences resulting in too small measured Soret coefficients. Ideally, the channel shape induces a one-dimensional temperature profile, but, due to the small dimensions, the linearity is easily affected by external thermal conditions through conduction and convection [36]. This requires a comprehensive thermal analysis of the device, and a direct measurement of temperature and concentration is required.

Herein, we suggest a thermophoretic microfluidic cell made of poly(methyl methacrylate) (PMMA). We designed large cooling and heating channels with high mass flow rates up to 0.94 m/s leading to high temperature gradients up to 34000 K/m corresponding to a temperature difference of 3°C across the measuring channel. A confocal microscope with a photomultiplier and a correlator is used to measure the fluorescent lifetime correlation function. The temperature dependence of the lifetime is used to characterize the temperature profile within the measuring channel. Additionally, in order to calculate the Soret coefficient, we determined the concentration profile by measuring the fluorescence intensity. Aqueous solutions of polystyrene particles containing a fluorescent dye (Firefly, green) in the core of the particle with a diameter of 25 nm (G25) are used for validating the cell compared to TDFRS.

2. Method and materials

2.1. Geometry and fabrication

Fig. 1 (a) and (b) show a schematic and a picture of the thermophoretic microfluidic cell. The cell is made of PMMA, a transparent, bio-compatible and hard polymer. The measuring channel has been micro-milled between a heating and cooling channel. The cell is sealed with a polyvinyl acetate (PVA) cover slip with a thickness

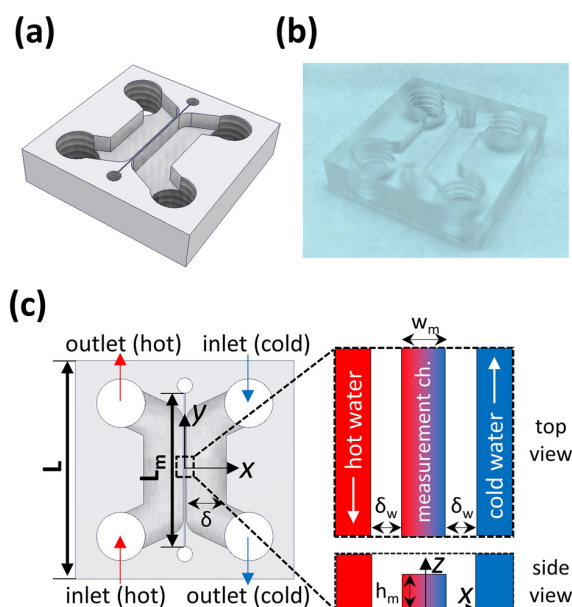


Fig. 1. (a) Schematic drawing and (b) picture of the thermophoretic microfluidic cell. (c) Geometrical target dimensions of the cell are given in the text. Note, that the origin of the coordinate system is in the center of the measuring channel.

of 170 μm . As an adhesive, we used a mixture of dichloromethane and cyclohexane with a volume ratio of 45 to 55.

Geometrical dimensions of the cell are presented in Fig. 1(c). The thickness of the PMMA block is 5 mm and its length is 22 mm to have sufficient space to attach connectors for the cooling and heating channels. The height and width (δ) of cooling and heating channels are 2.2 mm and 4.0 mm, respectively. We maximized the cross-section to reduce the pressure drop in the thermostating channels. The target width (w_m) and height (h_m) of the measuring channel are 127 μm and 100 μm , respectively. However, the fabrication process has a tolerance which is on the order of 20 μm [37] leading to slightly different dimensions which occur along the measuring channel. Using a fluorescent solution inside the measuring channel, we determined $w_m = 93.9$ μm and $h_m = 76$ μm for the fabricated cell. The length of the measuring channel (L_m) is 15 mm. The target wall thickness (δ_w) between the measuring channel and the cooling or heating channel is 100 μm . The ideal volume of the measuring channel is 0.2 μL .

2.2. Experimental set up

Fig. 2 (a) and (b) present the experimental setup of the light and flow path to monitor the sample in the thermophoretic microfluidic cell, respectively. A confocal microscope (Olympus IX-71 with FV3-294 confocal unit) was used for observing the fluorescence intensity and lifetime. A pulsed laser with a wavelength of 485 nm was selected for excitation of the dye in combination with a long-pass emission filter at 500 nm (HQ 500 LP, Leica Microsystems GmbH, Wetzlar, Germany). The fluorescence intensity was recorded by a photomultiplier and the fluorescence lifetime was probed by fluorescence lifetime imaging microscopy (FLIM) using a correlator (PicoQuant, Berlin, Germany). In order to regulate the temperature in the cooling and heating channel, we used two thermostats (cooling: Lauda eco RE 620, Lauda-Königshofen, Germany, heating: Lauda ecoline RE 306, Lauda-Königshofen, Germany). To compensate the heat exchange between thermostating channels, we used a counter-flow to maintain a constant temperature gradient along the measuring channel. The controlled mass

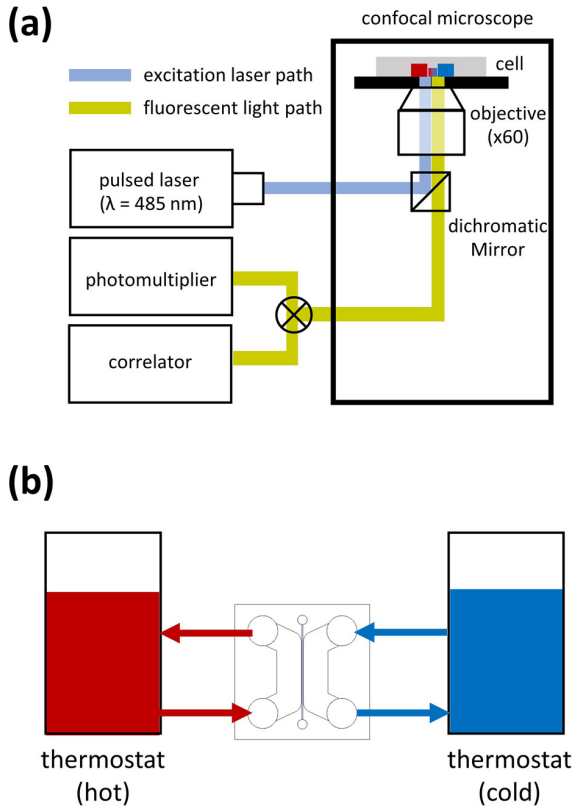


Fig. 2. (a) Light path in the confocal microscope for measuring the Soret coefficient by using the thermophoretic microfluidic cell. (b) Microfluidic cell with cooling and heating channel to induce the temperature gradient.

flow rate by thermostats was maximized to 520 ± 15 g/min. The low temperature was between 5°C and 15°C , and the high temperature was varied between 35°C and 45°C .

2.3. Sample preparation

We used polystyrene (PS) particles (G25, ThermoFisher Scientific Inc.) with a diameter of 25 nm without further treatment. The particles contained inside the core Firefly fluorescence green dye. At $T = 25^\circ\text{C}$ the particle density and the refractive index at a wavelength of 589 nm are $\rho = 1.05\text{g/cm}^3$ and $n = 1.59$, respectively. The particle concentration in a water-based solution with pH = 3.2 is 1 wt%. According to the supplier, ethylenediaminetetraacetic acid (EDTA) and an anionic surfactant were added to stabilize the solution and to prevent aggregation [38].

Solutions are injected into the measuring channel through tubes and syringes by hand. The solutions are filtered through a $0.2 \mu\text{m}$ filter (Whatman Anotop 10) which removes larger particles and the aggregation of the solutions. After that, the measuring channel is closed tightly by a lid to prevent evaporation and concentration changes during the measurement.

For measuring the solutions in TDFRS, the filtered solution is filled into an optical quartz cell (Hellma) with an optical path length 0.2 mm. Solutions were measured two times at the same temperature. Auxiliary parameters, concentration and temperature dependence of the refractive index, are required to calculate Soret coefficient S_T . The refractive index as function of concentration was measured with an Abbe refractometer (Anton Paar Abbemat MW) at a read-out wavelength of 632.8 nm. We measured the refractive index for 5 concentrations to determine $(\partial n/\partial c)_{p,T}$. The change of

the refractive index with respect to temperature, $(\partial n/\partial T)_{p,c}$ was measured interferometrically [39].

2.4. Temperature and concentration ratio measurement

The averaged decaying time of the fluorescence intensity from an excited to ground state typically depends on temperature, therefore we use this temperature sensitivity of the fluorescence lifetime to measure the temperature inside the measuring channel [40]. As fluorescent dye, we used Rhodamine B (RhB, Sigma Aldrich, grade: for fluorescence). The fluorescence correlation function can be recorded for each position in the measuring channel and is then analyzed with a commercial software (SymPhoTime provided by PicoQuant). Using a calibration curve between fluorescence lifetime and temperature (cf. Fig. S1 Supplementary information), the measured lifetime can be converted into a temperature profile. The spatial resolution of the temperature and concentration measurement is $1 \mu\text{m}$ and $0.25 \mu\text{m}$, respectively. The concentration ratio for the Soret coefficient was determined from the fluorescence intensity ratio. After reaching the equilibrium of the concentration profile, the concentration ratio $c(x, y)$ was evaluated as follows,

$$\frac{c(x, y)}{c(x_{\text{ref}}, y)} = \frac{I(x, y)}{I(x_{\text{ref}}, y)} \quad (2)$$

with the intensity $I(x, y)$. y_{ref} is the center of the measuring channel.

2.5. Data evaluation

In a diluted solution ($c \ll 1$), the flux equation in Eq. 1 in the steady state was expressed as,

$$\nabla c = -cS_T \nabla T, \quad (3)$$

with the temperature T and the Soret coefficient S_T . In the measuring channel, one-dimensional temperature gradient happened along a transverse direction of the measuring channel. For this reason, the averaged temperature $\bar{T}(x)$ and concentration ratio $\bar{c}(x)/\bar{c}(x_{\text{ref}})$ along the longitudinal direction of the measuring channel were used for the Soret coefficient. The size of the field of view is $256 \mu\text{m}$ (x) by $256 \mu\text{m}$ (y). The number of pixels for temperature measurement is 256 by 256, so that each pixel is $1 \mu\text{m} \times 1 \mu\text{m}$. The number of pixels for intensity measurements is 1024 by 892 where the length of each pixel is $0.25 \mu\text{m}$ (Δx) by $0.29 \mu\text{m}$ (Δy). The average temperature is calculated from 256 pixels along y -axis in the field of view. The average intensity is calculated by 892 pixels along y -axis. Based on averaged values, we rearranged Eq. 3 using $\nabla c = dc/dx$ and $\nabla T = dT/dx$ as follows:

$$\ln \frac{\bar{c}(x)}{\bar{c}(x_{\text{ref}})} = \ln \frac{\bar{I}(x)}{\bar{I}(x_{\text{ref}})} = S_T (\bar{T}(x_{\text{ref}}) - \bar{T}(x)) \quad (4)$$

According to Eq. 4, the logarithmic concentration ratio depends linearly on the temperature difference $T(x_{\text{ref},y,z}) - T(x, y, z)$. The logarithmic concentration ratio was determined from the logarithmic fluorescence intensity ratio. The slope in the linear relation is the Soret coefficient. The reference location in this study was at the center of the measuring channel.

2.6. Uncertainty analysis

The uncertainty of the Soret coefficient was calculated from the uncertainty of the logarithmic concentration ratio and the temperature. The averaged uncertainty of the intensity ratio was 3.4%. That of the temperature was $\delta T = 0.28$ K. Then, we calculated the uncertainty of the slope, which is identical with the Soret coefficient. We included the deviations of temperature and logarithmic

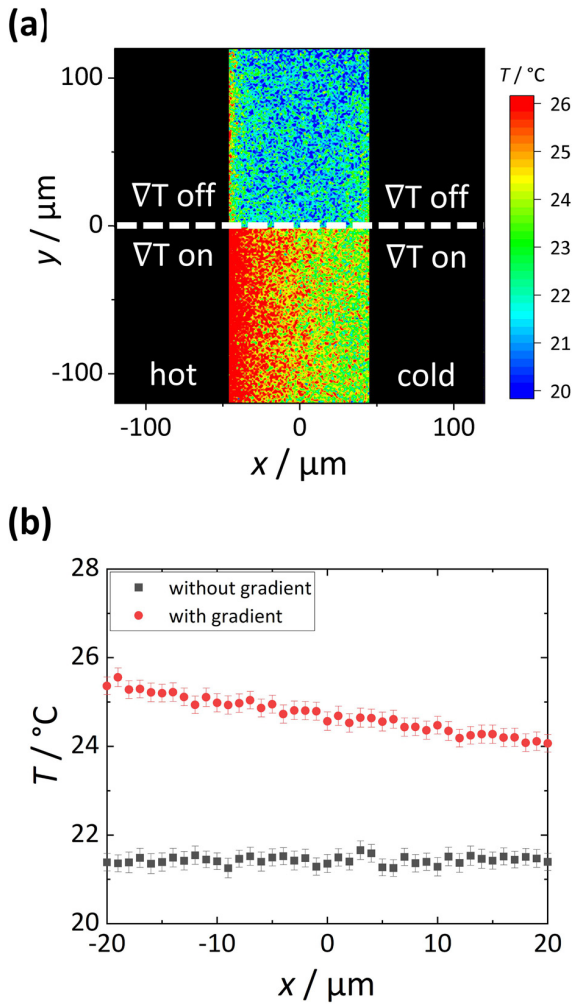


Fig. 3. Temperature distribution measured by fluorescence lifetime imaging microscopy (FLIM) without temperature gradient (upper figure, $T_{mean} = 21.4^{\circ}\text{C}$) and $\nabla T = 34207\text{ K/m}$ (bottom figure, $T_{mean} = 24.7^{\circ}\text{C}$). (b) Graph of the line-averaged temperature along the y-axis as function of x. The resolution of the temperature profile is $1\ \mu\text{m}$.

intensity ratio following the York method [41] implemented in the commercial plot software ORIGIN [42]. This resulted in an averaged uncertainty of the Soret coefficient of 9% based on the 95% confidence level [43].

3. Results

3.1. Temperature profile in the thermophoretic microfluidic cells

In the thermophoretic microfluidic cell, the precise characterization and stability of the temperature profile are crucial since this profile results in the concentration distribution in the measuring channel. Figure 3(a) presents the temperature distribution measured by FLIM without and with a temperature gradient. In the absence of a temperature gradient, we find a homogeneous temperature distribution. Increasing the temperature in the heating channel (left) to 40°C and decreasing the temperature in the cooling channel (right) to 10°C leads to a gradual temperature decrease along the x-axis. The measured temperature in Fig. 3(a) was independent of the y-direction, so that we achieved a one-dimensional temperature profile in the measuring channel as intended.

Fig. 3 (b) shows the y-axis averaged temperature profile across the channel. Without the temperature gradient, the mean temperature is 21.4°C , while with the temperature gradient, the mean temperature at the center of the measuring channel is 24.7°C and a gradient of around $33,000 \pm 1000\text{ K/m}$ establishes inside the measuring channel. Note, that the achieved temperature gradient depends not only on the temperatures of the thermostats, but also on the surrounding temperature. Typically observed gradients lie between of $32,000$ and 34000 K/m . Considering the temperatures in the heating and cooling channel of 10°C and 40°C , we would expect ideally an almost three-times larger temperature gradient of roughly 92000 K/m . The reason for the low temperature gradient is a large temperature drop within the PMMA-wall with a low thermal conductivity with $k = 0.19\text{ W/mK}$ [44] separating the measuring channel from the heating and cooling channel. This implies that the temperature gradient in the measuring channel can be increased by using a wall material with a high thermal conductivity.

In order to characterize the temperature profile for different mean temperatures, we varied the cooling and heating temperature between $5\text{--}15^{\circ}\text{C}$ and $35\text{--}45^{\circ}\text{C}$, respectively. The solid red line in Fig. 4(a) presents the calculated average $T_{calc} = 0.5(T_{cool} + T_{heat})$ in comparison with the measured mean temperature T_{mean} at the center of the measuring channel (diamonds). The mean temperature T_{mean} is the averaged temperature of the y-axis line-averaged temperature as a function of x-axis within $\pm 1\ \mu\text{m}$. In Fig. 4(a), it is shown that the slope of the measured mean temperature is lower than the expected mean temperature (red line). This is caused by a heat exchange between the cell and the surrounding environment at ambient temperature leading to higher temperatures at low and lower temperatures at higher temperatures. The influence of the ambient temperature might be estimated by taking the average of all three temperatures $T_{calc} = (1/3)(T_{cool} + T_{heat} + T_{ambi})$ indicated by the dotted green line in Fig. 4(a). It turns out that the actual measured temperatures lie between the two calculated lines. These observations emphasize that it is necessary to measure the temperature profile within the measuring channel as temperature changes in the environment will have an impact on the profile in the microfluidic cell.

We performed measurements at different mean temperatures by keeping the temperature difference between the heating and cooling channel the same and by varying the temperatures in steps of 2.5°C over a temperature range of 10°C . Figure 4(b) shows the y-axis averaged temperature profiles for different mean temperatures across the channel in the x-direction. In all cases, we observe a one-dimensional temperature profile independent of the mean temperature and similar temperature gradients. The gradients vary from 32000 K/m ($T_{cool} = 7.5^{\circ}\text{C}$, $T_{heat} = 37.5^{\circ}\text{C}$) to 34000 K/m ($T_{cool} = 5^{\circ}\text{C}$, $T_{heat} = 35^{\circ}\text{C}$). As can be seen in Fig. 4(c), the measured temperature gradient does not show a systematic trend with the mean temperature. The fluctuations of the temperature gradient are of the order of 10%.

Additionally, we characterized the temperature profile in y-direction and at different heights z inside the measuring channel to ensure a one-dimensional profile. Fig. 5(a) shows the temperature profile at three different y-positions as function of x, whereas the temperatures of the thermostats where set to 10°C and 40°C . We observe that the temperature profiles differ up-to about 1°C for the three different y-positions. Many factors may be responsible for this discrepancy, such as the heat exchange with the surrounding, fabrication tolerances of the cell and other geometrical differences such as flow connectors and the thermal contact with microscope. If we assume that the heat exchange between the measuring channel and the thermostated channels is the main reason, we expect a monotonous change of the temperature in y-direction gradually decreasing from 3 mm to -3 mm due to the cross flow configuration of the cooling and heating fluid as indicated in the

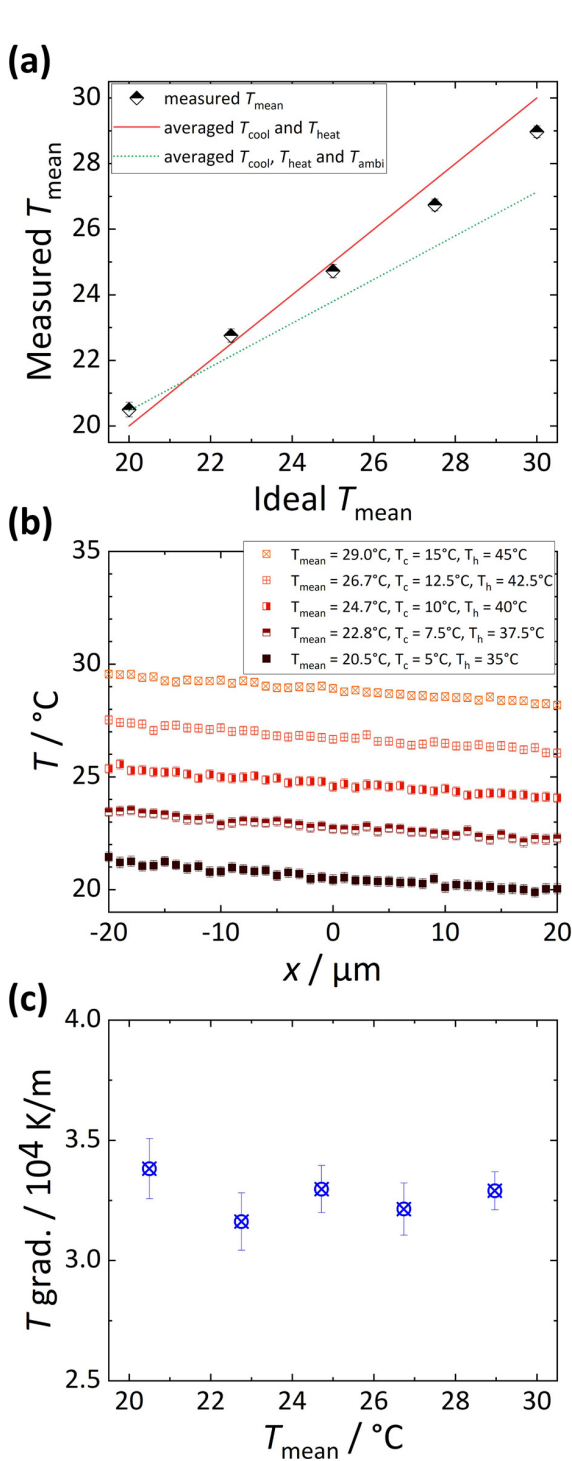


Fig. 4. (a) Comparison of measured and calculated mean temperatures in the measuring channel. The solid red line represents the ideal mean temperature $T_{\text{calc}^{\text{ch}}} = 0.5(T_{\text{cool}} + T_{\text{heat}})$ calculated from the temperatures of the heating and cooling water at T_{heat} and T_{cool} , respectively. The dotted green line corresponds to $T_{\text{calc}^{\text{ch}}} = (1/3)(T_{\text{cool}} + T_{\text{heat}} + T_{\text{ambi}})$ taking the ambient temperature T_{ambi} in the lab into account. (b) Change of the y-axis averaged temperature across the measurement channel for different temperatures in the thermostating channels. Note that only the temperature profile in the center of the measuring channel is shown. (c) Temperature gradient as a function of the mean temperature. (For interpretation of the references to colour in this figure legend, the reader is referred to the web version of this article.)

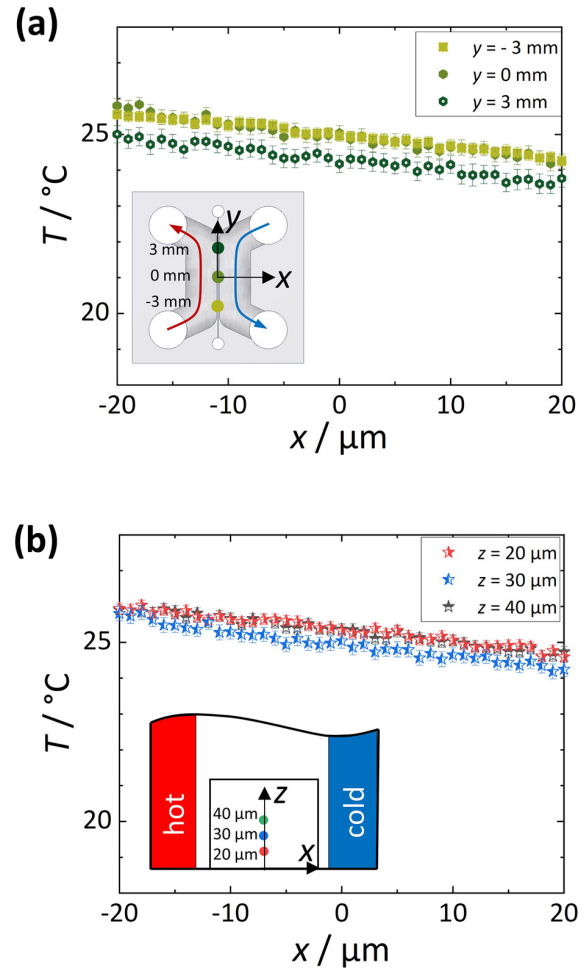


Fig. 5. Graphs of the y-axis averaged temperature as a function of x at (a) three different locations along the measuring channel ($y = -3, 0, 3 \text{ mm}$). The inset illustrates the measuring positions. (b) The y-axis line-averaged temperature at three different heights ($z = 20, 30, 40 \mu\text{m}$). Inset shows the locations.

inset of Fig. 5. However, since there is no systematic temperature variation, the heat exchange with the thermostated channels is not the only reason for this discrepancy. Although the influence of geometric factors cannot be quantified, from Fig. 4(a), we infer that the ambient temperature couples into the small microfluidic chip, but also manufacturing tolerances of the wall between measuring and thermostated channels will influence the observed temperature profile. As shown in Fig. 5(b), temperatures along the z -axis are also slightly different, even though the geometrical changes along the z -axis has a smaller variation than along the y -axis. From these results in Fig. 5(a) and (b), we conclude that the temperature differences along the channel are also caused by geometrical factors. However, the temperature gradient along the y -axis is with 333 K/m only 1% of the temperature gradient along the x -axis, so that we can neglect it. In the following, we consider a one-dimensional temperature gradient along the x -axis for the calculation of the Soret coefficient.

3.2. Intensity ratio profile in the thermophoretic microfluidic cells

Fig. 6 (a) shows an image of the intensity ratio $\bar{I}|_{x=0}$ distribution within the measuring channel. According to Eq. 2, the intensity ratio is identical to the concentration ratio $\bar{c}|_{x=0}$, which is required to calculate the Soret coefficient in Eq. 4. The upper and

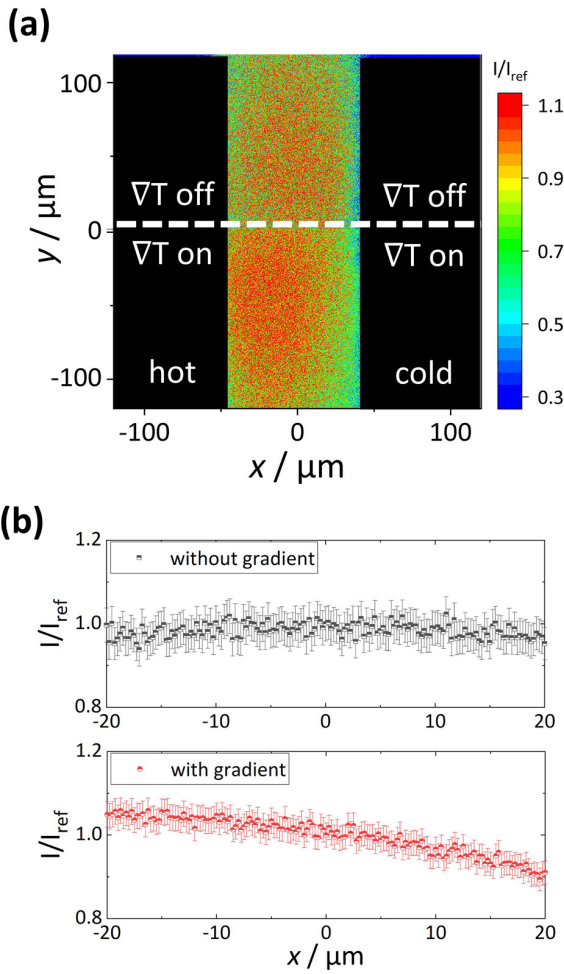


Fig. 6. Image of the intensity ratio distribution measured by fluorescence intensity without temperature gradient (upper figure, $T_{mean} = 21.4^{\circ}\text{C}$) and $\nabla T = 33000\text{ K/m}$ (bottom figure, $T_{mean} = 24.7^{\circ}\text{C}$). (b) Graph of y -axis averaged intensity ratio as a function of x without (top) and with (bottom) temperature gradient, respectively.

bottom parts of Fig. 6(a) have been taken at a mean temperature of $T_{mean} = 24.7^{\circ}\text{C}$ without and with a temperature gradient of $\nabla T = 33000\text{ K/m}$, respectively. In the absence of a temperature gradient, the intensity ratio is constant in the center of the channel, indicating a homogeneous distribution of particles. Towards the walls, we observe a drop of the intensity, which could be caused by reflections at the wall or interfacial effects close to the wall. Therefore, in the following, we restrict our analysis to the center of the cell.

To quantify the intensity ratio profile, the y -axis averaged intensity ratio is used. As shown in the upper part of Fig. 6(b), the intensity ratio is constant without an applied temperature gradient while we observe an asymmetric distribution, if a temperature gradient is applied (cf. bottom part of Fig. 6(b)). The intensity ratio is not linearly varying across the channel, but shows an exponential profile as expected according to Eq. 4.

Before calculating the Soret coefficient, we also need to check the dependence of the concentration ratio on the y - and z -axes in a similar way as for the temperature profile. Fig. 7(a) shows the averaged intensity ratio as a function of x along the y -direction. We observe that the intensity ratio is almost identical at the three locations. This is in contrast to the slight variation of the temperature profile along the y -direction. We assume that although the geometrical differences leading to a temperature difference along the

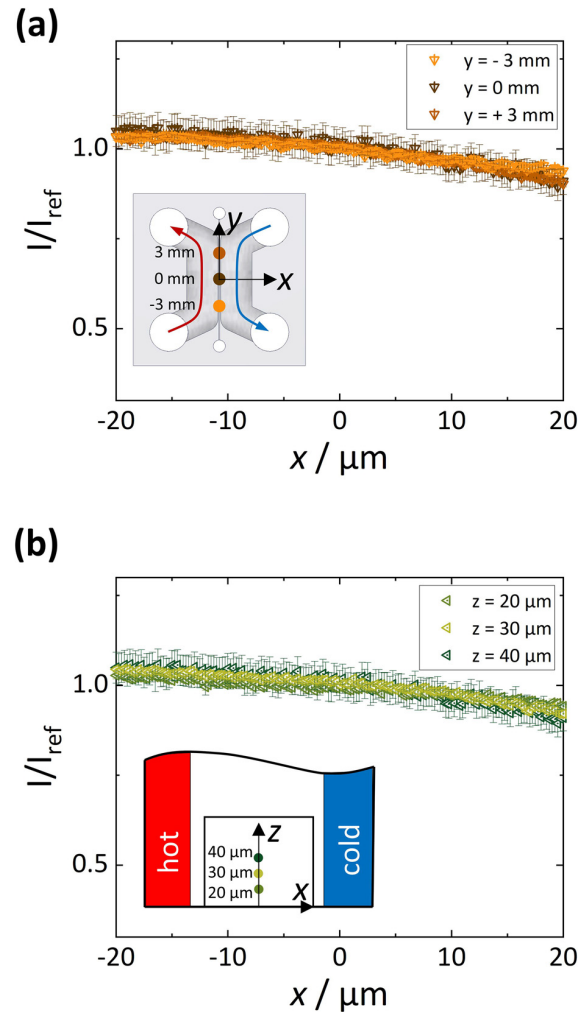


Fig. 7. Graphs of the line-averaged intensity ratio along the y -axis as function of x at (a) three different locations ($y = -3, 0, 3\text{ mm}$) and (b) three different heights ($z = 20, 30, 40\text{ }\mu\text{m}$).

measuring channel, the averaged variation of temperature is within 0.4 K resulting in an intensity ratio modulation of 0.04 , if we assume a Soret coefficient of 0.1 K^{-1} . This implies that the variation of the intensity ratio along the y -axis is negligible. Fig. 7(b) shows that the intensity ratio at different heights also overlaps. Therefore, we can conclude that we have one-dimensional temperature and the concentration ratio profiles in the measuring channel which can be used to calculate the Soret coefficient accordingly.

In addition, we investigated the effect of free convection on the concentration profile in the measuring channel, which would distort the concentration profile. Based on a one-dimensional temperature profile in the measuring channel, we can simulate the temperature and concentration profile. In the simulation, we observe free convection in the measuring channel, whereas the magnitude of free convection velocity is comparable with the thermophoretic velocity (cf. Fig. S2 in the Supplementary Information). Nevertheless, the obtained concentration profiles are almost the same with and without free convection (cf. Fig. S3 in the Supplementary Information). Additionally, the slopes of the logarithmic concentration ratios as function of x and $T - T_{ref}$ along the z -axis overlap, so that we can ignore free convection for the analysis of S_T . Furthermore, we investigate whether measurements of thermophobic particles ($S_T > 0$) are possible. The simulated results of thermophobic

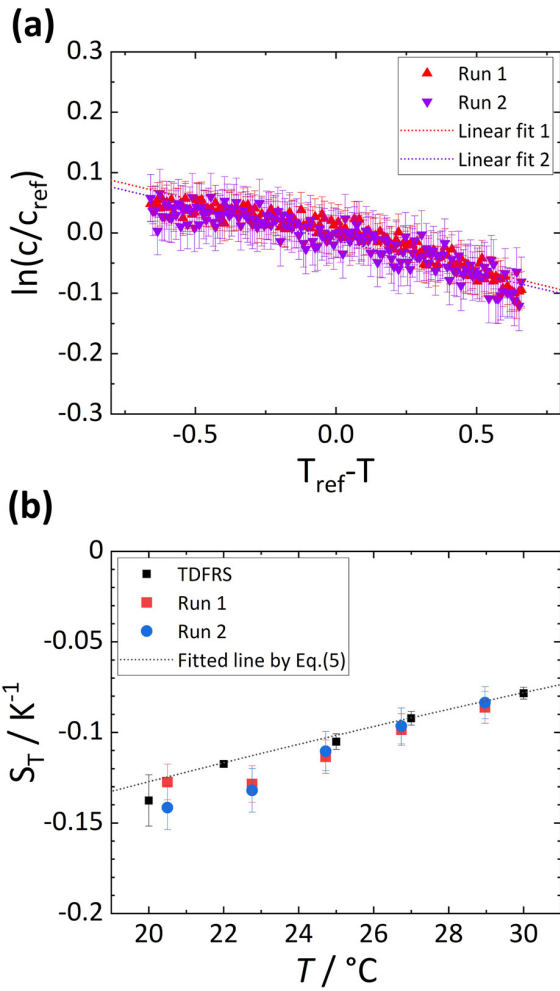


Fig. 8. (a) Logarithmic intensity ratio as a function of temperature difference for run 1 and 2. ($T_{cool} = 10^{\circ}C$, $T_{heat} = 40^{\circ}C$, $T_{mean} = 24.7^{\circ}C$) The red and blue dotted lines refer to a linear fit of the data of run 1 and run 2, respectively. (b) Comparison of the Soret coefficients of unwashed polystyrene particles ($d = 25$ nm, 1%) measured in run 1 (red square), run 2 (blue bullet) and with TDFRS (black square) connected with a dotted line). The dotted line corresponds to a fit of the TDFRS data using Eq. 5. (For interpretation of the references to colour in this figure legend, the reader is referred to the web version of this article.)

particles reveal that the effect on the concentration profile is weak (cf. Fig. S5 in the Supplementary Information). It means that the cell can be used to evaluate S_T of thermophobic particles using Eq. 4. Note that, since the natural convection velocity in the channel is confined by the shortest length of the channel, a smaller channel ensures reliable concentration profiles to determine Soret coefficients. A detailed description of the simulation of free convection and thermophoresis is presented in the Supplementary Information.

3.3. Evaluation of the Soret coefficient

The measured temperature and intensity ratio in the measuring channel were used to calculate the Soret coefficient according to Eq. 4. Figure 8(a) shows the natural logarithm of the measured intensity ratio as function of the temperature difference. During the experiments, we set the cooling and heating fluid temperatures to $10^{\circ}C$ and $40^{\circ}C$, respectively. The solid lines are linear fits of the logarithmic intensity ratio as function of the temperature difference. Note, that the linearly fitted lines of run 1 and

Table 1

Soret coefficients of G25-particles (1% wt) measured in the microfluidic channel cell in comparison with TDFRS results. The uncertainties include the errors of temperature differences and concentration ratios.

$T/^{\circ}C$	S_T/K^{-1} Run 1	S_T/K^{-1} Run 2	$T/^{\circ}C$	S_T/K^{-1} TDFRS
20.5	-0.127 ± 0.010	-0.142 ± 0.012	20	-0.138 ± 0.014
22.8	-0.129 ± 0.010	-0.132 ± 0.012	22	-0.117 ± 0.001
24.7	-0.114 ± 0.009	-0.110 ± 0.011	25	-0.105 ± 0.004
26.7	-0.099 ± 0.009	-0.097 ± 0.010	27	-0.092 ± 0.004
29.0	-0.086 ± 0.009	-0.084 ± 0.009	30	-0.078 ± 0.003

2 overlap. The corresponding slopes are $-0.114 \pm 0.009 K^{-1}$ and $-0.110 \pm 0.010 K^{-1}$, respectively. The uncertainties include the errors of temperature differences and concentration ratios.

Figure 8(b) shows the temperature dependence of the Soret coefficient measured in the microfluidic channel cell. In order to verify the cell, we compared the obtained S_T values with the data measured with the TDFRS set-up, which has been validated in the Fontainebleau benchmark using three binary organic mixtures [45]. Note that, it is impossible to certify the microfluidic cell using the same mixtures, [45] because, with a confocal microscope, we cannot measure concentration changes of organic solvents. The data points shown in Fig. 8(b) and their error bars are additionally listed in Table 1. The fitted curve is described by the empirical equation [46],

$$S_T = S_T^{\infty} \left[1 - \exp\left(\frac{T^* - T}{\tilde{T}}\right) \right], \quad (5)$$

where S_T^{∞} , T^* and \tilde{T} are empirical parameters that refer to the Soret coefficient at infinite temperature, the temperature at which a sign change of S_T occurs, and a parameter to describe the curvature, respectively. The empirical parameters S_T^{∞} , T^* and \tilde{T} determined for the TDFRS data are $0.20 \pm 0.03 K^{-1}$, $323.4 \pm 0.89 K$ and $61.6 \pm 6.32 K$, respectively. It turns out that the averaged deviation of Soret coefficients measured with the microfluidic cell is 7.8% from the fitted curve according to Eq. 5 in the investigated temperature range.

Another advantage of the instrument is that we can control the mean temperature between 20–30°C to perform temperature dependent measurements of the Soret coefficient. The obtained Soret coefficients of the G25-particles increase between 20°C and 30°C from $-0.138 K^{-1}$ to $-0.078 K^{-1}$. A similar weak temperature dependence has been observed before another batch of the same particles [38] and is typical for solutes in water at high dilution and can be described in Eq. 5 [46]. This empirical equation reflects that the thermophoretic behavior of aqueous systems is dominated by hydrogen bonds. With increasing temperature the strength of the hydrogen bonds is weakened leading to an increase of S_T and a decrease of the temperature dependent slope [6]. The latter cannot be observed for the G25 particles in the investigated temperature range, since the temperature dependent slope of S_T remains almost constant.

As mentioned before, the surrounding temperature influences the temperature profile within the measuring channel, therefore an expansion of the temperature range will require a thermostated housing of the set-up to reach a good temperature stability. In conclusion, the proposed thermophoretic microfluidic cell provides reliable and reproducible temperature dependent measurements of S_T .

4. Conclusion

In summary, we propose a thermophoretic microfluidic cell for quantitative measurements of the Soret coefficient of colloidal particles or proteins. In the developed microfluidic cell the actual

measuring channel is located between heating and cooling channel to establish a temperature gradient across the measuring channel. As a test system, we used fluorescently labeled polystyrene particles with a diameter of 25 nm. FLIM with RhB is utilized for probing the spatial temperature profile inside the measuring channel. The established concentration ratio in the steady state is determined from the fluorescence intensity ratio. The characterization of the thermophoretic cell reveals that a one-dimensional temperature profile is achieved. The established concentration ratio profile, which is equal to the measurable intensity ratio profile, is used to determine the Soret coefficient. In the entire investigated temperature range, the obtained S_T -values of the colloidal particles deviate on average by 7.8% from the fitted curve describing the TD-FRS results. We demonstrated further that the device is suitable to perform temperature dependent measurements. So far, we varied the mean temperature between 20°C and 30°C. An expansion of the temperature range will be possible, if a thermostated housing is used to reach a good temperature stability. As mentioned, characterization measurements revealed that the ambient surrounding temperature influences the temperature profile inside the measuring channel. This effect raises as the temperature difference between the measuring channel and the environment increases. In conclusion, the proposed thermophoretic microfluidic cell provides reliable and reproducible temperature dependent measurements of S_T for large colloids ($> 1 \mu\text{m}$) and smaller fluorescently labelled particles or (bio-)macromolecules.

The proposed cell has several advantages compared to conventional methods, which are often limited to binary mixtures. The presented thermophoretic microfluidic device allows the study of specific fluorescently labeled or large solute macromolecules in multi-component mixtures such as buffer solutions. For instance, it will be possible to study the thermophoretic behavior of solutes for buffer solutions of different ionic strength or pH. The thermophoretic microfluidic cell has also a fairly short equilibration time $\tau = w_m^2/(\pi^2 D)$, which depends on the measuring channel width w_m and the mass diffusion coefficient D [47]. Even for larger colloidal particles with a diameter of 1 μm , we find equilibration times of roughly 1 h, which should be accessible if evaporation of the solvent and photobleaching of the dye are prevented. Note that, the sedimentation velocity of 1 μm PS particle is 35.2 nm/s [48]. The channel height is 76 μm , which leads to the retention time of sedimentation of 1.5 hours. Therefore, sedimentation will influence the thermophoretic motion so that a mixture of water and heavy water (D_2O) should be used to match the density of the solvent with that of the particles. Another advantage of this cell is the small channel volume lower than 20 μL including connectors which makes it suitable for the study of rare biological compounds. With this cell, it will also be possible to investigate the thermophoretic movement in nematic phases or a crowded environment. The latter is especially interesting to study transport in biomimetic systems. This device will help to extend our fundamental understanding of thermophoresis in complex environments and might also be suitable to develop new analytical methods to characterize and separate colloidal synthetic and natural particles.

Declaration of Competing Interest

The authors declare that they have no known competing financial interests or personal relationships that could have appeared to influence the work reported in this paper.

CRedit authorship contribution statement

Namkyu Lee: Conceptualization, Investigation, Methodology, Visualization, Writing – original draft, Writing – review & editing.

Shilpa Mohanakumar: Formal analysis, Writing – review & editing. **Simone Wiegand:** Conceptualization, Methodology, Visualization, Writing – review & editing.

Acknowledgments

We thank the JCNS workshop and ZEA 1 for their advice and fabrication of the cells. We are grateful to Jan Dhont for inspiring ideas and his generous support of our work. NL acknowledges the support by the Humboldt foundation and SM acknowledges the support by the International Helmholtz Research School of Biophysics and Soft Matter (BioSoft).

Supplementary material

Supplementary material associated with this article can be found, in the online version, at doi:10.1016/j.ijheatmasstransfer.2022.123002.

References

- [1] S.R. de Groot, *Thermodynamics of Irreversible Processes*, North Holland, Amsterdam, 1966.
- [2] W. Köhler, K.I. Morozov, The Soret effect in liquid mixtures – a review, *J. Non-Equil. Thermodyn.* 41 (2016) 151–197.
- [3] P. Baaske, F.M. Weinert, S. Dühr, K.H. Lemke, M.J. Russell, D. Braun, Extreme accumulation of nucleotides in simulated hydrothermal pore systems, *Proc. Natl. Acad. Sci. USA* 104 (2007) 9346–9351.
- [4] D. Niether, D. Afanasenkau, J.K.G. Dhont, S. Wiegand, Accumulation of formamide in hydrothermal pores to form prebiotic nucleobases, *Proc. Natl. Acad. Sci. USA* 113 (2016) 4272–4277.
- [5] M. Asmari, R. Ratih, H.A. Alhazmi, S. El Deeb, Thermophoresis for characterizing biomolecular interaction, *Methods* 146 (2018) 107–119.
- [6] D. Niether, S. Wiegand, Thermophoresis of biological and biocompatible compounds in aqueous solution, *J. Phys. Condens. Matter* 31 (50) (2019) 503003.
- [7] F. Tian, Z. Han, J. Deng, C. Liu, J. Sun, Thermomicrofluidics for biosensing applications, *VIEW* (2021) 20200148.
- [8] T.J. Salez, B.T. Huang, M. Rietjens, M. Bonetti, C. Wiertel-Gasquet, M. Roger, C.L. Filomeno, E. Dubois, R. Perzynski, S. Nakamae, Can charged colloidal particles increase the thermoelectric energy conversion efficiency? *Phys. Chem. Chem. Phys.* 19 (2017) 9409–9416.
- [9] C.-G. Han, X. Qian, Q. Li, B. Deng, Y. Zhu, Z. Han, W. Zhang, W. Wang, S.-P. Feng, G. Chen, W. Liu, Giant thermopower of ionic gelatin near room temperature, *Science* 368 (6495) (2020) 1091–1098.
- [10] Y. Jia, Q. Jiang, H. Sun, P. Liu, D. Hu, Y. Pei, W. Liu, X. Crispin, S. Fabiano, Y. Ma, Y. Cao, Wearable thermoelectric materials and devices for self-powered electronic systems, *Adv. Mater.* 33 (2021) e2102990.
- [11] P. Ball, J.E. Hallsworth, Water structure and chaotropy: their uses, abuses and biological implications, *Phys. Chem. Chem. Phys.* 17 (2015) 8297–8305.
- [12] S.R. de Groot, P. Mazur, *Non-equilibrium Thermodynamics*, Dover, New York, 1984.
- [13] A. Parola, R. Piazza, Particle thermophoresis in liquids, *Eur. Phys. J. E* 15 (2004) 255–263.
- [14] P.A. Artola, B. Rousseau, G. Galliero, A new model for thermal diffusion: kinetic approach, *J. Am. Chem. Soc.* 130 (2008) 10963–10969.
- [15] A. Würger, Thermal non-equilibrium transport in colloids, *Rep. Prog. Phys.* 73 (2010) 126601.
- [16] S. Di Lecce, T. Albrecht, F. Bresme, The role of ion-water interactions in determining the Soret coefficient of LiCl aqueous solutions, *Phys. Chem. Chem. Phys.* 19 (2017) 9575–9583.
- [17] R. Rusconi, L. Isa, R. Piazza, Thermal-lensing measurement of particle thermophoresis in aqueous dispersions, *J. Opt. Soc. Am. B* 21 (2004) 605–616.
- [18] P. Polyakov, S. Wiegand, Investigation of the Soret effect in aqueous and non-aqueous mixtures by the thermal lens technique, *Phys. Chem. Chem. Phys.* 11 (2009) 864–871.
- [19] W. Köhler, P. Rossmanith, Aspects of thermal-diffusion forced Rayleigh-scattering – heterodyne-detection, active phase tracking, and experimental constraints, *J. Phys. Chem.* 99 (1995) 5838–5847.
- [20] S. Wiegand, H. Ning, H. Kriegs, Thermal diffusion forced Rayleigh scattering setup optimized for aqueous mixtures, *J. Phys. Chem. B* 111 (51) (2007) 14169–14174.
- [21] R. Piazza, Thermal diffusion in ionic micellar solutions, *Philos. Mag.* 83 (2003) 2067–2085.
- [22] A. Königer, B. Meier, W. Köhler, Measurement of the Soret, diffusion, and thermal diffusion coefficients of three binary organic benchmark mixtures and of ethanol-water mixtures using a beam deflection technique, *Philos. Mag.* 89 (2009) 907–923.
- [23] I. Dueramae, M. Yoneyama, N. Shinyashiki, S. Yagihara, R. Kita, Thermal diffusion of aqueous solution of acetylated dextran: the effect of hydrophobicity using optical beam deflection technique, *Int. J. Heat Mass Transf.* 132 (2019) 997–1003.

- [24] M.M. Bou-Ali, O. Ecnarro, J.A. Madariaga, C.M. Santamaria, J.J. Valencia, Thermogravimetal measurement of the solet coefficient of liquid mixtures, *J. Phys.: Condens. Matter* 10 (15) (1998) 3321–3331.
- [25] M. Gebhardt, W. Köhler, What can be learned from optical two-color diffusion and thermodiffusion experiments on ternary fluid mixtures? *J. Chem. Phys.* 142 (2015) 084506.
- [26] P. Blanco, M.M. Bou-Ali, J.K. Platten, D.A. de Mezquia, J.A. Madariaga, C. Santamaria, Thermodiffusion coefficients of binary and ternary hydrocarbon mixtures, *J. Chem. Phys.* 132 (11) (2010) 114506.
- [27] D. Vigolo, R. Rusconi, H.A. Stone, R. Piazza, Thermophoresis: microfluidics characterization and separation, *Soft Matter* 6 (15) (2010) 3489–3493.
- [28] S.A.I. Seidel, P.M. Dijkman, W.A. Lea, G. van den Bogaart, M. Jerabek-Willemsen, A. Lasic, J.S. Joseph, P. Srinivasan, P. Baaske, A. Simeonov, I. Katritch, F.A. Melo, J.E. Ladbury, G. Schreiber, A. Watts, D. Braun, S. Duhr, Microscale thermophoresis quantifies biomolecular interactions under previously challenging conditions, *Methods* 59 (3) (2013) 301–315.
- [29] Y. Zhou, C. Yang, Y.C. Lam, X. Huang, Thermophoresis of charged colloidal particles in aqueous media – effect of particle size, *Int. J. Heat Mass Transf.* 101 (2016) 1283–1291.
- [30] T. Tsuji, K. Kozai, H. Ishino, S. Kawano, Direct observations of thermophoresis in microfluidic systems, *Micro Nano Lett.* 12 (8) (2017) 520–525.
- [31] D. Lauster, S. Klenk, K. Ludwig, S. Nojoui, S. Behren, L. Adam, M. Stadtmüller, S. Saenger, S. Zimmer, K. Hönzke, L. Yao, U. Hoffmann, M. Bardua, A. Hamann, M. Witzernath, L.E. Sander, T. Wolff, A.C. Hocke, S. Hippenstiel, S. de Carlo, J. Neudecker, K. Osterrieder, N. Budisa, R.R. Netz, C. Böttcher, S. Liese, A. Herrmann, C.P.R. Hackenberger, Phage capsid nanoparticles with defined ligand arrangement block influenza virus entry, *Nat. Nanotechnol.* 15 (5) (2020) 373–379.
- [32] A.C. Walls, M.A. Tortorici, B.-J. Bosch, B. Frenz, P.J.M. Rottier, F. DiMaio, F.A. Rey, D. Velesler, Cryo-electron microscopy structure of a coronavirus spike glycoprotein trimer, *Nature* 531 (7592) (2016) 114–117.
- [33] A. Ittner, S.W. Chua, J. Bertz, A. Volkerling, J. van der Hoven, A. Gladbach, M. Przybyla, M. Bi, A. van Hummel, C.H. Stevens, S. Ippati, L.S. Suh, A. Macmillan, G. Sutherland, J.J. Kril, A.P.G. Silva, J.P. Mackay, A. Poljak, F. Delerue, Y.D. Ke, L.M. Ittner, Site-specific phosphorylation of tau inhibits amyloid- β toxicity in alzheimer's mice, *Science* 354 (6314) (2016) 904–908.
- [34] R.-Y. Dong, Y. Zhou, C. Yang, B.-Y. Cao, Experimental study on thermophoresis of colloids in aqueous surfactant solutions, *J. Phys.: Condens. Matter* 27 (49) (2015) 495102.
- [35] N. Lee, S. Wiegand, Thermophoretic micron-scale devices: practical approach and review, *Entropy* 22 (9) (2020) 950.
- [36] Y. Cengel, *Heat and Mass Transfer: Fundamentals and Applications*, McGraw-Hill Higher Education, 2014.
- [37] M. Annoni, L. Rebaioli, Q. Semeraro, Thin wall geometrical quality improvement in micromilling, *Int. J. Adv. Manuf.* 79 (5–8) (2015) 881–895.
- [38] O. Syschyk, D. Afanasenkau, Z. Wang, H. Kriegs, J. Buitenhuis, S. Wiegand, Influence of temperature and charge effects on thermophoresis of polystyrene beads, *Eur. Phys. J. E* 39 (12) (2016) 129.
- [39] A. Becker, W. Köhler, B. Müller, A scanning Michelson interferometer for the measurement of the concentration and temperature derivative of the refractive-index of liquids, *Ber. Bunsen-Ges. Phys. Chem. Chem. Phys.* 99 (4) (1995) 600–608.
- [40] C.B. Müller, K. Weiss, A. Loman, J. Enderlein, W. Richtering, Remote temperature measurements in femto-liter volumes using dual-focus-fluorescence correlation spectroscopy, *Lab Chip* 9 (9) (2009) 1248–1253.
- [41] D. York, N.M. Evensen, M.L. Martínez, J. de Basabe Delgado, Unified equations for the slope, intercept, and standard errors of the best straight line, *Am. J. Phys.* 72 (3) (2004) 367–375.
- [42] OriginPro 2019, Originlab corporation (Northampton, MA, USA).
- [43] R.J. Moffat, Describing the uncertainties in experimental results, *Exp. Therm. Fluid Sci.* 1 (1) (1988) 3–17.
- [44] M.J. Assael, S. Botsios, K. Gialou, I.N. Metaxa, Thermal conductivity of polymethyl methacrylate (PMMA) and borosilicate crown glass bk7, *Int. J. Thermophys.* 26 (5) (2005) 1595–1605.
- [45] J.K. Platten, M.M. Bou-Ali, P. Costeseque, J.F. Dutrieux, W. Köhler, C. Leppla, S. Wiegand, G. Wittko, Benchmark values for the solet, thermal diffusion and diffusion coefficients of three binary organic liquid mixtures, *Philos. Mag.* 83 (2003) 1965–1971.
- [46] S. Iacopini, R. Rusconi, R. Piazza, The macromolecular tourist: universal temperature dependence of thermal diffusion in aqueous colloidal suspensions, *Eur. Phys. J. E* 19 (2006) 59–67.
- [47] S. Wiegand, Thermal diffusion in liquid mixtures and polymer solutions, *J. Phys.: Condens. Matter* 16 (10) (2004) R357–R379.
- [48] M. Braibanti, D. Vigolo, R. Piazza, Does thermophoretic mobility depend on particle size? *Phys. Rev. Lett.* 100 (10) (2008) 108303-1–108303-4.

6 Complementary Experimental

Methods to Obtain Thermodynamic

Parameters of Protein Ligand Systems



Article

Complementary Experimental Methods to Obtain Thermodynamic Parameters of Protein Ligand Systems

Shilpa Mohanakumar ¹, Namkyu Lee ¹ and Simone Wiegand ^{1,2,*}

¹ IBI-4—Biomacromolecular Systems and Processes, Forschungszentrum Jülich GmbH, D-52428 Jülich, Germany

² Chemistry Department-Physical Chemistry, University of Cologne, D-50939 Cologne, Germany

* Correspondence: s.wiegand@fz-juelich.de; Tel.: +49-2461-61-6654

Abstract: In recent years, thermophoresis has emerged as a promising tool for quantifying biomolecular interactions. The underlying microscopic physical effect is still not understood, but often attributed to changes in the hydration layer once the binding occurs. To gain deeper insight, we investigate whether non-equilibrium coefficients can be related to equilibrium properties. Therefore, we compare thermophoretic data measured by thermal diffusion forced Rayleigh scattering (TDFRS) (which is a non-equilibrium process) with thermodynamic data obtained by isothermal titration calorimetry (ITC) (which is an equilibrium process). As a reference system, we studied the chelation reaction between ethylenediaminetetraacetic acid (EDTA) and calcium chloride (CaCl₂) to relate the thermophoretic behavior quantified by the Soret coefficient S_T to the Gibbs free energy ΔG determined in the ITC experiment using an expression proposed by Eastman. Finally, we have studied the binding of the protein Bovine Carbonic Anhydrase I (BCA I) to two different benzenesulfonamide derivatives: 4-fluorobenzenesulfonamide (4FBS) and pentafluorobenzenesulfonamide (PFBS). For all three systems, we find that the Gibbs free energies calculated from S_T agree with ΔG from the ITC experiment. In addition, we also investigate the influence of fluorescent labeling, which allows measurements in a thermophoretic microfluidic cell. Re-examination of the fluorescently labeled system using ITC showed a strong influence of the dye on the binding behavior.

Keywords: thermophoresis; thermodiffusion; Soret effect; protein-ligand binding; hydration effects; entropy–enthalpy compensation; thermal diffusion forced Rayleigh scattering; isothermal titration calorimetry; thermophoretic microfluidic cell



Citation: Mohanakumar, S.; Lee, N.; Wiegand, S. Complementary Experimental Methods to Obtain Thermodynamic Parameters of Protein Ligand Systems. *Int. J. Mol. Sci.* **2022**, *23*, 14198. <https://doi.org/10.3390/ijms232214198>

Academic Editor: Istvan Simon

Received: 2 November 2022

Accepted: 12 November 2022

Published: 17 November 2022

Publisher's Note: MDPI stays neutral with regard to jurisdictional claims in published maps and institutional affiliations.



Copyright: © 2022 by the authors. Licensee MDPI, Basel, Switzerland. This article is an open access article distributed under the terms and conditions of the Creative Commons Attribution (CC BY) license (<https://creativecommons.org/licenses/by/4.0/>).

1. Introduction

Quantification of biomolecular interactions is extremely valuable in applications such as drug discovery and understanding molecular disease mechanisms. Several techniques, such as Bioluminescence Resonance Energy Transfer (BRET) [1], Atomic Force Microscopy (AFM) [2], and Fluorescence Cross-Correlation Spectroscopy (FCCS) [3], have been developed providing binding affinities, kinetics, and/or thermodynamics of the interactions [4]. One of the newer methods is MicroScale thermophoresis (MST) [5]. MST measures the thermophoretic movement of solutes in a temperature gradient by recording the fluorescent intensity. Typically, the binding constant is derived by using multiple capillaries with constant concentrations of protein and increasing ligand concentration. The capillaries are scanned consecutively, so that K_a can be determined, which gives access to the change in Gibbs free energy ΔG and has been demonstrated in a series of experiments [6,7]. Since the technique uses fluorescent detection, either a fluorescent label is attached or the inherent fluorescence of the molecule of interest is detected [8,9]. The fluorescent labeling is very selective and allows low concentrations, but on the other hand the fluorescent label might influence the binding of the ligand. Although the underlying measurement effect is thermophoresis, the Soret and thermal diffusion coefficients are not determined in the commercial instrument, but this will be possible with a modified set-up [10].

Thermodiffusion is quantified by the Soret coefficient $S_T = D_T/D$, with the thermal diffusion coefficient D_T and the diffusion coefficient D [11,12]. A negative S_T indicates thermophilic behavior which means the solute accumulates on the warmer side. While S_T being positive (thermophobic) indicates a movement of the solute towards the colder side. Studies of aqueous systems suggest that the change in the thermodiffusive behavior is often connected with a variation in the hydration shells [13–15]. For certain solutions, a sign change from thermophilic to thermophobic behavior can be observed at a transition temperature T^* [16]. An empirical equation for diluted aqueous solutions proposed by Iacopini and Piazza [17] describes the temperature dependence by,

$$S_T(T) = S_T^\infty \left[1 - \exp\left(\frac{T^* - T}{T_0}\right) \right], \quad (1)$$

where S_T^∞ is a constant value approached at high temperatures, T^* is the temperature at which the sign change of S_T occurs and T_0 indicates the curvature. Equation (1) describes how S_T increases with increasing temperature: S_T is low at lower temperatures approaching a plateau value at high temperatures [13–15]. Solute-solvent interactions play a crucial role in the temperature sensitivity of S_T . In aqueous solutions, this contribution decreases with rising temperature due to breaking of hydrogen bonds [18]. For a number of aqueous systems, the difference of S_T at two different temperatures ΔS_T has found to correlate with $\log P$ (partition coefficient) [14,19]. This indicates that the hydrophilicity of the solute plays a crucial role in the thermophoretic behavior of aqueous systems. $\log P$ or the partition coefficient describes the concentration distribution of a solute between an aqueous and a 1-octanol phase in equilibrium. Thus, P is defined as

$$P = \frac{[\text{solute}]_{\text{octanol}}}{[\text{solute}]_{\text{water}}} \quad (2)$$

Solutes which are highly hydrophilic (low or negative $\log P$) show a stronger change of S_T with temperature compared to more hydrophobic solutes [14]. At low temperatures hydrophilic solutes form many hydrogen bonds with water, while their number and strength decrease with increasing temperature. This means that at lower temperature there is a greater change in the hydration layer, which affects the Soret coefficient to a greater extent [20–22].

To investigate the thermophoretic behavior quantitatively we use Thermal Diffusion Forced Rayleigh Scattering (TDFRS). This is an optical method which analyzes the diffraction efficiency of a refractive index grating due to temperature and concentration modulation. Ideally, the method is applied to binary mixtures, so biological systems with several components (buffer compounds) to stabilize the solution are more challenging because all compounds contribute to the refractive index contrast and complicate the analysis. So far only the strongly binding protein–ligand system streptavidin with biotin has been studied by TDFRS [18,23]. The measurements were supported by neutron scattering experiments and also isothermal titration calorimetry data were included in the analysis [24,25]. Experiments showed that the temperature sensitivity of the Soret coefficient was reduced for the complex compared to the free protein indicating that the complex was less hydrophilic leading to a larger entropy of the hydration layer. The outcome agreed with neutron scattering data. The study of this particular system illustrates that thermodiffusion and its temperature dependence are highly sensitive to changes in the hydration layer. Although the exact mechanism of these changes cannot be evaluated by the study of a single system, measurements of similar systems can give us a more explicit picture on the conformational and hydration changes that occur upon ligand binding.

Isothermal titration calorimetry (ITC) is a standard method for any chemical (binding) reaction [26]. It directly measures the heat released or consumed in the course of a molecular binding event. In addition to thermodynamic parameters, such as enthalpy ΔH , entropy ΔS , and Gibb's free enthalpies ΔG change, the equilibrium-binding affinity K_a and interaction

stoichiometry can be determined. Among the biophysical characterization methods ITC offers the highest information content [4].

A recently developed thermophoretic microfluidic cell was so far only tested with fluorescently labeled colloidal particles [27]. In principle, the cell can also be used to monitor quantitatively the thermophoretic properties of fluorescently labeled free proteins and complexes as used in MST.

Although the thermophoretic behavior of the free protein compared to the protein–ligand complex differs, the microscopic mechanism for this change is not yet understood. The underlying physical effect is one of the interesting unsolved puzzles in physical chemistry. Binding reactions are quite complex, strongly influenced by several factors, such as temperature, concentration, pH, ionic strength, etc., and, in turn, influence the thermophoretic motion [11,12,28]. In this work, due to the complexity of the system and the physical effect, we study chemical binding reactions with TDFRS and ITC. Based on the results of the complementary methods we want to establish a relation between thermodynamic parameters obtained by ITC and thermophoretic properties measured with TDFRS. Additionally, selective ITC measurements and studies in a thermophoretic microfluidic cell were performed to investigate the influence of a fluorescence label on the binding and thermophoretic behavior.

To connect the thermodynamic parameter determined with ITC with the non-equilibrium coefficient derived from TDFRS experiments, we start from an early work by Eastman [29]. In modern notation, his approach connects the Soret coefficient, S_T , to the Gibb's free energy as follows [29,30]:

$$S_T = \frac{1}{k_B T} \frac{dG}{dT} \quad (3)$$

This approach is not viewed uncritically, already de Groot wrote [31], that Eastman's theory is "... certainly not rigorous at all". Integrating Equation (3) with respect to temperature will give us access to a relation between S_T and ΔG for the individual compounds of the system (free protein, free ligand, and complex). A detailed derivation can be found in the Supporting Information Section S1.

How these individual contributions can be used to establish a relation between ITC and TDFRS measurements is illustrated in Figure 1. "A" and "B" correspond to the molecules which are used to form the complex "AB". We measure the free energy change ΔG at two different temperatures with ITC ($\Delta G_{T_{\text{low}}}$ and $\Delta G_{T_{\text{high}}}$). We hypothesize that $\Delta G_{T_{\text{high}}}$ can be calculated from the free energy change at low temperature $\Delta G_{T_{\text{low}}}$ measured by ITC and the differences in $\Delta\Delta G$ corresponding to two temperatures for the individual components probed by TDFRS using the following equation:

$$\Delta G_{T_{\text{high}}} = \Delta G_{T_{\text{low}}} + \Delta\Delta G_{AB} - \Delta\Delta G_A - \Delta\Delta G_B. \quad (4)$$

To test our hypothesis, we use EDTA and CaCl_2 in MES buffer as reference system. The chelation reaction between ethylenediaminetetraacetic acid (EDTA) and calcium chloride (CaCl_2) is a well known reaction which is used as a validation standard for ITC measurements [32]. EDTA exists in several forms in MES buffer [33–35]. Details of the existing forms (Figure S1a,b) can be found in the Supporting Information Section S2. In the next step, we use the same formalism for the protein Bovine Carbonic Anhydrase I (BCA I) with two different ligands. The enzyme BCA I is responsible for the conversion of carbon dioxide to bicarbonate [36] and inhibitors of this enzyme are used for the treatment of glaucoma and epilepsy [37]. Arylsulfonamides have the highest affinity and are mainly used as inhibitors for BCA I [38,39]. In our study, we used 4-fluorobenzenesulfonamide (4FBS) and Pentafluorobenzenesulfonamide (PFBS) (cf. Figure 2). A previous study of BCA II, which is a variant of our enzyme, shows that PFBS binds approximately 25 times stronger than 4FBS at 25 °C [40,41]. Therefore, we assume that the binding for these two ligands differs for BCA I as well, so that we can test our method for varying binding constants.

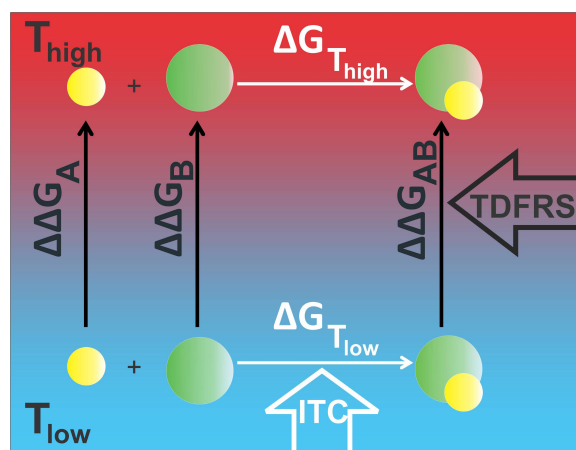


Figure 1. Schematic illustration of the calculation of ΔG and $\Delta\Delta G$ from ITC and TDFRS, respectively.

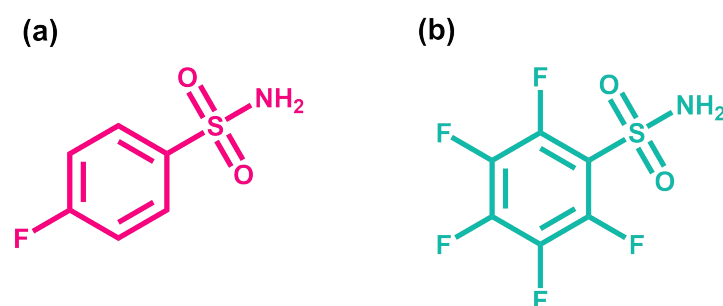


Figure 2. Chemical structure of the two investigated ligands: (a) 4-fluorobenzenesulfonamide (4FBS) and (b) Pentafluorobenzenesulfonamide (PFBS).

2. Results and Discussion

2.1. EDTA–CaCl₂ System

2.1.1. TDFRS Measurements

We conducted IR-TDFRS measurements for the individual components EDTA, CaCl₂, MES Buffer, and EDTA–CaCl₂ complex. Figure 3 shows the temperature dependence of S_T , D_T , and D for EDTA (1 mM), CaCl₂ (10 mM), MES buffer (10 mM), and EDTA–CaCl₂ complex. Temperature dependence of $(\partial n/\partial c)_{p,T}$ and $(\partial n/\partial T)_{p,c}$ used to analyze thermophoretic measurement for each temperature is shown in Supporting Information (Figure S5).

S_T of MES buffer is positive, while CaCl₂ in buffer displays thermophilic behavior ($S_T < 0$). For both systems, the temperature dependence of S_T can be described by Equation (1). The Soret coefficient of MES buffer and CaCl₂ in buffer is of the order of 10^{-3} K^{-1} , while S_T of EDTA and the complex EDTA–CaCl₂ are two orders of magnitude larger (cf. Figure 3(a1)). Therefore, we treat the solutions of EDTA and the complex (EDTA–CaCl₂) as a quasi-binary system analyzing the TDFRS data. The Soret coefficient of the complex shows an increase with temperature, but cannot be described by Equation (1) as it has a turning point. S_T of EDTA decays with increasing temperature with an unusual pronounced drop between 25 °C and 30 °C. In the literature [42–45], there are works reporting a change of behavior in properties of several systems in presence of EDTA around 30 °C compared to that of room temperature, but so far no explanation has been developed. A similar sudden change of S_T with temperature in the same temperature range has been reported for poly(*N*-isopropylacrylamide) (PNiPAM) in water [46]. PNiPAM is a temperature sensitive polymer showing a coil globule transition between 25 °C and 33 °C [47,48]. A small part of the drop of S_T is related to the increase in the diffusion coefficient, but the larger part is caused by the abrupt drop of D_T when the polymer coil collapses [46]. In the case of EDTA as well, the diffusion coefficient shows an abrupt increase between 20 °C and 25 °C, which is 5 K lower than the abrupt drop of S_T and D_T . The mechanism leading to the change in

S_T , D_T , and D of EDTA in water might have the same origin as in the case of PNiPAM as it happens in a similar temperature range so that it is very likely influenced by hydrogen bonds. Bischofsberger et al. [48] argue that at higher temperatures the system minimizes its free energy by gaining entropy through the release of water molecules from the hydration shell. Although the microscopic mechanism is still unclear, this is further evidence that changes in water structure affect thermophoretic motion.

We notice that the diffusion data of EDTA and EDTA–CaCl₂ agree at low temperatures, while they differ clearly at higher temperatures. This might indicate a similar hydrophilicity of EDTA and the complex at low temperatures. Further, we observe, that the diffusion coefficients of MES buffer and the CaCl₂ (10 mM) agree in both cases, as these are small molecules with similar diffusion behavior.

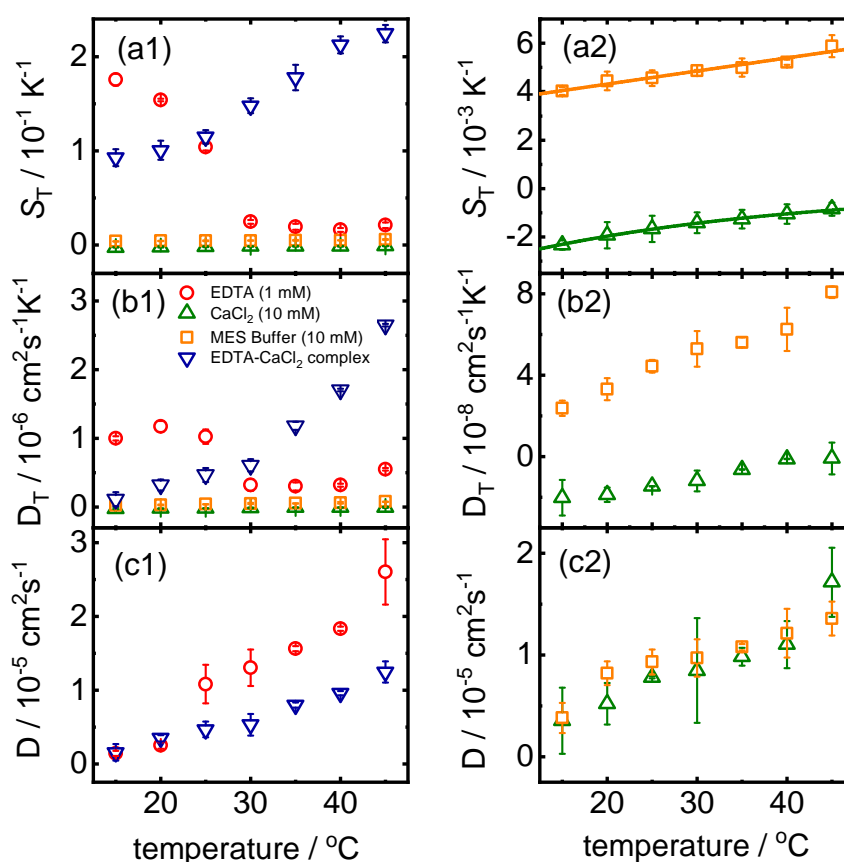


Figure 3. Temperature dependence of (a1) S_T and (b1) D_T for EDTA (1 mM), CaCl₂ (10 mM), MES buffer (10 mM), and EDTA–CaCl₂ complex. Figures on the corresponding right panel is a zoomed in image of temperature dependence of (a2) S_T and (b2) D_T for CaCl₂ and MES buffer. (c1,c2) show the temperature dependence of D for EDTA, EDTA–CaCl₂ complex and CaCl₂, MES buffer, respectively. The error bars correspond to the standard deviation of the mean of repeated measurements. Lines in (a2) corresponds to a fit according to Equation (1).

2.1.2. ITC Measurements

As mentioned before, EDTA–CaCl₂ is a system that has been well studied and characterized using ITC at room temperature [32,49,50]. For our goal we need binding parameters of the system in a wide temperature range. Our results are summarized in Table 1 and an example of a typical ITC measurement of the EDTA–CaCl₂ binding reaction at 25 °C is shown in Figure S7.

Table 1. Thermodynamic parameters of the binding reaction between EDTA and CaCl₂ measured using ITC at different temperatures by setting the stoichiometry of binding $m = 1$ for the fit.

Temperature (°C)	K_d (nM)	ΔH (kJ/mol)
20	510.0 ± 49.0	−17.0 ± 0.3
25	623.0 ± 70.3	−17.2 ± 0.8
30	699.0 ± 55.5	−17.3 ± 0.7
35	852.0 ± 78.9	−17.6 ± 0.5
40	1210.0 ± 123.0	−17.8 ± 0.5
45	1570.0 ± 134.0	−18.0 ± 0.8

The reaction is found to be temperature sensitive and is more favored at lower temperatures. This is similar to what has been observed by Arena et al., monitoring the association constant of the exothermic reaction between EDTA and Ca²⁺ [51], where they found a decrease with increasing temperature.

2.2. Protein–Ligand System

2.2.1. TDFRS Measurements

Temperature dependence of the thermophoretic behavior of the free protein (BCA I), free ligands (4FBS and PFBS), and protein–ligand complexes is shown in Figure 4. Change of D and D_T with temperature for the free protein (BCA I), both ligands (4FBS and PFBS), and protein–ligand complexes is shown in the Supporting Information (cf. Figures S3 and S4). Temperature dependence of $(\partial n/\partial c)_{p,T}$ and $(\partial n/\partial T)_{p,c}$ used to analyze thermophoretic measurement for each temperature is shown in Supporting Information (cf. Figure S6). As expected, the Soret coefficient S_T of free BCA I changes significantly once the ligand binds. S_T -values of the complexes BCA I–4FBS and BCA I–PFBS are higher compared to that of the free protein. It can also be noticed that S_T of both complexes are indistinguishable within the error bars. This means that the hydration shells of the complexes formed are very similar, but different from those of the free protein. Increase in S_T with temperature of BCA I–ligand complex compared to free BCA I is different from that observed for the Streptavidin–biotin (STV-B) system [23]. For STV-B the difference between S_T of the free protein and complex increases with increasing temperature. This was attributed to the stiffness of the protein at low temperatures so that the binding of the ligand (biotin) has a weaker effect at these temperatures [23]. In contrast to this, for both protein–ligand systems that we have studied the difference between S_T of free protein and complex decreases with temperature, so that it is almost negligible at high temperatures. This is an indication that the binding of both the ligands should become weaker with increasing temperature. This is in line with ITC measurements, which will be discussed in detail in Section 2.2.2.

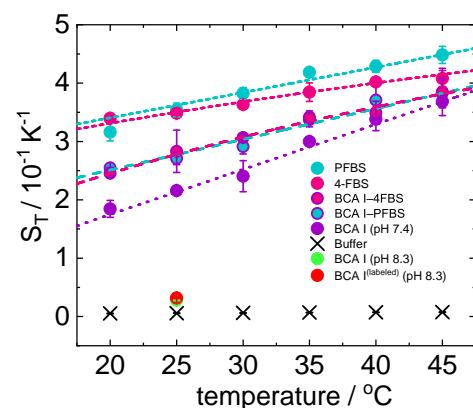


Figure 4. Temperature dependence of S_T for BCA I (10 μ M, pH 7.4, violet bullets), BCA I (10 μ M, pH 8.3, green bullets), labeled BCA I (pH 8.3, red bullets), 4FBS (110 μ M, pink bullets), and PFBS (110 μ M, turquoise bullets), corresponding protein–ligand complex, sodium phosphate buffer (20 mM, Black cross).

Hydrogen bonds have a clear influence on the variation of S_T with temperature. Change in S_T with temperature is more evident, if the solute can form more hydrogen bonds with water [12,23], therefore, we conclude that the free protein is more hydrophilic than the protein–ligand complex (cf. Figure 4). So far, the temperature dependence of the thermophoretic behavior has only been studied for two other binding systems; STV–B and various unmethylated cyclodextrins with acetylsalicylic acid [19,23]. In both cases, the stronger temperature dependence of the free protein or host molecule indicates a lower hydrophilicity of the formed complexes.

As we could not find studies which looked into the reaction mechanism of BCA I with the selected sulfonamide ligands, we compared Human Carbonic Anhydrase I (HCA I) with 4FBS and Bovine Carbonic Anhydrase II (BCA II) with both ligands which have been well characterized [40,52–55]. The active site of the different variants of carbonic anhydrase protein (HCA I, BCA II) is the Zn^{2+} ion that is tetrahedrally coordinated by three histidyl residues and a water molecule [56,57], to which sulfonamide ligands usually bind [39,58]. In the literature, two scenarios of binding of sulfonamide ligands are discussed. The first suggests that sulfonamides are present in the anionic form in their complexes with carbonic anhydrase [40,53–55,59], while the latter proposes neutral sulfonamides are bound to the active zinc ion [53]. The detailed mechanism in both the cases has been discussed by Krishnamurthy et al., [40]. It has to be noted that in both possible scenarios a water molecule is being released upon ligand binding. This implies that the complex is less hydrophilic than that of the free protein, which is what has also been concluded from the thermophoretic data.

In the literature, it has been reported that an increase in fluorination decreases the strength of hydrogen bond network between SO_2NH group and the active site of the target protein [40]. This implies that the complex of BCA I with PFBS (which is highly fluorinated) should show a weaker temperature sensitivity of S_T compared to 4FBS. This is what we observe from our TDFRS measurements as we find; $\Delta S_T = S_T(45^\circ C) - S_T(20^\circ C)$, $\Delta S_T(BCAI-4FBS) = 0.139\text{ K}^{-1}$ and $\Delta S_T(BCAI-PFBS) = 0.128\text{ K}^{-1}$.

2.2.2. Isothermal Titration Calorimetry Measurements

Thermodynamic parameters that have been obtained for the respective binding mechanisms at $25^\circ C$ are reported in Table 2. Figure 5 shows an increase in the dissociation constants for both complexation reactions with temperature which supports the TDFRS measurements. Both ligands show a stoichiometry of 1:1 binding to the protein.

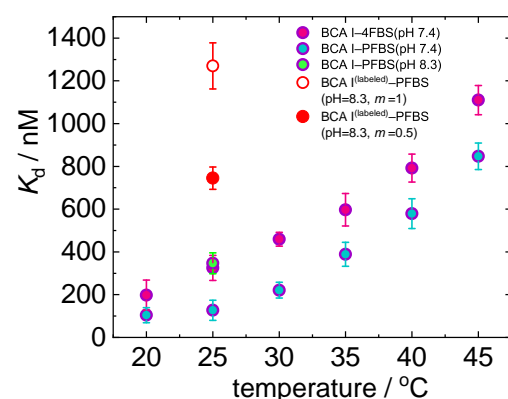


Figure 5. Temperature dependence of K_d for BCA I-4FBS and BCA I-PFBS complexes measured with ITC at $pH = 7.4$. For comparison we show also a single measurement at $25^\circ C$ of the labeled and unlabeled BCA I-PFBS complex at $pH = 8.3$. For the labeled BCA I-PFBS complex, we report two K_d values; red open circle (value that is obtained with $m = 1$) and red closed circle (value that is obtained with $m = 0.5$). More details about the difference in K_d and stoichiometry values of two fits for labeled BCA I are discussed in Section 2.2.3.

Table 2. Thermodynamic parameters of the binding reactions measured using ITC at 25 °C.

System	K_d (nM)	ΔH (kJ/mol)	ΔG (kJ/mol)
BCA I–PFBS	127.0 ± 47.2	− 12.5 ± 0.8	−37.4 ± 2.8
BCA I–4FBS	325.0 ± 58.7	−32.7 ± 0.4	−37.5 ± 1.3

Increase in fluorine substitution is found to enhance the inhibitor power of sulfonamide ligands [60], implying that the more fluorine substituted ligand (PFBS) exhibits a higher association with BCA I, which is reflected by a lower K_d value, compared to 4FBS for all temperatures. Note that the dissociation constants of two ligands differ for BCA I only by a factor of 2.5, while for BCA II a factor of 25 has been reported [40,41].

2.2.3. Measurements with a Thermophoretic Microfluidic Cell

We also used a thermophoretic microfluidic cell for measuring Soret coefficients [27]. This requires the system to be fluorescently labeled to determine the concentration profile. Details of the chemical structure of the dye (cf. Figure S2 in the Supporting Information) used for labeling and the procedure are given in the Supporting Information (cf. Section S3). Since the dye binds at a slightly higher pH = 8.3, we performed additional TDFRS measurements at this pH with the labeled and unlabeled protein. We found $S_T = 0.028 \pm 0.001 \text{ K}^{-1}$ and $S_T = 0.032 \pm 0.001 \text{ K}^{-1}$ for the unlabeled and labeled protein, respectively. Note, that the Soret coefficients measured at pH = 8.3 are roughly an order of magnitude smaller than at pH = 7.4 ($S_T = 0.216 \pm 0.003 \text{ K}^{-1}$). The reason might be that with increasing pH, the solute becomes more negatively charged and can form more hydrogen bonds, which often leads to lower S_T -values [12]. The Soret coefficient $S_T = 0.018 \text{ K}^{-1}$ measured in the microfluidic cell is roughly 40% lower than the TDFRS-value and has a high uncertainty. The measured fluorescence intensity is at the detection limit due to the low fraction of labeled proteins and decays due to photo bleaching. From repeated successful measurements we determine an uncertainty of 0.003 K^{-1} , but the real error might be higher due to systematic errors caused by bleaching.

To check the influence of the fluorescent label on the binding constant, we performed also ITC measurements. Since a change in pH is reported to affect the inhibitory power and activity of sulfonamides and protein, changes in the binding parameters are expected (cf. Figure 6) [61,62]. An increase in pH, shows a decrease in association of PFBS with BCA I (cf. Figure 5). Baronas et al. [63] report a weak increase in the dissociation constant of carbonic anhydrase with primary sulfonamides when the pH changes from 7.4 to 8.3. Once the protein is labeled, the association is only 30% compared to that of the unlabeled free protein at pH 8.3, so that we assume the dye blocks the binding site of the ligand (cf. Figure 5). Additionally, the stoichiometry of ligand:protein changes from 1:1 to 1:2. A hypothesis for this behavior could be the existence of protein dimer, thus a single ligand binding to two proteins as it has been previously reported for lysozyme [64]. Further experiments, e.g., using fluorescent correlation spectroscopy would have to be conducted to support this hypothesis. It has to be noted here that the K_d value reported for labeled BCA I–PFBS binding has a higher uncertainty due to the low protein concentration obtained after fluorescent labeling. More details are given in the Supporting Information (cf. Figure S8 in Section S7).

In conclusion, we refrained from more systematic measurements of fluorescently labeled proteins due to the change of the binding process and the high uncertainty in the microfluidic cell.

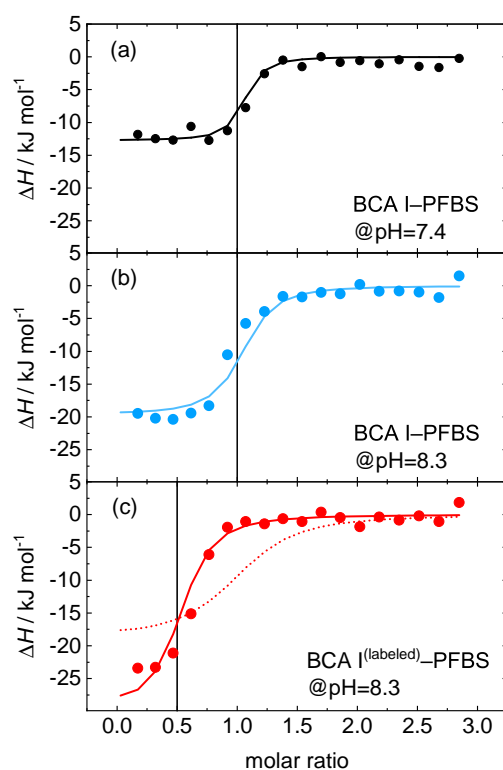


Figure 6. Molar change in enthalpy versus mole ratio of ligand over protein. (a) BCA I–PFBS at pH = 7.4 (b) BCA I–PFBS at pH = 8.3 and (c) the fluorescently labeled BCA I–PFBS at pH = 8.3. Dotted and solid lines corresponds to a fit with the stoichiometry of binding $m = 1$ and $m = 0.5$, respectively. All measurements have been performed at 25 °C.

2.3. Validation of the Relation between Soret Coefficient and Gibb’s Free Energy

This section mainly focuses on validating Equation (4) at two different temperatures which connects ΔG obtained from ITC with S_T obtained from TDFRS. In the forthcoming sections, the calculation corresponds to $T_{\text{high}} = 30$ °C and $T_{\text{low}} = 20$ °C.

2.3.1. EDTA–CaCl₂ System

As mentioned before, the first system that we chose for the validation of the derived mathematical expression is EDTA–CaCl₂. With the S_T values of EDTA, CaCl₂ and the complex measured at T_{high} and T_{low} , we have access to the change in Gibb’s energy ($\Delta\Delta G$) of the individual components. On the basis of our observations, we calculate ΔG (30 °C) to be -36.5 ± 1.2 kJ mol⁻¹, whereas from ITC measurements we obtained -36.4 ± 0.8 kJ mol⁻¹. Both values agree within the error limits. Repeating the calculations for other temperature pairs lead also to an agreement within 10% (cf. Table S1 in Supporting Information).

2.3.2. Protein–Ligand System

Now we apply the same procedure to the protein–ligand systems. In Table 3 we compare the calculated ΔG and the measured ΔG_{ITC} . For both the ligands values agree well within the error bars. Values for other temperature pairs can be found in the Supporting Information (Tables S2 and S3 in Supporting Information).

Table 3. Comparison of ΔG that has been calculated and that has been measured with ITC

System	T _{high} (°C)	T _{low} (°C)	$\Delta G_{\text{calculated}}$ (kJ/mol)	ΔG_{ITC} (kJ/mol)
BCA I-PFBS	30	20	-40.5 ± 1.1	-40.4 ± 1.3
BCA I-4FBS	30	20	-39.9 ± 3.9	-38.2 ± 1.5

3. Materials and Methods

3.1. Sample Preparation

3.1.1. EDTA–CaCl₂ System

Stock solutions of EDTA and CaCl₂ were prepared in 2-(N-morpholino)ethanesulfonic acid (MES) buffer of 10 mM, pH 5.8. EDTA solution of 1 mM and CaCl₂ of 10 mM were used for measurements. For TDFRS samples, these solutions were filtered (0.2 μm) to remove dust particles. The transparent solution was filled into an optical quartz cell (Hellma) with an optical path length of 0.2 mm. For ITC measurements, a calibration kit (Malvern Panalytical) was used as received.

3.1.2. BCA-Ligand System

To prepare the ligand and protein solutions, a sodium phosphate buffer (NaP buffer, pH 7.4, 20 mM) was used. Concentration of BCA I and ligand solutions were determined using UV-Vis absorption spectroscopy. Calibration curves (absorbance vs concentration) for BCA I, PFBS, and 4FBS were prepared starting from the stock solution of 1 mg/mL and measuring the absorbance maxima at 280, 268, and 257 nm, respectively. For BCA I, the concentration of the solution was reconfirmed using molar extinction coefficient of BCA I ($51.0 \times 10^3 \text{ M}^{-1} \text{ cm}^{-1}$) and absorbance measured at 280 nm [65]. For TDFRS experiments BCA I and ligand concentrations of 10 μM and 110 μM were used. For ITC experiments, the same concentration was used for BCA I–PFBS system, while for BCA I–4FBS we had to increase protein and ligand concentrations to 20 μM and 300 μM , respectively.

3.2. Methods

3.2.1. Thermal Diffusion Forced Rayleigh Scattering

Thermodiffusion of all the systems was measured by infrared thermal diffusion forced Rayleigh scattering (IR-TDFRS) [66,67]. This method uses the interference grating of two infrared laser beams ($\lambda = 980 \text{ nm}$) to generate a temperature grating inside an aqueous sample due to the inherent absorption of water at 980 nm [68]. A third laser beam ($\lambda = 633 \text{ nm}$) is refracted by this grating and the intensity of the refracted beam is measured. The intensity is proportional to the refractive index contrast of the grating, showing a fast rise over time due to the thermal gradient, then a slower change of intensity due to diffusion of the solute along the temperature gradient. The Soret, thermal diffusion and diffusion coefficient can be determined from the measurement signal when the refractive index contrast factors $(\partial n / \partial c)_{p,T}$ and $(\partial n / \partial T)_{p,c}$ are known [66].

3.2.2. Contrast Factor Measurement

The change of refractive index with concentration $(\partial n / \partial c)_{p,T}$ was measured by a refractometer (Abbemat MW Anton Paar) at a wavelength of 632.8 nm. Refractive indices for five concentrations at six different temperatures (20–45 °C with a 5 °C gap) were measured to determine $(\partial n / \partial c)_{p,T}$. The concentration dependence of n was linearly fitted to derive the slope $(\partial n / \partial c)_{p,T}$ for all measured temperatures. The refractive index increments with temperature $(\partial n / \partial T)_{p,c}$ were measured interferometrically [69]. Measurements were performed over a temperature range of 20–45 °C, with a heating rate of 1.6 mK/s.

3.2.3. Isothermal Titration Calorimetry

This technique has been extensively used to measure the thermodynamic parameters associated with protein–ligand binding interactions [70]. When a ligand binds to a protein,

thermodynamic potentials (ΔG , ΔH , ΔS) change which can be measured by highly sensitive calorimetry. All other conventional methods measure binding affinity whereas ITC measures the enthalpic and entropic contributions to binding affinity. This technique uses step wise injection of one reagent into the calorimetric cell. The working principle of the instrument has been discussed in the literature [26,70,71].

The calorimetric experiments for our study were performed with a MicroCal PEAQ ITC (Malvern Panalytical). For experiments on the reference system, EDTA (0.1 mM) in MES buffer (pH 5.8, 10 mM) was titrated with CaCl_2 (10 mM) in the same buffer at 6 different temperatures (20–45 °C with 5 °C gap). A typical experiment consisted of 19 injections, 2 μL each. The time interval between injections was 2.5 min. Measurements were conducted 2 times with a new stock solution of EDTA and CaCl_2 received from Malvern Panalytical. The same protocol was followed for BCA I–ligand systems with concentrations as mentioned in Section 3.1.2. For protein–ligand systems, measurements were also recorded at 6 temperatures between 20 and 45 °C at pH 7.4. Additionally, to study the effect of pH and labeling, extra measurements were carried out for BCA I–PFBS system. Binding of this system was monitored at 25 °C for two scenarios: (a) BCA I–PFBS at pH 8.3 and (b) labeled BCA I–PFBS at pH 8.3. Data were analyzed using a single-site binding model subtracting background enthalpies, whereas ΔH and K_d are treated as adjustable parameters.

3.2.4. Thermophoretic Microfluidic Cells

The thermophoretic microfluidic cell can be either operated with large colloids (>500 nm), which are visible under the microscope or with fluorescently labeled macromolecules. The cell was made of PMMA and consisted of three channels [27]. We created a 1D temperature gradient in the measurement channel between the heating and cooling channels. In order to measure the temperature and concentration profile in the channel, a confocal microscope (Olympus IX-71 with a FV3-294 confocal unit) is used. A pulsed laser ($\lambda = 485 \text{ nm}$) was used for probing the fluorescence intensity and lifetime. The fluorescence intensity for the concentration of proteins was measured by a photomultiplier and the fluorescence lifetime in the measurement channel was characterized by fluorescence lifetime imaging microscopy (FLIM) using a correlator and a photomultiplier. The sample concentration of protein (BCA I) in the solution was 20 μM . The labeled protein content was 2.2 μM , which corresponds to 11% of proteins in the solution.

4. Conclusions

The main goal of this work is to investigate whether it is possible to connect thermodynamic parameters obtained by ITC with thermodiffusion parameters determined by IR-TDFRS. For a low molecular weight reference system, EDTA– CaCl_2 and the protein BCA I with two ligands 4FBS and PFBS we were able to relate Soret coefficients with the Gibb's free energies measured at two different temperatures with ITC using an empirical expression suggested by Eastman [29]. For all temperature pairs that have been studied for the aforementioned systems, the Gibb's free energy values of the protein systems calculated agree within 8% with the values measured by ITC, which corresponds to 2-times the uncertainty of the ITC measurements. In the case of the system EDTA– CaCl_2 the agreement is with 3% well within the uncertainty of the ITC measurement. This implies that Soret coefficients measured at different temperatures can be used to predict the Gibb's free energy at other temperatures. This newly developed connection can be utilized to open promising gates in the accurate acquisition of the underlying binding and molecular dissociation mechanisms from the studied systems, if it is combined with molecular dynamic simulations [72] or complementary data obtained by AFM [73].

A second goal was to compare the results of the thermophoretic behavior of the protein and the complex with those obtained in a recently developed thermophoretic microfluidic cell. Fluorescent labeling of the protein is required to monitor the protein concentration using the thermophoretic microfluidic cell. For the here investigated protein BCA I, the flu-

orescent labeling influences the binding interactions severely so that we refrained from systematic thermophoretic measurements of the complex in the thermophoretic microfluidic cell. This is performed more efficiently with an intrinsic fluorescent protein, e.g., green fluorescent protein (GFP) or lysozyme. To gain a deeper microscopic understanding of the process, it would be desirable to perform neutron scattering experiments to determine the entropic contributions of the protein, thus unraveling the entire process [74,75].

Further, we found, that the Soret coefficients of EDTA and the EDTA–CaCl₂ complex show an unusual temperature dependence that cannot be described by Equation (1). Of particular note is the abrupt drop in the Soret coefficient of EDTA between 25 and 30 °C. One finds some studies in the literature that also indicate a change in the behavior of EDTA in the same temperature range, but the database is insufficient to draw clear conclusions. At this point more systematic pH-dependent measurements also of other chelating agents, such as diethylene triamine penta-acetic acid (DTPA) or hydroxyethylethylenediaminetriacetic acid (HEDTA) would be desirable.

Supplementary Materials: The following supporting information can be downloaded at: <https://www.mdpi.com/article/10.3390/ijms232214198/s1>.

Author Contributions: All authors designed the research, S.M. and N.L. performed measurements and the analysis of the data, S.M. prepared the original draft, all authors contributed to the interpretation of the data and the writing and editing of the manuscript. All authors have read and agreed to the published version of the manuscript.

Funding: This research received no external funding.

Data Availability Statement: The data presented in this study are available on request from the corresponding author.

Acknowledgments: Most grateful we are for the support by the group of Jörg Fitter (RWTH Aachen) especially to Olessya Yukhnoevets, who taught us the fluorescent labeling of the protein. We thank Mona Sarter and Andreas Stadler for fruitful and helpful discussions. We are grateful to Peter Lang and Jan Dhont for inspiring ideas and their generous support of our work. SM acknowledges the support by the International Helmholtz Research School of Bio-physics and Soft Matter (BioSoft) and NL acknowledges the support by the Humboldt foundation.

Conflicts of Interest: The authors declare no conflict of interest.

Abbreviations

The following abbreviations are used in this manuscript:

4FBS	4-fluorobenzenesulfonamide
BCA	Bovine Carbonic Anhydrase
EDTA	ethylenediaminetetraacetic acid
ITC	isothermal titration calorimetry
MES	2-(N-morpholino)ethanesulfonic acid
PFBS	Pentafluorobenzenesulfonamide
TDFRS	Thermal diffusion forced Rayleigh scattering

References

1. Verweij, E.W.E.; Bosma, R.; Gao, M.; van den Bor, J.; Al Araaj, B.; de Munnik, S.M.; Ma, X.; Leurs, R.; Vischer, H.F. BRET-Based Biosensors to Measure Agonist Efficacies in Histamine H1 Receptor-Mediated G Protein Activation, Signaling and Interactions with GRKs and β -Arrestins. *Int. J. Mol. Sci.* **2022**, *23*, 3184. [[CrossRef](#)]
2. Marcuello, C.; de Miguel, R.; Martínez-Júlvez, M.; Gómez-Moreno, C.; Lostao, A. Mechanostability of the Single-Electron-Transfer Complexes of Anabaena Ferredoxin-NADP(+) Reductase. *ChemPhysChem.* **2015**, *16*, 3161–3169. [[CrossRef](#)] [[PubMed](#)]
3. Jakobowska, I.; Becker, F.; Minguzzi, S.; Hansen, K.; Henke, B.; Epalle, N.H.; Beitz, E.; Hannus, S. Fluorescence Cross-Correlation Spectroscopy Yields True Affinity and Binding Kinetics of Plasmodium Lactate Transport Inhibitors. *Pharmaceuticals* **2021**, *14*, 757. [[CrossRef](#)]
4. Plach, M.; Schubert, T. Biophysical Characterization of Aptamer-Target Interactions. *Adv. Biochem. Engin. Biotechnol.* **2020**, *174*, 1–15.

5. Jerabek-Willemsen, M.; Andre, T.; Wanner, R.; Roth, H.M.; Duhr, S.; Baaske, P.; Breitsprecher, D. MicroScale Thermophoresis: Interaction analysis and beyond. *J. Mol. Struct.* **2014**, *1077*, 101–113. [[CrossRef](#)]
6. Duhr, S.; Braun, D. Why molecules move along a temperature gradient. *Proc. Natl. Acad. Sci. USA* **2006**, *103*, 19678–19682. [[CrossRef](#)]
7. Reichl, M.; Herzog, M.; Götz, A.; Braun, D. Why Charged Molecules Move Across a Temperature Gradient: The Role of Electric Fields. *Phys. Rev. Lett.* **2014**, *112*, 198101. [[CrossRef](#)]
8. Baaske, P.; Wienken, C.J.; Reineck, P.; Duhr, S.; Braun, D. Optical Thermophoresis for Quantifying the Buffer Dependence of Aptamer Binding. *Angew. Chem. Int. Edit.* **2010**, *49*, 2238–2241. [[CrossRef](#)] [[PubMed](#)]
9. Seidel, S.A.I.; Wienken, C.J.; Geissler, S.; Jerabek-Willemsen, M.; Duhr, S.; Reiter, A.; Trauner, D.; Braun, D.; Baaske, P. Label-Free Microscale Thermophoresis Discriminates Sites and Affinity of Protein-Ligand Binding. *Angew. Chem. Int. Ed.* **2012**, *51*, 10656–10659. [[CrossRef](#)]
10. Stein, J.A.C.; Ianeselli, A.; Braun, D. Kinetic Microscale Thermophoresis for Simultaneous Measurement of Binding Affinity and Kinetics. *Angew. Chem. Int. Ed. Engl.* **2021**, *60*, 13988–13995. [[CrossRef](#)]
11. Köhler, W.; Morozov, K.I. The Soret Effect in Liquid Mixtures—A Review. *J. Non-Equil. Thermody.* **2016**, *41*, 151–197. [[CrossRef](#)]
12. Niether, D.; Wiegand, S. Thermophoresis of biological and biocompatible compounds in aqueous solution. *J. Phys. Condens. Matter* **2019**, *31*, 503003. [[CrossRef](#)]
13. Niether, D.; Afanasenkau, D.; Dhont, J.K.G.; Wiegand, S. Accumulation of formamide in hydrothermal pores to form prebiotic nucleobases. *Proc. Natl. Acad. Sci. USA* **2016**, *113*, 4272–4277. [[CrossRef](#)]
14. Niether, D.; Kriegs, H.; Dhont, J.K.G.; Wiegand, S. Peptide model systems: Correlation between thermophilicity and hydrophilicity. *J. Chem. Phys.* **2018**, *149*, 044506. [[CrossRef](#)]
15. Niether, D.; Di Lecce, S.; Bresme, F.; Wiegand, S. Unravelling the hydrophobicity of urea in water using thermodiffusion: Implications for protein denaturation. *Phys. Chem. Chem. Phys.* **2018**, *20*, 1012–1020. [[CrossRef](#)]
16. Kishikawa, Y.; Wiegand, S.; Kita, R. Temperature Dependence of Soret Coefficient in Aqueous and Nonaqueous Solutions of Pullulan. *Biomacromolecules* **2010**, *11*, 740–747. [[CrossRef](#)]
17. Iacopini, S.; Rusconi, R.; Piazza, R. The “macromolecular tourist”: Universal temperature dependence of thermal diffusion in aqueous colloidal suspensions. *Eur. Phys. J. E* **2006**, *19*, 59–67. [[CrossRef](#)]
18. Niether, D.; Sarter, M.; König, B.; Zamponi, M.; Fitter, J.; Stadler, A.; Wiegand, S. Thermodiffusion as a probe of protein hydration for streptavidin and the streptavidin-biotin complex. *AIP Conf. Proc.* **2018**, *1929*, 020001.
19. Niether, D.; Kawaguchi, T.; Hovancova, J.; Eguchi, K.; Dhont, J.K.G.; Kita, R.; Wiegand, S. Role of Hydrogen Bonding of Cyclodextrin-Drug Complexes Probed by Thermodiffusion. *Langmuir* **2017**, *33*, 8483–8492. [[CrossRef](#)]
20. Schimpf, M.E.; Giddings, J.C. Characterization of Thermal-Diffusion in Polymer-Solutions by Thermal Field-Flow Fractionation—Dependence on Polymer and Solvent Parameters. *J. Polym. Sci. Pol. Phys.* **1989**, *27*, 1317–1332. [[CrossRef](#)]
21. Piazza, R.; Iacopini, S.; Triulzia, B. Thermophoresis as a probe of particle-solvent interactions: The case of protein solutions. *Phys. Chem. Chem. Phys.* **2004**, *6*, 1616–1622. [[CrossRef](#)]
22. Naumann, P.; Becker, N.; Datta, S.; Sottmann, T.; Wiegand, S. Soret Coefficient in Nonionic Microemulsions: Concentration and Structure Dependence. *J. Phys. Chem. B* **2013**, *117*, 5614–5622. [[CrossRef](#)] [[PubMed](#)]
23. Niether, D.; Sarter, M.; Koenig, B.W.; Fitter, J.; Stadler, A.M.; Wiegand, S. Thermophoresis: The Case of Streptavidin and Biotin. *Polymers* **2020**, *12*, 376. [[CrossRef](#)]
24. Sarter, M.; Niether, D.; Koenig, B.W.; Lohstroh, W.; Zamponi, M.; Jalarvo, N.H.; Wiegand, S.; Fitter, J.; Stadler, A.M. Strong Adverse Contribution of Conformational Dynamics to Streptavidin-Biotin Binding. *J. Phys. Chem. B* **2020**, *124*, 324–335. [[CrossRef](#)]
25. Sarter, M.; Niether, D.; Wiegand, S.; Fitter, J.; Stadler, A.M. Complementary approaches to obtaining thermodynamic parameters from protein ligand systems—challenges and opportunities. In Proceedings of the EPJ Web of Conferences, Santiago de Compostela, Spain, 24–28 October 2022.
26. Baranauskiene, L.; Petrikaite, V.; Matuliene, J.; Matulis, D. Titration calorimetry standards and the precision of isothermal titration calorimetry data. *Int. J. Mol. Sci.* **2009**, *10*, 2752–2762. [[CrossRef](#)]
27. Lee, N.; Mohanakumar, S.; Wiegand, S. Thermophoretic microfluidic cells for evaluating Soret coefficient of colloidal particles. *Int. J. Heat Mass Transf.* **2022**, *194*, 123002. [[CrossRef](#)]
28. Würger, A. Thermal non-equilibrium transport in colloids. *Rep. Prog. Phys.* **2010**, *73*, 126601. [[CrossRef](#)]
29. Eastman, E.D. Theory of the Soret effect. *J. Am. Chem. Soc.* **1928**, *50*, 283–291. [[CrossRef](#)]
30. Würger, A. Is Soret equilibrium a non-equilibrium effect? *C. R.-Mec.* **2013**, *341*, 438–448. [[CrossRef](#)]
31. de Groot, S.R. *Thermodynamics of Irreversible Processes*; North Holland: Amsterdam, The Netherlands, 1966.
32. Ràfols, C.; Bosch, E.; Barbas, R.; Prohens, R. The Ca²⁺-EDTA chelation as standard reaction to validate Isothermal Titration Calorimeter measurements (ITC). *Talanta* **2016**, *154*, 354–359. [[CrossRef](#)]
33. Reiter, J. CFD Analysis of EDTA–CaCl₂ Reaction in a Microfluidic Channel to Aid in Design of Novel Calorimeter Device. Ph.D. Thesis, Northeastern University Boston, Boston, MA, USA, 2015.
34. Kula, R.J.; Reed, G.H. Nuclear Magnetic Resonance Investigation of Ligand Exchange Kinetics in the Calcium(II)-EDTA System. *Anal. Chem.* **1966**, *38*, 697–701. [[CrossRef](#)]
35. Carr, J.D.; Swartzfager, D.G. Kinetics of the ligand exchange and dissociation reactions of calcium-aminocarboxylate complexes. *J. Am. Chem. Soc.* **1973**, *97*, 315–321. [[CrossRef](#)]

36. Maren, T.H. Carbonic anhydrase: General perspective and advances in glaucoma research. *Drug Dev. Res.* **1987**, *10*, 255–276. [[CrossRef](#)]
37. Cecchi, A.; Taylor, S.D.; Liu, Y.; Hill, B.; Vullo, D.; Scozzafava, A.; Supuran, C.T. Carbonic anhydrase inhibitors: Inhibition of the human isozymes I, II, VA, and IX with a library of substituted difluoromethanesulfonamides. *Bioorg. Med. Chem. Lett.* **2005**, *15*, 5192–5196. [[CrossRef](#)]
38. Innocenti, A.; Vullo, D.; Scozzafava, A.; Supuran, C.T. Carbonic anhydrase inhibitors: Interactions of phenols with the 12 catalytically active mammalian isoforms (CA I–XIV). *Bioorg. Med. Chem. Lett.* **2008**, *18*, 1583–1587. [[CrossRef](#)]
39. Supuran, C.T.; Scozzafava, A. and Casini, A. Carbonic anhydrase inhibitors. *Med. Res. Rev.* **2003**, *23*, 146–189. [[CrossRef](#)]
40. Krishnamurthy, V.M.; Bohall, B.R.; Kim, C.; Moustakas, D.T.; Christianson, D.W.; Whitesides, G.M. Thermodynamic parameters for the association of fluorinated benzenesulfonamides with bovine carbonic anhydrase II. *Chem. Asian J.* **2007**, *2*, 94–105. [[CrossRef](#)]
41. Krishnamurthy, V.M.; Kaufman, G.K.; Urbach, A.R.; Gitlin, I.; Gudiksen, K.L.; Wiebel, D.B.; Whitesides, G.M. Carbonic Anhydrase as a Model for Biophysical and Physical–Organic Studies of Proteins and Protein–Ligand Binding. *Chem. Rev.* **2008**, *108*, 946–1051. [[CrossRef](#)]
42. Sugiyama, T.; Dabwan, A.H.A.; Katsumata, H.; Suzuki, T.; Kaneco, S. Optimization of Conditions for the Photocatalytic Degradation of EDTA in Aqueous Solution with Fe-Doped Titanium Dioxide. *Open J. Inorg. Non met. Mater.* **2014**, *4*, 28–34. [[CrossRef](#)]
43. Minkevich, I.G.; Satroutdinov, A.D.; Dedyukhina, E.G.; Chistyakova, T.I.; Kaparullina, E.N.; Koshelev, A.V.; Okunev, O.N. The effect of temperature on bacterial degradation of EDTA in pH-auxostat. *World J. Microbiol. Biotechnol.* **2006**, *22*, 1205–1213. [[CrossRef](#)]
44. Yılmaz, Z.; Aktemur, S.; Buzoglu, H.D.; Gümüşderelioglu, M. The Effect of Temperature and pH Variations on the Surface Tension of EDTA Solutions. *J. Endod.* **2011**, *37*, 825–827. [[CrossRef](#)]
45. Pidard, D.; Didry, D.; Kunicki, T.; Nurden, A. Temperature-dependent effects of EDTA on the membrane glycoprotein IIb–IIIa complex and platelet aggregability. *Blood* **1986**, *67*, 604–611. [[CrossRef](#)]
46. Kita, R.; Wiegand, S. Soret coefficient of poly(N-isopropylacrylamide)/water in the vicinity of coil-globule transition temperature. *Macromolecules* **2005**, *38*, 4554–4556. [[CrossRef](#)]
47. Qiu, X.; Koga, T.; Tanaka, F.; Winnik, F.M. New insights into the effects of molecular weight and end group on the temperature-induced phase transition of poly(N-isopropylacrylamide) in water. *Sci. China Chem.* **2013**, *56*, 56–64. [[CrossRef](#)]
48. Bischofberger, I.; Calzolari, D.C.E.; de Los Rios, P.; Jelezarov, I.; Trappe, V. Hydrophobic hydration of poly-N-isopropyl acrylamide: A matter of the mean energetic state of water: A matter of the mean energetic state of water. *Sci. Rep.* **2014**, *4*, 4377. [[CrossRef](#)]
49. Griko, Y.V. Energetics of Ca²⁺-EDTA interactions: calorimetric study. *Biophys. Chem.* **1999**, *79*, 117–127. [[CrossRef](#)]
50. Christensen, T.; Gooden, D.M.; Kung, J.E.; Toone, E.J. Additivity and the physical basis of multivalency effects: A thermodynamic investigation of the calcium EDTA interaction. *J. Am. Chem. Soc.* **2003**, *125*, 7357–7366. [[CrossRef](#)]
51. Arena, G.; Musumeci, S.; Purrello, R.; Sammartano, S. Calcium- and Magnesium-EDTA complexes. Stability constants and their dependence on temperature and ionic strength. *Thermochimica Acta* **1983**, *61*, 129–138. [[CrossRef](#)]
52. Dugad, L.B.; Gerig, J.T. NMR studies of carbonic anhydrase-4-fluorobenzenesulfonamide complexes. *Biochemistry* **1988**, *27*, 4310–4316. [[CrossRef](#)]
53. Olander, J.; Bosen, S.F.; Kaiser, E.T. A study of the binding of two sulfonamides to carbonic anhydrase. *J. Am. Chem. Soc.* **1973**, *95*, 1616–1621. [[CrossRef](#)]
54. Kernohan, J.C. A method for studying the kinetics of the inhibition of carbonic anhydrase by sulphonamides. *Biochim. Biophys. Acta* **1966**, *118*, 405–412. [[CrossRef](#)]
55. Olander, J.; Kaiser, E.T. Binding of 4-hydroxy-3-nitrobenzenesulfonamide, a reporter group labeled inhibitor, to carbonic anhydrases. *J. Am. Chem. Soc.* **1970**, *92*, 5758. [[CrossRef](#)] [[PubMed](#)]
56. Vedani, A.; Huhta, D.W.; Jacober, S.P. Metal Coordination, -Bond Network Formation, and Protein–Solvent Interactions in Native and Complexed Human Carbonic Anhydrase I: A Molecular Mechanics Study. *J. Am. Chem. Soc.* **1989**, *111*, 4075–4081. [[CrossRef](#)]
57. Saito, R.; Sato, T.; Ikai, A.; Tanaka, N. Structure of bovine carbonic anhydrase II at 1.95 Å resolution. *Acta Crystallogr. Sect. D Biol. Crystallogr.* **2004**, *60*, 792–795. [[CrossRef](#)] [[PubMed](#)]
58. Abbate, F.; Supuran, C.T.; Scozzafava, A.; Orioli, P.; Stubbs, M.T.; Klebe, G. Nonaromatic sulfonamide group as an ideal anchor for potent human carbonic anhydrase inhibitors: Role of hydrogen-bonding networks in ligand binding and drug design. *J. Med. Chem.* **2002**, *45*, 3583–3587. [[CrossRef](#)]
59. Lindskog, S.; Thorslund, A. On the Interaction of Bovine Cobalt Carbonic Anhydrase with Sulfonamides. *Eur. J. Biochem.* **1968**, *3*, 453–460. [[CrossRef](#)] [[PubMed](#)]
60. Hansch, C.O.; McClarin, J.U.; Klein, T.E.; Langridge, R.O. A quantitative structure–activity relationship and molecular graphics study of carbonic anhydrase inhibitors. *Mol. Pharmacol.* **1985**, *27*, 493–498.
61. Henry, R.J. The mode of action of sulfonamides. *Bacteriol. Rev.* **1943**, *7*, 175–262. [[CrossRef](#)]
62. Henry, R.P. Techniques for Measuring Carbonic Anhydrase Activity in Vitro. In *The Carbonic Anhydrases*; Dodgson, S.J., Tashian, R.E., Gros, G., Carter, N.D., Eds.; Springer US and Imprint and Springer: Boston, MA, USA, 1991; pp. 119–125.

63. Baronas, D.; Dudutienė, V.; Paketurytė, V.; Kairys, V.; Smirnov, A.; Juozapaitienė, V.; Vaškevičius, A.; Manakova, E.; Gražulis, S.; Zubrienė, A.; et al. Structure and mechanism of secondary sulfonamide binding to carbonic anhydrases. *Eur. Biophys. J.* **2021**, *50*, 993–1011. [[CrossRef](#)]
64. Darby, S.J.; Platts, L.; Daniel, M.S.; Cowieson, A.J.; Falconer, R.J. An isothermal titration calorimetry study of phytate binding to lysozyme. *J. Therm. Anal. Calorim.* **2017**, *127*, 1201–1208. [[CrossRef](#)]
65. Osborne, W.R.A.; Tashian, R.E. Dissociation Constants for Carbonic Anhydrase-Sulfonamide Binding by High-Performance Liquid Chromatography. *Anal. Biochem.* **1984**, *137*, 302–306. [[CrossRef](#)]
66. Wiegand, S.; Köhler, W. Measurement of Transport Coefficients by an Optical Grating Technique. In *Thermal Nonequilibrium Phenomena in Fluid Mixtures*; Springer: Berlin/Heidelberg, Germany, 2002; Volume 584, pp. 189–210.
67. Blanco, P.; Kriegs, H.; Lettinga, M.P.; Holmqvist, P.; Wiegand, S. Thermal Diffusion of a Stiff Rod-Like Mutant Y21M fd-Virus. *Biomacromolecules* **2011**, *12*, 1602–1609. [[CrossRef](#)] [[PubMed](#)]
68. Wiegand, S.; Ning, H.; Kriegs, H. Thermal diffusion forced Rayleigh scattering setup optimized for aqueous mixtures. *J. Phys. Chem. B* **2007**, *111*, 14169–14174. [[CrossRef](#)] [[PubMed](#)]
69. Becker, A.; Köhler, W.; Müller, B. A Scanning Michelson Interferometer For the Measurement of the Concentration and Temperature Derivative of the Refractive- Index of Liquids. *Ber. Bunsen-Ges. Phys. Chem. Chem. Phys.* **1995**, *99*, 600–608. [[CrossRef](#)]
70. Velazquez-Campoy, A.; Leavitt, S.A.; Freire, E. Characterization of protein-protein interactions by isothermal titration calorimetry. In *Protein-Protein Interactions*; Humana Press: New York, NY, USA, 2004; Volume 261, pp. 35–54.
71. Thomson, J.A.; Ladbury, J.E. Isothermal Titration Calorimetry: A Tutorial. In *Biocalorimetry 2*; Ladbury, J.E., Doyle, M.L., Eds.; Wiley: Chichester, UK; Hoboken, NJ, USA, 2004; pp. 35–58.
72. Zhang, Q.; Han, J.; Zhu, Y.; Tan, S.; Liu, H. Binding Thermodynamics and Dissociation Kinetics Analysis Uncover the Key Structural Motifs of Phenoxyphenol Derivatives as the Direct InhA Inhibitors and the Hotspot Residues of InhA. *Int. J. Mol. Sci.* **2022**, *23*, 10102. [[CrossRef](#)]
73. Tapia-Rojo, R.; Marcuello, C.; Lostao, A.; Gómez-Moreno, C.; J Mazo, J.; Falo, F. A physical picture for mechanical dissociation of biological complexes: From forces to free energies. *Phys. Chem. Chem. Phys.* **2017**, *19*, 4567–4575. [[CrossRef](#)]
74. Stadler, A.M.; Koza, M.M.; Fitter, J. Determination of Conformational Entropy of Fully and Partially Folded Conformations of Holo- and Apomyoglobin. *J. Phys. Chem. B* **2015**, *137*, 72–82. [[CrossRef](#)]
75. Stadler, A.M.; Demmel, F.; Ollivier, J.; Seydel, T. Picosecond to nanosecond dynamics provide a source of conformational entropy for protein folding. *Phy. Chem. Chem. Phys.* **2015**, *18*, 21527–21538. [[CrossRef](#)]

7 Discussion and Conclusion

7.1 Discussion

This work mainly focused on the thermophoresis of aqueous ionic solutions and factors influencing this thermophoretic behavior. The study starts with simple salt solutions, which are the major components of buffer solutions in which protein-ligand reactions are studied. The thermophoretic behavior of aqueous salt solutions has been studied by systematically varying cations and anions (Ch. 2, Ch. 3). Certain salt solutions studied depicted a minimum in S_T with concentration. Ch. 4 focuses on understanding the physical picture behind the occurrence of this minimum.

The second part of the thesis investigates the thermodiffusive behavior of more complex systems, which includes binding reactions. A thermophoretic microfluidic cell was developed, which gives access to S_T of fluorescently labeled or inherently fluorescent systems (Ch. 5). Once a temperature gradient is applied, an established concentration gradient is measured from the fluorescent intensity ratio. Characterization of this microfluidic cell reveals that a one-dimensional temperature profile is achieved. Later, this cell is used to compare S_T of a free protein (BCA I) measured with IR-TDFRS (Ch. 6). As discussed in Sec. 1.2.1, the most important application of thermophoresis is monitoring protein-ligand interactions. Although the technique has been used to study different protein-ligand systems, there is very limited microscopic understanding about why the thermodiffusion of free protein changes when the ligand binds to it. S_T and D_T of free protein and protein-ligand complex have been so far reported for streptavidin-biotin complex using IR-TDFRS. Here, the thermophoretic behavior of BCA I-4FBS and BCA I-PFBS systems along with a simpler complex EDTA-CaCl₂ has been studied. The main goal of our investigation was to connect parameters obtained from IR-TDFRS and ITC. Obtained connection is verified using EDTA-CaCl₂

and protein-ligand systems (Ch. 6). This study also reports the difference in S_T between free protein and the protein-ligand complex formed and its connection with changes in the hydration layer.

7.1.1 Correlation with hydrophilicity

For several non-ionic systems, a clear correlation between ΔS_T ($\Delta S_T = S_T(T_2) - S_T(T_1)$), and $\log P$ has been derived from the temperature dependence studies. $\log P$ defines the hydrophilicity of the solute molecule [57]. Partition coefficient, P , is defined as the concentration of solute between two immiscible phases [96], commonly octanol and water, given by

$$P = \frac{[\text{solute}]_{\text{octanol}}}{[\text{solute}]_{\text{water}}}. \quad (7.1)$$

Non-ionic solutes, which are highly hydrophilic (low or negative $\log P$) show a stronger change in ΔS_T (ΔT). For non-ionic solutes, which are soluble in water, hydrogen bonds are predominantly present in the system. At low temperatures, hydrophilic solutes form many hydrogen bonds with water, which are broken as temperature rises. This leads to a stronger change of S_T . We investigated whether the same correlation holds for ionic solutes. As can be seen in fig. 7.1, ΔS_T (ΔT) for ionic solutes are more or less independent of $\log P$. This is an indication that the thermophoretic behavior of ionic solutes is determined predominantly by electrostatic interactions, which are independent of the hydrophilicity.

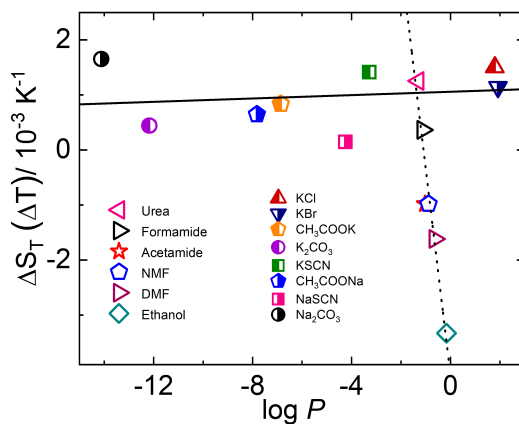


Figure 7.1: Change of $\Delta S_T(\Delta T)$ as a function of $\log P$ for salt systems in comparison with non-ionic systems

To investigate whether there is an influence of hydrophilicity, we further analyzed the temperature and concentration dependence with an ansatz developed by Wittko and Köhler [59], which describes the temperature and concentration dependence of S_T .

$$S_T(m, T) = \alpha(m)\beta(T) + S_T^i, \quad (7.2)$$

with polynomial serial expansions for $\alpha(m)$ and $\beta(T)$

$$\begin{aligned} \alpha(m) &= a_0 + a_1m + a_2m^2 + a_3m^3 + \dots, \\ \beta(T) &= 1 + b_1(T - T_0) + b_2(T - T_0)^2 + \dots \end{aligned} \quad (7.3)$$

T_0 is an arbitrary reference temperature, set to $T_0 = 25^\circ\text{C}$ and S_T^i is a temperature and concentration independent constant. It has to be noted here that a_0 is set to 0 in our analysis as it is strongly coupled with S_T^i . Except for the iodide salts and Na_2CO_3 , all the salt solutions are successfully described using Eq. 7.2.

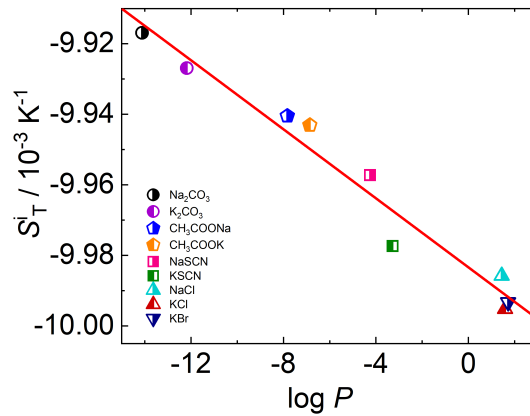


Figure 7.2: Change of S_T^i as a function of $\log P$ for salt systems

Calculated S_T^i values are found to be strongly correlated with $\log P$ as can be seen in Fig. 7.2. Correlation of S_T^i with hydrophilicity, which is existing for ionic solutes and also for non-ionic solutes, is most probably related to the ability of a molecule to form hydrogen bonds. Hence for ionic solutes, thermophoretic behavior is more influenced by specific interactions than by physical parameters such as mass and moment of inertia [57].

A comparison between the hydrophilicity of ions as suggested by Hofmeister and what has

been obtained from thermophoretic measurements is shown in Fig. 7.3. This study suggests that the highly hydrophilic ions tend to accumulate on the colder side or are thermophobic in nature.

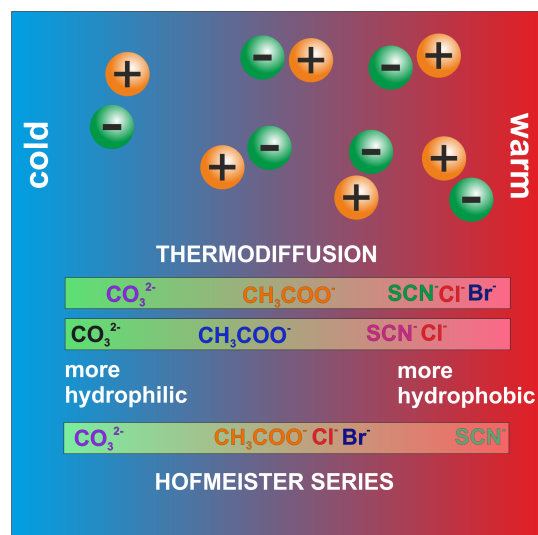


Figure 7.3: Comparison between hydrophilicity of ions suggested by Hofmeister and derived from the data from IR-TDFRS experiments.

7.1.2 Effect of cluster formation

To get a better physical picture of thermodiffusion in salt solutions, it is important to primarily identify what the diffusing entity is. It has often been reported, that with increasing salt concentrations, there are different entities present in the solution [49, 97, 98]. At low concentrations, dissociated ions and ion pairs are the major components of the solution. With increasing concentration, ion clusters can be formed in the solution. This implies that the solution becomes highly heterogeneous and different entities respond to the temperature gradient applied. This will have an effect on the thermodiffusive behavior and more dominantly on the diffusive behavior. In the past several theoretical models have been developed to describe the concentration dependence of D that has been observed experimentally for electrolyte solutions [99]. It has to be noted that most of these theories are only valid at dilute concentrations and are based on the Debye-Hückel ion atmosphere model that includes electrophoretic effects [100–102]. Ions in solution are generally moving under the influence

of two forces; the first one being the gradient of the chemical potential and the second, being an electric field produced by the movement of oppositely charged ions. D is expressed mathematically by following equation based on early work by Nernst [99] and later developed by Onsager and Fuoss [103]

$$D = (D_0 + \Delta_n) \left(1 + c \left(\frac{d \ln \gamma_{\pm}}{dc} \right) \right), \quad (7.4)$$

where D_0 is the Nernst limiting value of the diffusion coefficient, c is the concentration of solute in moles per volume, and γ_{\pm} is the mean molar activity coefficient of the salt. Contribution from the electrophoretic motion is incorporated in the term Δ_n . As per this approach, D shows a decrease with concentration until a point where a minimum is observed. After this point, there is an increase in D with concentration. This theoretical approach fails to explain a monotonous decrease in D with concentration that has been observed experimentally at high concentrations. This is where the formation of clusters plays a crucial role.

Different studies looked into the cluster formation of aqueous salt solutions. Simulation studies report cluster formation for LiCl, NaCl, KCl, NaSCN, KSCN, etc. [49, 98, 104, 105]. Experimental studies using 2C IR and pump/probe study reported cluster formation for aqueous solutions of NaSCN and KSCN [97]. With cluster formation, the size of diffusing entity increases, and a decrease in D is expected with concentration. This is experimentally observed for KSCN. For NaSCN (for which as well cluster formation is reported), an increase in D with concentration is observed as shown in fig. 7.4. Comparing the term $1 + c \left(\frac{d \ln \gamma_{\pm}}{dc} \right)$ from Eq. 7.4 for NaSCN and KSCN, it is found that the increase of the term for NaSCN is four times larger than for KSCN. Thus, there are contradictory contributions to D . For NaSCN, the influence of chemical potential is dominating. None of the studied systems showed a minimum in D in the investigated concentration range as predicted by the theoretical approach mentioned before [106].

Other studies of salt solutions suggest that different clusters are formed [104, 107]. While certain salt solutions form closely packed ion structures, some others build clusters that incorporate water molecules. The latter solutes tend to have a high solubility in water due to the formation of these clusters, which contains water molecules. Cations are found to have a prominent effect on deciding which type of cluster is formed in the solution [104].

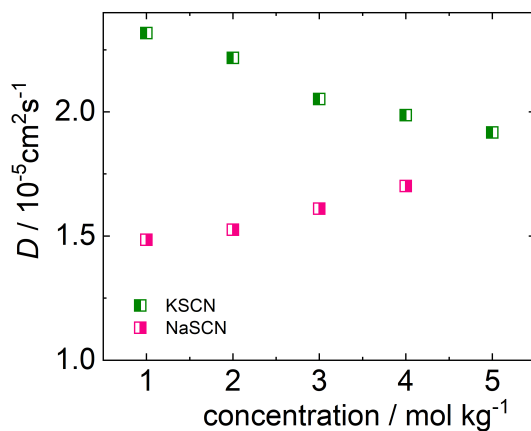


Figure 7.4: Change of diffusion coefficient D for KSCN and NaSCN with concentration at a temperature of 25 °C

The type of cluster formed will also have an effect on the thermophoretic behavior, although that has not yet been studied systematically.

7.1.3 Changes in the hydration shell

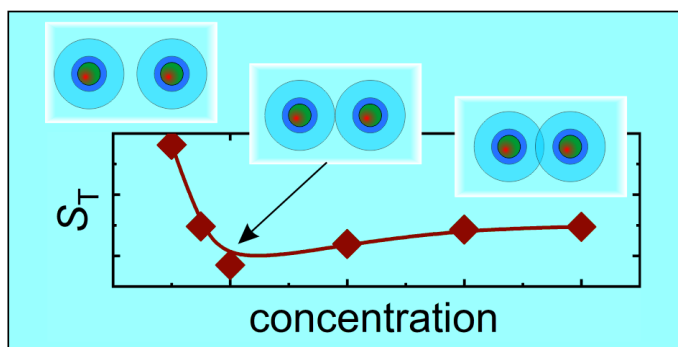


Figure 7.5: Graphical representation of the hydrated salt molecules overlapping with concentration. Corresponding variation of S_T with concentration is also shown.

A common thermophoretic behavior that has been observed for several aqueous salt systems like NaCl, LiCl, NaSCN, KSCN, etc. is a non-monotonous change in S_T with concentration. Some of the salt systems show a decrease in S_T until a concentration, where a minimum is observed and then an increase with concentration. For iodide salt solutions (LiI, NaI, and KI), it is observed that the concentration at which the minimum occurs is very almost

identical, hinting that the relevant length and energy scales are similar in all cases. Based on this observation, a preliminary model is developed to explain the occurrence of minimum in S_T , which primarily considers the changes, that happen in the hydration layer with an increase in salt concentration.

Ions have always been reported to interact with the hydrogen bonding network of water. Evidently, in dense solutions, solvent molecules have to reorganize their structure to incorporate the solute molecules. A simple model for the changes that happen in the water structure once an ion has been introduced is proposed by Frank and Wen [108]. The model suggests an immobilized layer of water molecules near the ion followed by a region of "broken water structure". This is then followed by the normal structure of water. This change in the structure of water around salt systems has been confirmed with simulations and neutron diffraction experiments [109–113]. From various studies, it can be concluded that beyond the first shell of water molecules (which is highly structured) a second shell of decreasingly perturbed water molecules is needed to gradually adjust to the structure of bulk water. It is important to note here that we treat salt molecules as single particles as the transport coefficients measured are assigned to non-dissociated salt molecules. A fully hydrated salt molecule (FHP), which is considered in the model consists of a bare salt molecule along with the closely packed first shell of water molecules and the shell of perturbed water molecules. The model assumes that S_T will monotonously decrease with concentration up to random close packing of FHPs. It is hypothesized that at this concentration where a minimum is observed, the perturbed layer of water molecules is touched. Beyond this concentration, they start to overlap, and hence a change in the behavior of S_T is observed. A schematic representation of this scenario is shown in Fig. 7.5.

The validity of the model can be tested in two ways; either by performing simulations or by extracting information from existing studies. We utilized the second option, where we extract the information from the simulation studies that were conducted by Artola and Rousseau for Lennard-Jones mixtures [16]. Simulations by them were performed over the full range of mole fractions. Results from the study by Artola and Rousseau [16] show that S_T changes linearly with mole-fraction. We use the reported data in their paper, with consideration of our model to predict how S_T changes beyond the concentration at which minimum is observed. At the minimum concentration, we estimate the size of the entity that could be present in the solution. This coincides with the size of the salt molecule with the strongly attached

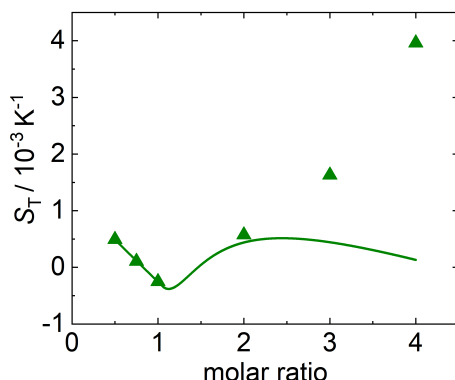


Figure 7.6: Concentration dependence of S_T of KI at a temperature of 25 °C. Line corresponds to fit that have been obtained with the model discussed in Sec. 7.1.3

first hydration shell and the perturbed layer of water molecules. A detailed discussion of these calculations can be seen in Ch. 4. An overlap between the perturbed water layers beyond the minimum concentration gives rise to a type of depletion interaction between the salt molecules. Our model is being mapped to the simulation results by Artola and Rousseau. A result of this mapping for KI at 25° C is shown in Fig. 7.6. As can be noticed, S_T values predicted by the model are in good agreement with the experimental data till a concentration of 2 mol/kg. Beyond this concentration, deviations between experimental and predicted data increase with concentration. Thus at larger concentrations, the model becomes inadequate. Pairwise addition of self energies, which have been considered in this model might be inappropriate at higher concentrations (discussed in detail in Ch. 4). Also, clusters are probably formed at higher concentrations, and contributions from these clusters are not considered in the current state of the model.

7.1.4 Thermodiffusion of complexes

As discussed in Sec. 1.1, thermodiffusion is very sensitive to complex formations. Hence, thermodiffusion can be used as an effective tool to probe complex formation and understand interactions involved. Previously, thermodiffusion has been used to study the complex formation of cyclodextrins (CD) with small drug molecules [114]. Later, the binding of biotin with the protein streptavidin has also been studied with thermodiffusion [80,81].

7.1.4.1 IR-TDFRS measurements

To have more insight into the complex formation a first investigation is carried out for a simple reaction, ethylenediaminetetraacetic acid (EDTA) with CaCl_2 in 2-(N-morpholino)ethanesulfonic acid (MES) buffer. The magnitude of S_T for EDTA and EDTA- CaCl_2 are two orders of magnitude larger than that of CaCl_2 and MES buffer. Only CaCl_2 and MES buffer follow the typical temperature dependence of S_T , which is described by Eq. 1.3. Although, S_T of complex shows an increase with temperature, it cannot be described with Eq. 1.3. S_T of EDTA shows a decrease in temperature with a drop between 25°C and 30°C. Alongside, D shows an abrupt increase between 20°C and 25°C. A similar behavior has been observed for a temperature sensitive polymer PNiPAM, which is connected to changes, that occur in the interaction between PNiPAM and water molecules [115]. Bischofsberger *et al.* [116] argue that at higher temperatures the system minimizes its free energy by gaining entropy through the release of water molecules from the hydration shell. EDTA is a molecule that exists in different charged forms in the solution, which will have interactions with water molecules. Hence in the temperature range where a behavior change is observed, it is more likely that the interactions, which include hydrogen bonds are influencing the thermodiffusive behavior. To fully unveil the microscopic mechanism, more studies have to be conducted with EDTA at different pH and that of other chelating agents.

As a next step, the complex formation of protein Bovine Carbonic Anhydrase I (BCA I) with two aryl sulfonamide ligands(4-fluorobenzene sulfonamide (4FBS) and Pentafluorobenzene sulfonamide (PFBS)) has been investigated. This has been discussed in detail in Ch. 6. S_T of the complexes formed are similar but different from that of the free protein. This indicates that the hydration shells of the complexes formed are very similar but different from that of the free protein. For streptavidin-biotin complex, which is a system that has been studied with thermodiffusion, the difference between S_T of the free protein and complex increases with increasing temperature [80,81]. Whereas for BCA I-ligand complexes, that are studied here, the difference between S_T of free protein and complex decreases with temperature. This is an indication that the binding of both ligands should become weaker with increasing temperature. Weakening the binding of ligand to BCA I with temperature is in line with the dissociation constant K_d , which increases with temperature as shown in Fig. 7.7(b).

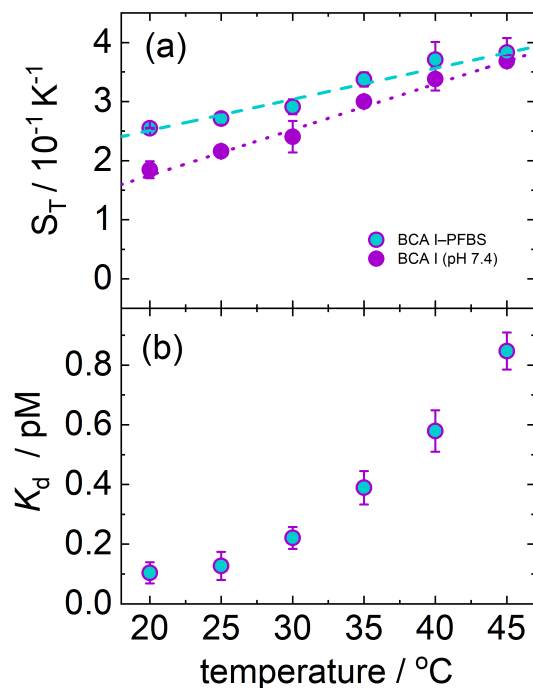


Figure 7.7: (a) Soret coefficient S_T against temperature for free protein BCA I and BCA I-PFBS complex in sodium phosphate buffer (b) Dissociation constant K_d against temperature for BCA I-PFBS complex.

From IR-TDFRS measurements, it can be concluded that the free protein is more hydrophilic than the protein-ligand complexes, in both cases. The interaction of different variants of this protein with both ligands has been well studied and characterized in literature [117–120]. Sulfonamides usually bind to the Zn^{2+} active site that is present in the protein. Two scenarios for this binding process have been proposed as shown in Eq. 7.5 and Eq. 7.6. Sulfonamides can bind to the free protein in anionic [117,119–122] (Eq. 7.5) or neutral form [119] (Eq. 7.6).



In both the above mentioned mechanisms, a water molecule is released once the ligand binds. This in turn implies that the complex is less hydrophilic than the free protein, which has also been concluded from IR-TDFRS measurements. To obtain a deeper microscopic

understanding of the process, it would be desirable to perform neutron scattering experiments to determine the entropic contributions of the protein.

7.1.4.2 Measurements using a thermophoretic microfluidic cell

A thermophoretic microfluidic cell, which is newly developed was also used to measure S_T of the free protein and compare it with IR-TDFRS measurements. The system needs to be fluorescently labeled to determine the concentration profile using the developed microfluidic cell. Fluorescent labeling required the pH of the system to be changed from 7.4 to 8.3 and the binding reactions are usually sensitive to changes in pH. Hence, fluorescent labeling also will influence the thermodiffusive behavior of the protein. Note that, S_T of BCA I at pH 8.3 is an order of magnitude lower than that at pH 7.4 measured with IR-TDFRS. This could be connected to the change, that happens with an increase in pH, where protein could become more negatively charged and hence could form more hydrogen bonds, which will give a lower S_T value. Besides, S_T measured with the microfluidic cell is roughly 40% lower than the TDFRS-value and has high uncertainty. It can be concluded that the measured fluorescence intensity is at the detection limit due to the low fraction of labeled proteins and decays due to photobleaching. Hence the real error might be higher due to systematic errors caused by bleaching.

7.1.4.3 Factors affecting thermodiffusion of complexes

As has already been discussed, thermophoretic microfluidic cell required the protein to be fluorescently labeled and hence pH of the system to be changed. A part of this work focused on investigating the effect of fluorescent labeling on binding reactions and thermodiffusive behavior. Fluorescent labeling can change the binding affinities for different proteins and hence it was necessary to check the same for the BCA I-ligand systems as well. A change in pH has been reported to affect the inhibitory power and activity of sulfonamides and protein [123,124]. The effect of fluorescent labeling and pH on the binding mechanism is investigated through ITC experiments. Changing pH from 7.4 to 8.3 increases the dissociation by 2.5 times. Additionally, fluorescent labeling of the protein increases the dissociation by 3.5 times compared to that at pH 8.3, which could be due to the dye blocking the binding site of the ligand. Hence changing the pH and fluorescently labeling the protein is found to have a

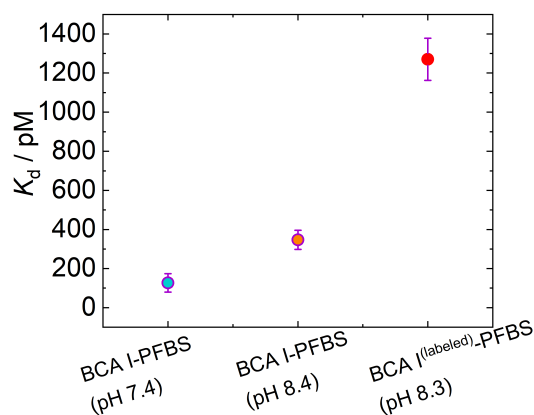


Figure 7.8: Dissociation constants at different experimental conditions (as explained in *x*-axis) for BCA I-PFBS complex measured at 25°C. K_d of BCA I(labeled)-PFBS at pH 8.3 corresponds to the value obtained with a fit of stoichiometry (m)=1

pronounced effect on the binding process. A comparison of the dissociation constants in different scenarios is shown in Fig. 7.8. Additionally, the stoichiometry of ligand:protein changes from 1:1 to 1:2 when the protein is fluorescently labeled. A hypothesis for this behavior could be the existence of protein dimer, thus a single ligand binding to two proteins as it has been previously reported for lysozyme [125], but this can only be confirmed with the help of fluorescent correlation spectroscopy.

7.1.5 Connecting parameters of equilibrium (ITC) and non-equilibrium (IR-TDFRS) experimental techniques

Two different experimental techniques have been utilized in this work to gain a deeper understanding of binding reactions. The first technique, IR-TDFRS which is a non-equilibrium technique measures the thermodiffusive behavior of the system. The latter one, ITC is an equilibrium technique that measures the thermodynamic parameters associated with the binding reaction. To get a profound insight into the binding mechanism, we investigated whether the non-equilibrium coefficient (S_T) can be related to equilibrium property (ΔG). To connect these parameters, we start from an early work by Eastman [126], which is expressed in modern notations [127] as

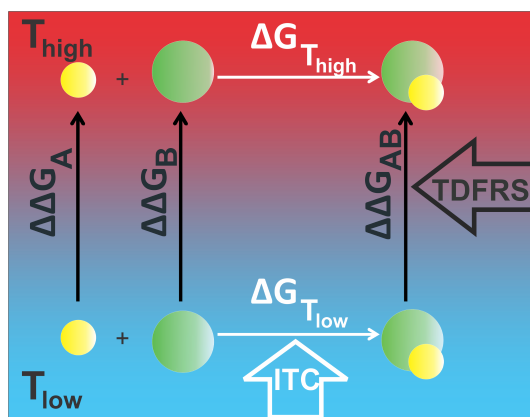


Figure 7.9: Schematic illustration which is used to calculate ΔG at a particular temperature from the calculated values.

$$S_T = \frac{1}{k_B T} \frac{dG}{dT}. \quad (7.7)$$

Assuming a linear T -dependence of S_T with T and integrating Eq. 7.7 will give access to a relation between S_T and ΔG for a mole of molecules of free protein, free ligand, or complex as follows

$$\Delta\Delta G = N_A k_B \left(S_T^{\text{slow}} + \Delta S_T \right) \left(\frac{T_{\text{high}}^2 - T_{\text{low}}^2}{2} \right). \quad (7.8)$$

IR-TDFRS measurements give access to S_T values of the free protein, free ligand, and complex at different temperatures. For systems in which the binding is not strong, there are chances of free ligands or free proteins present in the solution. The measured S_T value will have contributions from the complex and unbound compounds in such cases. How the various contributions can be separated and has been discussed in detail in Ch. 6.

Later, values obtained from Eq. 7.8 are utilized to calculate ΔG at a particular temperature and compare it with the value measured at the same temperature using ITC. An illustration of this is shown in Fig. 7.9. “A” and “B” correspond to the molecules, which are used to form the complex “AB”. Free energy change ΔG at two different temperatures are measured using ITC ($\Delta G_{T_{\text{low}}}$ and $\Delta G_{T_{\text{high}}}$). Following equation is proposed to calculate $\Delta G_{T_{\text{high}}}$

$$\Delta G_{T_{\text{high}}} = \Delta G_{T_{\text{low}}} + \Delta\Delta G_{\text{AB}} - \Delta\Delta G_{\text{A}} - \Delta\Delta G_{\text{B}}. \quad (7.9)$$

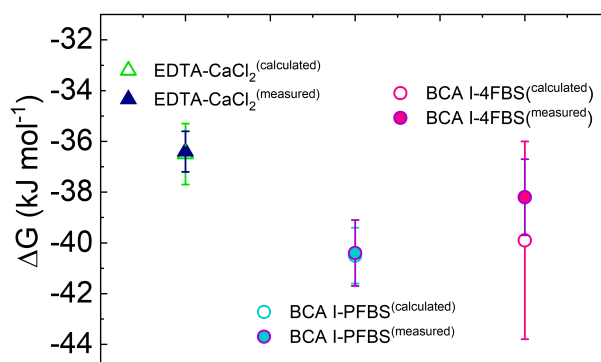


Figure 7.10: ΔG calculated with Eq. 7.9 plotted along with ΔG measured using ITC for EDTA-CaCl₂, BCA I-PFBS and BCA I-4FBS complexes. For the plotted values, $T_{\text{low}}=20^{\circ}\text{C}$ and $T_{\text{high}}=30^{\circ}\text{C}$

Three binding reactions that have been studied before are used to check the validity of the derived equation. Calculations are done considering different temperature pairs for all the systems. Of these three systems, EDTA-CaCl₂ is considered to be a model system since it is a well known reaction that is used as a validation standard for ITC measurements [128]. Once the equation was validated using EDTA-CaCl₂ model system, it was extended to BCA I-ligand systems. For all three systems, ΔG calculated using Eq. 7.9, agreed with the ΔG measured using ITC within the error limits. The agreement between ΔG calculated to that of measured with ITC for all three systems is shown in Fig. 7.10.

7.2 Conclusion

7.2.1 Thermodiffusion of aqueous salt solutions

In recent years, thermodiffusion has been used as a very sensitive tool to study biological reactions. Hence, a microscopic understanding of the thermal diffusion process in biological systems and biological reactions is of specific interest. Protein-ligand systems, which are of particular interest in this study, are quite complicated due to the multiple components that are present in the system. This includes hydrophobic, hydrophilic, and ionic chemical (side) groups of proteins, ligands, and buffer components. To reduce the complexity of the problem, we first looked into the thermodiffusive behavior of simple salt solutions, which act

as buffer components for protein-ligand systems. From the studies, it could be concluded that the presence of charges and the complex nature of *water* make the aqueous salt solutions itself complicated.

To investigate the sensitivity of Soret effect to the ionic species, the study was carried out for different sodium, potassium, and lithium salts. Thermodiffusive properties of all salt systems were studied as a function of concentration and temperature. It could be concluded that diffusive behavior is influenced by an exchange of cation and anion, whereas concentration dependence of S_T is primarily influenced by the change of the anion. This study once more underlined the sensitivity of thermodiffusion to the changes in hydration. On the other hand, the strong relation between $\Delta S_T(\Delta T)$ and $\Delta S_T(\Delta c)$ with the hydrophilicity $\log P$ found for non-ionic solutes, could not be confirmed for ionic solutes. For non-ionic solutes, hydrogen bonds are predominantly present in the system, which are influenced by changes in concentration and temperature. While for ionic solutes additionally, electrostatic interactions are present. The presence of two interactions, of which only one is strongly influenced by changes in temperature and concentration could be the reason that $\Delta S_T(\Delta T)$ and $\Delta S_T(\Delta c)$ of ionic solutes do not strongly dependent on hydrophilicity. This has been discussed in detail in Ch. 2, Ch. 3 and Sec. 7.1.1. The temperature and concentration independent empirical fitting parameter S_T^i (cf. Eq. 7.2) shows also for ionic systems a linear correlation with $\log P$.

Formation of clusters at high salt concentration influence mainly the diffusion coefficient D , while the influence on thermodiffusion coefficient D_T is minor. The effect of cluster formation is also not much pronounced on the behavior of S_T . Salts that are reported to form clusters, like KSCN, show a decrease in D with concentration due to the increase in the size of diffusing entity. Along with cluster formation, the chemical potential also has a pronounced influence on the diffusive behavior of salt systems, which has been discussed in Sec.7.1.2.

Several salt systems show a minimum in S_T with concentration. Until now, there exists no physical explanation for the occurrence of this minimum. Since ions change the hydrogen bonding network of water and thus form hydration layers around them, a preliminary model is developed based on this idea. It is assumed that the hydration layers of salt molecules start to touch at a concentration, where a minimum in S_T is observed. Beyond this concentration,

it is hypothesized that hydration layers of salt molecules start to overlap and an increase in S_T with concentration will be observed. Using the developed model calculations are done based on the results published by Artola and Rousseau for Lenard-Jones mixtures. Results indicate a minimum in S_T and later an increase with concentration. At larger concentrations, results using our model show a decay while experimental data continue to rise. This indicates that the model becomes inadequate at larger concentrations. Performing simulations with the developed model would be a future perspective of this work.

7.2.2 Development of a thermophoretic microfluidic cell

A thermophoretic microfluidic cell is developed for the quantification of S_T of colloidal particles or proteins, which are inherently fluorescent or fluorescently labeled. The development of this microfluidic cell is discussed in detail in Ch. 5. This cell allows thermophoretic measurements in multicomponent mixtures and requires small sample volumes (in μL). Such a cell is of particular advancement for studying thermophoresis of protein-ligand systems as it can be used to study specific fluorescently labeled or large macromolecules in multicomponent mixtures such as buffer solutions. S_T of colloidal particles measured using this thermophoretic microfluidic cell deviate on average by 7.8% from the fitted curve describing the TDFRS results.

S_T of fluorescently labeled protein (BCA I) has also been measured with this microfluidic device and compared with IR-TDFRS measurements in Ch. 6. S_T measured using the microfluidic cell of free BCA I has a higher uncertainty and is roughly 40% lower than what has been measured with IR-TDFRS. To make S_T measurement of BCA I viable with the microfluidic cell, it had to be fluorescently labeled and suffered from a low fluorescent labeling ratio. Besides, with the help of ITC, it was concluded that fluorescent labeling affects the binding of ligand to BCA I due to a change in pH. Hence, using this microfluidic cell to investigate inherently fluorescent proteins would be more beneficial.

7.2.3 Thermodiffusion of binding reactions

Investigating thermodiffusion of different complex formation reactions was motivated by different reasons as listed below.

1. To gain deeper understanding into the interactions involved in complex formation by comparing thermophoretic data (a non-equilibrium process) to the thermodynamic data (an equilibrium process)
2. How do the changes in the hydration layer once the complex is formed affect the thermodiffusive behavior?
3. Measure S_T of protein with the developed thermophoretic microfluidic cell and compare with IR-TDFRS measurement

To achieve the above-listed goals, two model systems were used: EDTA- CaCl_2 system and BCA I (protein) with two aryl sulfonamide ligands (4FBS and PFBS)

The temperature dependence of S_T for EDTA, CaCl_2 , and EDTA- CaCl_2 complex was measured. Also, the thermodynamics of this binding reaction was measured using ITC, which gave access to ΔG at different temperatures. A mathematical equation was derived, which connects S_T to ΔG . Corresponding values measured for EDTA- CaCl_2 binding reaction were substituted into the equation to validate the derived relation. Later, the same procedure was used for protein-ligand systems (BCA I-4FBS and BCA I-PFBS). The derived relation was validated for all three systems at different temperatures. This implies that S_T measured at different temperatures can be used to predict ΔG at a particular temperature.

Changes in thermodiffusion upon complex formation and its connection with the hydration layer have also been studied. Temperature dependence of S_T for EDTA- CaCl_2 complex and EDTA couldn't be described by Eq. 1.3. Especially, S_T of EDTA shows a decrease with temperature with an abrupt drop between 25 °C and 30 °C. A similar change in thermodiffusive behavior has been reported for PNiPAM in water, which is connected to the temperature sensitivity of the polymer. Change in thermodiffusive behavior of EDTA might also have the same origin as in the case of PNiPAM as it occurs at a similar temperature range, but further studies need to be conducted in this regard. As an extension, the next part of the study focused on the changes that happen in the thermodiffusive behavior of protein (BCA I) when ligands (4FBS and PFBS) bind to it. S_T of BCA I-4FBS and BCA I-PFBS complexes are very similar, but different from free BCA I. This is an indication that the hydration shells of complexes are different from that of free protein. The measured S_T of the complex becomes more similar to the free protein with increasing temperature, which might be explained by fewer formed complexes and more free protein and therefore a lower binding, which agrees

with the ITC measurements. The binding mechanism of aryl sulfonamide ligands with BCA I involves releasing water molecules and has been confirmed by thermodiffusion measurements.

S_T of free BCA I was measured with the developed thermophoretic microfluidic cell (Sec. 7.2.2) and was compared with IR-TDFRS measurement. Fluorescent labeling was required to monitor the protein concentration. For BCA I, from ITC experiments it was concluded that fluorescent labeling highly influences the binding reaction. S_T measured using microfluidic cell has a higher uncertainty and is roughly 40% lower than what has been measured with IR-TDFRS. Since fluorescent labeling of the protein highly influences the binding process, further measurements were not carried out.

7.3 Outlook

The main focus of this thesis lay in the investigation of ionic solutes in aqueous solution. We started with simple salts and found that the temperature dependence of S_T shifted with increasing concentration, but the shape of the curve remained. From aqueous solutions of non-ionic solutes, we know that the temperature dependent slope of S_T strongly varies with concentration. Two possible scenarios could be investigated in this direction, with the first one being

- Adding more organic groups to the salts
Inserting organic groups into the salts can be used to tune the hydrophilicity-hydrophobicity of salt systems. Hence such systems could be used to check whether the correlation between $\Delta S_T(\Delta T)$ and $\Delta S_T(\Delta c)$ with $\log P$ holds, as in the case for non-ionic systems.
- Increasing the valency of ions in the salts
So far, most of the salt systems studied here comprise ions with single valency. Increasing the valency of ions makes systems more complex and hence would influence the thermophoretic behavior.

In short, both of the above mentioned routes increase the complexity towards the multivalent proteins with several hydrophilic and hydrophobic groups.

We developed in this thesis a "sketchy" model to explain a minimum of S_T with concen-

tration. Preliminary results from the model that has been developed as a part of this thesis look promising in this aspect. As of now, this approach has been tested for alkali iodide salts, which have a big anion. On the experimental side, it could be investigated whether the observations are similar when iodide is replaced by other halide anions like chloride or bromide. Performing simulations with this model to predict the minimum and thus test the validity of the model would be another aspect of this work. This will also be helpful to analyze the limitations of the current model and rectify it. Simulations will also allow to vary the anion and cation size systematically, which could then be compared with experimental results. Raman Spectroscopy could be used to test the microscopic picture that has been proposed for the water molecules around the salt molecule in this model. This technique could be used to differentiate water molecules that are present near the salt molecule, perturbed water layer, and bulk water. Besides, this experimental technique can be utilized to see the difference in the spectra of water molecules under, at, and beyond the concentration at which a minimum in S_T is observed.

To study a system with the developed microfluidic cell, the system has to be inherently fluorescent or fluorescently labeled. S_T measured in the microfluidic cell for BCA I suffered from a low fluorescent labeling ratio. To explore the further possibilities of the cell, it would be beneficial to study inherently fluorescent proteins like Green Fluorescent Protein (GFP) or lysozyme. With these proteins, it would also be possible to perform systematic measurements as a function of pH, ionic strength, etc..

An abrupt change in the thermophoretic behavior of EDTA between 25°C and 30°C indicates that this change might be related to the interaction between EDTA and water molecules and hence changes in the hydrogen bond network. The existing database is insufficient to draw clear conclusions. More systematic measurements of EDTA at several other pHs would be helpful to connect the changes in the interaction of EDTA with water molecules and observed thermophoretic behavior. A study of other chelating agents such as diethylenetriaminepentaacetic acid (DTPA) or hydroxyethylethylenedimainetriacetic acid (HEDTA) would also be desirable in this regard.

Change in the thermodiffusive behavior of the protein followed by complex formation is often attributed to the changes in the hydration layer of the protein. Once complex formation happens, there is an entropy loss of protein, which can be measured with Quasi Elastic

Neutron Scattering (QENS). Calorimetry gives access to the total change in entropy, which includes the contribution from the protein and hydration layer. A difference between entropy values measured from calorimetry and QENS corresponds to $\Delta S^{\text{hydration}}$. It could be assumed that the entropy loss for protein is regained as an increase in the entropy of the hydration layer. This can be confirmed by the thermophoretic measurements, which are very sensitive to the changes in the hydration layer. To study whether a qualitative agreement between the entropy loss of protein and entropy gain of the hydration layer can be attained as in the case of the streptavidin-biotin system, QENS measurements of BCA I-4FBS and BCA I-PFBS would be desirable. From TDFRS measurements of BCA I-4FBS and BCA I-PFBS, it can be concluded that the protein is more hydrophilic than the complex. This in turn implies a lower change in entropy for protein, which could also be confirmed by QENS measurements.

We derived a mathematical relation between S_T and ΔG for three different complex formation reactions. This allows the calculation of change in Gibb's free energy of a complex formation from its thermophoretic measurements. It could also be tested if the same holds for other systems forming complexes.

Acknowledgement

Joining for my PhD was probably the most confusing, but at the same time most exciting decision that I have taken in my life. While starting this journey, little did I know about what life has kept in store for me. While writing this acknowledgment, it gives me a rewind of what happened for the last three and a half years.

To start with, I would like to express my foremost gratitude to Prof. Simone Wiegand, my supervisor. Be it on a scientific or personal front, she has been there for me in the last three and half years. Spending hours in front of her computer correcting my papers, looking into the results, guiding me everyday, I cannot imagine or wish for a more supportive supervisor.

I thank Prof. Jan K. G. Dhont and Prof. Peter Lang for providing with an opportunity to work in the group. I couldn't ask for a better group to start my scientific journey with.

I would also like to thank Prof. Annette Schmidt, my co-supervisor from University of Cologne for her interest in my work and also providing me an opportunity to do my PhD at University of Cologne. I would also like to thank Prof. Uwe Ruschwitz for taking the chair of my examination committee.

My sincere thanks to Dr. Harmut Kriegs for always making sure to solve any problems that the computer or setup came up with.

My sincere thanks go to all the people who collaborated with me - Prof. Wim Briels, Prof. Jutta Luettmmer-Strathmann, Dr. Andreas Stadler, Dr. Mona Sarter, Olessya Yukhnoevets, Dr. Namkyu Lee - for always answering my questions and keeping up the enthusiasm of the work when I felt short of it.

I would also like to thank International Helmholtz Research School of Biophysics and Soft Matter *BioSoft* for giving me an opportunity to be a fellow of the school. Thanks to Dr. Thorsten Auth for being the soul of *BioSoft* and always being there for help.

To all my colleagues in IBI-4; thank you for being a part of this journey. Apart from the scientific discussions, all the parties, games, outing will always stay in my memory. You all have contributed a lot for my growth scientifically as well as personally.

Dennis, Shammi, Vaibhav, Dhivya, Shivani, Sravan; my first and closest friends in Jülich. Thank you for being there even when I didn't ask to.

Team Jülich; Ashish, Akshay, Honey, Nithya, Vidhya, Nikhil. I might not have said this enough, but you all made my life here easier way more than you could imagine. Number of times I have been waiting for the weekend just to be there with you all and cook! It might sound very awkward, but thank you. This is a team that I am going to cherish for the rest of my life. Also to Vishakettan, Sindhuchechechi and Shanvik, for always keeping the door open with yummy food.

To Ashwathi, Theertha, Eldho, Deviyettan, Meghna, Amal, Pranchi ; you were all my escape routes when life was getting tough. Ashi and Febi; you both know how much you mean to me and that's it. Thank you for the long phone calls almost everyday which kept me sane throughout this journey. I wouldn't have stayed here for these three and half years without you both being here. To Anju, for making sure that you are there whenever I needed and nodding yes to all my research ideas and then saying "I didn't understand what you said but go on". Thank you!

Varun; Thank you for sticking me throughout this journey. Thank you for being the best partner I could ever ask for. For making mistakes, letting me make mistakes, and correcting it together with me. A formal thanks is not something I usually do to you, but this thesis is ours too as much as it is mine. For being my biggest cheerleader, my constant source of positivity, my fellow traveler; Thank you! Also to Varun's family for taking care of me as much as they take care of him and being beside me throughout this journey, thank you!

Now to my Achan, Amma, Kavya and Ammamma; I don't know where to start. Thank you would be a small word. To making sure for the past three and half years that I am not burning out and okay everyday, you all are my life. This thesis is deserving to you all as much as it is deserving to me.

Bibliography

- [1] C. Ludwig. Diffusion zwischen ungleich erwärmten Orten gleich zusammengesetzter Lösungen. *Sitz. ber. Akad. Wiss. Wien Math.-naturw. Kl.*, 20:539, 1856.
- [2] S.R. de Groot and P. Mazur. *Non-equilibrium Thermodynamics*. Dover, New York, 1984.
- [3] D. Niether and S. Wiegand. Thermophoresis of biological and biocompatible compounds in aqueous solution. *J. Phys. Condens. Matter*, 31:503003, 2019.
- [4] K. Clusius and G Dickel. Zur Trennung der Chlorisotope. *Naturwissenschaften*, 27:148–149, 1939.
- [5] B. C. Reed. Liquid thermal diffusion during the Manhattan project. *Phys. Perspect.*, 13:161–188, 2011.
- [6] B. Faissat, K. Knudsen, E. H. Stenby, and F. Montel. Fundamental statements about thermal-diffusion for a multicomponent mixture in a porous-medium. *Fluid Ph. Equilibria*, 100:209–222, 1994.
- [7] G. H. Thompson, M. N. Myers, and J. C. Giddings. An observation of a field-flow fractionation effect with polystyrene samples. *Sep. Sci.*, 2:797–800, 1967.
- [8] J. C. Giddings, V. Kumar, P. S. Williams, and M. N. Myers. Polymer separation by thermal field-flow fractionation - high- speed power programming. *Adv. Chem. Ser.*, 227:3–21, 1990.
- [9] M. E. Schimpf and J. C. Giddings. Characterization of thermal-diffusion in polymer-solutions by thermal field-flow fractionation - dependence on polymer and solvent parameters. *J Polym. Sci. Pol. Phys.*, 27:1317–1332, 1989.
- [10] J. C. Giddings, V. Kumar, P. S. Williams, and M. N. Myers. Polymer separation by thermal field-flow fractionation. *Adv. Chem.*, 227:3–21, 1990.

-
- [11] S. L. Brimhall, M. N. Myers, K. D. Caldwell, and J. C. Giddings. High-temperature thermal field-flow fractionation for the characterization of polyethylene. *Sep. Sci. Technol.*, 16:671–689, 1981.
- [12] M. Asmari, R. Ratih, H. A. Alhazmi, and S. El Deeb. Thermophoresis for characterizing biomolecular interaction. *Methods*, 146:107–119, 2018.
- [13] M. Jerabek-Willemsen, C. J. Wienken, D. Braun, P. Baaske, and S. Duhr. Molecular interaction studies using microscale thermophoresis. *ASSAY Drug Dev. Technol.*, 9:342–353, 2011.
- [14] M. Jerabek-Willemsen, T. André, W. Wanner, H.M. Roth, S. Duhr, P. Baaske, and D. Breitsprecher. Microscale thermophoresis: Interaction analysis and beyond. *J. Mol. Struct.*, 1077:101–113, 2014.
- [15] F. S. Gaeta, G. Perna, G. Scala, and F. Bellucci. Non-isothermal matter transport in sodium-chloride and potassium chloride aqueous solutions . 1. homogeneous system (thermal-diffusion). *J. Phys. Chem.*, 86:2967–2974, 1982.
- [16] P. A. Artola and B. Rousseau. Microscopic interpretation of a pure chemical contribution to the Soret effect. *Phys. Rev. Lett.*, 98:125901–1–125901–4, 2007.
- [17] S. Iacopini, R. Rusconi, and R. Piazza. The "macromolecular tourist": Universal temperature dependence of thermal diffusion in aqueous colloidal suspensions. *Eur. Phys. J. E*, 19:59–67, 2006.
- [18] Z. Wang, H. Kriegs, and S. Wiegand. Thermal diffusion of nucleotides. *J. Phys. Chem. B*, 116:7463–7469, 2012.
- [19] E. Ruckenstein. Can phoretic motions be treated as interfacial-tension gradient driven phenomena. *J. Colloid Interface Sci.*, 83:77–81, 1981.
- [20] J.K.G Dhont. Thermodiffusion of interacting colloids. I. a statistical thermodynamics approach. *J. Chem. Phys.*, 120:1632–1641, 2004.
- [21] J.K.G Dhont. Thermodiffusion of interacting colloids. II. a microscopic approach. *J. Chem. Phys.*, 120:1642–1653, 2004.
- [22] K. I. Morozov. Thermodiffusion in magnetic colloids. *J. Magn. Magn. Mater.*, 201:248–251, 1999.
- [23] E. Bringuier and A. Bourdon. Colloid transport in nonuniform temperature. *Phys.*

- Rev. E*, 67:011404, 2003.
- [24] J. K. G. Dhont, S. Wiegand, S. Duhr, and D. Braun. Thermodiffusion of charged colloids: Single-particle diffusion. *Langmuir*, 23:1674–1683, 2007.
- [25] H. Ning, J. K. G. Dhont, and S. Wiegand. Thermal-diffusive behavior of a dilute solution of charged colloids. *Langmuir*, 24:2426–2432, 2008.
- [26] S. Fayolle, T. Bickel, S. Le Boiteux, and A. Würger. Thermodiffusion of charged micelles. *Phys. Rev. Lett.*, 95:208301–1–208301–4, 2005.
- [27] S. Duhr and D. Braun. Why molecules move along a temperature gradient. *P. Natl. Acad. Sci. USA*, 103:19678–19682, 2006.
- [28] R. Piazza, S. Iacopini, and B. Triulzia. Thermophoresis as a probe of particle-solvent interactions: The case of protein solutions. *Phys. Chem. Chem. Phys.*, 6:1616–1622, 2004.
- [29] A. Würger. Thermal non-equilibrium transport in colloids. *Rep. Prog. Phys.*, 73:126601, 2010.
- [30] R. Piazza and A. Parola. Thermophoresis in colloidal suspensions. *J. Phys-Condens. Mat.*, 20:153102, 2008.
- [31] A. Parola and R. Piazza. Particle thermophoresis in liquids. *Eur. Phys. J. E*, 15:255–263, 2004.
- [32] Z. Wang, H. Kriegs, J. Buitenhuis, J. K. G. Dhont, and S. Wiegand. Thermophoresis of charged colloidal rods. *Soft Matter*, 9:8697–8704, 2013.
- [33] P. A. Artola and B. Rousseau. Thermal diffusion in simple liquid mixtures: what have we learnt from molecular dynamics simulations? *Mol. Phys.*, 111:3394–3403, 2013.
- [34] B. Hafskjold. Computer simulations of thermal diffusion in binary fluid mixtures. *LNP Vol. 584: Thermal Nonequilibrium Phenomena in Fluid Mixtures*, 584:3, 2002.
- [35] M. M. Zhang and F. Müller-Plathe. Reverse nonequilibrium molecular-dynamics calculation of the Soret coefficient in liquid benzene/cyclohexane mixtures. *J. Chem. Phys.*, 123:124502, 2005.
- [36] M. Klein and S. Wiegand. The Soret effect of mono-, di- and tri-glycols in ethanol. *Phys. Chem. Chem. Phys.*, 13:7059–7063, 2011.

- [37] G. Galliero and S. Volz. Thermodiffusion in model nanofluids by molecular dynamics simulations. *J. Chem. Phys.*, 128:064505, 2008.
- [38] M. C. Yang and M. Ripoll. Thermophoretically induced flow field around a colloidal particle. *Soft Matter*, 9:4661–4671, 2013.
- [39] P. Polyakov, F. Müller-Plathe, and S. Wiegand. Reverse nonequilibrium molecular dynamics calculation of the Soret coefficient in liquid heptane/benzene mixtures. *J. Phys. Chem. B*, 112:14999–15004, 2008.
- [40] P. Polyakov, M. Zhang, F. Müller-Plathe, and S. Wiegand. Thermal diffusion measurements and simulations of binary mixtures of spherical molecules. *J. Chem. Phys.*, 127:014502, 2007.
- [41] P. Kolodner, H. Williams, and C. Moe. Optical measurement of the Soret coefficient of ethanol/water solutions. *J. Chem. Phys.*, 88:6512–6524, 1988.
- [42] B. Rousseau, C. Nieto-Draghi, and J. B. Avalos. The role of molecular interactions in the change of sign of the Soret coefficient. *Europhys. Lett.*, 67:976–982, 2004.
- [43] K. J. Zhang, M. E. Briggs, R. W. Gammon, and J. V. Sengers. Optical measurement of the Soret coefficient and the diffusion coefficient of liquid mixtures. *J. Chem. Phys.*, 104:6881–6892, 1996.
- [44] C. Nieto-Draghi, J. B. Avalos, and B. Rousseau. Computing the Soret coefficient in aqueous mixtures using boundary driven nonequilibrium molecular dynamics. *J. Chem. Phys.*, 122:114503, 2005.
- [45] H. Ning and S. Wiegand. Experimental investigation of the Soret effect in acetone/water and dimethylsulfoxide/water mixtures. *J. Chem. Phys.*, 125:221102, 2006.
- [46] D. Niether, S. Di Lecce, F. Bresme, and S. Wiegand. Unravelling the hydrophobicity of urea in water using thermodiffusion: implications for protein denaturation. *Phys. Chem. Chem. Phys.*, 20:1012–1020, 2018.
- [47] P. A. Artola, B. Rousseau, and G. Galliero. A new model for thermal diffusion: Kinetic approach. *J. Am. Chem. Soc.*, 130:10963–10969, 2008.
- [48] S. Wiegand. Thermal diffusion in liquid mixtures and polymer solutions. *J. Phys.: Condens. Matter*, 16:R357–R379, 2004.
- [49] S. Di Lecce, T. Albrecht, and F. Bresme. The role of ion-water interactions in de-

- termining the Soret coefficient of LiCl aqueous solutions. *Phys. Chem. Chem. Phys.*, 19:9575–9583, 2017.
- [50] J. Colombani, J. Bert, and J. Dupuy-Philon. Thermal diffusion in (LiCl,rh₂o). *J. Chem. Phys.*, 110:8622–8627, 1999.
- [51] R. Kita, S. Wiegand, and J. Luettmmer-Strathmann. Sign change of the Soret coefficient of poly(ethylene oxide) in water/ethanol mixtures observed by thermal diffusion forced Rayleigh scattering. *J. Chem. Phys.*, 121:3874–3885, 2004.
- [52] Y. Kishikawa, S. Wiegand, and R. Kita. Temperature dependence of Soret coefficient in aqueous and nonaqueous solutions of pullulan. *Biomacromolecules*, 11:740–747, 2010.
- [53] K. Maeda, N. Shinyashiki, S. Yagihara, S. Wiegand, and R. Kita. Ludwig-Soret effect of aqueous solutions of ethylene glycol oligomers, crown ethers, and glycerol: Temperature, molecular weight, and hydrogen bond effect. *J. Chem. Phys.*, 143:124504, 2015.
- [54] D. Niether, D. Afanasenkau, J. K. G. Dhont, and S. Wiegand. Accumulation of formamide in hydrothermal pores to form prebiotic nucleobases. *Proc. Natl. Acad. Sci. USA*, 113:4272–4277, 2016.
- [55] A. L. Sehnem, D. Niether, S. Wiegand, and A. M. Figueiredo Neto. Thermodiffusion of monovalent organic salts in water. *J. Phys. Chem. B*, 122:4093–4100, 2018.
- [56] F. Römer, Z. Wang, S. Wiegand, and F. Bresme. Alkali halide solutions under thermal gradients: Soret coefficients and heat transfer mechanisms. *J. Phys. Chem. B*, 117:8209–8222, 2013.
- [57] D. Niether, H. Kriegs, J. K. G. Dhont, and S. Wiegand. Peptide model systems: Correlation between thermophilicity and hydrophilicity. *J. Chem. Phys.*, 149:044506, 2018.
- [58] R. Kita and S. Wiegand. Soret coefficient of poly(n-isopropylacrylamide)/water in the vicinity of coil-globule transition temperature. *Macromolecules*, 38:4554–4556, 2005.
- [59] G. Wittko and W. Köhler. On the temperature dependence of thermal diffusion of liquid mixtures. *Europhys. Lett.*, 78:46007, 2007.
- [60] C. C. Tanner. The Soret effect. part 1. *Trans. Faraday Soc.*, 23:75–95, 1927.
- [61] C. C. Tanner. The Soret effect. part 2. *Trans. Faraday Soc.*, 49:611–619, 1953.

- [62] P. N. Snowdon and J. C. R. Turner. The concentration dependence of the Soret effect. *Trans. Faraday Soc.*, 56:1812–1819, 1960.
- [63] P. N. Snowdon and J. C. R. Turner. The Soret effect in some 0.01 normal aqueous electrolytes. *Trans. Faraday Soc.*, 56:1409–1418, 1960.
- [64] J. Chanu, editor. *Thermal diffusion of Halides in aqueous solutions*. Interscience Publishers, 1967.
- [65] H. Ning, J. Buitenhuis, J. K. G. Dhont, and S. Wiegand. Thermal diffusion behavior of hard-sphere suspensions. *J. Chem. Phys.*, 125:204911, 2006.
- [66] Ph. Naumann, N. Becker, S. Datta, T. Sottmann, and S. Wiegand. Soret coefficient in nonionic microemulsions: Concentration and structure dependence. *J. Phys. Chem. B*, 117:5614–5622, 2013.
- [67] D. Vigolo, G. Brambilla, and R. Piazza. Thermophoresis of microemulsion droplets: Size dependence of the Soret effect. *Phys. Rev. E*, 75:040401, 2007.
- [68] Ph. Naumann, S. Datta, T. Sottmann, B. Arlt, H. Frielinghaus, and S. Wiegand. Isothermal behavior of the Soret effect in nonionic microemulsions: Size variation by using different n-alkanes. *J. Phys. Chem. B*, 118:3451–3460, 2014.
- [69] S. A. Putnam, D. G. Cahill, and G. C. L. Wong. Temperature dependence of thermodiffusion in aqueous suspensions of charged nanoparticles. *Langmuir*, 23:9221–9228, 2007.
- [70] M. Braibanti, D. Vigolo, and R. Piazza. Does thermophoretic mobility depend on particle size? *Phys. Rev. Lett.*, 100:108303–1–108303–4, 2008.
- [71] R. Dong, Y. Zhou, C. Yang, and B. Cao. Experimental study on thermophoresis of colloids in aqueous surfactant solutions. *J. Condens. Matter Phys.*, 27:495102, 2015.
- [72] J. Rauch and W. Köhler. On the molar mass dependence of the thermal diffusion coefficient of polymer solutions. *Macromolecules*, 38:3571–3573, 2005.
- [73] S. Duhr and D. Braun. Thermophoretic depletion follows boltzmann distribution. *Phys. Rev. Lett.*, 96:168301–1–168301–4, 2006.
- [74] O. Syshchyk, D. Afanasenkau, Z. Wang, H. Kriegs, J. Buitenhuis, and S. Wiegand. Influence of temperature and charge effects on thermophoresis of polystyrene beads. *The Eur. Phys. J. E*, 39:129, 2016.

- [75] K. A. Eslahian, A. Majee, M. Maskos, and A. Würger. Specific salt effects on thermophoresis of charged colloids. *Soft Matter*, 10:1931–1936, 2014.
- [76] K. A. Eslahian and M. Maskos. Hofmeister effect in thermal field-flow fractionation of colloidal aqueous dispersions. *Colloids Surf. A Physicochem. Eng.*, 413:65–70, 2012.
- [77] Z. Wang, D. Niether, J. Buitenhuis, Y. Liu, P. R. Lang, J. K. G. Dhont, and S. Wiegand. Thermophoresis of a colloidal rod: Contributions of charge and grafted polymers. *Langmuir*, 35:1000–1007, 2019.
- [78] P. Blanco, H. Kriegs, M. P. Lettinga, P. Holmqvist, and S. Wiegand. Thermal diffusion of a stiff rod-like mutant Y21M-fd-virus. *Biomacromolecules*, 12:1602–1609, 2011.
- [79] W. Köhler and K. I. Morozov. The Soret effect in liquid mixtures - a review. *J. Non-Equilib. Thermodyn.*, 41:151–197, 2016.
- [80] D. Niether, M. Sarter, B. König, M. Zamponi, J. Fitter, A. Stadler, and S. Wiegand. Thermodiffusion as a probe of protein hydration for streptavidin and the streptavidin-biotin complex. *AIP Conference Proceedings*, 1929:020001, 2018.
- [81] D. Niether, M. Sarter, B. W. Koenig, J. Fitter, A. M. Stadler, and S. Wiegand. Thermophoresis: The case of streptavidin and biotin. *Polymers*, 12:376, 2020.
- [82] D. E. Hyre, I. Le Trong, E. A. Merritt, J. F. Eccleston, N. M. Green, R. E. Stenkamp, and P. S. Stayton. Cooperative hydrogen bond interactions in the streptavidin-biotin system. *Protein Sci.*, 15:459–467, 2006.
- [83] M. Sarter, D. Niether, B. W. Koenig, W. Lohstroh, M. Zamponi, N. H. Jalarvo, S. Wiegand, J. Fitter, and A. M. Stadler. Strong adverse contribution of conformational dynamics to streptavidin-biotin binding. *J. Phys. Chem. B*., 124:324–335, 2020.
- [84] S. Wiegand, H. Ning, and H. Kriegs. Thermal diffusion forced Rayleigh scattering setup optimized for aqueous mixtures. *J. Phys. Chem. B*, 111:14169–14174, 2007.
- [85] B. Arlt, S. Datta, T. Sottmann, and S. Wiegand. Soret effect of n-octyl beta-d-glucopyranoside (C(8)G(1)) in water around the critical micelle concentration. *J. Phys. Chem. B*, 114:2118–2123, 2010.
- [86] K. F. Palmer and D. Williams. Optical-properties of water in near-infrared. *J. Opt. Soc. Am.*, 64:1107–1110, 1974.
- [87] W. Köhler and R. Schäfer. Polymer analysis by thermal-diffusion forced Rayleigh

- scattering. In *New Developments in Polymer Analytics II*, volume 151 of *Advances in Polymer Science*, pages 1–59. 2000.
- [88] A. Becker, W. Köhler, and B. Müller. A scanning michelson interferometer for the measurement of the concentration and temperature derivative of the refractive- index of liquids. *Ber. Bunsen-Ges. Phys. Chem. Chem. Phys.*, 99:600–608, 1995.
- [89] L. Baranauskiene, V. Petrikaite, J. Matuliene, and D. Matulis. Titration calorimetry standards and the precision of isothermal titration calorimetry data. *Int. J. Mol. Sci.*, 10:2752–2762, 2009.
- [90] A. Velazquez-Campoy, S. A. Leavitt, and E. Freire. Characterization of protein-protein interactions by isothermal titration calorimetry. *Methods Mol. Biol.*, 261:35–54, 2004.
- [91] W. H.J. Ward and G. A. Holdgate. 7 isothermal titration calorimetry in drug discovery. In *Progress in medicinal chemistry*, volume 38 of *Progress in Medicinal Chemistry*, pages 309–376. Elsevier, Amsterdam, op. 2001.
- [92] C. C. Liu, A. J. Richard, K. Datta, and V. J. LiCata. Prevalence of temperature-dependent heat capacity changes in protein-dna interactions. *Biophysical Journal*, 94:3258–3265, 2008.
- [93] A. I. Dragan, Z. Li, E. N. Makeyeva, E. I. Milgotina, Y. Liu, C. Crane-Robinson, and P. L. Privalov. Forces driving the binding of homeodomains to DNA. *Biochem.*, 45:141–151, 2006.
- [94] J. A. Thomson and John E. Ladbury. Isothermal titration calorimetry: A tutorial. In John E. Ladbury and Michael L. Doyle, editors, *Biocalorimetry 2*, pages 35–58. Wiley, Chichester and Hoboken, NJ, 2004.
- [95] W. R.A. Osborne and R. E. Tashian. Dissociation constants for carbonic anhydrase-sulfonamide binding by high-performance liquid chromatography. *Anal. Biochem.*, 137:302–306, 1984.
- [96] M. F. Mazzobre, M. V. Roman, A. F. Mourelle, and H. R. Corti. Octanol-water partition coefficient of glucose, sucrose, and trehalose. *Carbohydr. Res.*, 340:1207–1211, 2005.
- [97] H. Bian, X. Wen, J. Li, H. Chen, S. Han, X. Sun, J. Song, W. Zhuang, and J. Zheng. Ion clustering in aqueous solutions probed with vibrational energy transfer. *PNAS*, 108:4737–4742, 2011.

- [98] A. A. Chen and R. V. Pappu. Quantitative characterization of ion pairing and cluster formation in strong 1:1 electrolytes. *J. Phys. Chem. B*., 111:6469–6478, 2007.
- [99] W. Nernst. Zur Kinetik der in Lösung befindlichen Körper. *Z. Phys. Chem.*, 2U:613–637, 1888.
- [100] A. C. F. Ribeiro, J. J. S. Natividade, and A. J. M. Valente. Diffusion of electrolytes and non-electrolytes in aqueous solutions: A useful strategy for structural interpretation of chemical systems. In *Progress in Organic and Physical Chemistry*, pages 53–66. Apple Academic Press, 2013.
- [101] P. Anderko, A. Wang and M. Rafal. Electrolyte solutions: from thermodynamic and transport property models to the simulation of industrial processes. *Fluid Ph. Equilibria*, 194-197:123–142, 2002.
- [102] W. R. Fawcett and A. C. Tikanen. Role of solvent permittivity in estimation of electrolyte activity coefficients on the basis of the mean spherical approximation. *J. Phys. Chem.*, 100:4251–4255, 1996.
- [103] L. Onsager and R. M. Fuoss. Irreversible processes in electrolytes diffusion, conductance, and viscous flow in arbitrary mixtures of strong electrolytes. *J. Phys. Chem.*, 36:2689–2778, 1932.
- [104] J. Choi, H. R. Choi, J. Jeon, and M. Cho. Ion aggregation in high salt solutions. vii. the effect of cations on the structures of ion aggregates and water hydrogen-bonding network. *J. Chem. Phys.*, 147:154107, 2017.
- [105] S. A. Hassan. Computer simulation of ion cluster speciation in concentrated aqueous solutions at ambient conditions. *J. Phys. Chem. B*, 112:10573–10584, 2008.
- [106] G. Gao, H. Shi, and Y. Yu. Mutual diffusion coefficients of concentrated 1:1 electrolyte from the modified mean spherical approximation. *Fluid Ph. Equilibria.*, 256:105–111, 2007.
- [107] J. Choi and M. Cho. Ion aggregation in high salt solutions. vi. spectral graph analysis of chaotropic ion aggregates. *J. Chem. Phys.*, 145:174501, 2016.
- [108] H. S. Frank and W. Wen. Ion-solvent interaction. structural aspects of ion-solvent interaction in aqueous solutions: a suggested picture of water structure. *Discuss. Faraday Soc.*, 24:133, 1957.

- [109] M. Carrillo-Tripp, M. L. San-Román, J. Hernández-Cobos, H. Saint-Martin, and I. Ortega-Blake. Ion hydration in nanopores and the molecular basis of selectivity. *Biophys. Chem.*, 124:243–250, 2006.
- [110] A. K. Soper and K. Weckström. Ion solvation and water structure in potassium halide aqueous solutions. *Biophys. Chem.*, 124:180–191, 2006.
- [111] R. Mancinelli, A. Botti, F. Bruni, M. A. Ricci, and A. K. Soper. Hydration of sodium, potassium, and chloride ions in solution and the concept of structure maker/breaker. *J. Phys. Chem. B*, 111:13570–13577, 2007.
- [112] J. Gujt, M. Bester-Rogc, and B. Hribar-Lee. An investigation of ion-pairing of alkali metal halides in aqueous solutions using the electrical conductivity and the monte carlo computer simulation methods. *J. Mol. Liq.*, 190:34–41, 2014.
- [113] P. Gallo, D. Corradini, and M. Rovere. Do ions affect the structure of water? the case of potassium halides. *J. Mol. Liq.*, 189:52–56, 2014.
- [114] D. Niether, T. Kawaguchi, J. Hovancova, K. Eguchi, J. K. G. Dhont, R. Kita, and S. Wiegand. Role of hydrogen bonding of cyclodextrin-drug complexes probed by thermodiffusion. *Langmuir*, 33:8483–8492, 2017.
- [115] R. Kita, G. Kircher, and S. Wiegand. Thermally induced sign change of Soret coefficient for dilute and semidilute solutions of poly(n-isopropylacrylamide) in ethanol. *J. Chem. Phys.*, 121:9140–9146, 2004.
- [116] I. Bischofberger, D. C. E. Calzolari, and V. Trappe. Co-nonsolvency of PNiPAM at the transition between solvation mechanisms. *Soft Matter*, 10:8288–8295, 2014.
- [117] V. M. Krishnamurthy, B. R. Bohall, C. Kim, D. T. Moustakas, D. W. Christianson, and G. M. Whitesides. Thermodynamic parameters for the association of fluorinated benzenesulfonamides with bovine carbonic anhydrase ii. *Chem. Asian J.*, 2:94–105, 2007.
- [118] L. B. Dugad, J. T. Gerig. NMR studies of carbonic anhydrase-4-fluorobenzenesulfonamide complexes. *Biochemistry*, 27:4310–4316, 1988.
- [119] J. Olander, S. F. Bosen, E. T. Kaiser. A study of the binding of two sulfonamides to carbonic anhydrase. *J. Am. Chem. Soc.*, 95:1616–1621, 1973.
- [120] J. C. Kernohan. A method for studying the kinetics of the inhibition of carbonic anhydrase by sulphonamides. *Biochim. Biophys. Acta*, 118:405–412, 1966.

- [121] J. Olander and E. T. Kaiser. Binding of 4-hydroxy-3-nitrobenzenesulfonamide, a reporter group labeled inhibitor, to carbonic anhydrases. *J. Am. Chem. Soc.*, 92:5758, 1970.
- [122] S. Lindskog and A. Thorslund. On the interaction of bovine cobalt carbonic anhydrase with sulfonamides. *Eur. J. Biochem.*, 3:453–460, 1968.
- [123] R. P. Henry. Techniques for measuring carbonic anhydrase activity in vitro. In Susanna J. Dodgson, Richard E. Tashian, Gerolf Gros, and Nicholas D. Carter, editors, *The Carbonic Anhydrases*, pages 119–125. Springer US and Imprint and Springer, Boston, MA, 1991.
- [124] R. J. Henry. The mode of action of sulfonamides. *Bacteriol. Rev.*, 7(4):175–262, 1943.
- [125] S. J. Darby, L. Platts, M. S. Daniel, A. J. Cowieson, and R. J. Falconer. An isothermal titration calorimetry study of phytate binding to lysozyme. *J. Therm. Anal. Calorim.*, 127:1201–1208, 2017.
- [126] E. D. Eastman. Theory of the Soret effect. *J. Am. Chem. Soc.*, 50:283–291, 1928.
- [127] A. Würger. Is Soret equilibrium a non-equilibrium effect? *C. R. - Mec.*, 341:438–448, 2013.
- [128] C. Ràfols, E. Bosch, R.l Barbas, and R. Prohens. The ca(2+)-edta chelation as standard reaction to validate isothermal titration calorimeter measurements (itc). *Talanta*, 154:354–359, 2016.

Appendix

SUPPORTING INFORMATION:
Thermodiffusion of aqueous solutions of
various potassium salts

Shilpa Mohanakumar, Jutta Luettmmer-Strathmann
and Simone Wiegand

January 26, 2021

Contents

1	Aqueous solutions of KCl	3
1.1	Concentration dependence S_T , D and D_T of KCl	3
1.2	Temperature dependence S_T , D and D_T of KCl	5
1.3	Refractive index increments	6
2	Aqueous solutions of KBr	7
2.1	Concentration dependence of S_T , D and D_T of KBr	7
2.2	Temperature dependence of S_T , D and D_T of KBr	8
2.3	Refractive index increments	9
3	Aqueous solutions of KSCN	10
3.1	Concentration dependence of S_T , D and D_T of KSCN	10
3.2	Temperature dependence of S_T , D and D_T of KSCN	11
3.3	Refractive index increments	12
4	Aqueous solutions of CH₃COOK	13
4.1	Concentration dependence of S_T , D and D_T of CH ₃ COOK	13
4.2	Temperature dependence of S_T , D and D_T of CH ₃ COOK	14
4.3	Refractive index increments	15
5	Aqueous solutions of K₂CO₃	16
5.1	Concentration dependence of S_T , D and D_T of K ₂ CO ₃	16
5.2	Temperature dependence of S_T , D and D_T of K ₂ CO ₃	17
5.3	Refractive index increments	18

6	Concentration dependence of pH for CH₃COOK and K₂CO₃	19
7	Adjusted parameters and various correlations	21
7.1	Determined parameters: S_T^i and b_1	21
7.2	Parameters a_M and b_I for relative mass and moment of inertia differences	21
7.3	Correlation between b_1 and $\log P$	22
7.4	Correlation between $\Delta S_T(\Delta c)$ and $\log P$	23
7.5	Correlation between $\Delta S_T(\Delta T)$ and $\log P$	25
8	Diffusion coefficients of amides	26

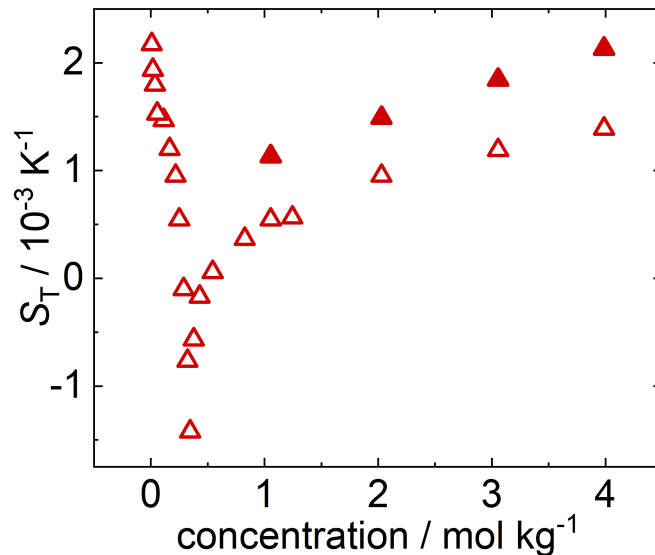


Figure 1: Concentration dependence of S_T of KCl in water at 30°C. Open triangles correspond to measurement from Gaeta *et al.* [1] and filled triangles correspond to our study.

1 Aqueous solutions of KCl

1.1 Concentration dependence S_T , D and D_T of KCl

Figure 1 shows a comparison of the KCl data for S_T by Gaeta *et al* [1] with our results. Note, that we converted molarities (mol per liter of the solution) specified by Gaeta *et al.* [1] in molalities (mol per kilogram solvent), which makes a difference at higher concentrations above 1 mol/kg.

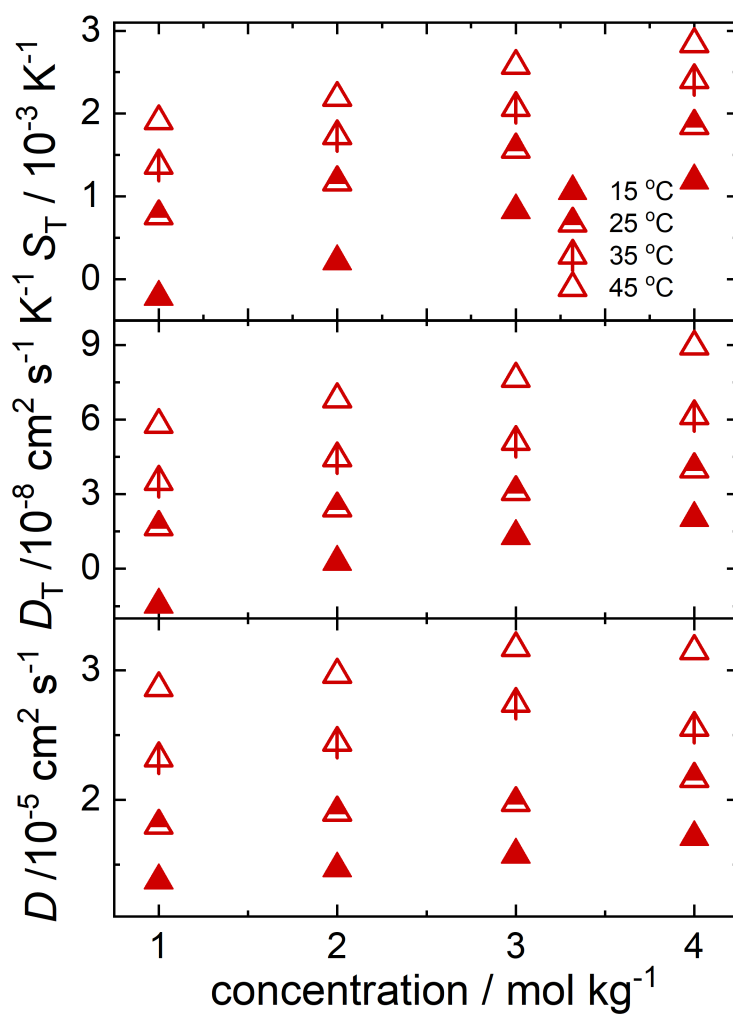


Figure 2: Concentration dependence of S_T , D and D_T of KCl in water at four different temperatures.

1.2 Temperature dependence S_T , D and D_T of KCl

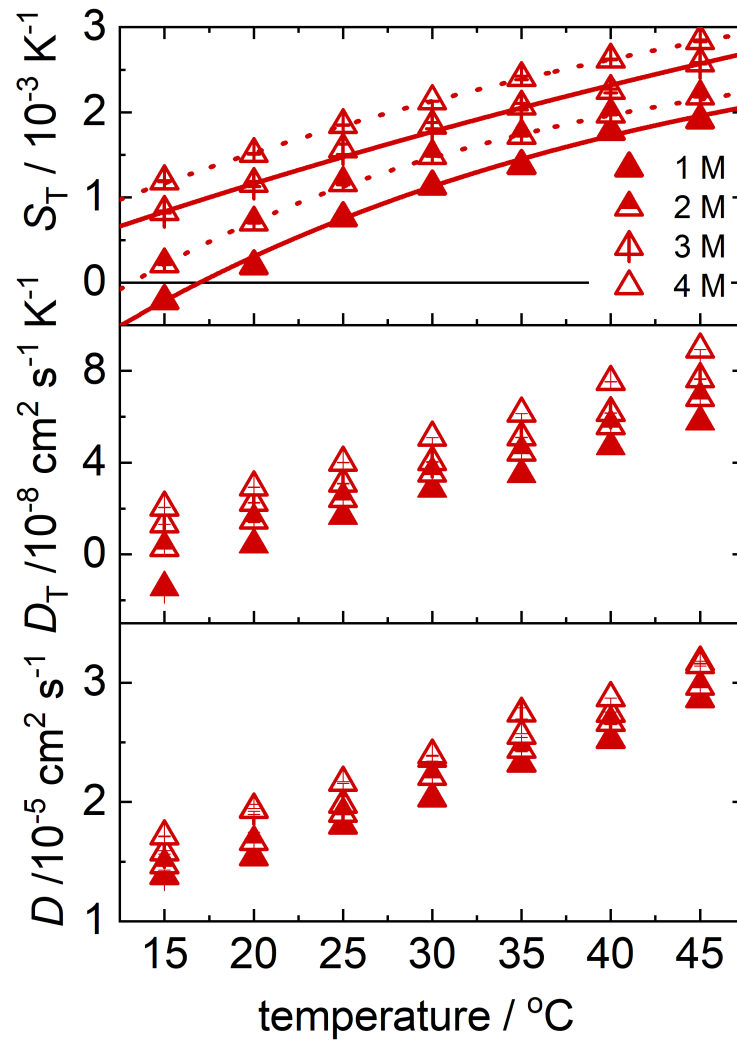


Figure 3: Temperature dependence of S_T , D and D_T of KCl in water at four different concentrations. The lines are fitted according to Eq. (2) in the main manuscript.

1.3 Refractive index increments

The following graphs show the refractive index increments $(\partial n/\partial T)_{p,c}$ and $(\partial n/\partial c)_{p,T}$ of KCl in water.

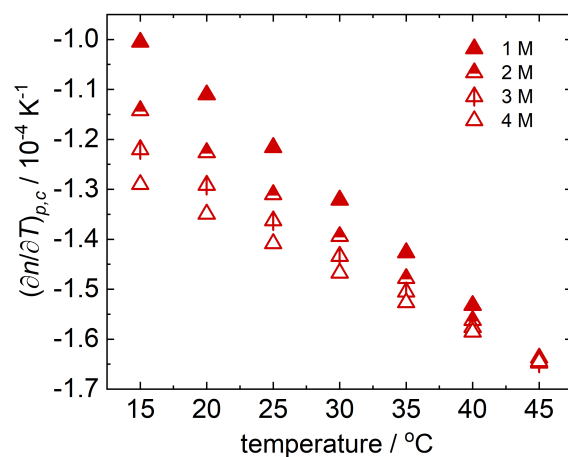


Figure 4: Temperature dependence of $(\partial n/\partial T)_{p,c}$ of KCl in water at four different concentrations.

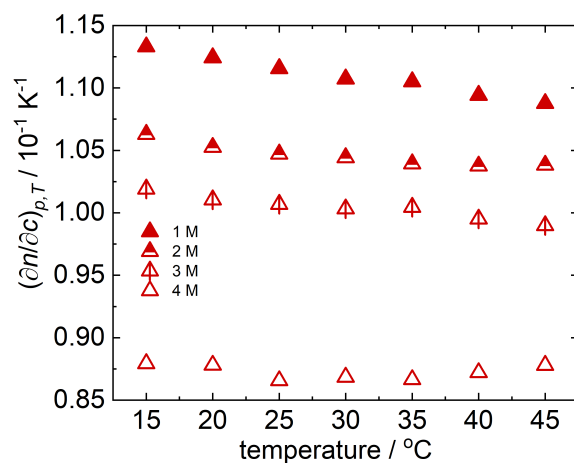


Figure 5: Temperature dependence of $(\partial n/\partial c)_{p,T}$ of KCl in water at four different concentrations.

2 Aqueous solutions of KBr

2.1 Concentration dependence of S_T , D and D_T of KBr

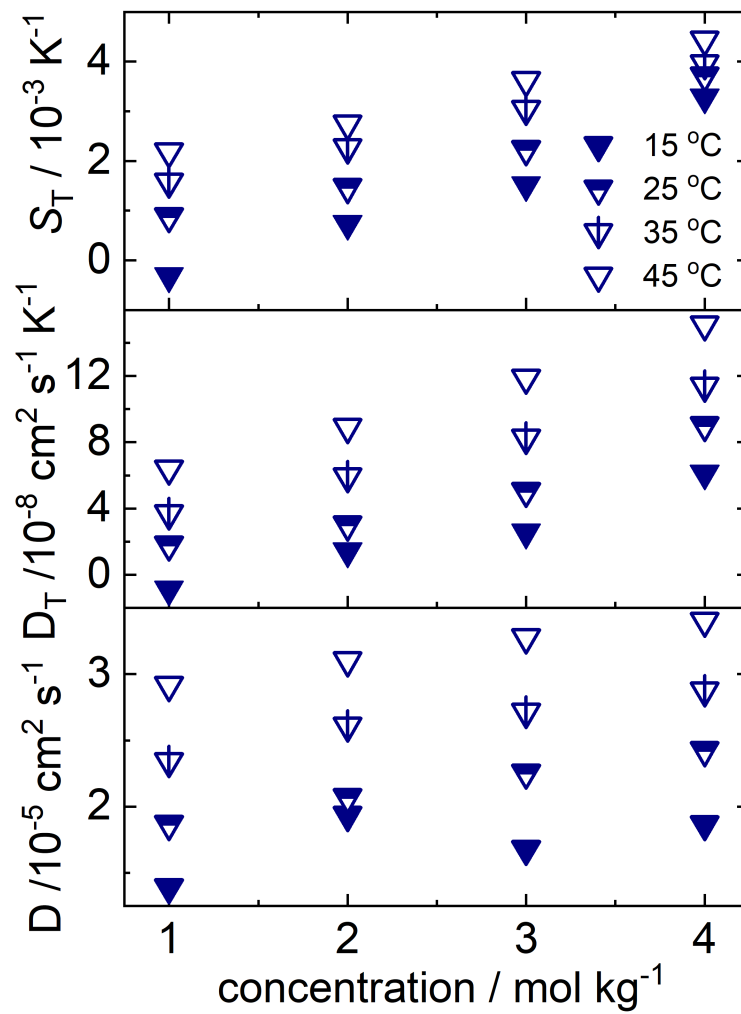


Figure 6: Concentration dependence of S_T , D and D_T of KBr in water at four different temperatures.

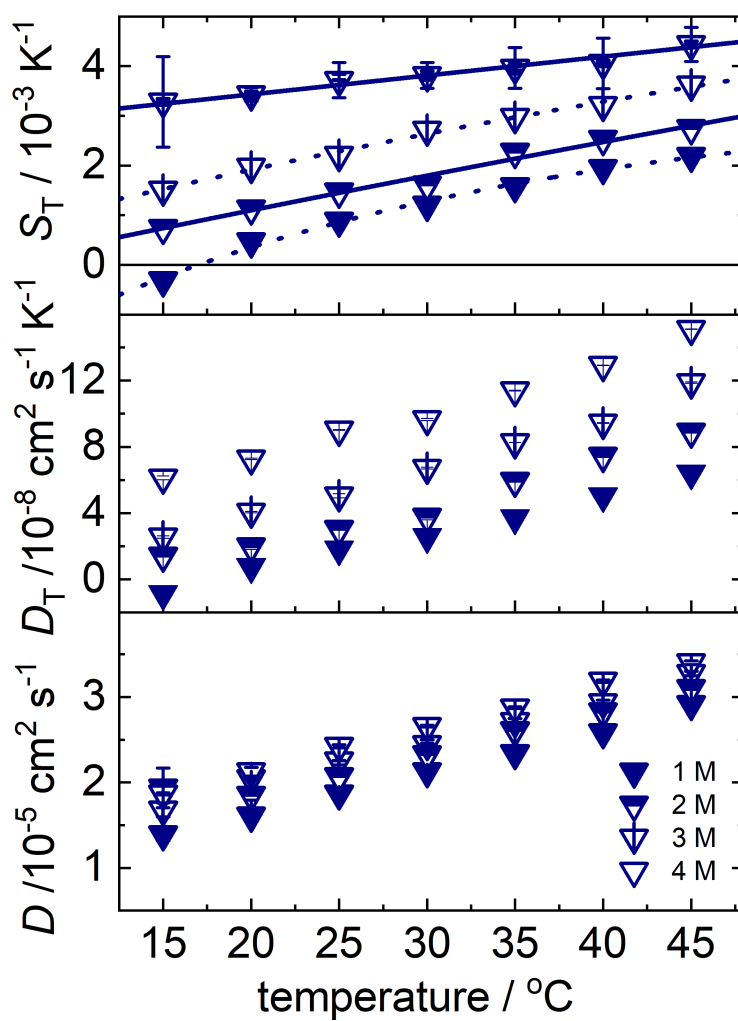
2.2 Temperature dependence of S_T , D and D_T of KBr

Figure 7: Temperature dependence of S_T , D and D_T of KBr in water at four different concentrations. The lines are fitted according to Eq. (2) in the main manuscript.

2.3 Refractive index increments

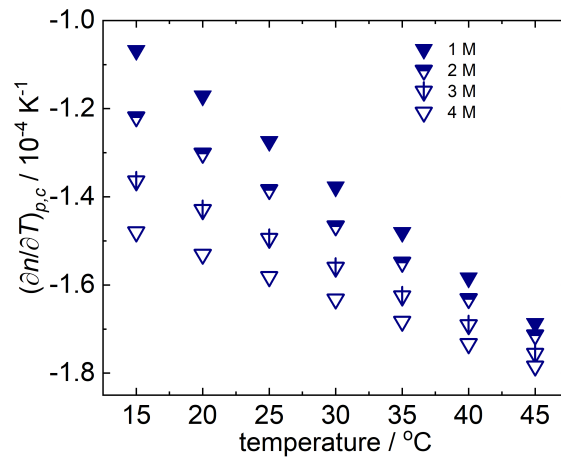


Figure 8: Temperature dependence of $(\partial n / \partial T)_{p,c}$ of KBr in water at four different concentrations.

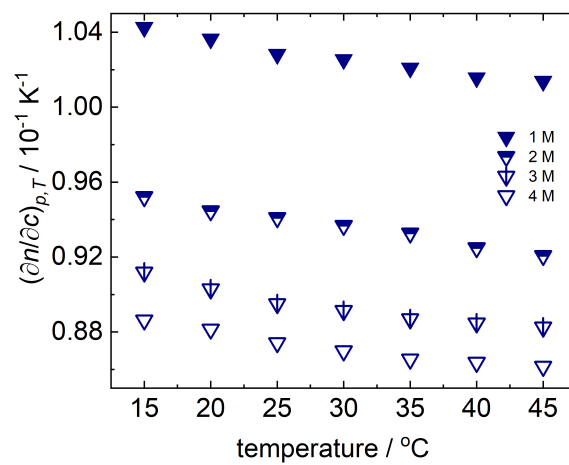


Figure 9: Temperature dependence of $(\partial n / \partial c)_{p,T}$ of KBr in water at four different concentrations.

3 Aqueous solutions of KSCN

3.1 Concentration dependence of S_T , D and D_T of KSCN

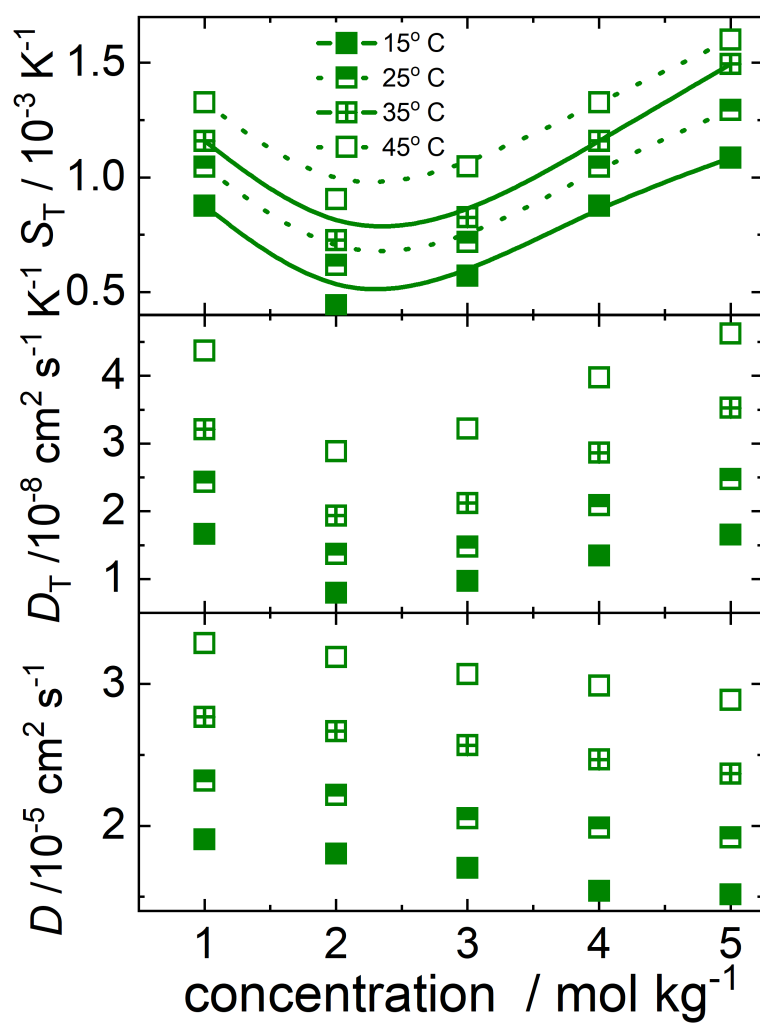


Figure 10: Concentration dependence of S_T , D and D_T of KSCN in water at four different temperatures. The lines are guide to the eye.

3.2 Temperature dependence of S_T , D and D_T of KSCN

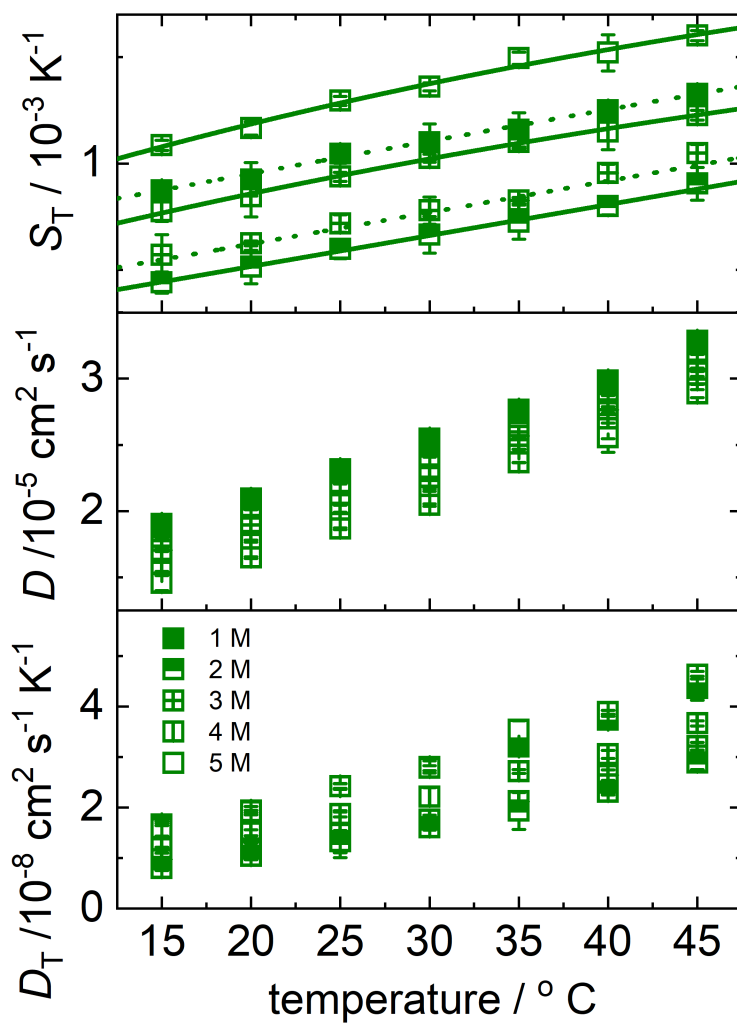


Figure 11: Temperature dependence of S_T , D and D_T of KSCN in water at five different concentrations. The lines are fitted according to Eq. (2) in the main manuscript.

3.3 Refractive index increments

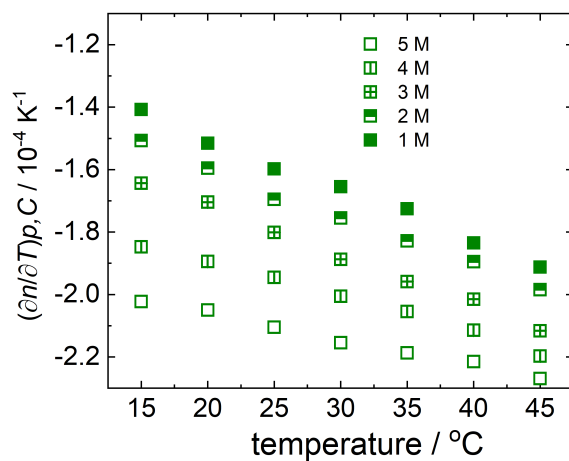


Figure 12: Temperature dependence of $(\partial n / \partial T)_{p,c}$ of KSCN in water at five different concentrations.

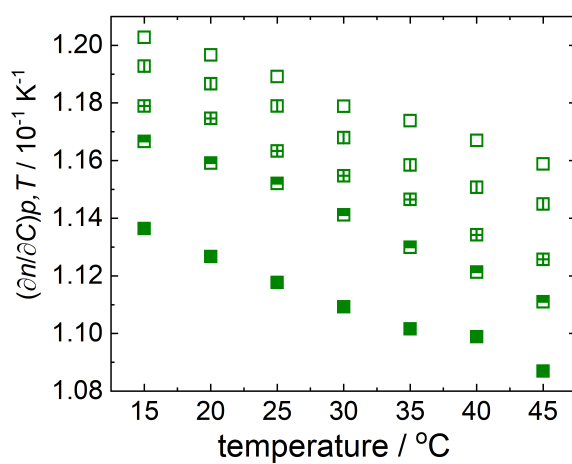


Figure 13: Temperature dependence of $(\partial n / \partial c)_{p,T}$ of CH_3COOK in water at five different concentrations.

4 Aqueous solutions of CH_3COOK

4.1 Concentration dependence of S_T , D and D_T of CH_3COOK

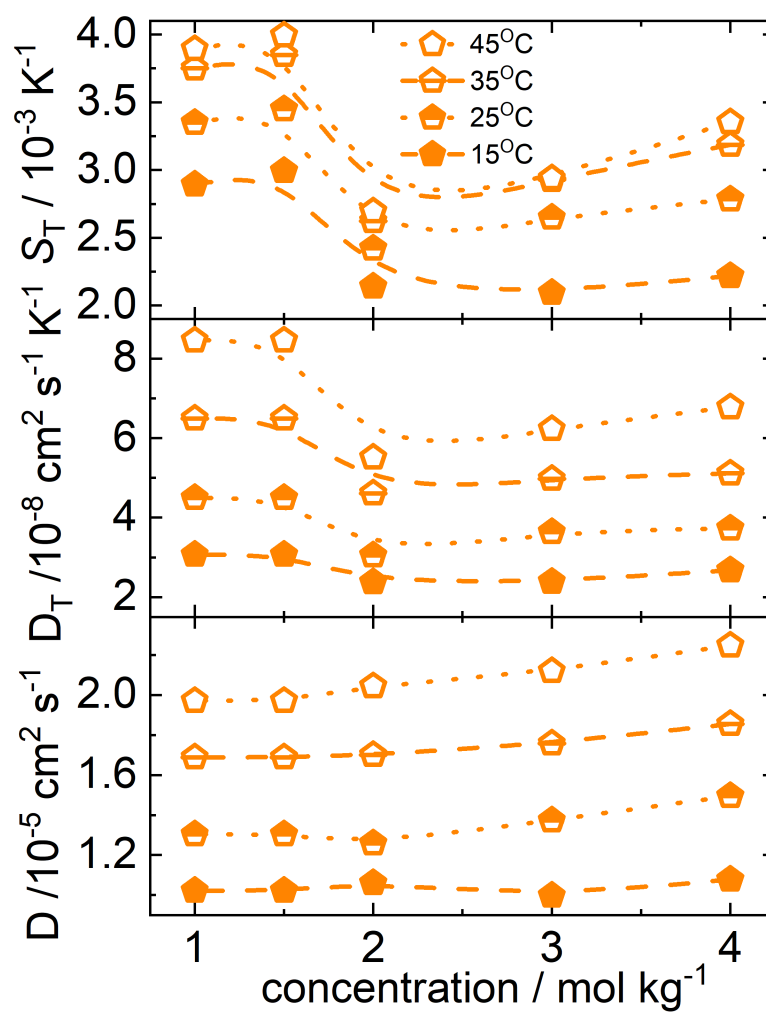


Figure 14: Concentration dependence of S_T , D and D_T of CH_3COOK in water at four different temperatures. The lines are a guide to the eye.

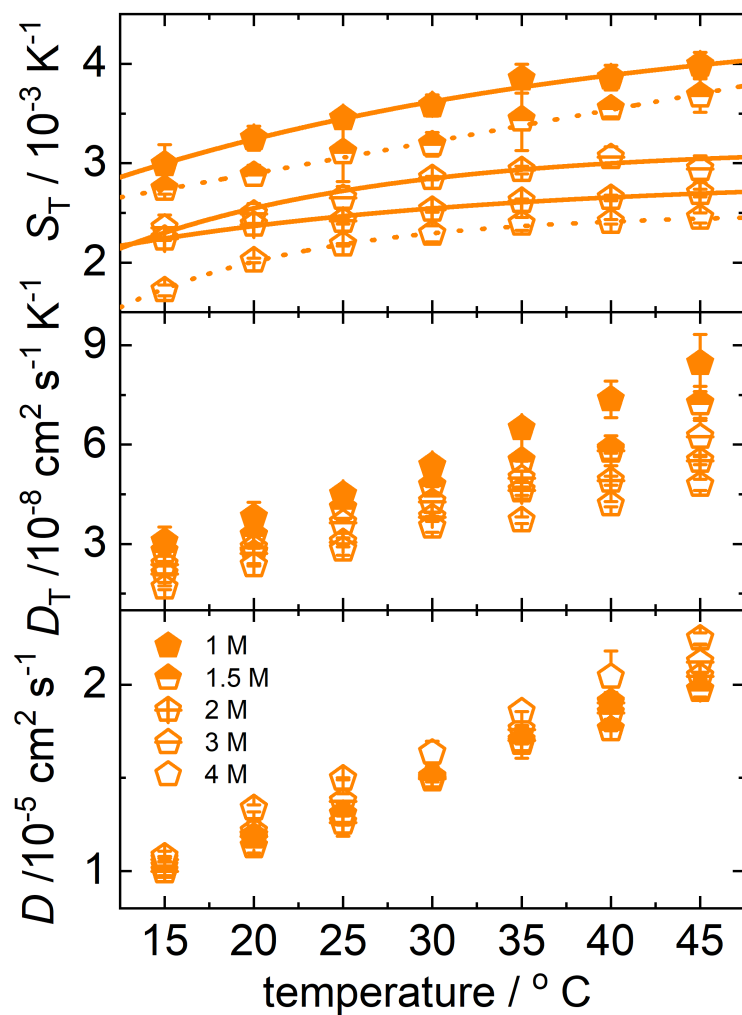
4.2 Temperature dependence of S_T , D and D_T of CH_3COOK 

Figure 15: Temperature dependence of S_T , D and D_T of CH_3COOK in water at five different concentrations. The lines are fitted according to Eq. (2) in the main manuscript.

4.3 Refractive index increments

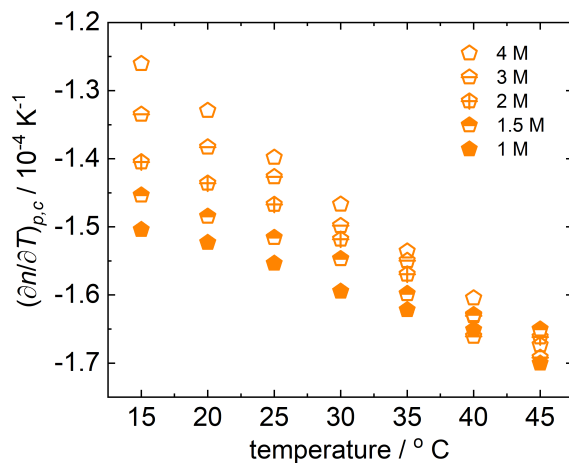


Figure 16: Temperature dependence of $(\partial n/\partial T)_{p,c}$ of CH_3COOK in water at four different concentrations.

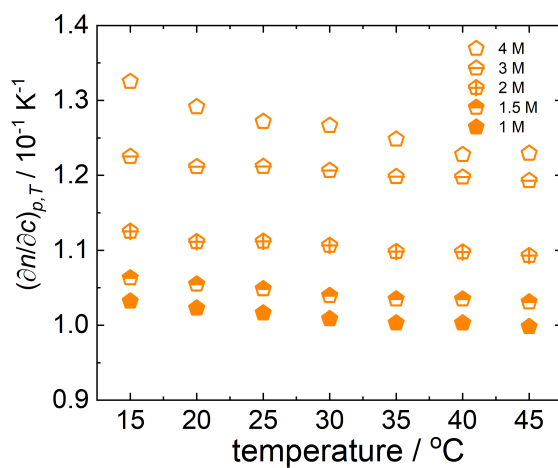


Figure 17: Temperature dependence of $(\partial n/\partial c)_{p,T}$ of CH_3COOK in water at four different concentrations.

5 Aqueous solutions of K_2CO_3

5.1 Concentration dependence of S_T , D and D_T of K_2CO_3

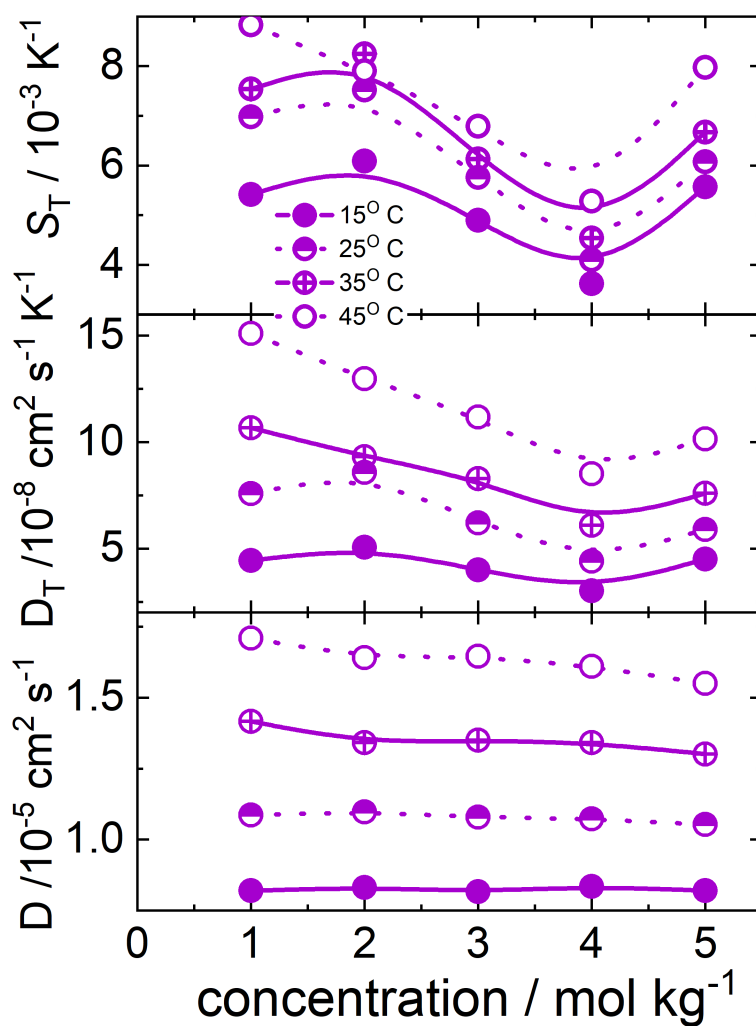


Figure 18: Concentration dependence of S_T , D and D_T of K_2CO_3 in water at four different temperatures. The lines are a guide to the eye.

5.2 Temperature dependence of S_T , D and D_T of K_2CO_3

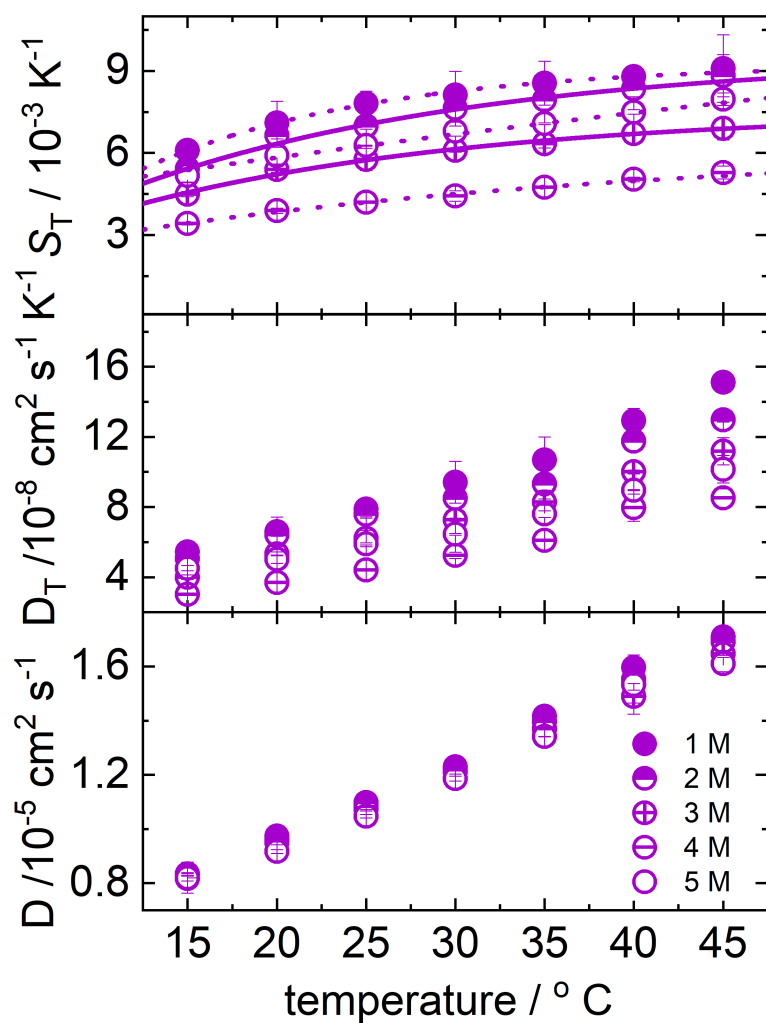


Figure 19: Temperature dependence of S_T , D and D_T of K_2CO_3 in water at five different concentrations. The lines are fitted according to Eq. (2) in the main manuscript.

5.3 Refractive index increments

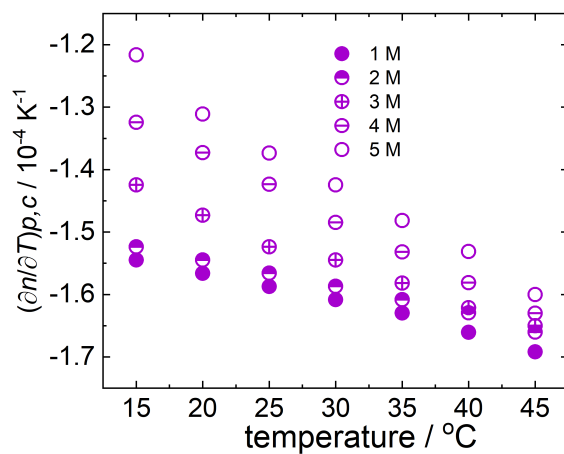


Figure 20: Temperature dependence of $(\partial n/\partial T)_{p,c}$ of K_2CO_3 in water at five different concentrations.

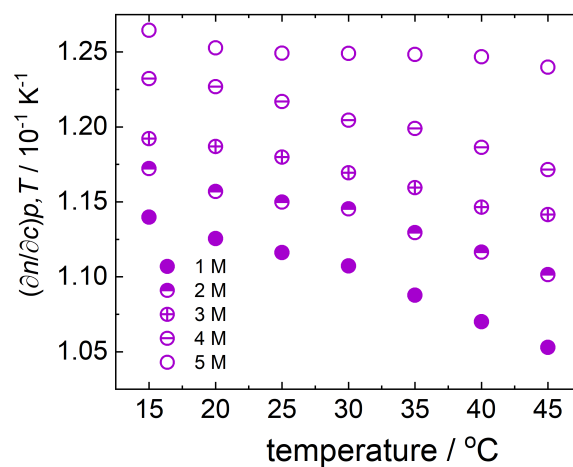


Figure 21: Temperature dependence of $(\partial n/\partial c)_{p,T}$ of CH_3COOK in water at five different concentrations.

6 Concentration dependence of pH for CH_3COOK and K_2CO_3

Since the salts CH_3COOK and K_2CO_3 are formed from weak acids, their aqueous solutions may contain several microspecies whose distribution depends on the pH of the solution. In Fig. 22 we show the species distribution as a function of pH for both salts obtained from ChemAxon's pKa Plugin [2]. Measured pH values of the salt solutions as a function of concentration are presented in Fig. 23 and show that the pH value increases with concentration.

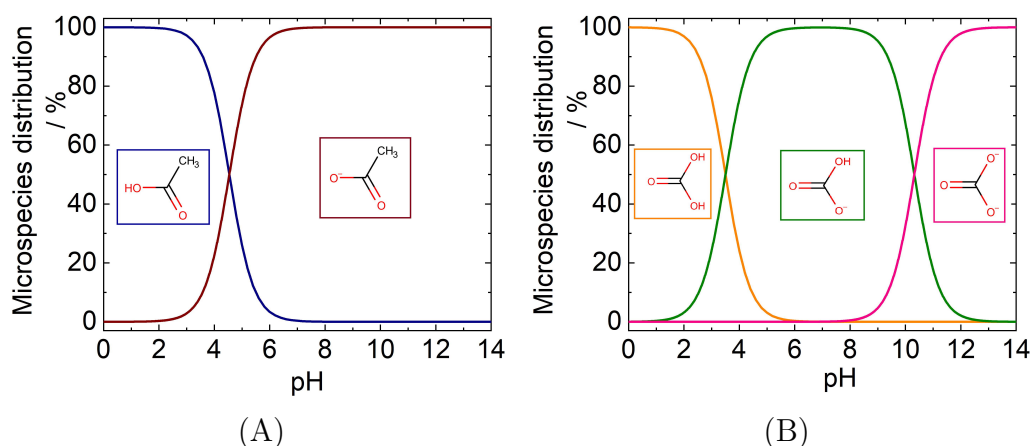


Figure 22: Microspecies distribution as a function of pH for aqueous solutions of (A) CH_3COOK and (B) K_2CO_3 . The lines show the fraction (in %) of the anionic species shown in the diagram framed in the same color.

For CH_3COOK at the lowest investigated concentration of 0.5 mol/kg we measured $\text{pH} = 8.6$, which corresponds to 99.99% of the conjugate base being fully charged, see Fig. 22. As the pH value increases with increasing concentration and since dissociation increases with pH, CH_3COO^- is the only species present at higher concentration. For K_2CO_3 at the lowest investigated concentration of 1 mol/kg we find $\text{pH} = 12.2$ and that 97% of the conjugate base molecules are fully charged and only a small fraction of 3% has a hydrated oxygen. At 5 mol/kg with $\text{pH} = 13.7$, 99.1% of the anions are fully charged. On the basis of these results, we conclude that in the investigated concentration range the dominant anions of the mono- and di-valent salt are CH_3COO^- and CO_3^{2-} , respectively.

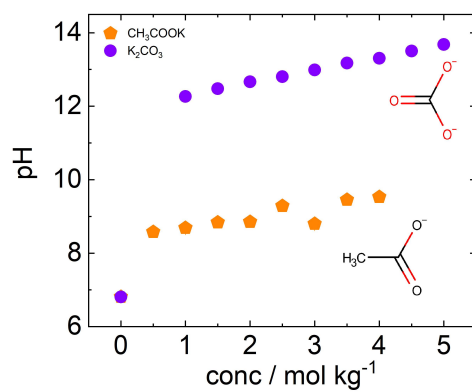


Figure 23: Measured pH values for CH_3COOK and K_2CO_3 as a function of salt concentration. The structure of the dominant anion species in the present pH range is also shown.

7 Adjusted parameters and various correlations

7.1 Determined parameters: S_T^i and b_1

We were able to describe the temperature and concentration dependence of the Soret Coefficient of the investigated salt solutions successfully using Eq. (4). We determined S_T^i and b_1 which are listed in Table 1. The maximum S_T^i value and the minimum b_1 value is observed for K_2CO_3 , which is a divalent salt.

Table 1: S_T^i and b_1 values of investigated systems

	$S_T^i (\times 10^{-3} K^{-1})$	$b_1 (\times 10^{-2} K^{-1})$
KCl	-10.6 ± 0.3	0.5 ± 0.7
KBr	-7.4 ± 0.1	0.8 ± 0.2
CH ₃ COOK	0.1 ± 0.1	1.7 ± 0.1
K ₂ CO ₃	7.6 ± 0.06	-0.8 ± 0.5
KSCN	-4.6 ± 0.3	0.3 ± 0.3

7.2 Parameters a_M and b_I for relative mass and moment of inertia differences

We used Eq. (4) to describe the temperature and concentration dependence of S_T , expressing the temperature and concentration independent fitting parameter S_T^i in respect to absolute differences in mass and moment of inertia according to Eq. (6). The absolute differences are given by,

$$\begin{aligned} \delta M &= M_{\text{solute}} - M_{\text{water}} \\ \delta I &= I_{\text{solute}} - I_{\text{water}} \end{aligned} \quad (1)$$

In the older literature the fitted values correspond often to relative differences in mass and moment of inertia.

The relative difference can be expressed as,

$$\begin{aligned} \delta M^{\text{relative}} &= \frac{M_{\text{solute}} - M_{\text{water}}}{M_{\text{solute}} + M_{\text{water}}} \\ \delta I^{\text{relative}} &= \frac{I_{\text{solute}} - I_{\text{water}}}{I_{\text{solute}} + I_{\text{water}}} \end{aligned} \quad (2)$$

The principal moments have been calculated using a commercial software (Chem3D Ver. 19, Perkiner Elmer). Values for all investigated systems are listed in Table 2. Note, that the mass and principal moment of inertia of water with 18.015 g/mol and $1.713 \text{ g mol}^{-1} \text{ \AA}^2$ have been used for all salts.

Table 2: Mass and moment of inertia differences (relative and absolute) of investigated systems

Solute	$\delta M /$ g mol^{-1}	$\delta M^{\text{relative}}$	$\delta I /$ $\text{g mol}^{-1} \text{ \AA}^2$	$\delta I^{\text{relative}}$
KCl	56.5	0.6	167.8	1.0
KBr	101.1	0.7	262.1	0.9
KSCN	79.2	0.7	367.4	1.0
CH ₃ COOK	80.1	0.7	399.1	1.0
K ₂ CO ₃	120.2	0.8	991.7	1.0
formamide	27.4	0.4	48.6	0.9
NMF	41.1	0.5	118.6	1.0
urea	42.1	0.5	91.2	0.9
DMF	55.2	0.6	165.7	0.9
acetamide	178.2	0.8	1319.7	1.0

Using relative differences we find $a_M^{\text{relative}} = (-5.2 \pm 0.4) \times 10^{-3} \text{ K}^{-1}$, $b_I^{\text{relative}} = (-2.1 \pm 0.7) \times 10^{-3} \text{ K}^{-1}$, which agrees with values reported by Rutherford [3] for substituted benzene systems $a_M^{\text{relative}} = (-5.3 \pm 0.4) \times 10^{-3} \text{ K}^{-1}$, $b_I^{\text{relative}} = (-2.6 \pm 0.7) \times 10^{-3} \text{ K}^{-1}$. Debuschewitz and Köhler [4] find for benzene-cyclohexane mixtures $a_M^{\text{relative}} = (-5.7 \pm 0.4) \times 10^{-3} \text{ K}^{-1}$, $b_I^{\text{relative}} = (-5.9 \pm 0.7) \times 10^{-3} \text{ K}^{-1}$. This shows that the reported values are in the same range.

As mentioned before, previous studies reported values of a_M and b_I on the basis of relative differences. For an easy comparison with our values, this was recalculated with respect to absolute differences. For the same, we had to multiply the values of a_M and b_I in the literature with $M_{\text{solute}} + M_{\text{water}}$ and $I_{\text{solute}} + I_{\text{water}}$ respectively.

7.3 Correlation between b_1 and $\log P$

Fig. 24 shows values of the parameter b_1 , which describes the first order temperature dependence in Eq. (4). While a study of amide systems [5]

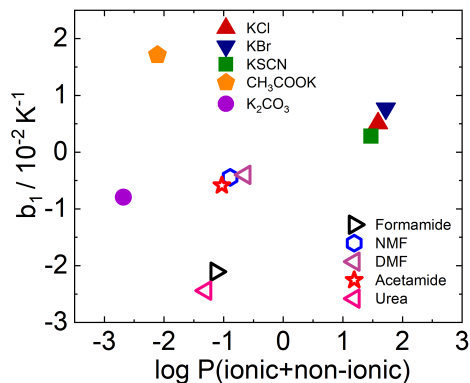


Figure 24: The parameter b_1 for all investigated potassium salts in water as a function of $\log P(\text{ionic+non-ionic})$. We added also the values for the amide systems previously studied by Niether *et al.* [5].

revealed an increase of b_1 with $\log P$, we cannot identify a correlation between b_1 and $\log P$ for the potassium salts.

7.4 Correlation between $\Delta S_T(\Delta c)$ and $\log P$

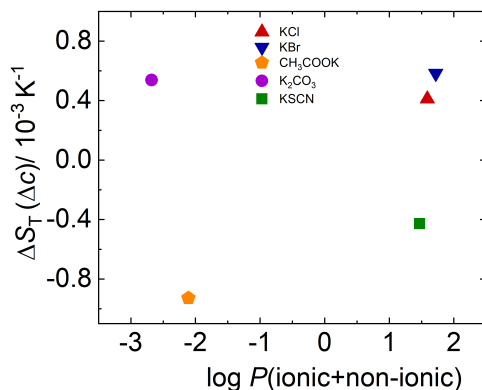


Figure 25: $\Delta S_T(\Delta c)$ of all investigated potassium salts in water as a function of $\log P(\text{ionic+non-ionic})$.

Fig. 25 shows values for $\Delta S_T(\Delta c)$, defined as the difference between S_T at 2 mol/kg and 1 mol/kg. Note that compared to the amide systems we had to choose a smaller concentration range as the concentration. We have chosen

the two lowest salt concentrations because a correlation with $\log P$ is not expected at high concentration since $\log P$ describes the interaction between the solute and water and, with increasing salt concentration, interactions between salt clusters become more likely.

Considering all investigated salts, $\Delta S_T(\Delta c)$ is not correlated with $\log P(\text{ionic}+\text{non-ionic})$. Considering only monovalent salts $\Delta S_T(\Delta c)$ seems to increase with $\log P(\text{ionic}+\text{non-ionic})$, but the correlation is weak. This observation cannot be generalized due to the limited number of investigated systems.

7.5 Correlation between $\Delta S_T(\Delta T)$ and $\log P$

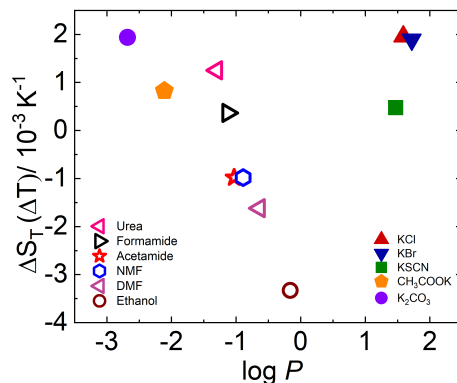


Figure 26: $\Delta S_T(\Delta T)$ of all investigated potassium salts in water as a function of $\log P$ (ionic+non-ionic). We added also the values for the amide systems at 5wt% previously studied by Niether *et al.* [5].

Fig.26 shows $\Delta S_T(\Delta T)$ measured at the lowest salt concentration of 1 mol/kg (solid symbols) as function of $\log P$ (ionic+non-ionic). A correlation between $\Delta S_T(\Delta T)$ and $\log P$ as it is observed for non-ionic solutes cannot be confirmed for the investigated salts. For comparison we added also the values obtained recently for various amide systems (open symbols) at a concentration of 5wt% [5]. Note, that potassium acetate and potassium carbonate, being able to form hydrogen bonds show a decrease of $\Delta S_T(\Delta T)$ with increasing $\log P$ as it is observed for non-ionic amides.

8 Diffusion coefficients of amides

Diffusion coefficients of non-ionic amides in water show a decrease with concentration (cf. Fig.27). This decay of D is similar to the behavior of K_2CO_3 and $KSCN$. Except for DMF we observe for all amides a weaker decay for lower temperatures.

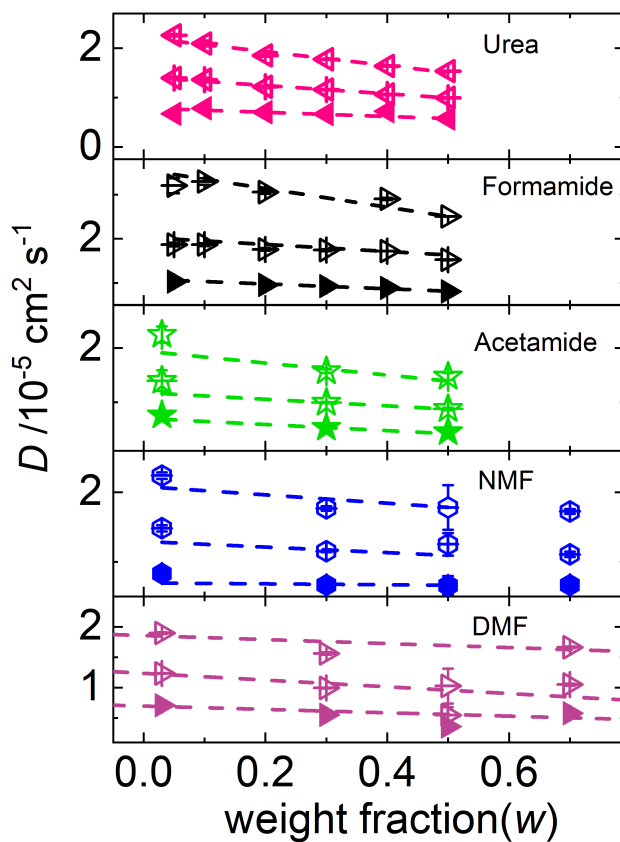


Figure 27: D as a function of concentration for amide systems, which had been studied by Niether *et al.* [5]. Note that these are unpublished diffusion coefficients that have been determined by Niether *et al.* [5] using thermophoretic measurements. Filled symbols correspond to $T = 10^\circ\text{C}$, crossed symbols to $T = 30^\circ\text{C}$ and open symbols to $T = 50^\circ\text{C}$. The dashed lines are linear fits up to a weight fraction of 0.5 in the case of urea, formamide, acetamide and NMF and up to 0.7 for DMF.

References

- [1] F. S. Gaeta, G. Perna, G. Scala, and F. Bellucci. Non-isothermal matter transport in sodium-chloride and potassium chloride aqueous solutions. 1. homogeneous system (thermal-diffusion). *J. Phys. Chem.*, 86:2967–2974, 1982.
- [2] ChemAxon. pK_a Plugin. <https://docs.chemaxon.com/display/docs/pka-plugin.md>, 2020. online protonation calculator.
- [3] W. M. Rutherford. Effect of mass-distribution on the isotopic thermal-diffusion of substituted benzenes. *J. of Chem. Phys.*, 81:6136–6139, 1984.
- [4] C. Debuschewitz and W. Köhler. Molecular origin of thermal diffusion in benzene plus cyclohexane mixtures. *Phys. Rev. Lett.*, 87:055901, 2001.
- [5] D. Niether, H. Kriegs, J.K.G. Dhont, and S. Wiegand. Peptide model systems: Correlation between thermophilicity and hydrophilicity. *J Chem Phys*, 149:044506, 2018.

SUPPORTING INFORMATION:
Effect of cation on the thermodiffusive
behavior of aqueous salts solutions

Shilpa Mohanakumar
and Simone Wiegand

Contents

S1 Experimental Methods	S2
S1.1 Thermal Diffusion Forced Rayleigh Scattering	S2
S1.2 Refractive index contrast measurements	S2
S2 Temperature dependence of S_T for CH_3COOK and CH_3COONa	S3
S3 Concentration dependence of S_T	S3
S4 TDFRS signal	S6
S5 Determined and used parameters	S6
S5.1 Determined parameters: S_T^i and b_1	S6
S5.2 Used log P -values	S7
S6 Concentration and temperature dependence of D_T	S9
S7 Concentration dependence of activity coefficient	S11

S1 Experimental Methods

S1.1 Thermal Diffusion Forced Rayleigh Scattering

Thermodiffusion of the electrolyte solutions was measured by infrared thermal diffusion forced Rayleigh scattering (IR-TDFRS) [1, 2]. This method uses the interference grating of two infrared laser beams ($\lambda = 980$ nm) to generate a temperature grating inside an aqueous sample due to the inherent absorption of water in that range [3]. A third laser beam is refracted by this grating and the intensity of the refracted beam is measured. This intensity is proportional to the refractive index contrast of the grating, showing a fast rise over time due to the thermal gradient, then a slower change of intensity due to diffusion of the solute along the temperature gradient (cf. Fig 1).

The heterodyne scattering intensity $\zeta_{het}(t)$ of the read-out beam is measured and fitted with

$$\zeta_{het}(t) = 1 - \exp\left(-\frac{t}{\tau_{th}}\right) - A(\tau - \tau_{th})^{-1} \times \left\{ \tau \left[1 - \exp\left(-\frac{t}{\tau}\right) \right] - \tau_{th} \left[1 - \exp\left(-\frac{t}{\tau_{th}}\right) \right] \right\}. \quad (S1)$$

With the lifetimes $\tau_{th} = (D_{th}q^2)^{(-1)}$ and $\tau = (Dq^2)^{(-1)}$ of the temperature and concentration grating, respectively, where q , D_{th} and D denote the grating wave vector, the thermal diffusivity and the mutual diffusion coefficient, respectively. The Soret coefficient (S_T) can be calculated from the amplitude A , if the so-called contrast factors, the change of refractive index with temperature and concentration, $(\partial n/\partial T)_{c,p}$ and $(\partial n/\partial c)_{T,p}$, are known:

$$A = \left(\frac{\partial n}{\partial c}\right)_{p,T} \left(\frac{\partial n}{\partial T}\right)_{p,c}^{-1} S_T c (1 - c). \quad (S2)$$

S1.2 Refractive index contrast measurements

Refractive index contrast factors are required to calculate S_T . The refractive index as function of concentration was measured with an Abbe refractometer (Anton Paar Abbemat MW) at a wavelength of 632.8 nm. For all salts, refractive index at five concentrations around the desired contraction were measured. The slope of the linear interpolation of the refractive index as a function of concentration gives $(\partial n/\partial c)_{p,T}$. The refractive index increments with temperature $(\partial n/\partial T)_{p,c}$ was measured interferometrically [4]. Measurements were performed over a temperature range of 25-45°C, with a heating rate of 1.6 mK/sec. The refractive index varied linearly with concentration and temperature in the investigated range.

S2 Temperature dependence of S_T for CH_3COOK and CH_3COONa

As mentioned in the main manuscript, temperature dependence of S_T of CH_3COOK and CH_3COONa is similar to that of carbonate salts. This is shown in Fig.S1.

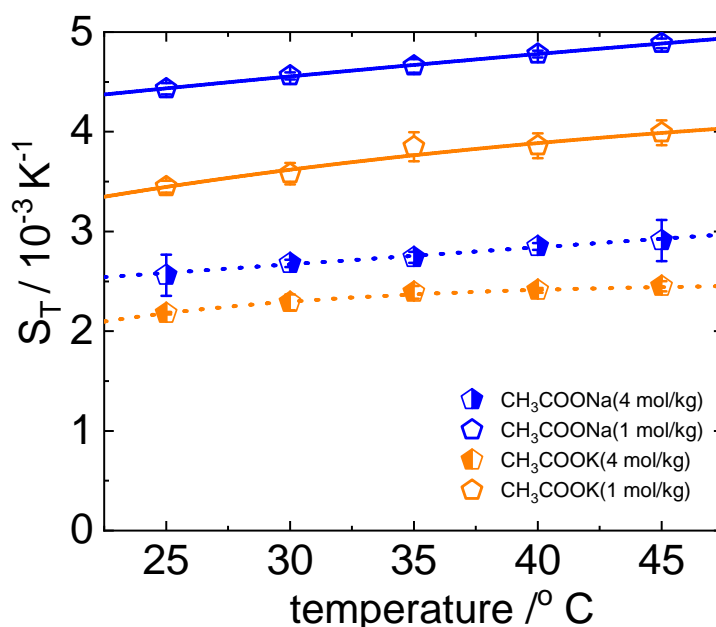


Figure S1: Soret coefficient of CH_3COOK and CH_3COONa as a function of temperature. Open and half-filled symbols correspond to concentrations 1 and 4 mol kg^{-1} , respectively. The lines correspond to fit according to Eq. (1) in the main manuscript.

S3 Concentration dependence of S_T

The concentration dependence of different salt systems studied at three different temperatures (25°C, 35°C, 45°C) is shown in Figs.S2, S3 and S4. It can be seen that the concentration dependent slope of all the studied systems doesn't change vastly with temperature.

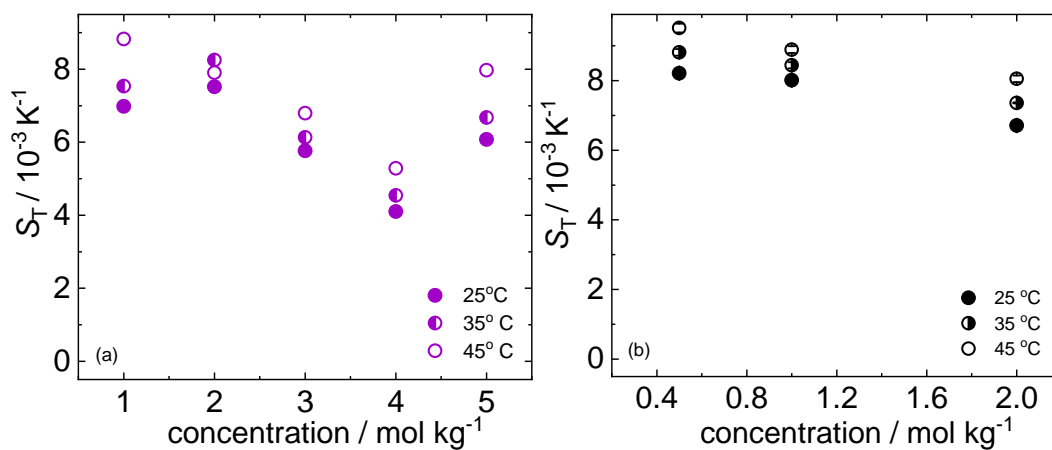


Figure S2: Concentration dependence of S_T of (a) K_2CO_3 and (a) Na_2CO_3 at 25° C, 35° C and 45° C

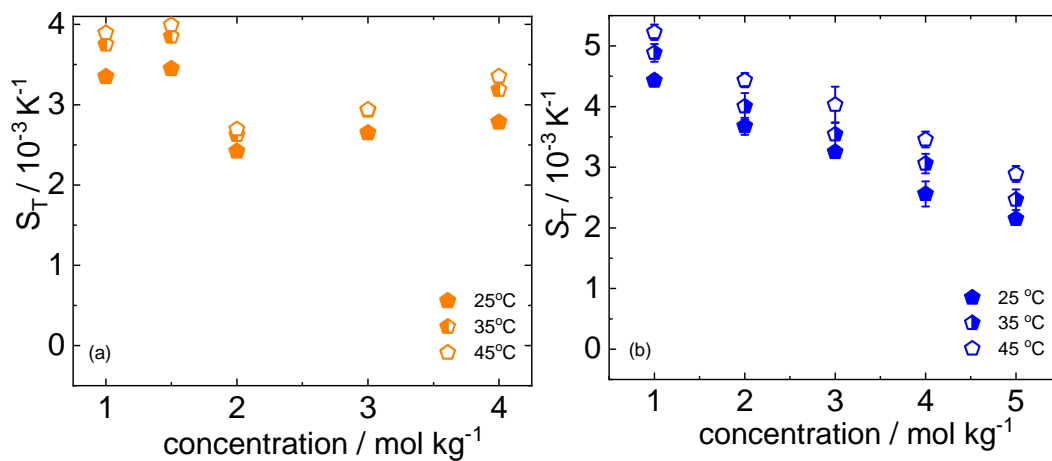


Figure S3: Concentration dependence of S_T of (a) CH_3COOK and (a) CH_3COONa at 25° C, 35° C and 45° C

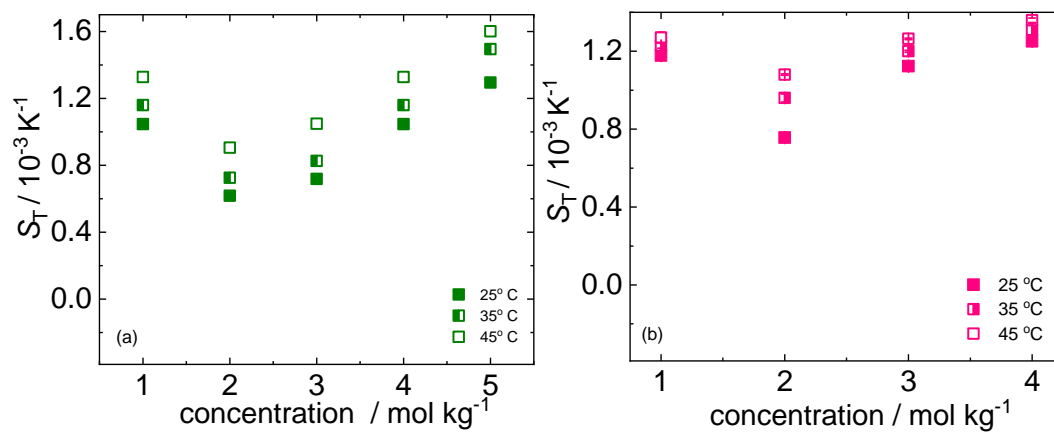


Figure S4: Concentration dependence of S_T of (a) KSCN and (b) NaSCN at 25°C, 35°C and 45°C

S4 TDFRS signal

An example of the TDFRS raw-data is shown in Fig.S5. Fig.S5(a) and Fig.S5(b) corresponds to the signal measured for NaSCN, at 1 mol kg^{-1} and 4 mol kg^{-1} respectively at 25°C and the corresponding residual plots. The black dots marks the data points, the red line represents the fit according the Eq.S2 and the red dots mark the residuals, which are within the 2σ range and do not show systematic deviations.

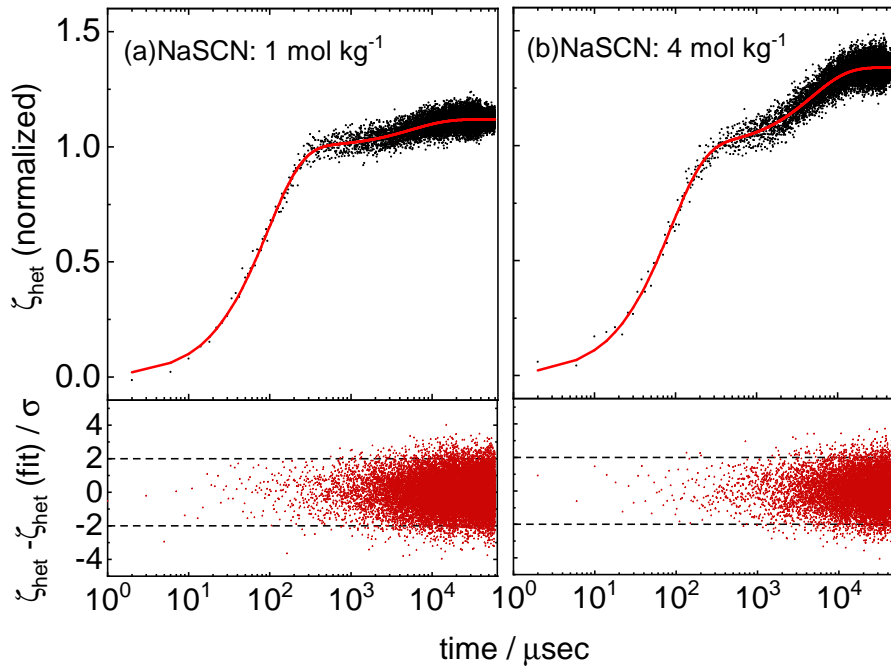


Figure S5: Normalized heterodyne diffraction intensities of NaSCN at 25°C as a function of time at (a) 1 mol kg^{-1} and (b) 4 mol kg^{-1} . The black dots marks the data points, the red line represents the fit according the Eq.S2 and the red dots mark the residuals.

S5 Determined and used parameters

S5.1 Determined parameters: S_T^i and b_1

We described the temperature and concentration dependence of the Soret coefficient of the investigated salt solutions successfully using Eq. (2) in the main manuscript. The determined S_T^i values are listed in Table S1. It has to be noted here that for all salts except Na_2CO_3 the fitting corresponds to

third order and second order polynomials for concentration and temperature respectively. Due to the low solubility of Na_2CO_3 , we were only able to measure the three lowest concentration, therefore we had to reduce the number of fit parameters by using first order polynomials of concentration and temperature to describe the data. For NaCl as well, for which the S_T values were only reported at three concentrations[5], we used first order polynomials of concentration and temperature to fit the data.

Table S1: S_T^i values of investigated systems

	$S_T^i (\times 10^{-1} \text{K}^{-1})$	$b_1 (\text{K}^{-1})$
CH_3COONa	9.94 ± 0.3	12.7 ± 0.6
CH_3COOK	9.94 ± 0.1	13.6 ± 0.1
Na_2CO_3	9.92 ± 0.4	19.7 ± 0.1
K_2CO_3	9.93 ± 0.1	19.6 ± 0.5
NaSCN	9.96 ± 0.2	3.5 ± 0.9
KSCN	9.97 ± 0.3	3.3 ± 0.3
NaCl	9.98 ± 0.2	2.9 ± 0.4
KCl	9.99 ± 0.3	1.0 ± 0.7
KBr	9.99 ± 0.1	4.0 ± 0.2

S5.2 Used log P -values

In order to correlate S_T^i with the hydrophilicity, we also determined the log P . Calculator Plugins were used for calculation of log P within Marvin 16.5.2.0, 2016, ChemAxon (<http://www.chemaxon.com>). The calculation method is based on the publication by Viswanadhan *et al.* [6]. Note that different methods exists, which give slightly different values and it is important to stay in one method to compare results. Values obtained are listed in Table S2. It has to be noted that log P has ionic and non-ionic contributions and the values listed here corresponds to the sum of these contributions.

Table S2: $\log P$ values of investigated systems

	$\log P$
CH ₃ COONa	-7.83
CH ₃ COOK	-6.86
Na ₂ CO ₃	-14.12
K ₂ CO ₃	-12.18
NaSCN	-4.25
KSCN	-3.28
NaCl	1.44
KCl	1.59
KBr	1.72

S6 Concentration and temperature dependence of D_T

Dependence of D_T with concentration at 25° C is shown in Fig.S6. The behavior of D_T is similar to that of S_T , which has been discussed in the main manuscript in Sec. 3.

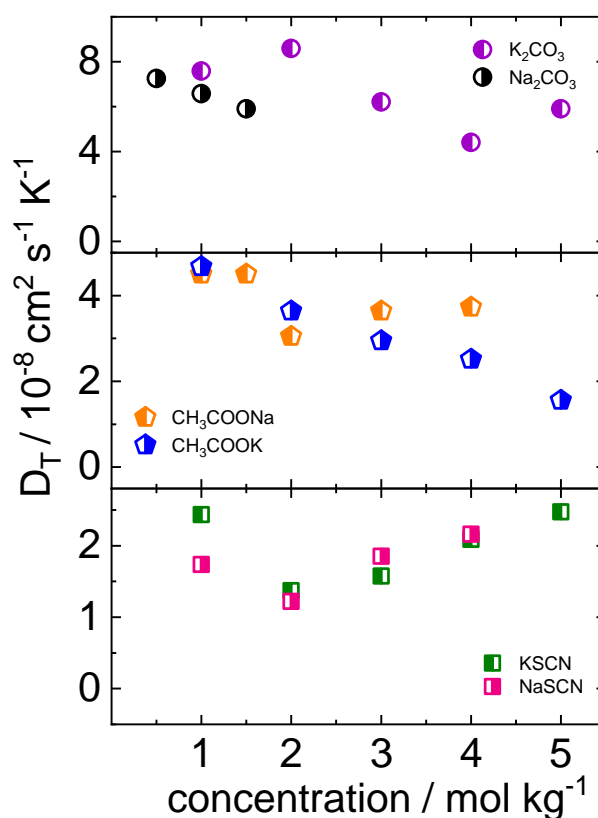


Figure S6: Thermal diffusion coefficient of all investigated salts as a function of concentration at a temperature of 25°C. We used the symbols as follows: CH₃COOK (orange pentagons), CH₃COONa (blue pentagons), K₂CO₃ (violet circles), Na₂CO₃ (black circles), KSCN (green squares) and NaSCN (pink squares).

Temperature dependence of D_T at the lowest concentration measured (1 mol kg⁻¹) is shown in Fig.S7.

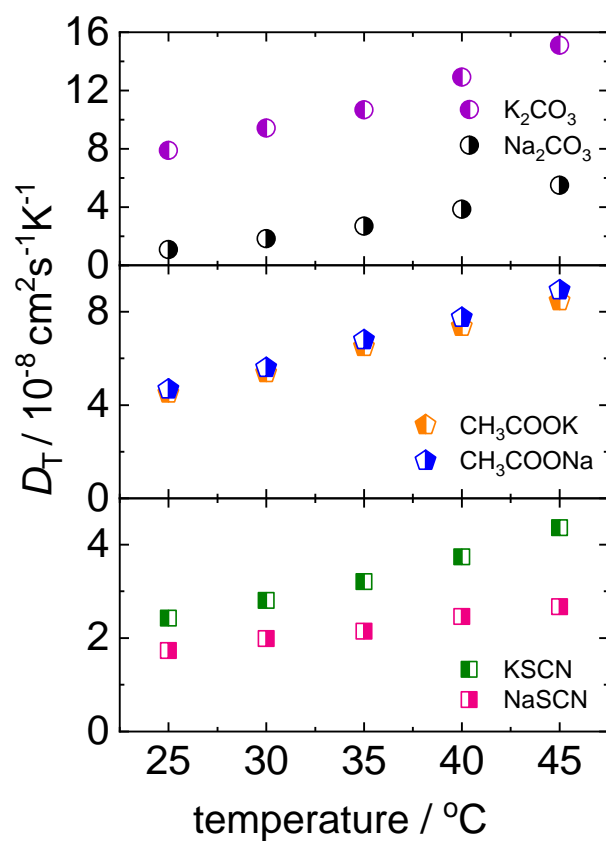


Figure S7: Thermal diffusion coefficient of all investigated salts as a function of temperature at a concentration of 1 mol kg^{-1} . We used the symbols as follows: CH_3COOK (orange pentagons), CH_3COONa (blue pentagons), K_2CO_3 (violet circles), Na_2CO_3 (black circles), KSCN (green squares) and NaSCN (pink squares).

S7 Concentration dependence of activity coefficient

As discussed in the main manuscript (cf. Eq.4), D of electrolyte solutions depends on the mean ionic activity coefficient, γ_{\pm} . The concentration dependence of D for aqueous solutions of KSCN and NaSCN shows an decrease and increase, respectively. Both systems show an increase of the viscosity with increasing concentration. To understand the difference in the concentration dependence in the diffusion of the two salts, we examined additionally the concentration dependence of the mean ionic activity coefficient γ_{\pm} , which has been studied by Robinson *et al.* [7]. We have used these values to calculate the corresponding term $1 + c(d \ln \gamma_{\pm}/dc)$ in Eq.4 in the main manuscript. This term shows for both salts a minimum at a low concentration around 0.25 mol/Kg and a gradual increase with increasing concentration. Within the measured concentration range (1-4 mol kg⁻¹), the increase of $1 + c(d \ln \gamma_{\pm}/dc)$ is 4-times steeper for NaSCN compared to KSCN.

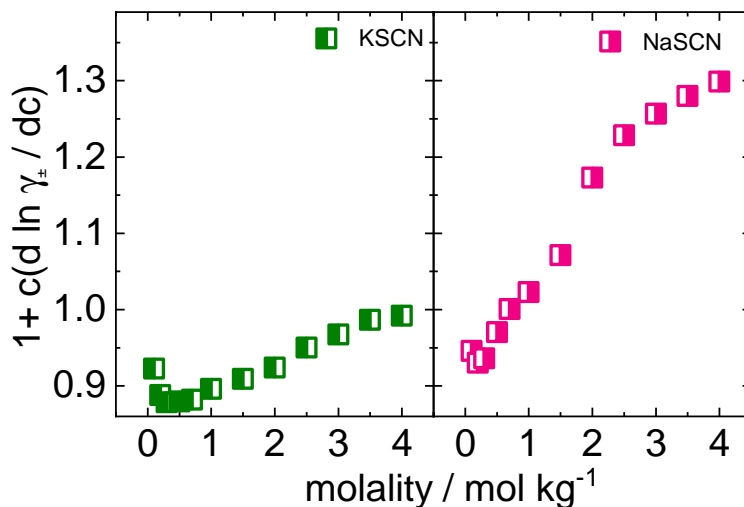


Figure S8: Concentration dependence of $1 + c(d \ln \gamma_{\pm}/dc)$ of NaSCN and KSCN.

References

- [1] S. Wiegand and W. Köhler. Measurement of transport coefficients by an optical grating technique. *LNP Vol. 584: Thermal Nonequilibrium Phenomena in Fluid Mixtures*, 584:189–210, 2002.

-
- [2] P. Blanco, H. Kriegs, M. P. Lettinga, P. Holmqvist, and S. Wiegand. Thermal diffusion of a stiff rod-like mutant y21m fd-virus. *Biomacromolecules*, 12:1602–1609, 2011.
- [3] S. Wiegand, H. Ning, and H. Kriegs. Thermal diffusion forced rayleigh scattering setup optimized for aqueous mixtures. *J. Phys. Chem. B*, 111:14169–14174, 2007.
- [4] A. Becker, W. Köhler, and B. Müller. A scanning michelson interferometer for the measurement of the concentration and temperature derivative of the refractive- index of liquids. *Phys. Chem. Chem. Phys.*, 99:600–608, 1995.
- [5] F. Römer, Z. Wang, S. Wiegand, and F. Bresme. Alkali halide solutions under thermal gradients: Soret coefficients and heat transfer mechanisms. *J. Phys. Chem. B*, 117:8209–8222, 2013.
- [6] Vellarkad N. Viswanadhan, Arup K. Ghose, Ganapathi R. Revankar, and Roland K. Robins. Atomic physicochemical parameters for three dimensional structure directed quantitative structure-activity relationships. 4. additional parameters for hydrophobic and dispersive interactions and their application for an automated superposition of certain naturally occurring nucleoside antibiotics. *J. Chem. Inf. Model.*, 29:163–172, 1989.
- [7] R. A. Robinson. The activity coefficients of sodium and potassium thiocyanate in aqueous solution at 25 degrees from isopiestic vapor pressure measurements. *J. Am. Chem. Soc.*, 62:3131–3132, 1940.

Supplementary information:
Thermophoretic microfluidic cells for
evaluating Soret coefficient of colloidal
particles

Namkyu Lee, Shilpa Mohanakumar and Simone Wiegand

April 13, 2022

Contents

S1 Thermal Diffusion Forced Rayleigh Scattering	S2
S2 Calibration of rhodamine B for fluorescence lifetime imaging microscope (FLIM)	S2
S3 Effect of free convection on the concentration profile in the measuring channel	S3
S4 Feasibility of the cell measuring thermophobic particles	S6

S1 Thermal Diffusion Forced Rayleigh Scattering

We used infrared Thermal Diffusion Forced Rayleigh Scattering (IR-TDFRS) setup to measure the thermal diffusion properties of the solution. This is a transient grating technique which has been used to study the transport properties in different aqueous systems of non-ionic surfactants[1, 2], biocolloids[3] and saccharide solutions[4]. IR laser beams are used which creates a temperature grating inside the sample due to inherent absorption of water in that wavelength range. This induced temperature gradient leads to the migration of particles which results in concentration grating. A readout laser beam that probes the optical contrast of the interference grating is used and the heterodyne intensity of this scattered beam is measured and fitted with

$$\zeta_{\text{het}}(t) = 1 - \exp\left(-\frac{t}{\tau_{\text{th}}}\right) - A(\tau - \tau_{\text{th}})^{-1} \times \left\{ \tau \left[1 - \exp\left(-\frac{t}{\tau}\right) \right] - \tau_{\text{th}} \left[1 - \exp\left(-\frac{t}{\tau_{\text{th}}}\right) \right] \right\}. \quad (\text{S1})$$

with the lifetimes $\tau_{\text{th}} = (D_{\text{th}}q^2)^{(-1)}$ and $\tau = (Dq^2)^{(-1)}$ of the temperature and concentration grating, respectively, where q , D_{th} and D denote the grating wave vector, the thermal diffusivity and the mutual diffusion coefficient, respectively. When change of refractive index with temperature and concentration, $(\partial n/\partial T)_{c,p}$ and $(\partial n/\partial c)_{T,p}$, are known the Soret coefficient can be calculated from the following equation,

$$A = \left(\frac{\partial n}{\partial w}\right)_{p,T} \left(\frac{\partial n}{\partial T}\right)_{p,w}^{-1} S_{\text{T}} w (1 - w) \quad (\text{S2})$$

where w is the mass fraction. Thus, the transport coefficients are determined by fitting Eq. S2 to the measured heterodyne signal.

S2 Calibration of rhodamine B for fluorescence lifetime imaging microscope (FLIM)

For fluorescence lifetime imaging microscope (FLIM), the calibration curve of fluorescent dyes is needed for converting fluorescence lifetime into temperature. In this study, Rhodamine B (RhB) was used as fluorescent dyes for FLIM to measure temperature. The concentration of RhB solution was 10^{-4} M. For the calibration, we used the copper block with a micro-sized cavity by

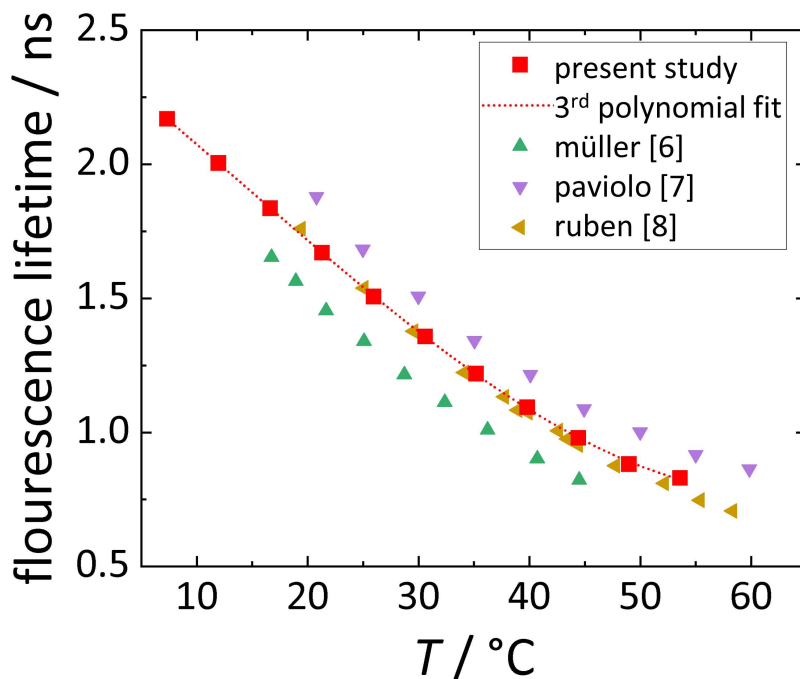


Figure S1: Calibration curve (red dot) with 3rd polynomial fit of RhB solution used in this study and compared with other research.

attaching the spacer and the cover slip on the block. The copper block was thermostated by the thermostats (Lauda eco RE 620, Lauda-Königshofen, Germany). Figure S1 showed the calibration curve fitted with 3rd polynomial equation compared to literatures [5, 6, 7]. It showed that the measured lifetime with temperature was well-matched with literature values. Therefore, we infer that the calibrated curve with 3rd polynomial fit can be used for measuring the temperature.

S3 Effect of free convection on the concentration profile in the measuring channel

Free convection in the measuring channel is inevitable because the temperature gradient induces a density change inducing a buoyancy force in the solution. However, we cannot measure the velocity profile in the microchannel directly, so that we performed simulations to check the effect of free convection on the concentration profile in the measuring channel. COMSOL

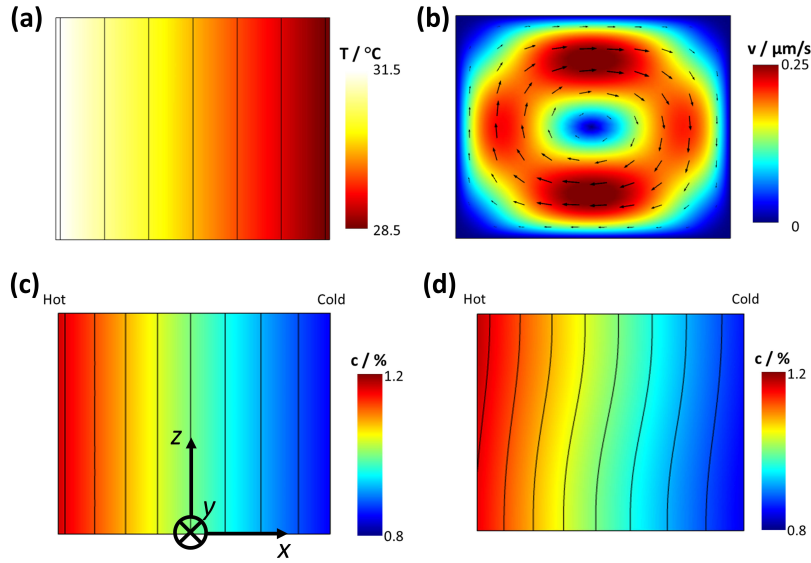


Figure S2: (a) Temperature and (b) Velocity distribution on cross-sectional ($x - z$) plane in the measuring channel. Comparison of concentration distribution on cross-sectional ($x - z$) plane in the measuring channel (c) without and (d) with free convection.

v.5.4, a commercial program, was used to simulate the heat and mass transfer, fluid dynamics in the measuring channel. The transport of particles is considered as follow:

$$\frac{\partial c}{\partial t} + \nabla(-D\nabla c - D_T c(1-c)\nabla T) + v\nabla c = 0 \quad (\text{S3})$$

with the diffusion coefficient D , the thermal diffusion coefficient D_T , the concentration c , the velocity v , respectively. The measured D and D_T obtained in the TDFRS-setup were used in the simulation. Furthermore, we used the physical properties of pure water supplied by NIST Chemistry WebBook, SRD 69 because the investigated solutions are very dilute (weight fraction $c \ll 1$). Since we know that a one-dimensional temperature profile forms in the measuring channel, we performed only a two-dimensional simulation in the $x - z$ plane. Figure S2 shows the temperature, velocity and concentration profiles in the measuring channel. The velocity magnitude due to free convection in Fig. S2(b) reaches up to $0.25 \mu\text{m/s}$, however, it does not distort the temperature profile in Fig.S2(a). Figure S2 (c) and (d) compare the concentration profile without and with free convection. The concentration profile without free convection is one-dimensional, whereas the profile with

the free convection is distorted along the velocity direction. We need to check how much free convection affects the concentration profile quantitatively.

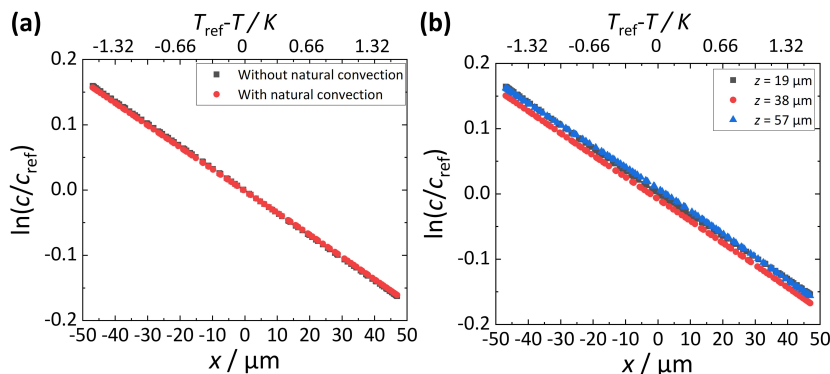


Figure S3: Graphs of (a) the logarithmic concentration ratio without and with free convection ($z = 38 \mu\text{m}$, the center of height) and (b) the height dependence ($z = 19 \mu\text{m}$, $38 \mu\text{m}$ and $57 \mu\text{m}$) on the logarithmic concentration ratio as function of x and $T - T_{\text{ref}}$.

Figure S3(a) compares the logarithmic concentration ratio without and with free convection in the measuring channel. Even though the concentration profile is distorted by free convection, the quantitative values in Fig. S2(d) overlap. Additionally, we need to check the height dependence on the logarithmic concentration ratio. Figure S3(b) shows $\ln(c/c_{\text{ref}})$ as function of x and $T - T_{\text{ref}}$, respectively. Although there is a small variation of $\ln(c/c_{\text{ref}})$ with height, the slope, which is used to calculate S_T (cf. Eq. 4), is the same for all heights. Therefore, we conclude that free convection can be neglected in the thermophoretic microfluidic cell.

Furthermore, we should ensure that the simulated results agree with the measured results. Figure S4 shows a comparison of the logarithmic concentration ratio as function of the temperature difference for the simulation and the measurement. S_T determined from the simulation results using Eq.4 is -0.102 K^{-1} , which agrees with the TDFRS result of $S_T = -0.105 \text{ K}^{-1}$ and the cell results ($S_T = -0.114 \text{ K}^{-1}$ in run 1, $S_T = -0.110 \text{ K}^{-1}$ in run 2). Therefore, we are convinced that the simulations reproduce the measurements reasonably well, so that we can use the simulation to investigate convection effects in the measurements.

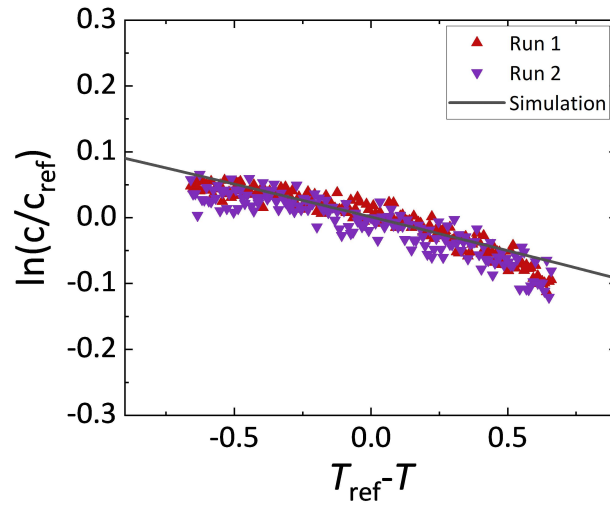


Figure S4: Logarithmic concentration ratio as function of the temperature difference determined by the simulation result in comparison with the measurements. Run 1 and 2 refer to the measurements with the thermophoretic microfluidic cell at $T_{ave} = 24.7^{\circ}C$ in the manuscript.

S4 Feasibility of the cell measuring thermophobic particles

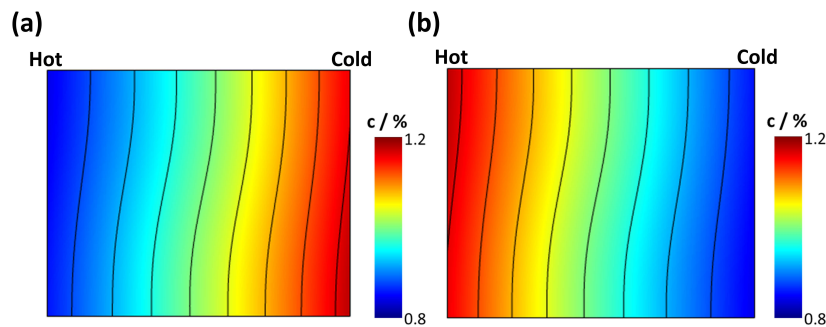


Figure S5: Comparison of the concentration profile between (a) the thermophobic ($S_T > 0$) and (b) the thermophilic ($S_T < 0$) particles.

We checked the variation of the concentration profile in the cell for thermophilic and thermophobic particles. In the simulation of thermophobic

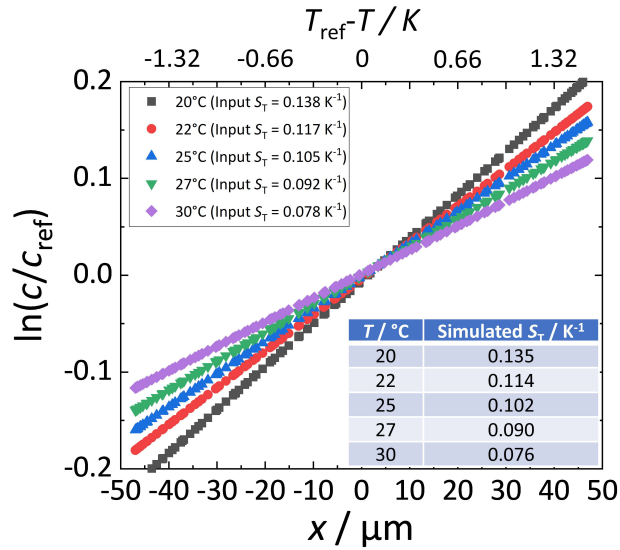


Figure S6: Graphs of the logarithmic concentration ratio as function of x and $T - T_{\text{ref}}$. Inset table presents the calculated Soret coefficient from the simulation.

particles ($S_T > 0$), we used the same magnitude of S_T changing only the sign of S_T . Figure S5 compares the concentration profile between the thermophobic and thermophilic ($S_T < 0$) particles. Both concentration profiles are distorted similarly due to free convection. However, the influence on the concentration profile is weak leading to a S_T , which is for the lowest value of S_T at 30°C 2.6% smaller than the expected S_T without convection (cf. Fig. S6). Note that the deviations will increase for systems with a lower thermal diffusion coefficient.

References

- [1] H. Ning, S. Datta, T. Sottmann, and S. Wiegand. Soret effect of nonionic surfactants in water studied by different transient grating setups. *J. Phys. Chem. B*, 112:10927–10934, 2008.
- [2] B. Arlt, S. Datta, T. Sottmann, and S. Wiegand. Soret effect of n-octyl beta-d-glucopyranoside (c(8)g(1)) in water around the critical micelle concentration. *J. Phys. Chem. B*, 114:2118–2123, 2010.
- [3] P. Blanco, H. Kriegs, M. P. Lettinga, P. Holmqvist, and S. Wiegand. Thermal diffusion of a stiff rod-like mutant Y21M fd-virus. *Biomacromolecules*, 12:1602–1609, 2011.
- [4] P. Blanco and S. Wiegand. Study of the soret effect in monosaccharide solutions. *J. Phys. Chem. B*, 114:2807–2813, 2010.
- [5] C. B. Müller, K. Weiss, A. Loman, J. Enderlein, and W. Richtering. Remote temperature measurements in femto-liter volumes using dual-focus-fluorescence correlation spectroscopy. *Lab Chip*, 9(9):1248–1253, 2009.
- [6] C. Paviolo, A. H. A. Clayton, S. L. Mcarthur, and P. R. Stoddart. Temperature measurement in the microscopic regime: a comparison between fluorescence lifetime- and intensity-based methods. *J. Microsc.*, 250:179–188, 2013.
- [7] R. Mercadé-Prieto, L. Rodriguez-Rivera, and X. D. Chen. Fluorescence lifetime of rhodamine b in aqueous solutions of polysaccharides and proteins as a function of viscosity and temperature. *Photoch. photobio. Sci.*, 16:1727–1734, 2017.
- [8] NIST. Chemistry webbook, srd 69. <https://webbook.nist.gov/chemistry/fluid/>, 2022.

SUPPORTING INFORMATION:
Overlapping hydration shells in salt solutions
causing non-monotonic Soret coefficients with
varying concentration

Shilpa Mohanakumar, Hartmut Kriegs
Wim Briels and Simone Wiegand

October 18, 2022

Contents

S1 IR-Thermal diffusion Forced Rayleigh scattering set-up	S2
S2 Refractive index contrast measurements	S4
S3 Concentration dependence of S_T, D_T and D	S5
S4 Temperature dependence of S_T, D_T and D	S8

S1 IR-Thermal diffusion Forced Rayleigh scattering set-up

A detailed description of the thermal diffusion forced Rayleigh scattering technique can be found in the literature [1, 2, 3, 4, 5, 6]. We used the infrared thermal diffusion forced Rayleigh scattering (IR-TDFRS) setup [7], which is optimal for aqueous solutions. The main difference is that no dye is needed to convert the light energy into heat energy in aqueous solutions, due to the absorption of water at the wavelength of the infrared laser beam ($\lambda_w=980$ nm).

Summarizing what is explained in more detail in the above given references, the infrared laser beam is split into two beams that interfere in the sample cell, creating an intensity grating. The intensity grating is absorbed by the fluid and as a consequence, a temperature gradient builds up, which in turn causes a concentration grating by the effect of thermal diffusion. Both temperature and concentration gratings contribute to a combined refractive index grating which is read out by the Bragg diffraction of an He-Ne laser ($\lambda_w=633$ nm). The typical fringe spacing of the grating is $20\mu\text{m}$ and the amplitude of the temperature grating will be in the order of $100\mu\text{K}$ [7]. The total heterodyne scattering intensity $\zeta_{\text{het}}(t)$ assuming an ideal excitation with a step function is given by

$$\begin{aligned} \zeta_{\text{het}}(t) = & 1 - \exp\left(-\frac{t}{\tau_{\text{th}}}\right) \\ & - A(\tau - \tau_{\text{th}})^{-1} \left\{ \tau \left[1 - \exp\left(-\frac{t}{\tau}\right) \right] - \tau_{\text{th}} \left[1 - \exp\left(-\frac{t}{\tau_{\text{th}}}\right) \right] \right\} \end{aligned} \quad (\text{S1})$$

with the steady state amplitude A

$$A = \left(\frac{\partial n}{\partial c}\right)_{p,T} \left(\frac{\partial n}{\partial T}\right)_{p,c}^{-1} S_T c (1 - c) \quad (\text{S2})$$

where c is the mass concentration, τ_{th} the heat diffusion time, $(\partial n/\partial c)_{p,T}$ and $(\partial n/\partial T)_{p,c}$ are refractive index contrast factors in respect to mass concentration at constant pressure and temperature, and in respect to temperature at constant pressure and mass concentration, respectively. The Soret coefficient $S_T = D_T/D$ can be expressed as ratio of the thermal diffusion coefficient, D_T , and the collective diffusion coefficient, D . Whereas $D = 1/(q^2\tau)$ can be calculated from the diffusion time, τ , in Eq. S1 using q the magnitude of the grating vector which is given by

$$q = \frac{4\pi}{\lambda_w} \sin\frac{\theta}{2} \quad (\text{S3})$$

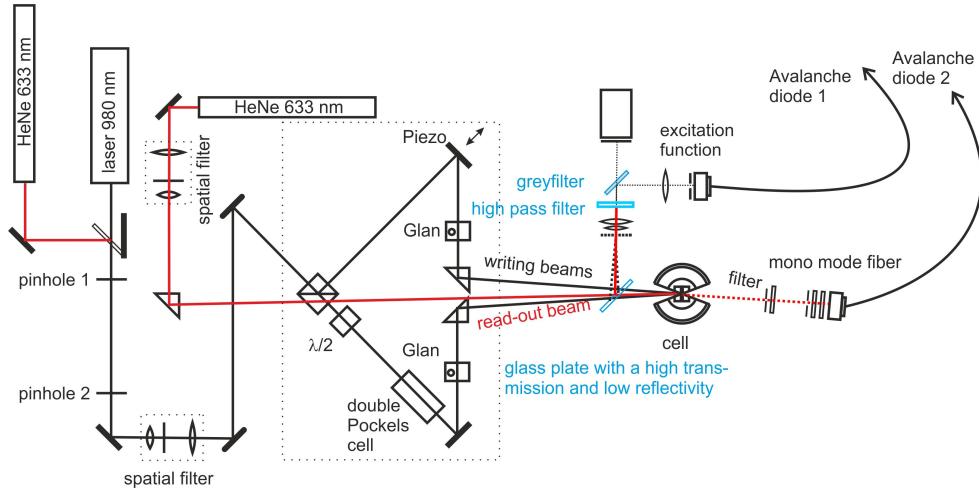


Figure S1: Sketch of the infrared TDFRS setup.

where θ is the angle between the two writing beams at the wavelength λ_w . The transport coefficients are determined by fitting Eq. S1 to the measured heterodyne signal and deconvoluting the excitation function [8, 9].

A sketch of the IR-TDFRS setup is shown in Fig. S1. We simultaneously record the excitation function and diffracted signal (through the cell), so any external disturbance (thermal or mechanical) will affect both recorded signals in the same way. This has been achieved by replacing the original flip mirrors [7] in front of the cell and the camera, by a glass plate with a high transmission and a low reflectivity and by a grey filter, respectively. Using a grey filter in front of the camera avoids ghost images on the camera due to internal reflections within the glass. For the phase synchronization of the excitation function we use a line grating, with the same period as the optical grating in its image plane. This line grating is mounted on a motorized translational stage. This can be moved perpendicular to the optical axis, so that the phase of the excitation function can be determined and adjusted. Using this additional grating reduces the noise in the determination of the phase.

S2 Refractive index contrast measurements

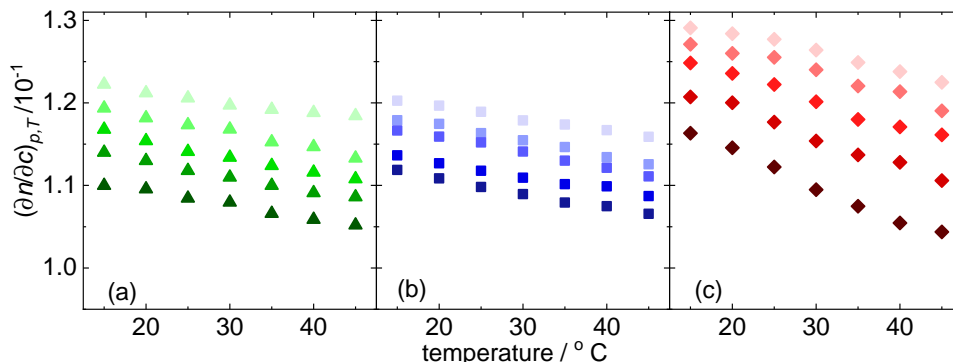


Figure S2: Contrast factor calculated from the refractive index measurements $(\partial n / \partial c)_{p,T}$ for (a) KI, (b) NaI and (c) LiI are plotted against temperature. Concentration follows the order 0.5, 1, 2, 3 and 4 mol/kg from top to bottom with highest concentration corresponding to darkest of symbols.

In order to calculate the Soret coefficient S_T from the intensity of the diffracted read-out beam, it is necessary to know the dependence of the refractive index on concentration. This was measured with an Abbe refractometer (Anton Paar Abbemat MW) at a wavelength of 632.8 nm. Fig.S2 shows the derivative of $n(c, T)$ with respect to concentration determined by linear fitting of the experimental refractive index values. $(\partial n / \partial c)_{p,T}$ decreases with increase in temperature. Measurements of the refractive index were conducted for 7 concentrations.

The dependence of the refractive index on temperature, $(\partial n / \partial T)_{p,c}$, is also necessary for the calculation of the Soret coefficient. This was measured interferometrically [10]. For the calculation of S_T from the IR-TDFRS measurements, the contrast factors were interpolated from these measurement series for temperatures and concentrations at which the TDFRS experiment had been performed. In the measured concentration and temperature range, $(\partial n / \partial T)_{p,c}$ is negative for all salts. The absolute value of $(\partial n / \partial T)_{p,c}$ increases with increasing salt concentration.

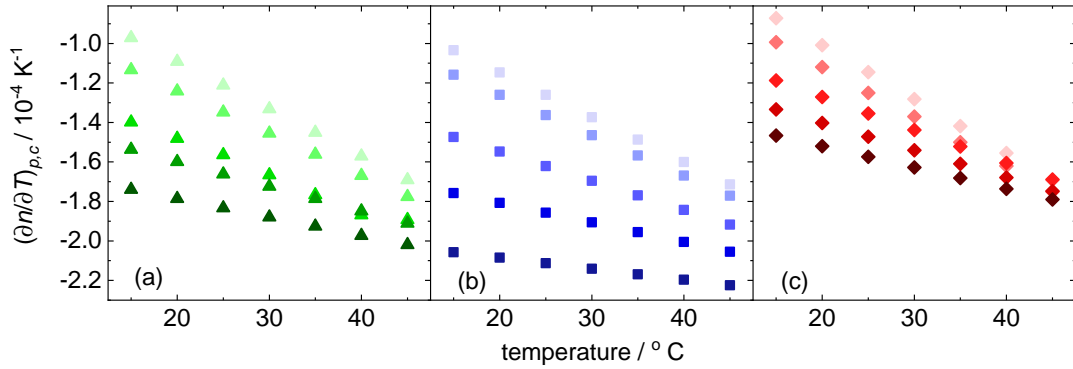


Figure S3: Results of the interferometrically measured contrast factors $(\partial n / \partial T)_{p,c}$ for (a) KI, (b) NaI and (c) LiI at different concentrations. Concentration follows the order 0.5, 1, 2, 3 and 4 mol/kg from top to bottom with highest concentration corresponding to darkest of symbols.

S3 Concentration dependence of S_T, D_T and D

As it can be seen in Fig. S4 and Fig. S5, both KI and LiI show minimum with concentration for S_T and D_T . D shows a monotonous increase with concentration for both salts. Thus behavior of these coefficients is very similar to that of NaI discussed in the main manuscript. LiI for concentrations $c > 0.75$ mol/kg shows thermophilic behavior for all temperatures. Where as KI shows thermophilic behavior at very low concentrations, $c < 2$ mol/kg at $T=15^\circ\text{C}$.

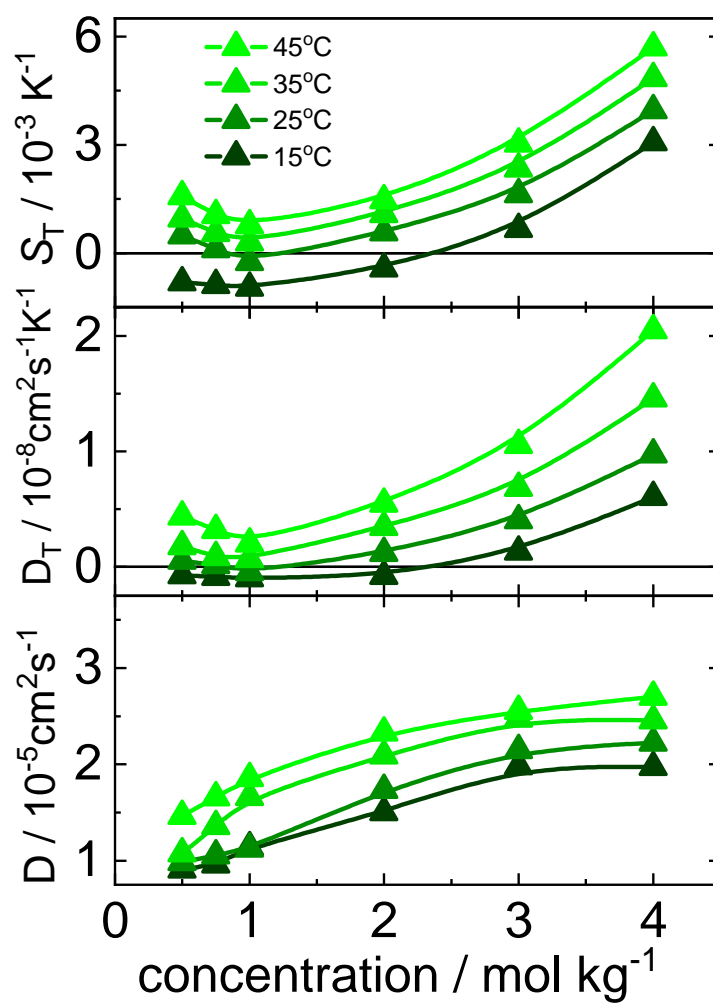


Figure S4: Concentration dependence of S_T , D_T and D of KI at four different temperatures. In each panel temperatures are 15, 25, 35 and 45 °C in the order with the darkest symbol corresponding to lowest temperature as shown in inset.

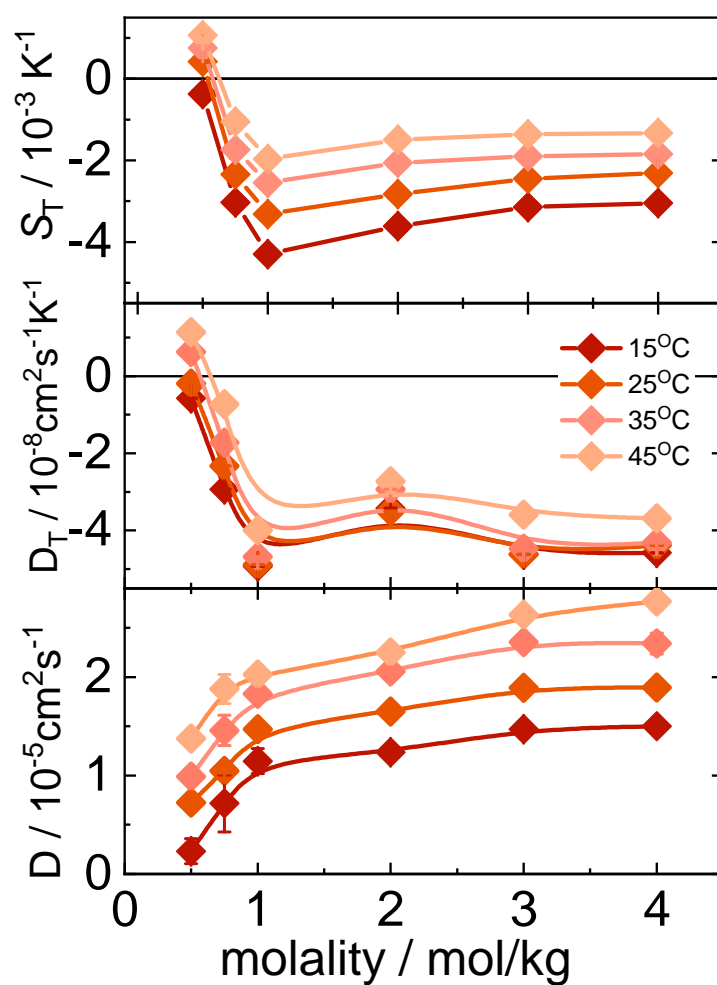


Figure S5: Concentration dependence of S_T , D_T and D of LiI at four different temperatures. In each panel temperatures are 15, 25, 35 and 45 °C in the order with the darkest symbol corresponding to lowest temperature as shown in inset.

S4 Temperature dependence of S_T , D_T and D

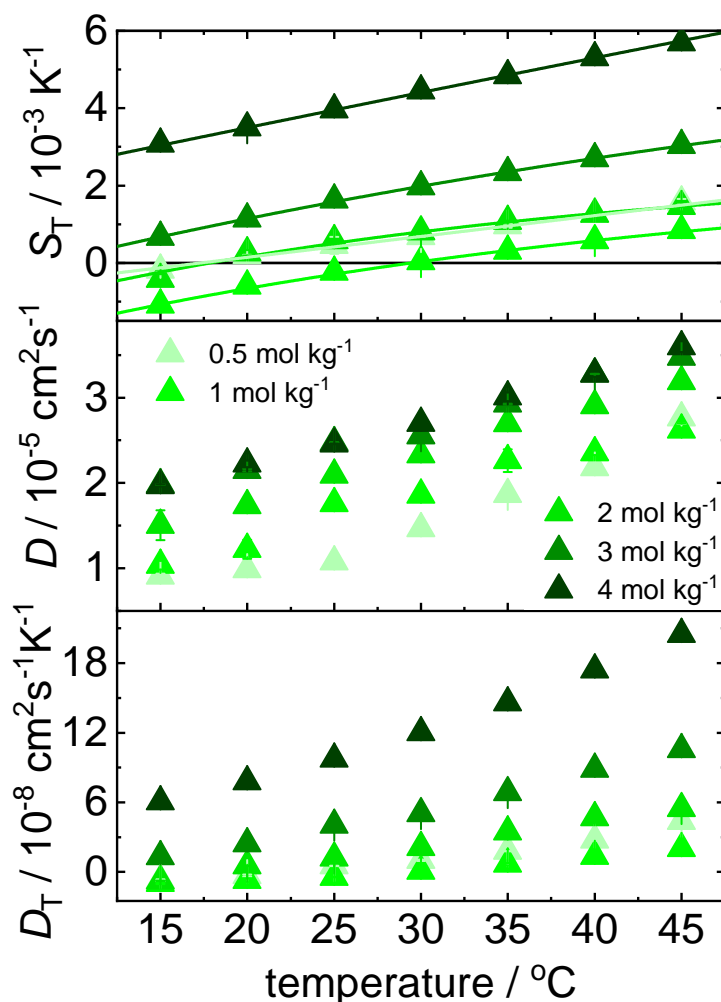


Figure S6: Temperature dependence of S_T , D_T and D of KI at different concentrations as shown in inset. The darkest symbol corresponds to the highest concentration 4 mol/kg followed by lower concentrations of 3, 2, 1 and 0.5 mol/kg (faded symbol).

Temperature dependence of S_T , D_T and D for KI, NaI and LiI is shown in Fig.S6, Fig.S7 and Fig.S8, respectively. S_T , D_T and D of all the systems increases with temperature at all concentrations measured.

Table S1: The table enlists the fitting parameters obtained for KI using Eq.2 in the main manuscript for all the concentrations studied

m / mol/kg	$S_T^\infty / 10^{-3} K^{-1}$	T^* / K	T^0 / K
0.5	2.40 ± 0.03	22.45 ± 0.21	22.7 ± 3.8
1	3.54 ± 0.08	29.45 ± 0.06	59.4 ± 6.8
2	2.61 ± 0.04	17.88 ± 1.04	32.9 ± 9.1
3	7.23 ± 0.09	8.40 ± 0.49	67.5 ± 10.1
4	8.54 ± 0.06	17.45 ± 2.33	69.4 ± 7.8

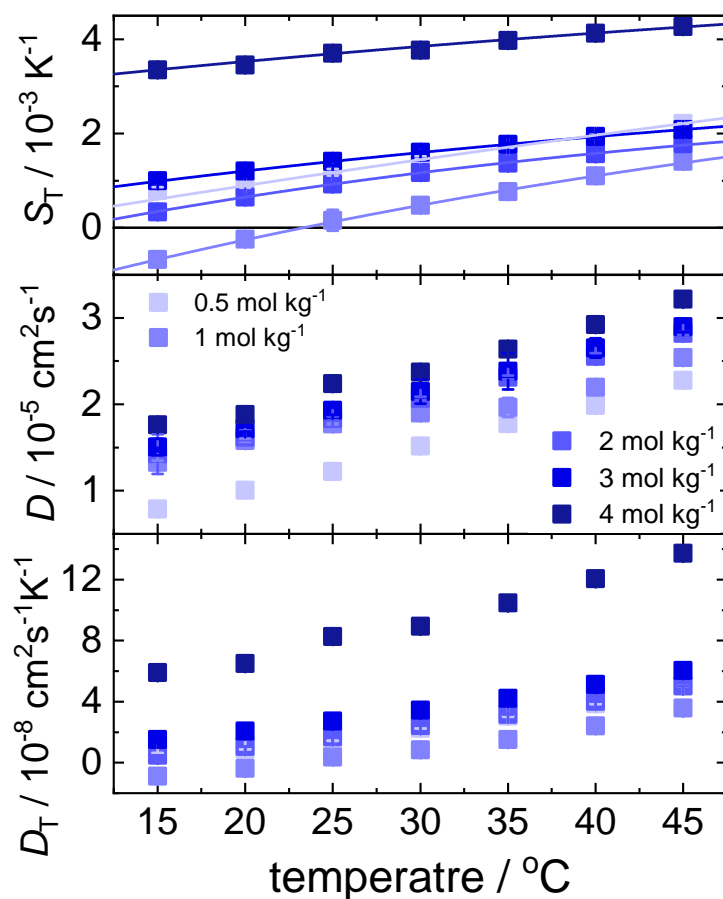


Figure S7: Temperature dependence of S_T, D_T and D of NaI at different concentrations as shown in inset. The darkest symbol corresponds to the highest concentration 4 mol/kg followed by lower concentrations of 3, 2, 1 and 0.5 mol/kg (faded symbol).

Table S2: The table enlists the fitting parameters obtained for NaI using Eq.2 in the main manuscript for all the concentrations studied

m / mol/kg	$S_T^\infty / 10^{-3} K^{-1}$	T^* / K	T^0 / K
0.5	10.32 ± 0.01	24.92 ± 2.16	52.7 ± 2.9
1	4.56 ± 0.12	23.31 ± 0.02	60.4 ± 2.3
2	3.20 ± 0.03	9.92 ± 0.52	44.1 ± 6.0
3	4.03 ± 0.02	-3.80 ± 0.50	67.0 ± 5.3
4	6.28 ± 0.01	-46.78 ± 10.28	81.00 ± 10.5

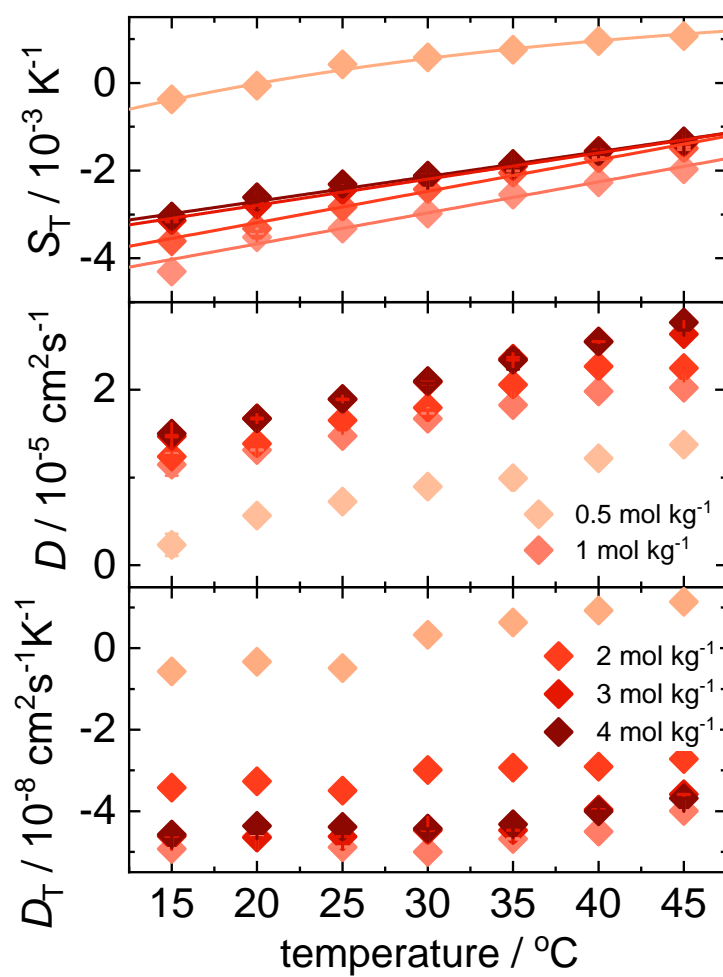


Figure S8: Temperature dependence of S_T , D_T and D of LiI at different concentrations as shown in inset. The darkest symbol corresponds to the highest concentration 4 mol/kg followed by lower concentrations of 3, 2, 1 and 0.5 mol/kg (faded symbol).

Table S3: The table enlists the fitting parameters obtained for LiI using Eq.2 in the main manuscript for all the concentrations studied

m / mol/kg	$S_T^\infty / 10^{-3} K^{-1}$	T^* / K	T^0 / K
0.5	1.91 ± 0.06	20.24 ± 0.49	28.2 ± 11.0
1	-2.58 ± 0.02	23.31 ± 0.02	23.1 ± 2.4
2	-2.39 ± 0.03	28.95 ± 0.089	32.6 ± 4.6
3	-3.59 ± 0.17	36.29 ± 0.59	46.9 ± 2.9
4	-8.95 ± 0.03	42.56 ± 1.03	48.5 ± 3.8

References

- [1] K. Thyagarajan and P. Lallemand. Determination of thermal-diffusion ratio in a binary mixture by forced rayleigh-scattering. *Opt. Commun.*, 26:54–57, 1978.
- [2] W. Köhler. Thermodiffusion in polymer-solutions as observed by forced rayleigh-scattering. *J. Chem. Phys.*, 98:660–668, 1993.
- [3] W. Köhler and P. Rossmanith. Aspects of thermal-diffusion forced rayleigh-scattering - heterodyne-detection, active phase tracking, and experimental constraints. *J. Phys. Chem.*, 99:5838–5847, 1995.
- [4] W. Köhler and R. Schäfer. Polymer analysis by thermal-diffusion forced rayleigh scattering. In *New Developments in Polymer Analytics II*, volume 151 of *Advances in Polymer Science*, pages 1–59. 2000.
- [5] S. Wiegand and W. Köhler. Measurement of transport coefficients by an optical grating technique. In Werner Köhler and Simone Wiegand, editors, *Thermal Nonequilibrium Phenomena in Fluid Mixtures*, volume 584, pages 189–210. Springer Berlin Heidelberg, Berlin, Heidelberg, 2002.
- [6] P. Blanco, H. Kriegs, M. P. Lettinga, P. Holmqvist, and S. Wiegand. Thermal diffusion of a stiff rod-like mutant y21m fd-virus. *Biomacromolecules*, 12:1602–1609, 2011.
- [7] S. Wiegand, H. Ning, and H. Kriegs. Thermal diffusion forced rayleigh scattering setup optimized for aqueous mixtures. *J. Phys. Chem. B*, 111:14169–14174, 2007.
- [8] G. Wittko and W. Köhler. Precise determination of the solet, thermal diffusion and mass diffusion coefficients of binary mixtures of dodecane, isobutylbenzene and 1,2,3,4-tetrahydronaphthalene by a holographic grating technique. *Philos. Mag.*, 83:1973–1987, 2003.
- [9] H. Ning, R. Kita, H. Kriegs, J. Luettmer-Strathmann, and S. Wiegand. Thermal diffusion behavior of nonionic surfactants in water. *J. Phys. Chem. B*, 110:10746–10756, 2006.
- [10] A. Becker, W. Köhler, and B. Müller. A scanning michelson interferometer for the measurement of the concentration and temperature derivative of the refractive-index of liquids. *Ber. Bunsen-Ges. Phys. Chem. Chem. Phys.*, 99:600–608, 1995.

SUPPORTING INFORMATION:
Complementary experimental methods to
obtain thermodynamic parameters of protein
ligand systems

Shilpa Mohanakumar, Namkyu Lee
and Simone Wiegand

Contents

S1 Mathematical relation between Soret coefficient and Gibb's free energy	S2
S2 Various existing forms of EDTA in MES buffer	S4
S3 Protein-ATTO 532 dye labeling	S4
S3.1 Labeling BCA	S4
S3.2 BCA purification	S5
S4 Temperature dependence of the thermal diffusion D_T and diffusion coefficient D for protein-ligand systems	S6
S5 Refractive index increments with temperature	S8
S6 Data analysis and fitting of ITC measurements	S10
S7 Analysis curves of ITC measurement for labeled BCA I with PFBS	S12
S8 Validation of the relation between Soret coefficient and Gibb's free energy at other temperatures	S13
S8.1 EDTA-CaCl ₂	S13
S8.2 Protein-ligand	S13
S8.2.1 BCA I-PFBS	S13
S8.2.2 BCA I-4FBS	S13

S1 Mathematical relation between Soret coefficient and Gibb's free energy

Soret coefficient and Gibb's free energy at different temperatures have been measured by TDFRS and ITC, respectively. A relation between S_T starts from a relation originally proposed by Eastman [1] and later rewritten by Würger [2] in a modern nomenclature,

$$S_T = \frac{1}{k_B T} \frac{dG}{dT} \quad (\text{S1})$$

The Soret coefficients S_T^{low} and S_T^{high} correspond to T_{low} and T_{high} , respectively. Assuming a linear T -dependence of S_T with T , we write

$$S_T(T) = (S_T^{\text{low}} + \Delta S_T)T \quad (\text{S2})$$

with

$$\Delta S_T = S_T^{\text{high}} - S_T^{\text{low}} \quad (\text{S3})$$

Integration of Eq. S1 with respect to temperature in the range from T_{low} to T_{high} leads to

$$\int_{T_{\text{low}}}^{T_{\text{high}}} dG = \int_{T_{\text{low}}}^{T_{\text{high}}} k_B T S_T(T) dT \quad (\text{S4})$$

using Eq. S2 we obtain

$$\Delta \Delta G = k_B (S_T^{\text{low}} + \Delta S_T) \left(\frac{T_{\text{high}}^2 - T_{\text{low}}^2}{2} \right) \quad (\text{S5})$$

For a mole of molecules holds

$$\Delta \Delta G = N_A k_B (S_T^{\text{low}} + \Delta S_T) \left(\frac{T_{\text{high}}^2 - T_{\text{low}}^2}{2} \right). \quad (\text{S6})$$

S_T values of ligand, macromolecule and the complex at two different temperatures, T_{high} and T_{low} can be measured with TDFRS. $\Delta \Delta G$ corresponding to ligand, macromolecule and the complex can then be calculated with Eq. (S6). For systems like EDTA-CaCl₂ and protein-ligand for which binding is not strong, there are chances to find free ligands and macromolecules in the solution. In such cases, $S_T(\text{complex})$ will have also contributions from the individual compounds that are remaining in the solution. Hence there will be two main contributions to the S_T measured;

1. Contribution from the complex

2. Contribution from free macromolecule or free ligand

$S_T(\text{complex})$ for such systems has to be calculated excluding the contribution from free protein/free ligand (whichever is present in the system). It has to be noted that in EDTA–CaCl₂ system, EDTA acts as the macromolecule (in the cell of ITC) and CaCl₂ as the ligand (injected through a syringe into the cell of ITC). Dissociation constant K_d measured by ITC is;

$$K_d = \frac{[\text{protein}][\text{ligand}]}{[\text{complex}]} \quad (\text{S7})$$

where [protein], [ligand] and [complex] are the concentrations of free protein, free ligand and complex, respectively. Since the total concentration of protein (protein(total)) and ligand (ligand(total)) is known, Eq. (S7) can be rearranged as follows,

$$K_d = \frac{[\text{protein}(\text{total}) - [\text{complex}]][\text{ligand}(\text{total}) - [\text{complex}]]}{[\text{complex}]} \quad (\text{S8})$$

Solving the quadratic equation Eq. (S8) gives access to [complex], from which we can calculate the fraction of the free protein f_P and ligand f_L accordingly,

$$f_P = \frac{[\text{protein}(\text{total}) - [\text{complex}]]}{\text{protein}(\text{total})} \quad (\text{S9})$$

$$f_L = \frac{[\text{ligand}(\text{total}) - [\text{complex}]]}{\text{ligand}(\text{total})} \quad (\text{S10})$$

$$f_C = 1 - (f_P + f_L) \quad (\text{S11})$$

Analysis of K_d values indicates that for EDTA–CaCl₂ and both protein-ligand systems, the fraction of free ligand (or CaCl₂) is higher than that of the free protein (or EDTA) (at 25°C, for BCA I–4FBS system, fraction of free protein and ligand are 0.008 and 0.7, respectively). Hence for the further calculations, we neglect the contribution from the free protein. We propose the following equation for the $S_T(\text{total})$ that is measured using our IR-TDFRS setup :

$$\frac{1}{S_T^{\text{total}}} = \frac{1 - f_C}{S_T^{\text{complex}}} + \frac{f_L}{S_T^{\text{ligand}}} \quad (\text{S12})$$

where S_T^{total} is the S_T measured using IR-TDFRS, S_T^{ligand} is the S_T of ligand, f_C is the fraction of complex and f_L is the fraction of free ligand. Rearranging Eq. (S12) leads to

$$S_T^{\text{complex}} = \frac{1 - f_C}{\frac{1}{S_T^{\text{total}}} - \frac{f_L}{S_T^{\text{ligand}}}} \quad (\text{S13})$$

Access of $S_T(\text{complex})$ at T_{high} and T_{low} enables the calculation of $\Delta\Delta G$ corresponding to the complex. Obtained values can be used to establish a relation between ITC and TDFRS measurements as shown in the main manuscript.

S2 Various existing forms of EDTA in MES buffer

EDTA ($\text{C}_{10}\text{H}_{16}\text{N}_2\text{O}_8$) exists in several forms in MES buffer [3]. EDTA is a hexadentate ligand which has six lone pairs of electrons that are available for binding. Protonation enables EDTA to exist in various states ranging from a fully protonated (Fig.S1a) to fully deprotonated stage (Fig.S1b). It can also exist in some intermediate stages between these two forms with one to three protons. Experimental studies confirm that EDTA^{4-} and HEDTA^{3-} exist, playing a crucial role in forming complexes with the metal ion [4, 5, 3]. It has to be noted that the complexation reaction primarily proceeds through EDTA^{4-} forms, but HEDTA^{3-} reacts also with a lower probability [3]. The majority form depends on the pH (cf. Fig.1 [4, 5] and Fig.9 in [3])

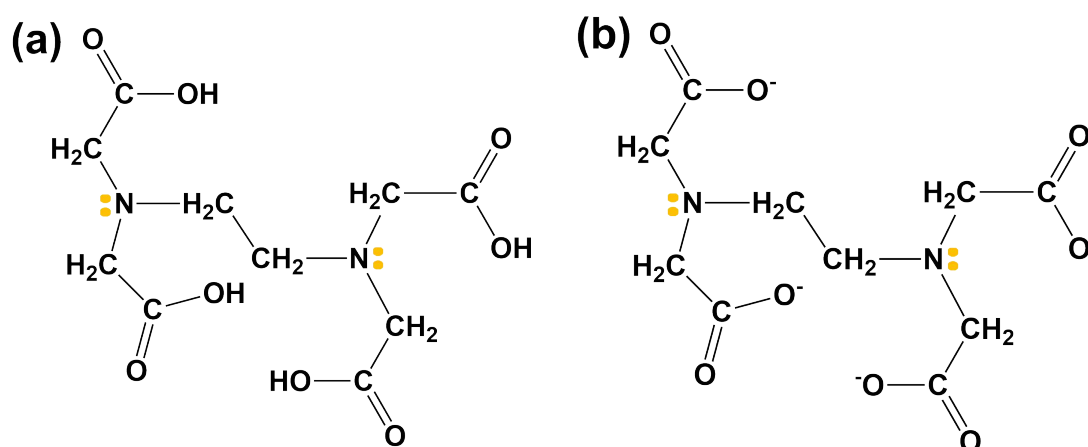


Figure S1: (a) Protonated form of EDTA (b) Deprotonated form of EDTA

S3 Protein-ATTO 532 dye labeling

S3.1 Labeling BCA

ATTO 532 dye (cf. Fig.S2) was used for labeling Bovine Carbonic Anhydrase (BCA) I. Protein standard (100 μM) was prepared in sodium phosphate

buffer (20 mM). For NHS-ester labeling the pH of the sample was adjusted to 8.3 by adding drops of a NaHCO_3 solution (2.1 g in 50 ml water). 1 mg of ATTO 532 was dissolved in 200 μl of dimethyl sulfoxide (DMSO) which is used as the standard solvent for the dye. The dye solution was mixed with the protein solution so that the final concentration ratio dye:protein is 200 μM :20 μM in 1 ml of the solution. The rest of the volume was filled up with buffer solution of pH 8.3. The sample were kept in shaker overnight for thorough mixing.

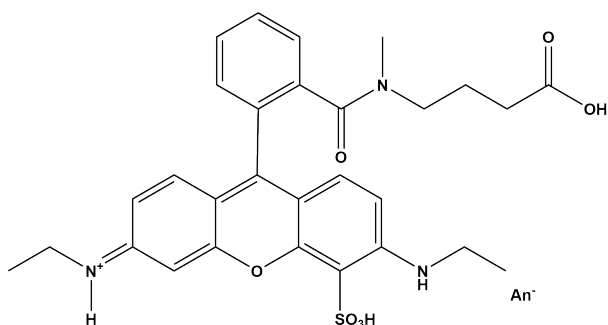


Figure S2: Chemical structure of ATTO 532 dye

S3.2 BCA purification

The following procedure was followed to remove the unbound dye. Zeba™ Spin-Säulen columns were used for the purification of the mixture. Once the column is settled after centrifugation (1000 rpm for 2 minutes), the process was repeated with buffer of pH 7.4. 300 μl of the mixture was transferred to the column and purified. Absorption of the solution was measured using UV-VIS spectrophotometer. Labeled proteins have an absorption at 532 nm, which gives the corresponding concentration.

S4 Temperature dependence of the thermal diffusion D_T and diffusion coefficient D for protein-ligand systems

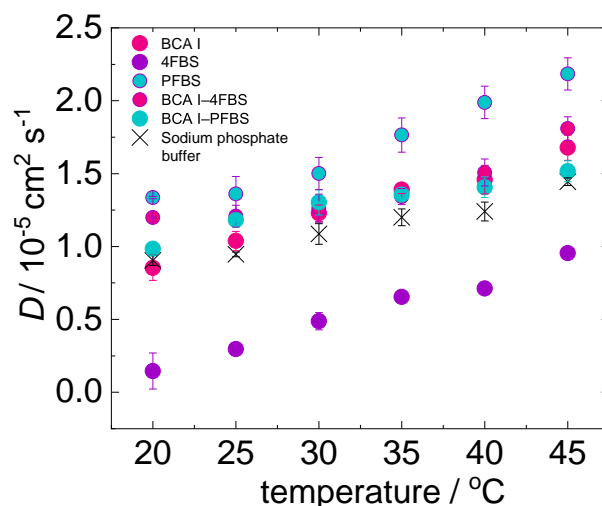


Figure S3: Temperature dependence of D for BCA I (protein), 4FBS and PFBS (ligands), corresponding protein-ligand complex, sodium phosphate buffer

Dependence of diffusion coefficients on temperature is shown in Fig.S3. Diffusion of protein gets faster when ligand binds to it. This could be related to the fact, that the complex is less hydrophilic, so that it can move faster compared to the free protein, which shows the slowest diffusion. The increase in D with temperature due to decrease in viscosity can also be seen in Fig.S3. Dependence of thermodiffusion coefficient on temperature is shown in Fig.S4. here it is striking that the thermal diffusion coefficients of the complexes and the ligands are very similar, which D_T is much lower, which could also be related to the higher hydrophilicity of the free protein.

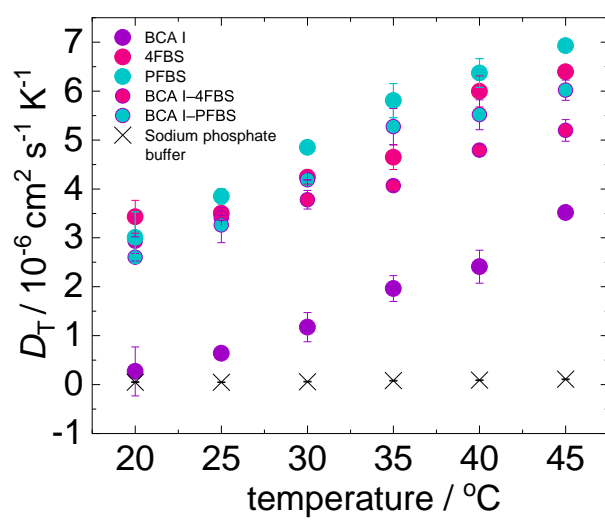


Figure S4: Temperature dependence of D_T for BCA I (protein), 4FBS and PFBS (ligands), corresponding protein-ligand complex, sodium phosphate buffer

S5 Refractive index increments with temperature

Figure S5 and S6 shows the refractive index increments for EDTA–CaCl₂ and both protein-ligand systems.

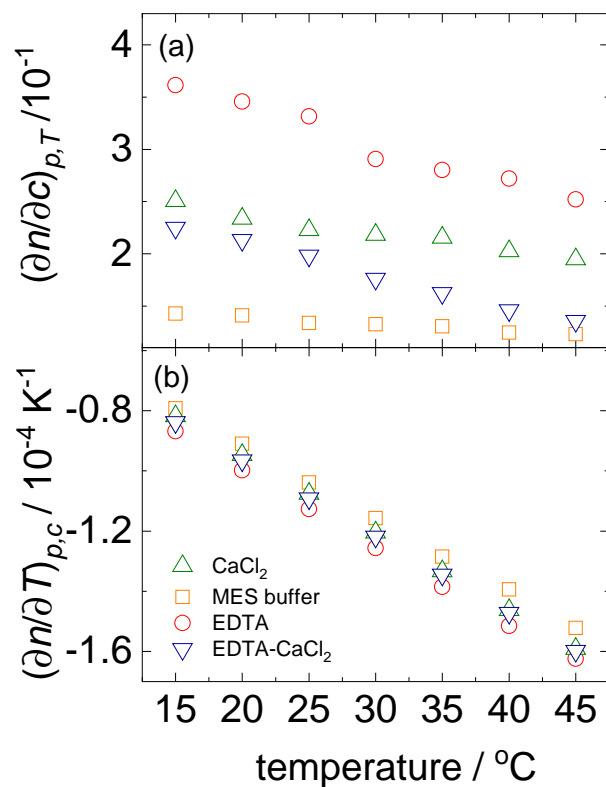


Figure S5: (a) Temperature dependence of $(\partial n/\partial c)_{p,T}$ for EDTA–CaCl₂ system (b) Temperature dependence of $(\partial n/\partial T)_{p,c}$ for EDTA–CaCl₂ system

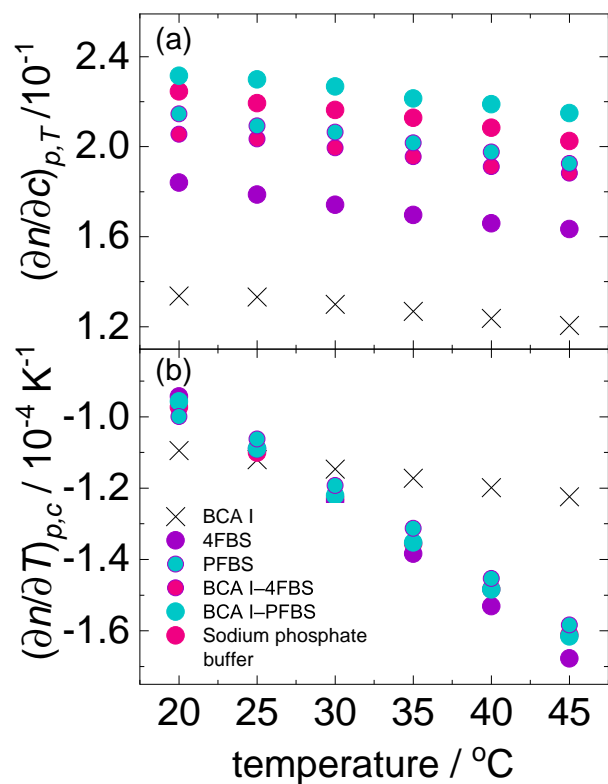


Figure S6: (a) Temperature dependence of $(\partial n/\partial c)_{p,T}$ for protein-ligand systems (b) Temperature dependence of $(\partial n/\partial T)_{p,c}$ for protein-ligand systems

S6 Data analysis and fitting of ITC measurements

We have used the most common binding model (1:1 binding) for the analysis of our ITC data. The following notations are used further: m is the number of binding sites, θ is the fraction of sites occupied by ligand X, M_t and M are the bulk and free concentration of macro molecule, X_t and X are the bulk and free concentration of ligand, ΔH is the molar heat of ligand binding, V_0 is the active cell volume. Binding constant,

$$K = \frac{\theta}{(1 - \theta)X} \quad (\text{S14})$$

Total ligand concentration,

$$X_t = X + m\theta M_t \quad (\text{S15})$$

Combining Eq. S14 and Eq. S15;

$$\theta^2 - \theta \left[1 + \frac{X_t}{mM_t} + \frac{1}{mKM_t} \right] + \frac{X_t}{mM_t} = 0 \quad (\text{S16})$$

The total heat content of the solution Q at a given time for an ITC measurement is

$$Q = m\theta M_t \Delta H V_0 \quad (\text{S17})$$

Solving Eq. S16 for θ and substituting it in Eq. S17 gives,

$$Q = \frac{mM_t \Delta H V_0}{2} \left[1 + \frac{X_t}{mM_t} + \frac{1}{mKM_t} - \sqrt{\left(1 + \frac{X_t}{mM_t} + \frac{1}{mKM_t} \right)^2 - \frac{4X_t}{mM_t}} \right] \quad (\text{S18})$$

Once an injection of ligand into the cell occurs, software calculates the heat associated with the injection. What is of primary interest for the study is the change in heat content of i^{th} injection to that of $i - 1^{th}$ injection. Change in heat after i^{th} injection is given by;

$$\Delta Q(i) = Q(i) + \frac{dV_i}{V_0} \left[\frac{Q(i) + Q(i - 1)}{2} \right] - Q(i - 1) \quad (\text{S19})$$

where dV_i is the correction factor introduced to compensate the heat contribution from the displaced volume. This is because, for each injection there is a volume of protein-ligand complex that is expelled from the cell which is identical to the volume of ligand that is injected. Fitting involves initial guesses of m , ΔH and K which allows to calculate $\Delta Q(i)$ for each injection. This is then compared with the experimental $\Delta Q(i)$ which is measured and then improving m , ΔH and K values until the best fit. A typical ITC measurement curve and molar enthalpy curve is shown in Fig.S7.

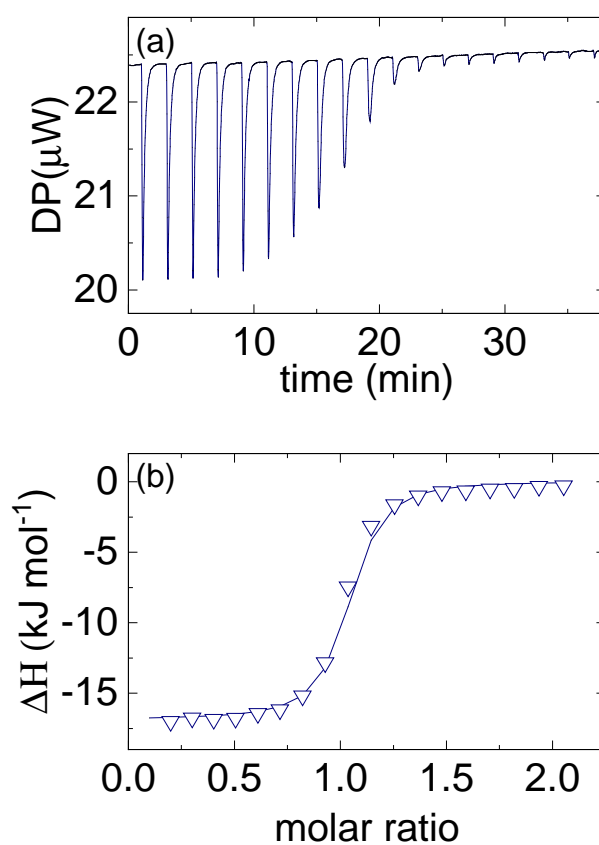


Figure S7: (a) Raw data output for EDTA-CaCl₂ binding reaction measured at 25°C (b) Integrated data output for EDTA-CaCl₂ binding reaction measured at 25°C plotted as molar change in enthalpy against molar ratio

S7 Analysis curves of ITC measurement for labeled BCA I with PFBS

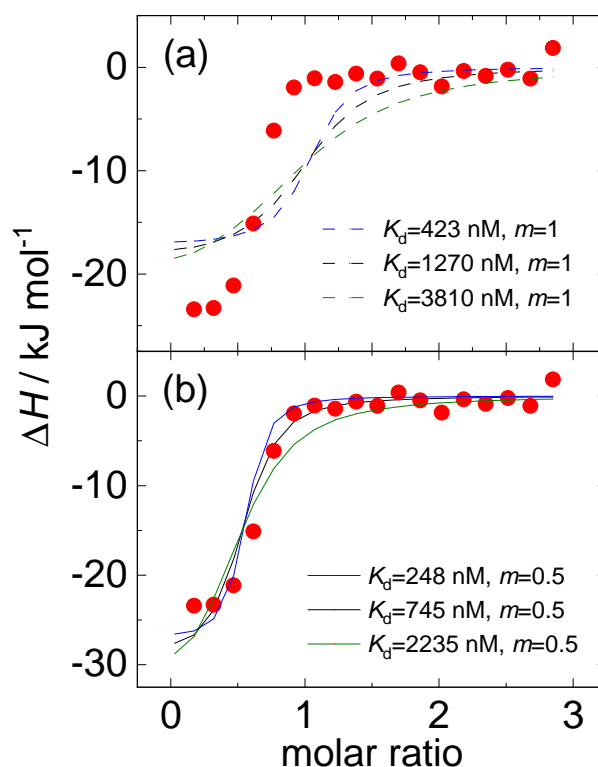


Figure S8: Integrated data output for labeled BCA I–PFBS binding measured at 25°C. (a) and (b) corresponds to the fit obtained with $m=1$ and $m=0.5$, respectively. The black line corresponds to the optimum fit generated by the analysis software with $K_d(\text{optimum})$. The blue line corresponds to the fit obtained by fixing K_d to a three times lower value of $K_d(\text{optimum})$ and green line corresponds to the fit obtained by fixing K_d to a three times higher value of the optimum fit $K_d(\text{optimum})$. Lower and higher K_d values used for the fits are listed in the legend.

Fixing the value of K_d and m adjusting ΔH gives the results shown in Fig. S8. Changing the value of K_d changes the shape of the curve, but the data are not compatible with $m = 1$. For $m = 0.5$ the lower K_d -value gives also a reasonable description, which implies that the uncertainty of K_d is at least 50%.

S8 Validation of the relation between Soret coefficient and Gibb's free energy at other temperatures

ΔG calculated at higher temperatures using Eq. 4 (cf. Sec.1 of main manuscript) and its comparison to the ITC measurements will be discussed for all systems in the following paragraphs.

S8.1 EDTA–CaCl₂

Table S1 lists the calculated $\Delta G_{\text{calculated}}$ and ΔG_{ITC} measured with ITC for EDTA–CaCl₂. Both values agree within the error bars.

Table S1: Table enlists ΔG values that are calculated and measured using ITC at different temperature combinations for EDTA–CaCl₂ system

T _{high} (°C)	T _{low} (°C)	$\Delta G_{\text{calculated}}$ (kJ/mol)	ΔG_{ITC} (kJ/mol)
20	30	-36.5 ± 1.2	-36.4 ± 0.8
25	35	-36.1 ± 3.2	-35.5 ± 1.8
30	40	-35.7 ± 3.4	-34.8 ± 2.4
35	45	-33.3 ± 1.4	-34.2 ± 1.9

S8.2 Protein-ligand

S8.2.1 BCA I–PFBS

Table S2 lists the calculated $\Delta G_{\text{calculated}}$ and ΔG_{ITC} measured with ITC for BCA I–PFBS. Both values agree within the error bars.

S8.2.2 BCA I–4FBS

Table S3 lists the calculated $\Delta G_{\text{calculated}}$ and ΔG_{ITC} measured with ITC for BCA I–PFBS. Both values agree within the error bars.

Table S2: Table enlists ΔG values that are calculated and measured using ITC at different temperature combinations for BCA I-PFBS system

T_{high} ($^{\circ}\text{C}$)	T_{low} ($^{\circ}\text{C}$)	$\Delta G_{\text{calculated}}$ (kJ/mol)	ΔG_{ITC} (kJ/mol)
20	30	-40.5 ± 1.1	-40.4 ± 1.3
25	35	-44.0 ± 2.6	-46.8 ± 0.6
30	40	-48.2 ± 3.1	-52.1 ± 1.2
35	45	-54.9 ± 2.9	-55.9 ± 1.1

Table S3: Table enlists ΔG values that are calculated and measured using ITC at different temperature combinations for BCA I-4FBS system

T_{high} ($^{\circ}\text{C}$)	T_{low} ($^{\circ}\text{C}$)	$\Delta G_{\text{calculated}}$ (kJ/mol)	ΔG_{ITC} (kJ/mol)
20	30	-39.9 ± 3.9	-38.2 ± 1.5
25	35	-36.6 ± 3.4	-39.4 ± 1.1
30	40	-40.3 ± 1.8	-40.7 ± 0.8
35	45	-45.5 ± 3.5	-42.1 ± 1.3

References

- [1] E. D. Eastman. Theory of the Soret effect. *J. Am. Chem. Soc.*, 50:283–291, 1928.
- [2] A. Würger. Is Soret equilibrium a non-equilibrium effect? *C. R. - Mec.*, 341:438–448, 2013.
- [3] J. Reiter. *CFD analysis of EDTA-CaCl₂ reaction in a microfluidic channel to aid in design of novel calorimeter device*. PhD thesis, Northeastern University Boston, Massachusetts, 2015.
- [4] R. J. Kula, G. H. Reed. Nuclear magnetic resonance investigation of ligand exchange kinetics in the calcium(II)-EDTA system. *Analytical chemistry*, 38:697–701, 1966.
- [5] J. D. Carr and D. G. Swartzfager. Kinetics of the ligand exchange and dissociation reactions of calcium-aminocarboxylate complexes. *J. Am. Chem. Soc.*, 97:315–321, 1973.

Declaration of Individual Contribution and Accessibility of Data and Materials

The complete primary data are stored and are available on request from the corresponding author, while the displayed data in the main manuscripts are accessible via ZENODO.

Article no. 1

Title: Thermodiffusion of Aqueous Solutions of Various Potassium Salts

Corresponding Thesis Chapter: Chapter 2

Status: Published. DOI: 10.1063/5.0038039

Data: 10.5281/zenodo.7545048

S. Mohanakumar, J. Luettmer-Strathmann, S. Wiegand, J. Chem. Phys. 154, 84506 (2021);

The independent contribution of the candidate:

I did all experiments 100% by myself. I contributed 60% of data analysis, interpretation of the results and writing the manuscript.

Article no. 2

Title: Towards understanding specific ion effects in aqueous media using thermodiffusion

Corresponding Thesis Chapter: Chapter 3

Status: Published. DOI: 10.1140/epje/s10189-022-00164-8

Data: 10.5281/zenodo.7545078

S. Mohanakumar, S. Wiegand, The Eur. Phys. J. E 45, 10 (2022);

The independent contribution of the candidate:

I did all experiments and the data analysis 100% by myself. I contributed about 80% to the interpretation of the results and writing of the manuscript.

Article no. 3

Title: Overlapping hydration shells in salt solutions causing non-monotonic Soret coefficients with varying concentration

Corresponding Thesis Chapter: Chapter 4

Status: Published. DOI: 10.1039/D2CP04089A

Data: 10.5281/zenodo.7545116

S. Mohanakumar, Hartmut Kriegs, W. J. Briels, S. Wiegand, *Phys. Chem. Chem. Phys.* 24, 27380 (2022);

The independent contribution of the candidate:

I did all TDFRS experiments and data analysis 100%. Performing the calculations, I was involved 50%. I contributed about 60% to the interpretation of the data and the writing of the manuscript.

Article no. 4

Title: Thermophoretic microfluidic cells for evaluating Soret coefficient of colloidal particles

Corresponding Thesis Chapter: Chapter 5

Status: Published. DOI: 10.1016/j.ijheatmasstransfer.2022.123002

Data: 10.5281/zenodo.7545093

N. Lee, **S. Mohanakumar**, S. Wiegand, *Int. J. Heat Mass Transf.* 194, 123002 (2022);

The independent contribution of the candidate:

I performed TDFRS experiments and data analysis and Dr. Lee designed microfluidic cell and performed the experiments. I contributed about 50% to the interpretation of the results and writing the manuscript.

Article no. 5

Title: Complementary Experimental Methods to Obtain Thermodynamic Parameters of Protein Ligand Systems

Corresponding Thesis Chapter: Chapter 6

Status: Published. DOI: 10.3390/ijms232214198

Data: 10.5281/zenodo.7545129

S. Mohanakumar, N. Lee, and S. Wiegand, *Int. J. Mol. Sci.* 23, 14198 (2022);

The independent contribution of the candidate:

I performed all TDFRS and ITC experiments and the data analysis, while Dr. Lee did the experiments with the microfluidic cell and the analysis. In total I did 80% of the experimental work. I contributed 80% of interpretation of results and writing of the manuscript.

Erklärung zur Dissertation

„Hiermit versichere ich an Eides statt, dass ich die vorliegende Dissertation selbstständig und ohne die Benutzung anderer als der angegebenen Hilfsmittel und Literatur angefertigt habe. Alle Stellen, die wörtlich oder sinngemäß aus veröffentlichten und nicht veröffentlichten Werken dem Wortlaut oder dem Sinn nach entnommen wurden, sind als solche kenntlich gemacht. Ich versichere an Eides statt, dass diese Dissertation noch keiner anderen Fakultät oder Universität zur Prüfung vorgelegen hat; dass sie - abgesehen von unten angegebenen Teilpublikationen und eingebundenen Artikeln und Manuskripten - noch nicht veröffentlicht worden ist sowie, dass ich eine Veröffentlichung der Dissertation vor Abschluss der Promotion nicht ohne Genehmigung des Promotionsausschusses vornehmen werde. Die Bestimmungen dieser Ordnung sind mir bekannt. Darüber hinaus erkläre ich hiermit, dass ich die Ordnung zur Sicherung guter wissenschaftlicher Praxis und zum Umgang mit wissenschaftlichem Fehlverhalten der Universität zu Köln gelesen und sie bei der Durchführung der Dissertation zugrundeliegenden Arbeiten und der schriftlich verfassten Dissertation beachtet habe und verpflichte mich hiermit, die dort genannten Vorgaben bei allen wissenschaftlichen Tätigkeiten zu beachten und umzusetzen. Ich versichere, dass die eingereichte elektronische Fassung der eingereichten Druckfassung vollständig entspricht.“

Teilpublikationen::

1. **S. Mohanakumar**, J. Luettmer-Strathmann, S. Wiegand, J. Chem. Phys. 154, 84506 (2021)
2. **S. Mohanakumar**, S. Wiegand, The Eur. Phys. J. E 45, 10 (2022)
3. N. Lee, **S. Mohanakumar**, S. Wiegand, Int. J. Heat Mass Transf. 194, 123002 (2022)
4. **S. Mohanakumar**, Hartmut Kriegs, W. J. Briels, S. Wiegand, Phys. Chem. Chem. Phys. 24, 27380 (2022)
5. **S. Mohanakumar**, N. Lee, and S. Wiegand, Int. J. Mol. Sci. 23, 14198 (2022)

Shilpa Mohanakumar

✉ s.mohanakumar@fz-juelich.de

🌐 https://www.fz-juelich.de/profile/mohanakumar_s



Education

- 2019-present **Ph.D., Forschungszentrum Jülich** in Experimental Soft Matter.
Thesis title: *Thermophoresis of electrolyte solutions and protein-ligand systems*, Supervisor: Prof. Dr. Simone Wiegand
- 2014 – 2019 **BS-MS Dual degree. Chemistry, IISER Bhopal** GPA: 8.73/10
Thesis title: *Interaction of Epirubicin Hydrochloride with Lysozyme: A spectroscopic and Calorimetric Investigation*, Supervisor: Prof. Dr. Saptarshi Mukherjee
- 2012 – 2014 **Intermediate (Class XII), GMVHSS Nilambur, Kerala, India** Cumulative percentage: 98.5
- 2011 – 2012 **Matriculation (Class X), LFEMHSS Nilambur, Kerala, India** Cumulative percentage: 97.5

Research Publications

- S. Mohanakumar, N. Lee, and S. Wiegand, “Complementary experimental methods to obtain thermodynamic parameters of protein ligand systems,” *Int. J. Mol. Sci.*, vol. 23, p. 14198, 2022.
- S. Mohanakumar, H. Kriegs, W. J. Briels, and S. Wiegand, “Overlapping hydration shells in salt solutions causing non-monotonic soret coefficients with varying concentration,” *Phys. Chem. Chem. Phys.*, vol. 24, pp. 27380–27387, 2022.
- N. Lee, S. Mohanakumar, and S. Wiegand, “Thermophoretic microfluidic cells for evaluating soret coefficient of colloidal particles,” *Int. J. Heat Mass Transf.*, vol. 194, p. 123002, 2022.
- S. Mohanakumar and S. Wiegand, “Towards understanding specific ion effects in aqueous media using thermodiffusion,” *Eur. Phys. J. E*, vol. 45, p. 10, 2022.
- S. Mohanakumar, J. Luettmmer-Strathmann, and S. Wiegand, “Thermodiffusion of aqueous solutions of various potassium salts,” *J. Chem. Phys.*, vol. 154, p. 084506, 2021.
- L. Khamari, U. Pramanik, S. Shekhar, S. Mohanakumar, and S. Mukherjee, “Thermal reversibility and structural stability in lysozyme induced by epirubicin hydrochloride,” *Langmuir*, 37, pp. 3456–3466, 2021.

Oral Presentations

- **IBI-INM Retreat 2022**, Forschungszentrum Jülich, Germany
- **Bonn International Graduate School of Chemistry (BIGS Chemistry) Summer School**, Clausius Institute for Physical and Theoretical Chemistry, Universität Bonn, Germany

- **14th International Meeting on Thermodiffusion**, Norwegian University of Science and Technology, Trondheim, Norway

Awards and Achievements

- 2022 ■ **Best Poster Award**, Bunsen-Tagung 2022, Justus-Liebig-University Gießen, Gießen, Germany
- 2018 ■ **IASc-INSA-NASI Summer Research Fellowship**, Summer Internship, Jadavpur University, Kolkata, India.

- 2014 ■ **INSPIRE-SHE Scholarship**. Innovation in Science Pursuit for Inspired Research for motivated undergraduate science students by Department of Science Technology, India (Belonging to top 1 percent of the students who appeared in the exam).

Lab Skills

- Infra-red Thermal Diffusion Forced Rayleigh Scattering (IR-TDFRS)
- Isothermal Titration Calorimetry (ITC)
- UV-Vis Spectrophotometer, Spectrofluorometer
- Time-resolved fluorometer using the time-correlated using single-photon counting (TCSPC) technique.
- Circular Dichroism (CD) Spectroscopy
- Lab courses and on-hand experience on HPLC, NMR, MS during graduate studies and various summer internships